Performance-related properties of large particle sized tire-derived aggregate (TDA) for leachate collection and removal systems (LCRS)

by

Adedoyinsola (Doyin) Adesokan

A Thesis submitted to the College of Graduate and Postdoctoral Studies in partial fulfilment of the requirements for the degree of Doctor of Philosophy in the Department of Civil, Geological and Environmental Engineering University of Saskatchewan Saskatoon, Saskatchewan, Canada

Permission to use

In presenting this thesis in partial fulfillment of the requirements for the degree of Doctorate of Philosophy from the University of Saskatchewan, I agree that the Libraries of the University may make it freely available for inspection. I further agree that permission for copying this thesis in any manner, in whole or in part, for scholarly purposes may be granted by the professor or professors who supervised my thesis work or, in their absence, by the Head of the Department or the Dean of the College in which my thesis work was done. It is understood that any copying or publication or use of this thesis or parts thereof for financial gain shall not be allowed without my written permission. It is also understood that due recognition shall be given to me and to the University of Saskatchewan in any scholarly use, which may be made of any material in my thesis.

Requests for permission to copy or to make other use of material in this thesis in whole or in part should be addressed to:

The Head of the Department of Civil, Geological and Environmental Engineering

University of Saskatchewan

57 Campus Drive Saskatoon, SK S7N 5A9 Canada

OR

The Dean

College of Graduate and Postdoctoral Studies

University of Saskatchewan

116 Thorvaldson Building, 110 Science Place,

Saskatoon, SK CANADA S7N 5C9 Canada

Abstract

The compressive response of large particle sized tire derived aggregate (TDA) (>50 mm in size) to large applied stress, and the resulting effects on void ratio, vertical and horizontal hydraulic conductivity were studied to evaluate the use of the material in constructing the leachate collection and drainage layer of landfills. The applied stress studied ranged from 28 kPa to 375 kPa to simulate 2 m to 40 m of overlying waste over a landfill drainage layer. The performance of a drainage layer in a landfill depends on a high hydraulic conductivity to rapidly transmit leachate from the base of the landfill into collection and removal units to prevent excessive mounding of leachate on basal liner materials. It also depends on a high void volume to store inevitable biogeochemical clog material that will accumulate around the TDA particles as leachate flows through the drainage layer.

Given that TDA compresses under applied stress, unlike gravel – which is typically used in constructing the drainage layer of landfills, the hydraulic conductivity of TDA and void volume will change under applied stress with time. The individual and combined effects of immediate compression (the instantaneous response upon application of stress) and creep (the time delayed compression following immediate compression) on void ratio under applied stress were studied. Study of biogeochemical clogging was outside the scope of work; however, parameters such as void ratio under applied stress and specific surface area were measured. These can be used in the simulation and evaluation of biogeochemical clogging in future studies.

The inherent nature of TDA required innovative design of the laboratory testing equipment and iterative re-design and modification of the units and their components. The testing units had to be large to accommodate the testing of the large particle sized TDA, whilst minimizing the effects/inevitable artifacts of constrained large scale testing (such as sidewall friction). Despite all efforts to minimize sidewall friction loss, this was still highly prevalent during the testing, causing higher applied stress and compression in TDA sublayers closer to the applied surface stress and

lower applied stress and compression in the sublayers farther away from the surface stress. Sidewall friction loss during compression testing was accounted for by determining the vertical distribution of applied stress and void ratio across the TDA thickness. In the evaluation of permeability and hydraulic conductivity, sidewall friction effects were removed from the data using some formulated analytical forms. High velocities and inertia effects were also accounted for in the analyses of the permeability and hydraulic conductivity data.

Laboratory testing was carried out using two main large sized, purpose built units – a one dimensional (1D) consolidometer (1.8 m high, 0.7 m diameter) and a two dimensional (2D) permeameter and consolidometer (1 m high, 1.2 m long, 0.6 m wide). The 1D cell was used to measure immediate compression and creep under applied stress. The 2D cell was used to measure vertical, horizontal air permeability, and hydraulic conductivity under sustained applied stress; compression data was also collected from testing in the 2D cell. Eight compression/creep tests were completed in the 1D cell over a combined 705 days, individual duration ranged from 24 to 317 days. The duration of testing in the 2D cell was over 430 days (combined for all the tests), individual duration ranged from 112 to 316 days. Air permeability and hydraulic conductivity were evaluated from several dozens of tests completed at different flow rates and pressures.

The results from this study show that the void ratio of TDA can decrease to as low as 0.2 at applied stress of 224 kPa (20 m to 25 m of overlying waste on a landfill drainage layer). Nonetheless, the corresponding vertical and hydraulic conductivity values at a void ratio of 0.2 were both greater than 0.01 m/s. Projections of void ratio to higher applied stress up to 800 kPa (70 m – 85 m of overlying waste) showed a decrease to 0.01 and beyond that, void ratio was considerably less than 0.01. Corresponding vertical and horizontal hydraulic conductivity values at a void ratio of 0.01 were both higher than 0.001. These thus imply that void ratio alone is not sufficient for evaluating the performance of a TDA drainage layer, as even at considerably low

void ratios, adequate flows can still be maintained in a TDA drainage layer. Many landfill regulations (for instance *Standard for landfills in Alberta* – used in Saskatchewan) stipulate a hydraulic conductivity of 0.0001 m/s. The measured and projected values (up to 800 kPa) meet and exceed the common stipulation for landfills, and are comparable to the typical range of values for gravel used in landfill leachate drainage layers. Given these results, large particle sized TDA can be considered adequate for use as drainage material in the leachate collection and removal systems of landfills.

The results from this research work were used in an existing analytical form for evaluating maximum leachate head in a drainage layer. The maximum leachate head values obtained from the analytical form were validated and corrected using finite element numerical modeling. The corrected values were presented in the form of design charts. The design charts and the results from this work were used to prepare a design guidance that may be used when constructing a landfill drainage layer with large particle sized TDA.

Acknowledgement

My sincere gratitude goes to Dr. Ian Fleming for providing the opportunity for this graduate studies. I am deeply grateful for his invaluable supervision, ideas, and suggestions, and for supporting me in various capacities throughout the program.

I would like to thank the members of my committee – Dr. James (JD) Johnston, Dr. David Elwood, Dr. Grant Ferguson, committee chair – Dr. Christopher Hawkes, external examiner – Dr. Craig Lake, and also, Dr. Lee Barbour, for the time and effort invested.

I would like to thank Loraas Disposal, Shercom Industries, SNC Lavalin, Adelantar Consulting, Alberta Recycling Management Authority for providing the funding and resources for this research work.

I would like to thank the many helpful people at the University of Saskatchewan (U of S), who supported and assisted in various capacities – Adam Hammerlindl, Helen Yin, Dale Pavier, Brennan Pokoyoway, Kyle Scales, Jake Hartl, Minh Nguyen, Yan Bedin, Brody Smith, Jamie Fleming, Richard Heese, Cynthia Hanke, Alison Draude, the team at the Engineering Shops, Blair Cole, Mike Miller, and Emmanuel Neye – PhD candidate Department of Mathematics and Statistics, U of S. You are all very much appreciated.

Dedication

This work is dedicated to Jürgen and Todd – my entire world. Jürgen, thank you for bringing new meaning to my life. Todd, thank you for the support.

Preface

Sections of this thesis have been submitted as multi-authored papers in refereed journals. The research was performed by me and some data collection (such as some portions for the solid volume compression, immediate completion and creep and hydraulic conductivity) were carried out by one of the co-authors – Adam Hammerlindl, in coordination with graduate and undergraduate students who were trained by me in the data collection and experimental processes. Data analyses and manuscript preparation were carried out by me, in conjunction with Dr. Ian Fleming – supervisor and co-author, who provided helpful suggestions, as well as reviewed and edited the manuscripts for submission to refereed journals.

Published, Accepted and Submitted Manuscripts

1. **D. Adesokan**, I. Fleming, A. Hammerlindl, and J. McDougall, "Strategies for One Dimensional (1D) Compression Testing of Large-Particle-Sized Tire Derived Aggregate," Geotechnical Testing Journal 42, no. 5 (September/October 2019): 1336–1358. https://doi.org/10.1520/GTJ20170091

   Authors' contribution: Doyin Adesokan was jointly responsible for the original ideas behind the paper, equipment design, experimental strategies, collection of experimental data, data analyses, presentation of the findings, and writing and editing of the original paper. Adam Hammerlindl was jointly responsible for the original ideas behind the equipment design, experimental strategies and collection of experimental data. Dr. McDougall provided revision and edits on this paper. Dr. Ian Fleming was jointly responsible for the original ideas, equipment design, and experimental strategies, and provided supervision, revision and edits on this paper. This research is discussed in **Chapter 3** of this thesis.

2. **D. Adesokan**, I. Fleming and A. Hammerlindl, "One-dimensional (1D) immediate compression and creep in large particle sized Tire Derived Aggregate (TDA) for leachate

collection and removal systems (LCRS)," Canadian Geotechnical Journal, manuscript ID cgj-2019-0722.R2 Accepted for publication May 25, 2020

Authors' contribution: Doyin Adesokan was jointly responsible for the original ideas behind the paper, equipment design, experimental strategies, collection of experimental data, data analyses, presentation of the findings, and writing and editing of the original paper. Adam Hammerlindl was jointly responsible for the original ideas behind the equipment design, experimental strategies and collection of experimental data. Dr. Ian Fleming was jointly responsible for the original ideas, equipment design, and experimental strategies, and provided supervision, revision and edits on this paper. This research is discussed in **Chapter 4** of this thesis.

3. **D. Adesokan**, I. Fleming and A. Hammerlindl, "Hydraulic Conductivity of Tire Derived Aggregate for Leachate Collection and Removal," Environmental Geotechnics Journal, Submitted August 2, 2020.

   Authors' contribution: Doyin Adesokan was jointly responsible for the original ideas behind the paper, equipment design, experimental strategies, collection of experimental data, data analyses, presentation of the findings, and writing and editing of the original paper. Adam Hammerlindl was jointly responsible for the original ideas behind the equipment design, experimental strategies and collection of experimental data. Dr. Ian Fleming was jointly responsible for the original ideas, equipment design, and experimental strategies, and provided supervision, revision and edits on this paper. This research is discussed in **Chapter 5** of this thesis.

Table of contents

List of figures

List of tables

1.0 Introduction

1.1 Background

Modern-day engineered landfills typically have leachate collection and removal systems (LCRS) that act to control leachate mounding, thus reducing the buildup of excessive hydraulic head on the landfill basal liner system or sub grade of the landfill cell (Rowe and Fleming, 1998; Rowe, 2005; Warith et al., 2004). The LCRS systematically collects and removes leachate and contaminated water that could be transported into the environment (McIsaac and Rowe, 2005; Rowe, 2005). The LCRS consists of a subgrade, perforated leachate collection pipes, leachate collection sump(s), leachate evacuation pumps and a drainage media. The drainage media connects the landfill waste to the leachate collection pipes and sumps, and it is the channel through which infiltrated water and leachate are collected and removed from the landfill into leachate collection pipes and sumps (Reddy and Saichek, 1998; Qian et al., 2002; Warith et al., 2004; McIsaac and Rowe, 2005; Rowe, 2005; Yu and Rowe, 2012).

One of the essential requirements of the drainage media of a LCRS is high hydraulic conductivity over a long term. The hydraulic conductivity of the drainage media influences the buildup of hydraulic head on the landfill basal liner system and this has an impact on the efficient and effective functioning of the LCRS. Excessive hydraulic head on the basal liner system has various adverse consequences, one of which is slope instability in the landfill, another is the increased potential for contaminant transport through the basal liner as overlying hydraulic head increases (Reddy and Marella, 2001; Rowe, 2005). In order to control hydraulic head buildup in landfills, environmental regulations exist that stipulate both the thickness and the hydraulic conductivity requirements of the drainage media during the service life of the landfill.

Generally, the landfill drainage layer should have a thickness of at least 0.3 m and a hydraulic conductivity greater than or equal to 0.0001 m/s (Duffy, 1995; Narejo and Shettima, 1995; Warith et al., 2004). In certain situations and countries, the regulatory hydraulic conductivity of the LCRS drainage layer could be as low as 0.0000001 m/s (Beaven et al., 2007). In Saskatchewan, the *Standards for Landfills in Alberta* (2010) is used and this requires a minimum hydraulic conductivity of 0.0001 m/s for LCRS drainage materials at the time of placement, and no more than 0.3 m of leachate head over the basal liner system during the active landfill life, final landfill closure and post closure. In view of these, a suitable material for use as the drainage media in a LCRS is required to have and maintain a sufficiently high hydraulic conductivity for extended periods; even after being subjected to various loading and biogeochemical conditions within the landfill, the drainage media is expected to continue to perform effectively to meet or exceed regulatory stipulations (Warith et al., 2004; McIsaac and Rowe, 2005; Rowe, 2005; Yu and Rowe 2013).

Another important function of the drainage media is to protect the landfill base barrier (e.g. geomembrane), from damage during construction and after the placement of waste (Reddy and Saichek, 1998; Warith et al., 2004; Dickinson and Brachman, 2008; Marcotte and Fleming, 2020). The drainage media of the LCRS is thus expected to perform a dual function of leachate conduit and base barrier protector.

Uniformly graded gravel has been a suitable drainage material for LCRS because it can maintain a sufficiently high hydraulic conductivity under high applied stress for extended periods (Rowe and McIsaac, 2005; McIsaac and Rowe, 2005; Rowe 2005; Yu and Rowe, 2012; Yu and Rowe, 2013). A few drawbacks relating to cost, material availability, and inability to protect the landfill base barrier from damage – Dickinson and Brachman (2008), have resulted in the need to source for suitable alternatives to gravel (Evans, 1997; Warith et al., 2004; Moo-Young et al., 2003; Rao and Dutta, 2006).

Tire derived aggregate (TDA), obtained from the shredding of waste tires into sizes from 12 mm to over 305 mm, have been proposed (Hall 1991; Duffy, 1995; Reddy and Saichek, 1998; Warith et al., 2004), researched (McIsaac and Rowe, 2005; Rowe and McIsaac, 2005; Hudson et al., 2007; Beaven et al., 2007; Beaven et al., 2013; Adesokan et al., 2019[1]) and used (Donovan et al., 1996; Evans, 1997; Zimmerman, 1997; Reddy and Saichek, 1998; Warith et al., 2004; Adesokan et al., 2019[2]; Adesokan et al., 2020[3]) as an alternative to gravel as drainage media in LCRS. TDA is a suitable alternative because it is relatively cheaper and lighter in weight than gravel and can maintain a high hydraulic conductivity under applied stress (Hall, 1991, Edil et al, 1992, Ahmed and Lovell, 1993; Duffy, 1995; Moo-young et al., 2003). Although the hydraulic conductivity of TDA can reduce significantly under applied stress because of both immediate compression and long-term creep (Wartman et al., 2006), various researches have shown that under low to moderate loading, some TDA materials can maintain a high hydraulic conductivity that meets regulatory stipulations throughout the service life of the LCRS (Hall, 1991; Beaven, 1994; Duffy, 1995; Narejo and Shettima, 1995; Reddy and Saichek, 1998; Warith et al., 2004; Beaven et al., 2007; Hudson et al., 2007).

Another reason for the suitability of TDA as LCRS drainage material is that it can perform the second important function of the drainage media, which is to protect the landfill base barrier (geomembrane) from damage during construction and after landfill waste placement (Reddy and Saichek, 1998; Warith et al., 2004; Dickinson and Brachman, 2008; Marcotte and Fleming, 2020). This function is best performed by TDA with no protruding, exposed or loose wires (Dickinson and Brachman, 2008; Marcotte and Fleming, 2020).

In LCRS, TDA with particle size over 50 mm (“large” particle sized TDA), are preferred over small particle sized TDA because of the relatively larger void volume that is achievable within

[1] Chapter 3
[2] Chapter 3
[3] Chapter 4

large particle sized TDA. A large void volume is needed for a high hydraulic conductivity, and to store biogeochemical clog as leachate permeates through the drainage layer (Reddy and Saichek 1998; Rowe and Fleming 1998; Fleming et al. 1999; Fleming and Rowe 2004; Rowe et al., 2004; Rowe 2005; McIsaac and Rowe 2005; McIsaac and Rowe 2005; Rowe and Babcock 2007; Yu and Rowe 2012; Beaven et al., 2013). Large particle sized TDA typically have exposed wires – loose and protruding, thus recent studies by Marcotte and Fleming (2019) are investigating localized strains and damage to geomembrane from the exposed wires in large particle sized TDA.

Particle size matters in the response of TDA to applied stress (Hall 1991; Reddy and Saichek 1998; Warith et al. 2004; Rowe and McIsaac 2005; McIsaac and Rowe 2005; Beaven et al., 2006; Strenk et., 2007; Mwai et al. 2010), and the results from testing small particle sized TDA have not been clearly shown to be applicable for estimating the behaviour of large particle sized TDA. Hence, size specific testing is needed to determine the performance-related properties of large particle sized TDA.

Most of the evaluation and testing to date have focused on showing that TDA can be an adequate substitute for gravels i.e. perhaps not quite as good but good enough and relatively cheaper. However, if the drainage performance is as good, and pore volume is sufficient to provide a service life against biogeochemical clogging that is adequate, also, if localized strains and damage in underlying geomembranes are lesser than with gravel, these may represent an advantage in performance over gravel as landfill drainage layer material.

These advantages may also ease some of the existing restrictions surrounding the use of TDA as drainage material in LCRS. For instance – a waste height restriction of no more than 15 m of waste over a drainage layer constructed using TDA (The Saskatchewan Environmental Code, landfill chapter draft (2010)). Major waste management companies and municipalities in Saskatchewan are interested in increasing the height of waste in their landfills and waste

disposal grounds to 25 m or more to maximize landfill capacity. Evaluating the performance of TDA under applied stress equivalent to over 25 m of overlying waste i.e. over 200 kPa (see Zekkos et al., 2006) will enable its unrestricted use in these instances.

In view of these, this research work studied the performance-related properties of large particle sized TDA, including immediate compression and creep, vertical and horizontal hydraulic conductivity, anisotropy in the hydraulic conductivity, and pore geometry, in relation to its use in the LCRS of waste disposal sites. The applied stress were up to 375 kPa to simulate 30 – 40 m of waste above a TDA drainage layer.

Four different large particle-sized TDA types, sourced from two different tire processing facilities in the provinces of Saskatchewan and Alberta, Canada were used in the studies. Several TDA types were tested because various studies (such as Hall 1991; Reddy and Saichek 1998; Warith et al., 2004, Rowe and McIsaac 2005; McIsaac and Rowe 2005; Fleming and Marshall, 2013) have shown that not all TDA is the same, and different types of TDA (differing in terms of shape, particle size, mode of shredding, exposed and loose wire content) perform differently in compression under similar applied stress and loading conditions. Testing several different TDA types provided an opportunity to extensively investigate the material and performance related properties of TDA for use as drainage medium in LCRS.

1.2 Problem definition

Various properties of TDA have been investigated in the literature (see Chapter 2), however information is still lacking on some of the fundamental properties of TDA essential to its use and performance in civil engineering applications such as in LCRS. For instance:

1. In one of the key studies to date on TDA usage as drainage medium in LCRS (McIsaac and Rowe, 2005), compression and drainable porosity were measured for both gravels and TDA materials, while simultaneously permeating both materials with landfill leachate

for up to two years. As the study progressed, biogeochemical minerals from the leachate clogged up the pore volume of both materials, reducing their drainable porosities. The results of the study showed more clogging of the TDA pore volume than that of the gravel, and the key conclusions were not supportive of the use of TDA in LCRS. There were however, a few issues with how the study was carried out. For instance, the study did not first set out to establish some fundamentals such as:

a. How much of the pore volume reduction was attributable to biogeochemical clogging and how much was from immediate compression and/or creep?

b. Did solid volume compression of the individual TDA particles contribute to the total void volume reduction or was this solely from the reduction in bulk void volume as with solid minerals in classical soil mechanics? (Figure 1-1)

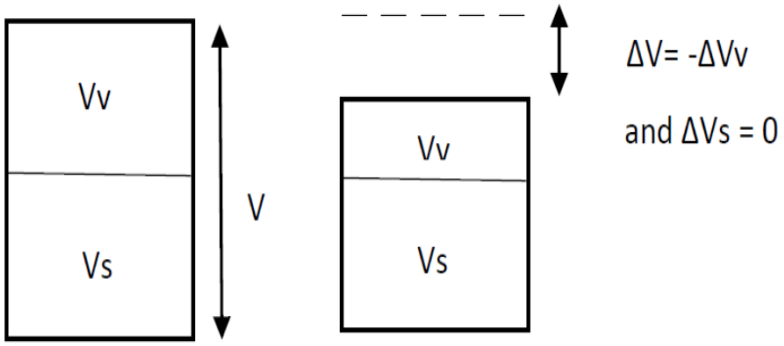

Where V_v is volume of voids, V_s is volume of solids and V is total volume

Figure 1-1: A schematic of volumetric compression in solid minerals

2. Most of the hydraulic conductivity results of TDA reported in the literature have been in the vertical direction. Vertical hydraulic conductivity is needed to understand how leachate might infiltrate within the landfill waste into the drainage media; but it is not sufficient to describe how the leachate might flow laterally through the drainage media into leachate collection pipes and sumps (Hudson et al., 2007). Current methods for calculating the maximum leachate head over the landfill base barrier require a

knowledge of the horizontal hydraulic conductivity. Given the elongated flat shape of some large TDA particles, especially under high-applied stress, it is expected that there will be anisotropy in the hydraulic conductivity of TDA, resulting a higher horizontal than vertical hydraulic conductivity (Donovan et al., 1996; Hudson et al., 2007). An understanding of the horizontal conductivity of TDA and anisotropy in the hydraulic conductivity is required to fill this knowledge gap and to better estimate the hydraulic head buildup on a landfill base barrier overlain by a TDA drainage layer.

3. Previous studies of TDA under applied stress have not widely considered long-term creep under sustained loading. The few studies to have looked at creep in TDA (such as Tweedie et al., 1998; Youwai and Bergado 2003; Rao and Dutta, 2006; Wartman et al., 2007) studied small particle sized TDA – tire chips (particle size less than 50 mm), and mixtures of the tire chips and soil. Only one study (Humphrey et al., 2000) is known to have studied creep in large particle sized TDA. Because TDA is a polymeric composite, a mass of TDA is expected to undergo creep under sustained loading. Hence, further research into creep was needed to evaluate the parameters affecting creep in TDA and the contribution of creep to void volume reduction in TDA.

4. Various parameters that affect void volume reduction and hydraulic performance of TDA such as the shape, particle size, exposed wire content and mode of shredding of TDA as well as the effects of prolonged loading and biogeochemical clogging have been investigated (Hall 1991; Reddy and Saichek, 1998; Warith et al., 2004, Rowe and McIsaac, 2005; McIsaac and Rowe, 2005). However, the individual and combined effects of elevated temperatures and applied stress over time have not been evaluated. There was a need to investigate this, at the typical temperatures that may arise at the base of a landfill over time, which could be as high as 50 C in some cases.

These four main areas formed the focus of this research work. The findings in this research work are expected to provide useful information and guidance on designing with TDA as drainage medium in the LCRS of engineered landfills and other waste disposal facilities. The experimental and analytical approaches utilized can be applied to similar highly compressible materials that undergo large void volume reduction under applied stress.

1.3 Research goal

The goal of this research work was to gain a better understanding of the immediate and time dependent performance-related properties of TDA for use as drainage medium in the LCRS of engineered landfills and other waste disposal facilities. To achieve this, the properties of TDA that can change under instant loading and over time, and which can affect performance in service, such as the compression of the solid and total volume, long term creep, hydraulic conductivity and specific surface under high applied loads/stress sustained for various amounts of time were investigated.

1.4 Research objectives

In view of the above, the specific objectives of the research were as follows:

1. develop and implement experimental strategies to address the challenges with the laboratory testing of large particle sized TDA

2. determine if there is isotropic solid volume compression in TDA or if volume change is solely because of reduction in void ratio such that:

   $\frac{\Delta H}{H} = \frac{\Delta e}{1+e_0}$ and $\Delta V_s = 0$

   Where ΔH is the change in height, Δe is the change in void ratio and ΔV_s is the change in volume of solids

3. determine the contribution of solid volume provide an assessment of void volume reduction in large particle sized TDA under sustained applied stress up to 375 kPa – equivalent to 30 to 40 m of waste over a TDA drainage layer in a waste disposal facility
4. quantify the individual and combined effects of factors such as immediate compression, creep, applied stress, duration of the applied stress, loading rate and temperature that may influence void volume reduction in TDA under the sustained applied stress
5. provide an assessment of the vertical and horizontal hydraulic conductivity of large particle sized TDA and anisotropy in the hydraulic conductivity under sustained applied stress
6. provide values for parameters relating to the pore geometry of TDA such as specific surface that may be used in existing biogeochemical clogging models to assess clogging in a TDA drainage layer in a LCRS.

1.4 Organization of thesis

This thesis contains three research manuscripts, presented in Chapters 3 to 5, and a Chapter with some design guidance for constructing a leachate collection and drainage layer with TDA.

Chapter 1 contains some background information into the research work, including the problem definition, research goal, objectives and methodology. Chapter 2 contains the review of literature relating to various aspects of the study.

Chapter 3 (Strategies for One Dimensional (1D) Compression Testing of Large-Particle-Sized Tire Derived Aggregate), was submitted as Manuscript 1, and it addresses objectives 1 - 4. Chapter 4 (One-dimensional (1D) immediate compression and creep in large particle sized Tire Derived Aggregate (TDA) for leachate collection and removal systems (LCRS)), was submitted as Manuscript 2, and it addresses objectives 3 - 4.

Chapter 5 (Hydraulic Conductivity of Tire Derived Aggregate for Leachate Collection and Removal), was submitted as Manuscript 3, and it addresses objectives 5 and 6. Chapter 6 contains the design guidance, and Chapter 7 contains the summary of key findings in the research work, and areas for future research.

1.5 Research methodology

The scientific method, consisting of *Observe, Measure, Explain and Verify* (Barbour and Krahn, 2004) was used in the research work.

- *Observe* – the focus of the research (problem definition – Section 1.2) was defined based on the knowledge gaps and deficiencies with studies in existing literature that are paramount to the use of TDA in LCRS
- *Measure* – data specific to the defined problems were collected by performing laboratory tests and synthesizing these with existing literature (Chapters 3-5)
- *Explain* – analyses and interpretation of data including the formulation of relevant analytical forms for data analysis, and assessment of parameters and factors were completed using resources available in the literature and new approaches developed in this work. The practical implications of the various results and findings were presented (Chapters 3-5)
- *Verify* – the results from the various aspects of the research were verified with supplementary experimental approaches. In addition, findings from the research were used in a theoretical model for designing leachate collection layers to generate design charts and provide guidance for TDA drainage layers in LCRS. The results obtained from the theoretical model were validated and corrected using finite element numerical modeling (Chapters 3-6).

2.0 Literature review

2.1 Leachate collection and removal system (LCRS)

A typical LCRS (Figure 2-1) consist of a leachate filter, drainage layer, a perforated leachate collection pipe system, pumps, sumps, riser pipes/manholes, clean out ports and leachate storage tanks (Fleming et al., 1999; Qian et al., 2002).

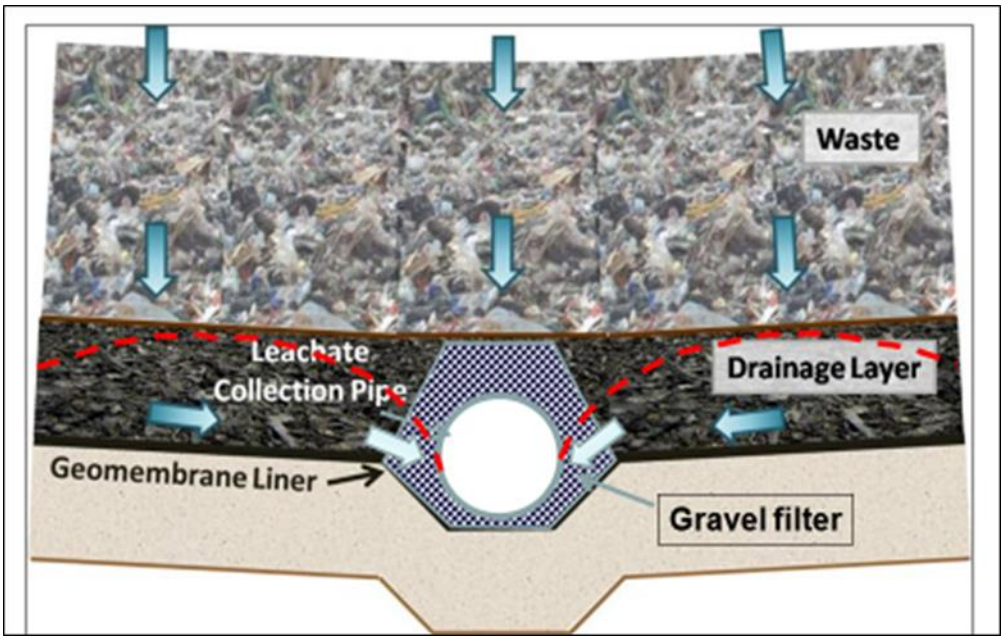

Figure 2-1: Schematic of a LCRS showing the major components of the drainage layer (Source: Fleming and Marshall, 2013)

One of the functions of a landfill LCRS is to remove leachate constantly from the base of the landfill into leachate collection pipes and sumps for treatment or disposal. Another function, performed majorly by the drainage layer component, is to prevent the build-up of excessive leachate head on the landfill base liner, reducing the potential for contaminant seepage through the liner (Fleming et al., 1999; McIsaac et al., 2000; Qian et al., 2002; Rowe et al., 2005). These functions require that the drainage layer have sufficiently high hydraulic conductivity to last the contaminating lifespan of the landfill, and prolong the service life of the LCRS – i.e., the period for which the LCRS performs in accordance with design assumptions (Fleming et al., 1999;

Fleming and Rowe et al., 2004; Rowe, 2005). The contaminating lifespan of a landfill and service life of the LCRS can be over a century, depending on factors such as the performance of the drainage layer, design details, waste characteristics, biogeochemical conditions, landfill practices and mode of operation (Rowe, 2005). Thus, processes and operations that can reduce or optimize the long-term performance of the LCRS must be factored into their design (Rowe and McIsaac, 2005). For this, the drainage layer requires particular attention. This is because if the LCRS drainage layer reaches its service level – i.e., the point at which the leachate head at the base of the landfill can no longer be controlled to the design level (Rowe, 2005; Yu and Rowe, 2012), the performance of some other components of the landfill barrier system may become compromised. For instance, if the hydraulic conductivity of the drainage layer is significantly reduced, such that excessive leachate mound builds up at the base of the landfill, the resulting high head could increase fluid and contaminant flow through the basal geomembrane liner into the environment, compromising the barrier function of the geomembrane. Excessive leachate mound could also result in elevated temperatures over 50 C on the landfill basal geomembrane, which may adversely affect the service life of the geomembrane (Rowe, 2005).

Some references consider a LCRS to have failed when the maximum leachate mound exceeds the widely used design value of 0.3 m (Rowe et al. 2004; Yu and Rowe, 2012). However, some other references (such as I. Fleming, personal communication, May 2020) have stated that while 0.3 m is a good conservative value for design, for practical considerations and from experience, leachate mounds of 0.4 m to 0.6 m is hardly a “failure”. A design approach that has been widely employed to extend the service life of the LCRS is the use of uniformly graded large diameter gravel as the drainage material (Rowe 2000 a,b; Rowe et al., 2004; Rowe and McIsaac, 2005). Gravel is widely used because it can maintain a high hydraulic conductivity for

extended periods under landfill conditions (Rowe, 2000). Drainage geosynthetics have also been used to this end (Fleming et al., 1999; Qian et al., 2002; McIsaac and Rowe., 2005).

In the past two decades however, various studies have indicated that TDA (section 2.2) may be equally suitable for the purpose, while providing economic and environmental benefits (Hall 1991; Beaven, 1994; Duffy, 1995; Donovan et al., 1996; Evans, 1997; Zimmerman, 1997; Reddy and Saichek, 1998; Warith et al., 2004; Hudson et al., 2007; Beaven et al., 2007; Beaven et al., 2013). Several studies (including this) have been carried out globally to investigate the hydraulic conductivity and other performance related properties of different TDA types for use in LCRS under various simulated landfill conditions.

2.2 Tire derived aggregate (TDA)

TDA (Figure 2-2) is obtained from shredding scrap automobile tires into sizes from 12 mm to over 305 mm; TDA with particle sizes ranging from 12 to 50 mm are referred to as tire chips, while TDA with particle sizes ranging from 50 to 305 mm are referred to as tire shreds (Wartman et al., 2007; ASTM D6270-98, *Standard Practice for Use of Scrap Tires in Civil Engineering Applications*).

Figure 2-2: TDA processing at the Shercom tire recycling facility, SK Canada; (a) Whole scrap tires to be shredded; (b) Tire shredder; (c) TDA (and some whole tires to be shredded)

Automobile tires, and consequently TDA, consist of materials such as natural and synthetic rubber, polymers, carbon black, sulfur, oil, paraffins, pigments, fabrics, additives, steel reinforcement, beads or belt materials (Reddy and Marella, 2001; Warith et al., 2004). The properties of TDA differ according to the original composition of the tire and this varies with tire manufacturer, type of tire, and the portion of whole tire shredded (Reddy and Marella, 2001).

Shredding of scrap tires into TDA is completed in one or more shredding passes, usually, the fewer the passes, the larger the TDA particles produced (Donovan et al., 1996; Moo-young et al., 2003). The material properties of TDA are not only dependent on the original composition of the parent whole tire, but also on the TDA particle size (whether chips, shreds or large particle sized), the mode of shredding, exposed wire content, and the portion of the tire used for TDA. When TDA is tested, a knowledge of the type of TDA used is required to characterize the TDA and evaluate its properties relative to other TDA types.

TDA can be described qualitatively, for instance in terms of the nature of cut (e.g. P and G shreds in McIsaac and Rowe, 2005; higher and lower quality shreds in Warith et al., 2004) or in terms of the shape of the particles (e.g. Beaven et al., 2007). Beaven et al (2007) used terms such as rotund for tire chips because they could be so small (<50 mm) that their three orthogonal dimensions were almost equal, and used terms such as plate-like and flat for tire shreds because they could be large enough (> 50 mm) to have such shapes.

TDA can also be described quantitatively. This can be in terms of the particle size distribution (PSD), which can be obtained by mechanical sieving for particles <50 mm, and by manual measurements or modified cumulative frequency methods for particles >50 mm (e.g. Mwai et al., 2010; Adesokan et al., 2019[4]). Quantitative descriptions can be in terms of density/unit weight – for instance, Warith et al (2004) showed that the average loose density of TDA is related to the size of the shreds. It can be in terms of the specific gravity – for instance, Geosyntec (2008) reported specific gravity values of 1.02 to 1.27 for TDA with the higher values corresponding to TDA with high wire content. It can be in terms of nominal size i.e., the average of 50% or more of the sample (Beaven et al., 2007), or aspect ratio (Warith et al., 2004; McIsaac and Rowe, 2005; Rowe and McIsaac, 2005; Beaven et al., 2007. An effective way of describing TDA types used in studies is to utilize a combination of the both qualitative (visual description) and quantitative methods.

2.3 TDA in LCRS

The use of TDA as drainage media in LCRS can be both environmentally and economically beneficial (Duffy, 1995; McIsaac and Rowe, 2005). The environmental benefits relate to the removal and use of stockpiles of whole tires that would have been potential fire hazards or breeding grounds for disease transmitting vectors (Duffy, 1995, Donovan et al., 1996; Moo-Young et al., 2003). The economic benefits relate to the cheaper cost of sourcing TDA relative to gravel (Duffy, 1995; Moo-Young et al., 2003), or drainage geosynthetics.

In order to use TDA as a substitute for primarily gravel in LCRS, it should be demonstrable that its performance will match or exceed that of gravel. The initial consideration, decades ago, for the use of TDA as a potential drainage material in LCRS was its high hydraulic conductivity that was found to match and in some cases exceed that of gravel (Hall, 1991; Zimmerman 1997; Beaven,

[4] Chapters 3,4

1995; Reddy and Saichek, 1998). However, hydraulic conductivity alone is not sufficent to assess the overall performance of TDA in LCRS. Other performance-related properties such as compression and creep and void volume to store biogeochemical clog also need to be assessed individually and in combination with hydraulic conductivity.

A database of information is developing for some performance based properties of TDA relating to its use as a drainage material in LCRS. The available information however contains a wide range of disparities. These disparities exist because researchers tend to test different TDA types that are different in terms of the particle size, type and part of tire used, particle size, aspect ratio and more. In addition, testing processes, methods, applied stress, and more are different, even for similar TDA types, making it difficult to correlate or extrapolate results or make direct comparisons between the results presented by various researchers.

Nonetheless, there are some commonalities in the results presented for some individual properties of TDA. For instance, many researchers have tested the hydraulic conductivity of different TDA types and regardless of the differences in the tested materials, results from these various tests have shown that TDA has a high hydraulic conductivity. This high hydraulic conductivity (especially when TDA is in an uncompressed state), often exceeds commonly prescribed regulatory limits for LCRS and can be maintained even at high applied stress over 400 kPa (Beaven, 1994; Duffy, 1995; Donovan et al., 1996; Evans, 1997; Zimmerman, 1997; Warith et al., 2004; Hudson et al., 2007; Beaven et al., 2007; Beaven et al., 2013) and up to 100 kPa (Hall 1991; Reddy and Saichek, 1998). Void volume reduction from compression and biogeochemical clogging have also been studied, and while all studies have found significant void volume reduction in TDA from compression depending on various parameters including the applied stress and particle size (Section 2.6), conclusions on the biogeochemical clogging of TDA have varied widely (Section 2.5).

2.4 Hydraulic conductivity of TDA

The results of different studies have shown that TDA, regardless of particle size, shape, wire content and more, exhibit an initially high hydraulic conductivity that decrease as applied vertical stresses increase (Hall, 1991; Beaven, 1994; Duffy, 1995; Narejo and Shettima, 1995; Reddy and Saichek, 1998; Warith et al., 2004; Beaven et al., 2007; Hudson et al., 2007). Biogeochemical clogging induced by the flow of leachate through the void spaces of TDA have also been found to reduce the hydraulic conductivity of TDA (Rowe and McIsaac, 2005; McIsaac and Rowe, 2005; Rowe and Babcock, 2007; Beaven et al., 2013). A summary of some of the hydraulic conductivity measurements in the literature are presented in Table 2-1; an overview of the studies in Table 2-1 is presented afterwards.

Table 2-1: Summary results of some hydraulic conductivity measurements in the literature

TDA particle size (mm)	Applied vertical load/stress (kPa)	Hydraulic conductivity - vertical (m/s)	Reference	
			Author	Year
19	22 kPa	0.019	Hall*	1991
38		0.021		
Whole tires	not stated	>0.7 to 0.025	Beaven	1994
12.7	163	0.001	Reddy and Saichek	1998
19.7	1006	0.00001		
<46	not stated	0.00002 to 0.000005	Reddy and Marella	2001
>25.4	5 to 20	>0.01		
76.2	60	0.134	Warith et al.,	2004
	330	0.0067		
>50	150	0.007 to 0.02	Rowe and McIsaac	2005
50	<100 to 600	0.01 to 0.001	Hudson et al.,	2007
200	<200 to 600			
450				

*the applied stress in study was stated as 6450 pounds, this was converted into kPa in the Table. See notes below

Hall (1991) tested the hydraulic properties of 38 mm and 19 mm TDA. The 38 mm material had protruding wires while the 19 mm material contained no wires. The vertical load applied to the

TDA samples ranged from 0 to 30 kN to simulate 0 to 11 m of MSW, based on an in place unit weight of 7.3 kN/m^3. The author reported applied load in pounds (6450 pounds). This value could be pounds per square inch (psi) or pounds force (lbf). Pounds force appears more logical going by the height of waste the author was trying to simulate with the applied load. In addition, going by the guidelines provided in Zekkos et al (2006) for estimating unit weight of municipal solid waste, the height of waste simulated by applying 30 kN of load would realistically be about 3 m of waste. Thus, the load in kN reported here for this author is thus based on the assumption that the pounds meant lbf. The average hydraulic conductivity reported for the 38 mm material was 0.021m/s while that for the 19 mm material was 0.019 m/s.

Although not stated in the Hall article, it appears that both the particle size and exposed wire content had effects on the hydraulic conductivity of the TDA tested as the material with protruding wires had a slightly higher hydraulic conductivity than the one without protruding wires and the material with the protruding wire was the larger sized material. Although the Hall experiment was able to show that TDA can maintain a high hydraulic conductivity under large applied stresses, in addition to being able to indicate a connection between hydraulic conductivity, TDA size and wire protrusion, the study was inconclusive in attributing high hydraulic conductivity independently to either TDA size or wire protrusion.

Beaven (1994) tested the hydraulic conductivity of whole scrap and van (truck) tires. The hydraulic conductivities obtained were in a range of > 0.7 m/s to 0.025 m/s. These reported values are on par with those for conventional LCRS materials, such as uniformly graded gravel, that have hydraulic conductivities ranging from 0.1 m/s to 1 m/s (Beaven, 1994; Fleming and Rowe, 2004). Fleming and Rowe (2004) measured 0.1 m/s for uneven, 37 mm angular gravels. Although the hydraulic conductivity values reported by Beaven are high, they noted in the report that the piezometer tubes used in the hydraulic conductivity test were only inserted a few centimeters into the very large test chamber (the Pitsea cell – capable of accommodating samples up to 2m in

diameter and 2.5 m high). Thus, the hydraulic gradient measured was at the edge of the cell; hence, preferential flow along the side of the Pitsea cell could have resulted in higher hydraulic conductivities than actually were. The hydraulic conductivity values reported by Beaven were in the range of what Hall (1991) reported, however there was no detail on the vertical stress or strain levels at which the hydraulic conductivities observed by Beaven were measured. Thus, a direct comparison of Beaven's results with Hall's would not be very accurate.

Reddy and Saichek (1998) tested TDA materials ranging in size from 12.7 mm to 139.7 mm. At a normal stress of 163 kPa, they measured hydraulic conductivity of approximately 0.001 m/s. At 1006 kPa, the hydraulic conductivity reduced by two orders of magnitude to approximately 0.00001 m/s.

Reddy and Marella (2001) summarized the hydraulic conductivity of TDA from results available in the literature. From the summary, TDA less than 4.6 mm in size had the lowest hydraulic conductivity values ranging from 0.00002 m/s to 0.000005 m/s. The applied vertical stresses, which resulted in these hydraulic conductivities, were not stated. TDA greater than 25.4 mm in size had hydraulic conductivities higher than 0.01 m/s, under vertical stresses of 5 to 20 kPa.

One might be quick to conclude from the review by Reddy and Marella that smaller sized TDA materials have lower hydraulic conductivities than larger TDA materials; however, the vertical stresses under which the hydraulic conductivities of the smaller sized TDA materials were measured were not stated. In addition, the larger sized TDA materials were subjected to a maximum stress of 20 kPa. Subjecting the different sizes of TDA materials to the same loading conditions will provide a means for better performance evaluation of the hydraulic conductivity of the different materials. An important finding from the review of literature carried out by Reddy and Marella was that larger sized TDA have an acceptable hydraulic conductivity to perform effectively as drainage materials in LCRS. This finding is important because of the potential cost savings from the fewer number of shredding passes for large particle sized TDA (Donovan et al., 1996).

Warith et al (2004) measured the hydraulic conductivity of two different TDA materials, which they termed “higher quality” and “lower quality” shreds, having nominal sizes of 76.2 mm. The hydraulic conductivity values ranged from 0.134 m/s to 0.0067 m/s corresponding to strains of 0.3 to 0.5 and average applied normal stresses of 60 to 330 kPa (Warith et al., 2007).

Rowe and McIsaac (2005) tested two different types of TDA; G shred with dimensions 101.6 mm x 50.8 mm x 10.2 mm having few exposed wires and P shred with dimensions 127 mm x 40.6 mm x 10.2 mm having many exposed wires. The hydraulic conductivity tests were carried out as part of a clogging analysis of TDA. The initial hydraulic conductivities reported for the TDA materials, before the onset of clogging under a stress of 150 kPa, were 0.007 m/s and 0.02 m/s for the G and P shreds respectively. The hydraulic conductivity values are in the range of what was reported by previous researchers for TDA materials having sizes less than 203 mm (e.g. Hall, 1994; Reddy and Saichek, 1998; Warith et al., 2004).

Hudson et al (2007) tested four different TDA materials - TS450 having a nominal size of 450 mm, ST 200 with a nominal size of 200 mm, ST 50 with a nominal size of 50 mm. and ST 29 with a nominal size of 20 mm. The authors noted that the hydraulic conductivity of the different sizes of TDA could reduce by up to one order of magnitude when the average vertical stress increases from 100 kPa to 700 kPa. For instance, the hydraulic conductivity of the ST 200 materials decreased from 0.01 m/s to 0.001 m/s as applied vertical stress increased from 100 to 400 kPa. The article also indicated that the hydraulic conductivity of TDA materials reduces with increasing particle size for the various applied vertical stress.

Although the various results discussed above do not show a clearly defined relationship between hydraulic conductivity and TDA particle size as one would expect for gravel, one thing unique to all the results was that TDA materials with particle size >25.4 mm nominal size, exhibited a high hydraulic conductivity greater than 0.0001 m/s. This value is comparable to that for gravel, which is in the range of 10 m/s to 0.001 m/s (Beaven, 1994; Fleming and Rowe, 2004). The hydraulic

conductivity values reported here were all vertical hydraulic conductivity values; none of the studies reported values for horizontal hydraulic conductivity.

Only one study (Beaven et al., 2013) is known by the author to have completed horizontal hydraulic conductivity tests in TDA (large particle sized TDA). However, the tests were completed on the TDA at constant volume, not constant applied stress. Some stress relaxation may have occurred that may have relaxed the compression of the voids a bit, and it was not stated in the article if the applied stress on the TDA was sustained long enough to capture additional void volume reduction from creep. Not accounting for creep may result in some overestimation of the hydraulic conductivity.

2.5 Drainable porosity of TDA

Drainable porosity, also known as effective porosity, is one of the properties widely used to assess the hydraulic performance of TDA. The drainable porosity of TDA is the ratio of the volume of voids from which water will drain freely under gravity having been saturated, to the total volume (Beaven, 1994; Beaven et al., 2008).

Drainable porosity, although very useful, does not present a true picture of the hydraulic performance of TDA. TDA, especially those greater than 50 mm in size, come in different shapes – including cup-shaped, mound-shaped or elongated/flat-like. The cup-shaped ones would retain water during draining, while the mound-shaped ones may not be completely filled with water during filling (Figure 1-1). This results in lower draining and filling porosities than the actual porosity in the TDA, and erroneous assessment of void volume and hydraulic performance of the TDA. In a continuous flow scenario, such as hydraulic conductivity, the cup-shaped TDA will be filled with water and will contribute to the overall flow even though they may not drain completely during a drainable porosity test.

The connectivity of the void spaces in TDA, and how the voids may contribute to continuous flow through a TDA material, measured in hydraulic conductivity or permeability tests should be the hydraulic property used when assessing TDA performance as a drainage media and not drainable porosity. One of the great uses of drainable porosity is that it can be used to estimate changes in TDA void volume with time (McIsaac and Rowe, 2005). Thus, void ratio values calculated from drainable porosity tests can be used to validate values obtained from other forms of compression measurements.

2.5.1 Biogeochemical clogging of TDA – measured from drainable porosity

McIsaac and Rowe (2005) performed one of the key works to date on the effects of clogging on the drainable porosity of TDA. After 254 days of permeating leachate through a column of TDA and a column of gravel, drainable porosity was lower in the TDA column than in the gravel column. This was attributed to higher clogging rates in the TDA columns than in the gravel column and because of that; the study was unsupportive of the use of TDA drainage material in LCRS (McIsaac and Rowe, 2005).

Beaven et al (2013) conducted a similar study in the UK, on the effects of clogging on TDA drainable porosity. As part of the study, the authors reviewed the work of McIsaac and Rowe (2005), and stated that leachate permeated into the TDA tested by McIsaac and Rowe was acidogenic and had a high concentration of calcium. They stated that to better simulate real life conditions, methanogenic leachate should be used, based on the premise that new waste deposited in landfill cells are under acidogenic conditions, but after a few months, methanogenic conditions become established as methane production commences.

High strength acidogenic leachate are produced in the first few months as newly deposited waste decompose, but with time, acidogenic leachate is converted to a stable methanogenic form (Beaven et al., 2013). Although Rowe (2005) observed a contradiction to this at the Keele Valley

Landfill, where after a decade of operation some acidogenic leachate was found in older waste layers deep within the landfill, Beaven et al maintained that in many landfills, especially those that are significantly saturated, the leachate reaching the LCRS drainage layer is methanogenic.

Accordingly, Beaven et al assessed the susceptibility of LCRS drainage materials (TDA and gravel) to clogging from methanogenic leachates and reported a high drainable porosity and little evidence of significant clogging in both the TDA and gravel materials after about 60 days of permeating the materials with leachate. Although the results from that study were favourable to the use of TDA in LCRS, there are a few downsides to the results. First, the experiment was performed at constant volume not constant stress. Second, the individual effects of compression were not considered or separated from the clogging results. Third, because of time constraints, leachate was permeated through the test chambers at an accelerated flow rate. The high flow rate could have resulted in some deposited clog being washed off from the TDA particles, which may have contributed to the low clogging observed. In addition, the experiment was not run for a very long time, it was run for about 60 days compared to the McIsaac and Rowe's, which was run for 254 days. In the 1998 article by Rowe and Fleming, it was noted that clogging is dependent on rate of clogging, and, as the drainage layer clogs, a greater residence time is created which may increase the deposition of clog materials used.

While the debate on leachate composition may continue, neither of the studies discussed above considered the individual and combined effects of solid volume compression, immediate compression and creep on the void volume reduction measured. Separating these is useful for evaluating the performance of a TDA drainage medium under various conditions, and at various stages, in the life cycle of a landfill.

2.6 Immediate compression and creep of TDA

The compressive behaviour of a material is a design factor that needs to be considered when a material is to be subjected to high normal stresses (Donovan et al., 1996); as it shows the susceptibility of the material to bulk volume change as applied stress increase (Reddy and Marella, 2001). When evaluating the feasibility of using TDA in LCRS drainage systems, adequate knowledge of the compressive response of TDA to applied stress is important, especially for large particle sized TDA that are preferred in such applications. This is because the TDA drainage layer will be subjected to high applied stress in the form of waste overburden, for extended periods.

TDA is highly compressible; it compresses under both its own self-weight and under applied stress. As it compresses, its thickness (height), void volume and hydraulic conductivity reduce (ASTM D6270-98; Reddy and Marella, 2001; Rowe and McIsaac, 2005). Creep under sustained applied stresses also decreases the void volume in TDA (Humphrey et al., 2000; Wartman et al., 2007; Adesokan et al., 2019[5]). ASTM D2990-09 and ASTM D7406-07 describe creep as time dependent compression under sustained applied stresses.

The height and hydraulic conductivity of the drainage layer of a LCRS should be maintained at specified values in order to meet stipulated regulatory design criteria. Typically, a hydraulic conductivity of ≥0.0001 m/s and a layer thickness ≥0.3 m. Thus, for a TDA drainage layer in a LCRS, any changes that may occur in the height, void volume and hydraulic conductivity from compression under applied stress over time will have to be well understood and accounted for in the design.

Different researchers have described the compression of TDA in different ways. Warith et al (2004) described it as initially plastic under vertical stresses, the plastic compression being up to

[5] Chapters 3,4

40% of the initial placement thickness and afterwards compression is elastic relative to reduction in porosity. Ahmed and Lovell (1993) described it as consisting of three mechanisms. The first is the re-arrangement of the TDA materials resulting in minimal plastic compression during initial loading. The second is the bending and flattening of the TDA materials resulting in the major percentage of mostly recoverable compression and the third is the elastic compression of the TDA (compression of the TDA solid volume), which is minimal and fully recoverable (Ahmed and Lovell, 1993; Beaven et al., 2007).

Reddy and Marella (2001) provided a more condensed form of the compression mechanism presented by Ahmed and Lovell (1993), describing the compression of TDA under applied stress as consisting of two stages. The first stage was described as resulting in the bending and re-arrangement of the TDA materials into a denser form, and the second stage was described as resulting in the compression of the individual tire shreds (Reddy and Marella, 2001). Donovan et al (1996) stated that a difference between TDA (tire chips) and other gravel is that the solid volume of individual TDA material is compressible in addition to the compression of the TDA mass. They however did not support this assertion with any studies of their own or from other researchers.

Wartman et al (2007) alluded to solid volume compression in TDA. They studied the compressibility of a mixture of 50% tire chips and 50% sand and 100% tire chips. They differentiated between the processes involved in the immediate compression and time dependent compression of TDA. They reported that in the immediate compression of TDA, pore volume reduction is dominant while TDA solid volume compression is negligible or nonexistent. However, in the time dependent compression of TDA, the effects of solid volume compression becomes more significant, in addition to reduction of void volume (Wartman et al., 2007). From the findings of Wartman et al (2007), there is an indication that solid volume compression in TDA is time dependent, occurring as TDA ages. However, it should be noted that tire chips (TDA with particle

size <50 mm) not large particle sized TDA (TDA with particle size >50 mm) were tested. The material properties of TDA have been found to be particle size dependent (Strenk et al., 2007).

Compression in TDA can be expressed as vertical strain (Eq. 2-1) resulting from vertical stress or as a percentage of the original sample height (McIsaac and Rowe, 2005; Beaven et al., 2007) (Eq. 2-2).

$$\text{Vertical strain } (\varepsilon) = ((L_i - L_0))/L_0 \quad (2\text{-}1)$$

$$\text{Compression } (\%) = ((L_i/L_0))/L_0 \times 100 \quad . \quad (2\text{-}2)$$

Where:

L_i = the instantaneous length under applied vertical stress;

L_i-L_0 = the instantaneous deformation relative to applied vertical stress;

L_0 = the initial sample thickness.

Some TDA compression results from the literature are presented in Table 2-2. The Table indicates a few aspects of the compressive behaviour of TDA, for instance, the compression of TDA appeared to decrease as the applied stress increased; although not stated by those authors; this is an indication of strain stiffening in the TDA with increased loading. Strain stiffening in TDA, which may be related to the movement and realignment of particles under applied stress (Chapter 8), is desirable because it implies that after a certain applied stress, void volume reduction under applied stress may become minimal or negligible.

Table 2-2: Some TDA compression results from the literature

TDA size (mm)	Applied vertical load/ stress (kPa)	Compression (%)	Reference	
			Author	Year
38	6450 pounds[1]	30	Hall	1991
19				
Whole tires	40	70	Beaven	1994
	600	87		
12.7 to 19.7	163	50	Reddy and Saichek	1998
	1006	65		
76.2	440	50	Warith et al	2004
101.6 x 50.8 x 10.2 (G shred)	150	48	Rowe and McIsaac	2005

127 x 40.6 x 10.2 (P shred)		44		
450	50	52		
	100	62		
	400	71		
200	50	21		
	100	38		
	400	50	Beaven et al[2]	2007
50	50	19		
	100	33		
	400	45		
	600	48		
20	50	22		
	100	32		
	400	44		

[1]see section 2.4; [2]Values for Beaven et al (2007) were obtained by extrapolation from the "compression (%) vs. average stress (kPa)" plot presented in their article.

Also, from the results of the Rowe and McIsaac (2005) study (Table 2-2), there seemed to be an indication that TDA with more exposed and interconnecting wires (as with the P shred) may compress less than that with fewer exposed wires and no interconnecting wires (as with the G shred).

The results from Beaven (1994) and Beaven et al (2007) in Table 2-2 also show more compression in larger particle sized TDA (> 200 mm) than in the smaller particle sized TDA at similar applied stress. The higher compression in the larger particle sized TDA probably relates to a higher initial void volume that undergoes higher reduction under applied stress relative to a lower initial void volume in the smaller particle sized TDA. The results in Table 2-2 highlight that particle size matters in the compressive behaviour of TDA, and further indicate the need to test TDA with particle size that is suitable for particular applications. For instance, testing of large particle sized TDA for LCRS applications as was done in this work.

ASTM D6270–98 recommends that TDA compression tests be carried out in a rigid cylinder having a diameter several times greater than the largest particle size and the ratio of the initial sample thickness to diameter in the test cell should be greater than one to allow for the large

strains that will occur in the TDA bulk volume. Using an initial sample thickness to diameter ratio greater than one will however require that steps be taken to overcome sidewall friction (ASTM D6270-98; Beaven et al., 2007; Adesokan et al., 2019[6]).

2.6.1 Sidewall friction loss in one-dimensional (1D) compression tests

Sidewall friction loss occurs when a substantial portion of the applied surface stress is transferred to the walls of the test cell to overcome frictional forces between the TDA particles and the walls of the test cell (ASTM D6270-98). Up to 50% of the applied surface stress can be lost to sidewall friction (Beaven, 1994; Warith et al., 2004), causing decrease in applied surface stress across the TDA thickness and non-uniform stress distribution within the TDA.

Sidewall friction, if not accounted for, causes an underestimation of the overall compression of the TDA being tested (ASTM D6270-98).Higher applied stress in TDA closer to the top will undergo higher compression and those farther away will undergo lower compression relative to the applied stress. The effects of sidewall friction increases as the height of test cell and thickness of TDA in the cell increases (ASTM D6270-98). To account for sidewall friction, a widely used method is to measure the applied surface stresses, and the stress reaching the bottom of the TDA using measurement units, and then calculate the average stress within the sample (ASTM D6270-98; Warith et al., 2004; Rowe and McIsaac, 2005; McIsaac and Rowe, 2005).

Beaven et al (2007) and Hudson et al (2007) accounted for sidewall friction using data from their drainable porosity tests, based on the hypothesis that drainable porosity of TDA varies with applied vertical stress. Thus, during the determination of drainable porosity, a linear relationship between volume of water added at the bottom of the sample and water level rise was indicative of uniform drainable porosity, and hence uniform stress throughout the sample thickness. However, if the rise in water level per unit volume of water added at the bottom is smaller at the

[6] Chapter 3

bottom than at the top, this was indicative of a reduction in the degree of compression with depth because of loss in applied vertical stress with depth (Beaven et al., 2007; Hudson et al., 2007). This approach worked with the cell used (the Pitsea cell – see section 2.4) because with a very large cell diameter to particle size ratio, sidewall friction was not nearly the issue for them. In a cell with significant sidewall friction, such an approach will not be accurate because of the non-uniform distribution of stress caused by sidewall friction loss.

Different methods have been employed in the literature to minimize sidewall friction. ASTM D6270-98 recommends lubricating the walls of the test cylinder prior to testing. Beaven (1994) lubricated the walls of the test cell with hydraulic oil prior to TDA testing, and the ratio of measured to applied stress varied from 78 % to 51% at the centre of the test cell, and 63 to 65% near the perimeter of the test cell. Warith et al (2004) utilized silicon based lubricant spray. For this treatment, the measured stress at the bottom of the test cell was 40% of the applied stress at the top. Wartman et al (2007) lubricated the walls of the steel test vessel with a light coat of non-silicon grease; this resulted in 75% of the applied stress reaching the bottom of the test cell. Some other methods involved placing layers of plastic sheets between the TDA and the walls of the test cell, which resulted in 80% of the applied stress at the top reaching the bottom of the test cell (Rowe and McIsaac, 2005; McIsaac and Rowe, 2005).

2.6.2 Creep – time dependent compression

Significant research has been carried out to determine short term (immediate) compression of TDA, however, since TDA will be buried under applied stress (waste overburden) for extended periods if used as the drainage layer in LCRS, it is essential to understand the creep in TDA resulting from increased and sustained loading with time. Creep (Figure 2-3) is the progressive deformation of a material while being subjected to a constant long-term stress (ASTM D2990-09).

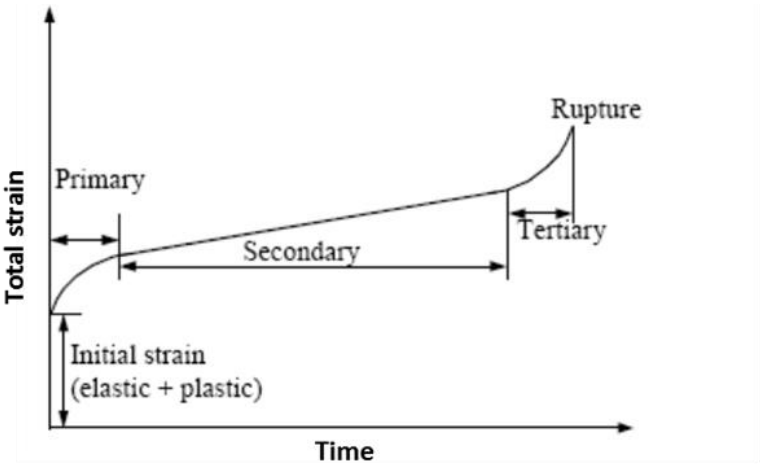

Figure 2-3: An idealized curve for stages of creep (Re-drawn from ASTM D2990-09). Idealized because some materials do not have the secondary or tertiary stages (ASTM D2990-09).

Creep tests are required to predict creep modulus and measure dimensional changes in materials under constant long-term static applied stresses (ASTM D2990-09). To measure compressive creep in a test material, a constant stress is applied at constant temperature and the resultant deformation is measured as a function of time (ASTM D2990-09; ASTM D7406-07). Upon application of surface stress, initial strain (consisting of both elastic and plastic deformations) take place, followed by a decrease in the creep rate with time (primary deformation), followed by a steady state strain with time (secondary deformation) and then rupture (tertiary deformation) (Figure 2-3).

At low temperatures, the rate of creep is usually very low and strain is often found to vary as the logarithm of time; a rapid increase in creep effects is noticed as temperature increases (ASTM D2990-09; ASTM D7406-07). Given that TDA is a polymeric composite, an understanding of its creep behaviour is needed to predict the dimensional changes that may occur under sustained applied stresses, particularly at elevated temperatures. There are currently no standard test methods for creep in TDA. However, since TDA is a polymeric composite (Reddy and Marella, 2001; Warith et al., 2004), methods for measuring creep in polymers, in ASTM D2990-09 and ASTM D7406-07, were adapted for TDA (see Chapter3, Section 3.10.3).

3.0 Strategies for one dimensional (1D) compression testing of large-particle-sized tire derived aggregate

Overview

Presented in this Chapter are the equipment design and experimental methodologies for the one dimensional (1D) compression testing of large particle sized TDA, addressing research objectives 1 and 2. Also presented in this Chapter are preliminary results and findings from the study to illustrate the successful implementation of the design methodologies. This Chapter is a precursor to Chapter 4, *immediate compression and creep in large particle sized TDA*.

This Chapter was published in the Geotechnical Testing Journal as follows:

D. Adesokan, I. Fleming, A. Hammerlindl, and J. McDougall, "Strategies for One Dimensional (1D) Compression Testing of Large-Particle-Sized Tire Derived Aggregate," Geotechnical Testing Journal 42, no. 5 (September/October 2019): 1336–1358. https://doi.org/10.1520/GTJ20170091

Additional information relating to this Chapter, which were not included in the submitted published paper are included as footnotes within the Chapter, and as supplementary data in Section 3.10.

3.1 Introduction

Over the past two decades, in large part for economic considerations and as a means for reusing the large stream of scrap tires generated at the end of the useful life of automobile tires, TDA derived from scrap tires shredding into sizes from 25 mm to over 305 mm has been suggested (Hall 1991; Duffy 1995; Reddy and Saichek 1998; Warith et al. 2004), researched (McIsaac and Rowe 2005; Rowe and McIsaac 2005; Hudson et al. 2007; Beaven et al. 2006; Beaven et al. 2013), and used (Donovan et al. 1996; Evans 1997; Zimmerman 1997; Reddy and Saichek 1998; Warith et al. 2004) as a substitute for gravel in the blanket drainage layers of leachate collection and disposal systems. In the western Canadian provinces of Saskatchewan

and Alberta, TDA is used in over thirty landfills that receive between a quarter and a third of the combined municipal solid waste stream of the two provinces.

TDA is a polymeric composite, as such a mass of TDA subjected to vertical loading is expected to exhibit viscoelastic behavior (Reddy and Marella 2001; Warith et al. 2004) typically consisting of an immediate elastic spring-like response followed by a time-dependent viscous dashpot-like response (creep). It is important to understand both responses and their individual and combined effects on long-term performance and service life when designing load-bearing applications such as drainage layers in waste disposal sites with TDA. The performance and service life of any drainage layer is expected to exceed the contaminating lifespan of the waste disposal facility, which has been estimated to be several centuries (Rowe and Fleming 1998; Fleming et al. 1999; Fleming and Rowe 2004; Rowe 2005; Yu and Rowe 2012).

This expected service life and performance depends on a number of factors including: (1) the ability of the drainage layer to maintain a sufficient vertical and more importantly horizontal permeability to rapidly transmit infiltrating leachate from the overlying waste into collection pipes and sumps to minimize excessive head on basal barrier materials (Fleming et al. 1999; Qian et al. 2001; Rowe et al. 2004; Yu and Rowe 2012); (2) the ability of the drainage layer to retain a sufficient pore volume following physical and inevitable biogeochemical clogging to ensure continuous transmission of leachate into collection and removal units (Fleming et al.1999; Qian et al. 2001; Rowe and McIsaac 2005; Rowe and Babcock 2007; Beaven et al. 2013); (3) the ability of the drainage layer to transfer vertical stress to underlying basal barrier materials without inducing or making worse localized strains and other forms of physical damage (Dickinson and Brachman 2008).

Various studies such as Hall (1991), Reddy and Saichek (1998), Warith et al (2004), Rowe and McIsaac (2005), and McIsaac and Rowe (2005) have shown that different TDA (differing in terms of shape, particle size, mode of shredding, exposed and loose wire content) perform

differently in compression under similar applied stress and loading conditions. Strenk et al. (2007) highlighted the variability and scale dependence of TDA particle size and performance-related properties. Similarly, studies by Beaven et al. (2006), Mwai et al (2010), and Beaven et al. (2013) showed that particle size matters in the behavior of a TDA mass under applied stress.

The one dimensional (1D) compression results presented in the Beaven and Mwai studies showed that TDA masses with large-sized particles (particles greater than 200 mm) compressed more than those with smaller-sized particles (200 mm and less) under similar applied stress. A higher compression implies a higher void volume reduction, and void volume reduction is a key parameter for assessing the performance of TDA in service, especially for drainage applications under service stresses. For these reasons, testing smaller particle-sized TDA in smaller test equipment to eliminate the need for large-sized testing equipment may result in errors in estimating the performance and service life of large-particle-sized TDA.

In assessing the service life of a TDA mass for drainage applications in waste disposal sites under high compressive stresses imposed by overlying materials, it is imperative to perform the required tests on a TDA mass with particle sizes and attributes that are suitable for such applications—ideally, large-particle-sized TDA with the longest particle dimension from 50 mm to over 305 mm. Testing such large-sized particles will require large test cells and large systems for applying and sustaining high compressive stresses on the test cells.

Such large scale testing may present a number of challenges. Zimmerman (1997) appeared to have alluded to this in the study in which 200-mm to 400-mm particle-sized TDA mass was tested. The author stated that it was “impractical” to have a test chamber several times larger than the largest particle size. “Practicality,” as stated by Zimmerman, could have been related to potential challenges associated with having a large-sized test chamber, and in the study, a smaller test chamber equal in width to the longest TDA particle dimension was used.

Testing a mass of TDA in a chamber with the same dimensions as the longest particle size may increase sidewall friction along the walls of the test chamber. Sidewall friction is an artefact of 1D constrained loading tests (Olson 1986; Sarby and Vickers 1986) and, given the flexibility of TDA particles, there is an increased tendency for the particles to “stick” to the walls of test cells, potentially increasing sidewall friction. Sidewall friction reduces the amount of applied surface stress reaching the bottom of a test specimen, causing larger strains in materials at the top of the test cell compared to that at the bottom (Sarsby and Vickers 1986).

Sidewall friction has been noted to increase as the ratio of chamber size to longest TDA particle dimension decreases (ASTM D6270-08). The effects of sidewall friction could result in the erroneous estimation of the properties of the TDA mass, potentially causing an underestimation of compression and an overestimation of porosity in the TDA mass if unaccounted for in the analyses of the laboratory test results.

It was deemed important from the outset to be able to measure and account for sidewall friction. Because sidewall friction was anticipated to be significant, the stress state could be expected to vary across the thickness of the TDA mass in the consolidometer. Accordingly, it was deemed necessary to measure the total vertical stress reaching the base of the TDA mass and to estimate compressive response at intermediate positions within the test specimen.

Because the test cell was fabricated from transparent acrylic (Figure 3-3 a), coloured lacrosse balls were placed as visual markers at intermediate levels to enable the TDA mass to be treated as if it were a stack of thinner slices, each subjected to differing vertical and horizontal stress conditions. In later tests, the coloured balls were replaced by fluorescent paint spots applied to individual particles of TDA placed near the cylinder sidewall. In order to determine the actual vertical stress reaching the base of the TDA mass, a total stress (TS) cell was placed on the acrylic base of the apparatus prior to filling with TDA.

Each slice created by a top and bottom visual marker thus may be considered to represent a compression test at an applied stress. The progression of compression in each slice was measured from the displacement of the visual markers, and each slice was analyzed as an individual compression test at the applied stress reaching the slice. The vertical stress reaching each slice was estimated from considerations of sidewall friction along with the observed variation in vertical strain and the measured TS at the base of the TDA mass.

Evaluating the performance determining properties of large-particle-sized TDA under large applied and sustained vertical stresses is the basis of a series of completed and ongoing studies at the University of Saskatchewan (U of S), Canada. Two pieces of custom, large scale laboratory testing equipment—a one dimensional consolidometer, and a consolidometer/permeameter unit for determining two dimensional (vertical and horizontal) flows under sustained stresses[7], were designed and fabricated at the U of S as part of these studies.

The equipment and procedures for the 1D consolidometer for evaluating compression, creep and ensuing void ratio reduction in the TDA mass are described in this article. The consolidometer/permeameter unit was used to evaluate the effects of void volume reduction on horizontal and vertical permeability under increasing applied vertical stress; this equipment and the experimental methodologies employed will be discussed in a complementary article.

The equipment design and experimental methodologies for the 1D consolidometer are presented in this article as a series of technical challenges that were overcome in order to successfully operate large scale geotechnical laboratory equipment to evaluate the field performance of a mass of TDA under large sustained stresses. The challenges described include the following:

[7] Chapter 5

- The geometry of the test chamber and the associated structural considerations, given the large particle size of the TDA mass;
- A system for applying and sustaining high stresses on the TDA mass under large compressive strains;
- Managing differential compression in the heterogeneous TDA mass;
- Measuring and reducing sidewall friction; and
- Measuring phase (solid and void) volume change under increasing applied stress.

In view of the previously mentioned challenges, the three fold objectives of this article are to (1) describe the design aspects of the 1D consolidometer and the experimental challenges that were encountered, (2) describe the strategies that were developed and implemented to overcome these challenges, and (3) present some test results from the implementation of the experimental designs and test equipment.

3.2 Material

The TDA used in this study (Figure 3-1) was supplied by Shercom industries, Saskatoon, Saskatchewan. Shercom produces TDA from scrap passenger and light truck tires.

Figure 3-1: TDA used in the study

Quantitative analyses were performed to determine the particle size distribution (PSD) and specific gravity of the TDA mass. For the PSD, approximately 20 kg of TDA was selected randomly and the length, width, thickness, and mass of individual shreds (particles) were measured. Plots of PSD using the cumulative percentage smaller than the longest dimension of each TDA particle and the cumulative percentage smaller than the smallest dimension of each particle are presented in Figure 3-2. The specific gravity of the TDA mass was measured according to ASTM C127-12 to be 1.27.

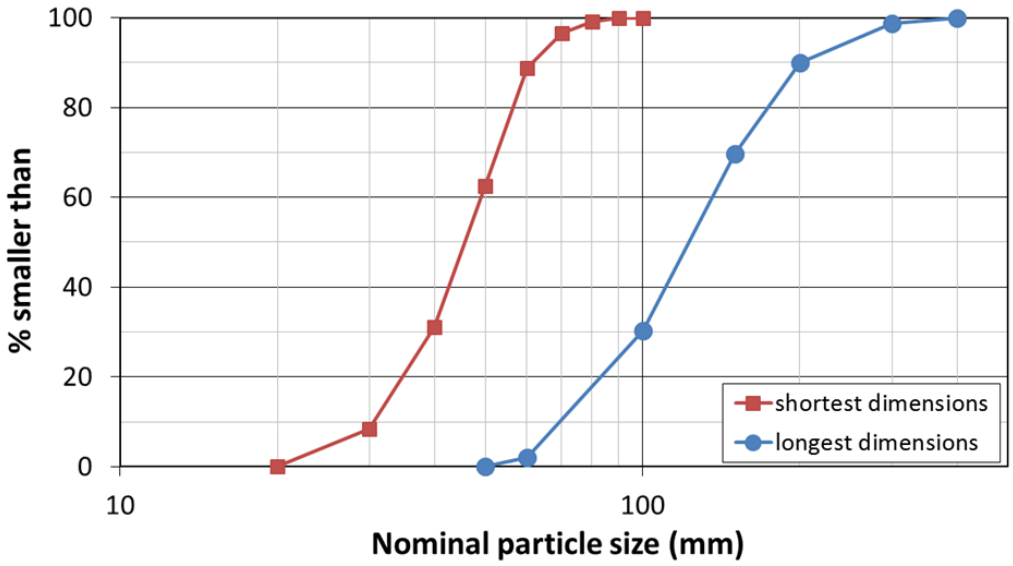

Figure 3-2: Particle size distribution plots for the TDA mass using both longest and shortest dimensions of individual particles.

3.3 Challenge 1: A suitable test chamber

Given the large dimensions of the TDA particles, a large test chamber several times larger in diameter than the longest dimension of the TDA particles was required to minimize sidewall friction as recommended in ASTM D6270-08. In addition, the height of the test chamber had to be sufficient to accommodate an initially greater thickness of a mass of TDA that would undergo large compressive strains as loading progressed.

A 1.8-m-high 1D consolidometer with a diameter of 0.7 m was fabricated from a cylinder of transparent acrylic material with a wall thickness of 0.1 m, an ultimate tensile strength of approximately 50 MPa, and an elastic modulus of 3.2 GPa (Figure 3-3a). In the load frame, the consolidometer was placed on a wooden base plate of the same diameter as the outer diameter of the consolidometer; the base plate had sufficient clearance underneath for a forklift to move the consolidometer in and out of the load frame. A schematic of the 1D consolidometer setup with details of the load/stress application system is presented in Figure 3-3b.

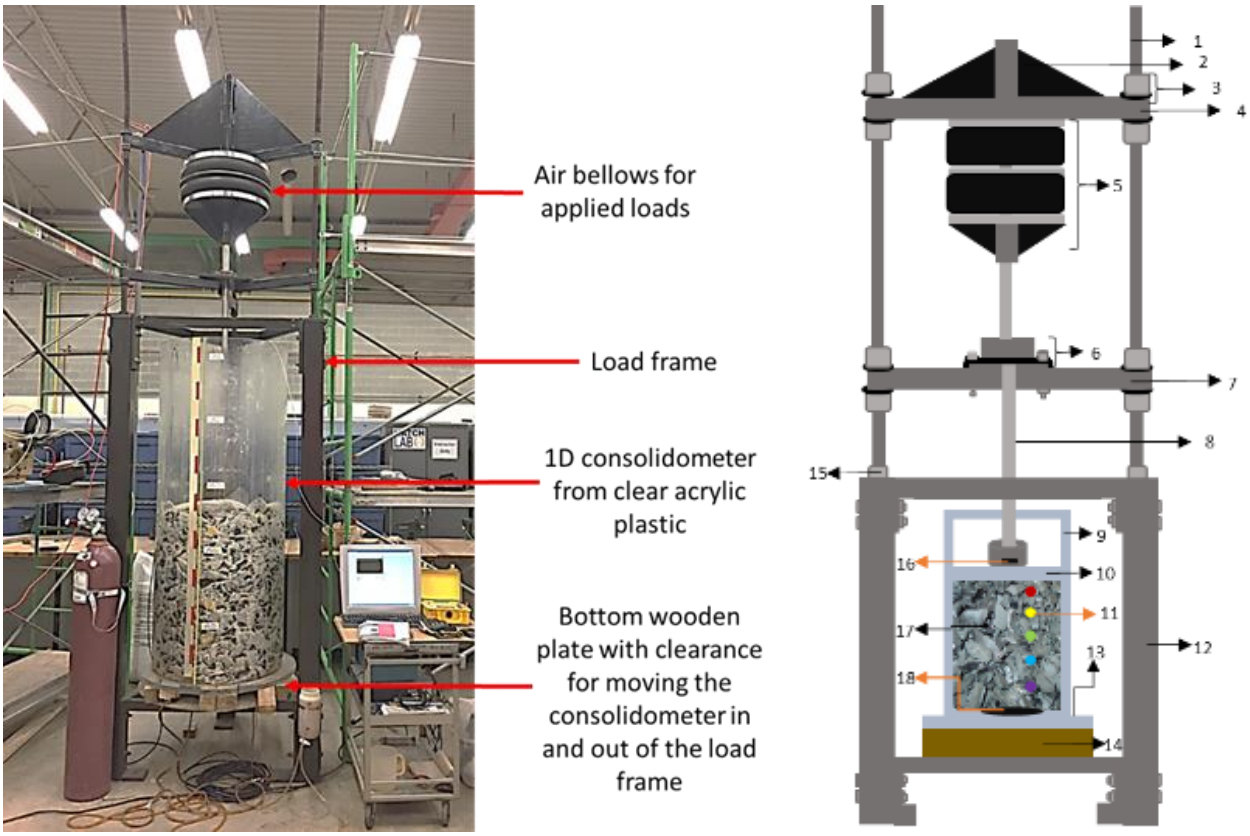

(a) (b)

Figure 3-3: (a) The 1D consolidometer placed in the triangular-shaped load frame showing a compression test in progress; (b) schematic of the 1D consolidometer and its components. 1. Threaded rod for winding bellows up and down; 2. Steel gusset plate reinforcement for air bellows; 3. Nut and washer securing load frame "arms"; 4. Upper "arms" of load frame; 5. Air bellows; 6. Piston guide; 7. Lower "arms" of load frame; 8. Piston rod; 9. 1D consolidometer cell; 10. Press plate; 11. Coloured marker balls to measure vertical displacement; 12. Load frame; 13. Base of consolidometer; 14. Wooden support for consolidometer; 15. Nut securing threaded rods to load frame; 16. Load cell; 17. TDA test sample; 18. Total stress (TS) cell.

It was important to be able to move the consolidometer in and out of the loading frame with minimal obstructions and to have a load frame that was sufficiently sturdy with adequate capacity to withstand applied stress. It was also important to have a system for loading and unloading the consolidometer. A triangular design was implemented for the load frame to facilitate easy movement of the consolidometer in and out of the load frame (Figure 3-3a), and a gantry system allowing for various degrees of inclination of the consolidometer was fabricated for loading and unloading the consolidometer (Figure 3-4).

Figure 3-4: Gantry system for unloading and loading the consolidometer outside the load frame

3.4 Challenge 2: The loading system

The large-sized consolidometer meant a large loaded area, the application of large vertical loads of over 150 kN, and a loading system capable of applying and maintaining the large vertical loads constantly at high strains greater than 50 %. A loading system such as this would require a long extension stroke with means for lowering and raising the system while maintaining constant stress on the TDA mass.

In addition, components that would facilitate the transfer and distribution of the applied vertical stress uniformly across the surface of the TDA mass in the consolidometer were required. To apply the large constant stresses, 21 ½-inch-diameter stock units of double convolution air bellows (model 9109150) were sourced from Parker Hannifin, Cleveland, OH. The air bellows were subsequently modified by removing the factory-fitted upper and lower plates—items “f” and “h” in Figure 3-5a— and replacing them with steel plates and gusset reinforcement (Figure 3-5b)

to enhance the load bearing capacity of the air bellows and prevent excessive bending of the inset ring plates during loading.

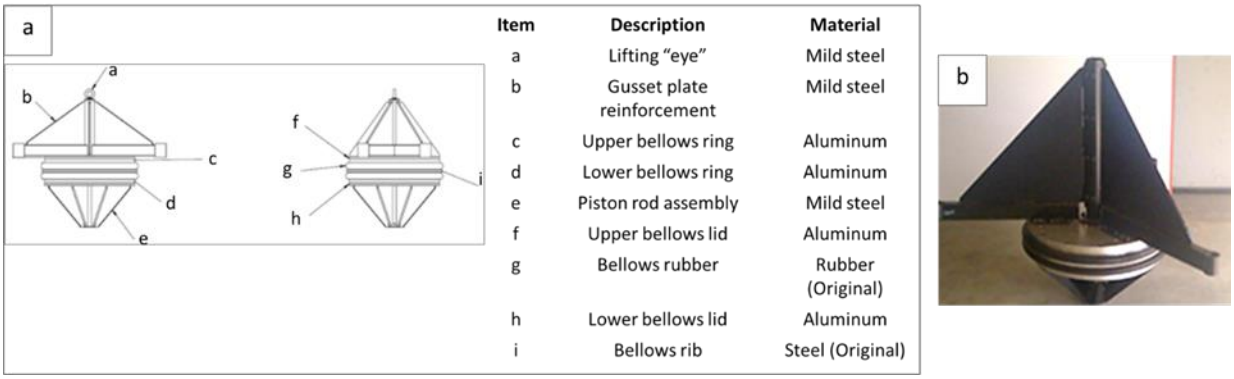

Figure 3-5: (a) Components of re-engineered air bellows; (b) re-engineered air bellows with gusset reinforcement.

The re-engineered air bellows (Fig. 3-5b) weigh 123 kg and have the capacity to generate over 150 kN, which could be used to apply vertical stresses of up to 600 kPa. The maximum applied vertical stress in the testing described in this article was 224 kPa to simulate 20 m to 25 m of overlying waste (Zekkos et al. 2006) above a mass of TDA in a landfill drainage application.

A 0.04-m by 1.64-m piston rod fabricated out of steel was used to transfer the applied load from the air bellows to the loading plate on the test sample. The loading plate was fabricated from the same acrylic material as the consolidometer, is 20 mm thick, and is 5 mm smaller in diameter than the inner diameter of the consolidometer, providing sufficient clearance along the walls of the consolidometer during loading.

A piston guide was incorporated into the loading system to provide alignment for the piston rod during loading. Both the piston guide and air bellows were connected to the load frame by upper and lower "arms" that were attached to threaded rods bolted onto the top of the load frame (see Fig. 3-3b). The length of threaded rods was designed to allow for sustained loading on the TDA mass over a total displacement associated with vertical strains exceeding 50 %.

The “arms” were manually wound down[8] while maintaining constant pressure in the air bellows by means of pressure relief valves. This ensured that a constant applied stress was supplied to the TDA mass as the applied vertical stress increased and compressive strains became larger.

A button-type load cell[9] with a capacity of over 150 kN, sourced from Futek Inc., Irvine, CA, USA (model LLB500), was positioned between the lower end of the piston rod and the press plate to determine the actual load/stress supplied by the air bellows to the consolidometer. The load cell was placed in a housing and this was bolted to the top of the press plate to ensure that the load cell was held in place during the tests. The load cell was connected to a PC-controlled readout unit, and the vertical stress supplied to the TDA mass was displayed in real time.

A pancake-type vibrating wire (VW) TS cell[10] (P/N 52608220, S/N 11-1282) with a capacity of over 300 kPa manufactured by Durham Geo-Enterprises, Inc., (Durham Geo Slope Indicator (DGSI), Richmond, BC, Canada) was used to measure the stress reaching the bottom of the consolidometer. The TS cell readings were useful for estimating the effectiveness of the sidewall treatments that were applied to the walls of the 1D consolidometer for reducing sidewall friction. They were also useful for developing a theoretical approach for estimating the loss of applied surface stress across the thickness of the TDA mass resulting from sidewall friction.

The TS cell was placed in the 1D consolidometer prior to filling with TDA, resting flat on the rigid base of the consolidometer to avoid poor conformance and stiffness– compatibility related errors in the TS measurement that may occur with placing the TS cell within the TDA mass. Descriptions of poor conformance and stiffness compatibility errors in TS measurements are provided in Dunicliff (1988). A 25-mm-thick plywood disc that was the same diameter as the TS cell was placed on top of the TS cell before loading the consolidometer with TDA to ensure an

[8] See Figure 3-20, Section 3.10.6
[9] See Figure 3-15, Section 3.10.3
[10] See Figure 3-15, Section 3.10.3

even distribution of applied stresses on the TS cell. The TS cell was connected to a VW data recorder (P/N 52613500, S/N 42182) by DGSI to obtain readings.

3.5 Challenge 3: Differential compression

Because of the variations in shapes and sizes of the particles in the TDA mass and an initially large void volume from the large sizes of the TDA particles, differential compression and misalignment of the load application system occurred at the early stages of the research work, during trial runs. Following an increase of applied stress from 112 kPa to 224 kPa, uneven settlement of the TDA mass occurred, and this caused the press plate to tilt and the piston rod misaligned such that only a small portion of the lower end of the piston rod was left in contact with the load cell. A diagnostic evaluation of the occurrence showed that the clearance between the piston rod and the annulus of the piston guide was insufficient, and this had caused the piston rod to bind at the ends of the piston guide during the misalignment (Figure 3-6a). This binding resulted in significant fluctuations in the applied stress reaching the surface of the TDA mass.

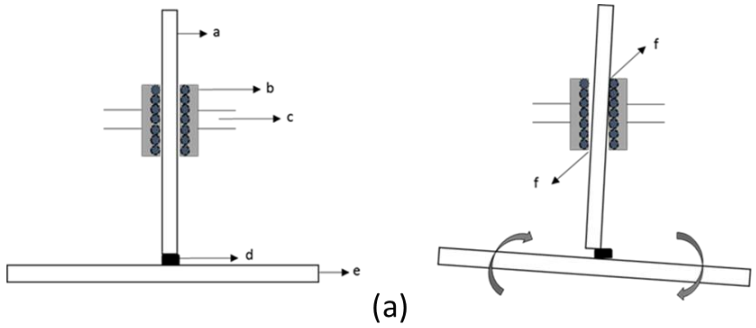

Figure 3-6: (a) Representation of the initial piston guide design and deflection of the load application system; a. Piston rod; b. Linear bearing cartridge piston guide; c. Lower "arms" of the load frame; d. Load cell; e. Press plate; f. Binding and loss of applied vertical load to the piston guide. (b) Representation of the redesigned piston guide and deflection of the load application system; a. Piston rod; b. Annular single row piston guide; c. Lower "arms" of the load frame; d. Conical tip fitting for piston rod; e. Load cell; f. Press plate; g. No binding – sufficient clearance between piston guide and piston rod.

The piston guide that was originally used (Figure 3-6a) had been a linear bearing cartridge placed inside a cylindrical canister base. Embedded inside the cartridge were rings of small-sized ball bearings to provide alignment of the piston rod. The linear bearing design provided motion and full contact in the direction of the cartridge but did not allow for misalignment of the piston rod. The piston guide had to be redesigned and refabricated to accommodate deflections and misalignments in subsequent tests.

The redesigned piston guide (Figure 3-6b)[11] has an annular single row consisting of 5/8-sized ball bearings to provide a single point of contact around any given point of the piston rod. The ball bearings in the piston guide are capped in two halves that are bolted together to form a canister base. The redesigned piston guide provides better alignment and freer movement of the piston rod and is able to accommodate misalignments up to 15°, creating a diametric clearance of almost 3 mm within the annulus of the piston guide.

In addition to redesigning the piston guide, the lower end of the piston rod was fitted with a cylindrical hollow base having a conical tip[12] to create a wider contact area between the lower end of the piston rod and the surface of the load cell during misalignment. With the conical tip attachment, the piston rod is able to revolve or rotate on the load cell during differential settlements and misalignments without slipping off completely (Fig. 3-6b).

With the re-engineered piston assembly, during subsequent testing, the piston rod was able to move freely within the annulus of the piston guide and was able to misalign slightly without

[11] Also see Figure 3-15, Section 3.10.3
[12] See Figure 3-15, Section 3.10.3

binding at the edges of the piston guide while maintaining maximum contact with the load cell. The re-engineered piston assembly reduced the fluctuations in applied stress reaching the TDA mass during subsequent tests considerably.

3.6 Challenge 4: Measuring compressive strains and void volume reduction

There are currently no standard test methods for evaluating compression and void volume reduction in a mass of TDA under applied stress. The following standard methods for evaluating creep in polymers were adapted as required: ASTM D2990–09 and ASTM D7406–07.

3.6.1 Evaluating solid volume compression in TDA particles

Before setting out to measure the compression and void volume reduction in the TDA mass, it was deemed essential to identify the contribution of solid volume compression in individual TDA particles to the overall void volume reduction so that appropriate means for evaluating the resulting void volume reduction may be established. A complementary study was completed as part of this research work to evaluate the contribution of solid volume compression of individual TDA particles to overall compression and creep.

In that study, isotropic stresses from 50 kPa to 200 kPa were applied incrementally to a mass of TDA in a 0.6-m by 0.3-m triaxial cell for over 90 days. Upon application of the surface stress, there appeared to be some elastic compression, but subsequently, there was little or no further compression over the test period to the end of the final isotropic stress of 200 kPa[13].

Given the minimal solid volume compression observed in that study, it was determined that void volume reduction may be the principal mechanism for compressive strains in a mass of TDA under applied stress and compressive solid volume change in the individual TDA particles may

[13] See Figure 3-13, Section 3.10.1 for the experimental data

be ignored. Hence, any change in void volume in a mass of TDA under applied stress may be represented by the change in the height of the TDA mass using Eq. 3-1.

$$\frac{\Delta H}{H} = \frac{\Delta e}{1+e_0} \text{ and } \Delta V_s = 0 \qquad (3\text{-}1)$$

Where:

ΔH = change in height;

H = initial height;

Δe = change in void ratio;

e_o = initial void ratio;

ΔV_s = volume of solids.

3.6.2 Measuring 1D compression and change in void volume in the TDA mass—primary strategy

Having fabricated the consolidometer cell from transparent plastic, it was possible to place visual markers at various depths within the TDA mass and the vertical displacement of the markers could be tracked periodically to measure intermediate strains[14]. Three coloured four inch diameter balls with a comparable elastic modulus to the modulus of individual TDA particles were placed at predetermined heights as visual markers against the inside walls of the consolidometer adjacent to three 1.8-m-long measuring tapes that had been glued to the outside wall of the cell 120 degrees apart.

The positions of the visual markers were read across the measuring tapes as loading progressed. Adjacent visual markers separated the TDA mass into slices. The slices were analyzed to represent a series of tests running simultaneously in the test cell. The mass of TDA placed in each slice separated by the visual markers was determined during loading, and

[14] The steps taken for data collection are presented in Section 3.10.3

because the specific gravity of the TDA had been previously measured, the dry unit weight of each mass of TDA slice was estimated. Knowing these, it was possible to estimate the initial void volume in the slices and the change in void volume with the progression of the test using Eq. 3-2[15].

$$e = \left(\frac{G_s \gamma_w}{\gamma_{dry}}\right) - 1 \qquad (3\text{-}2)$$

Where:

G_s = specific gravity

γ_w = the unit weight of water (kN/m^3)

γ_{dry} = the unit weight of dry TDA mass in the slices (kN/m^3)

3.6.3 Measuring 1D compression and change in void volume in the TDA mass—auxiliary strategy

Drainable porosity was measured periodically as an auxiliary method for estimating compression and change in the void ratio within the TDA mass. Drainable porosity measurements for void ratio evaluation in a mass of TDA have been done by previous researchers, e.g., McIsaac and Rowe (2005), Rowe and McIsaac (2005), and Hudson et al. (2007).

The fabrication of the consolidometer included threaded ports at the base for introducing fluids into the TDA mass. The threaded ports made it easy to remove the fittings when they were not in use to recover a smooth flush base for transporting the cell around on a forklift. The ports were barb fitted to allow for connection of flexible tubing for fluid flow. The barb fitting design was to ensure a smooth flush on the inside of the consolidometer at the base and to prevent

[15] As for solid minerals

intrusion of fittings into the consolidometer or standing water at the base during drainable porosity tests.

Both filling and draining porosities were evaluated in the drainable porosity tests. For the filling porosity, a graduated cylinder was placed on a scaffold and a flexible tubing was connected to the bottom of the graduated cylinder and to the ports at the bottom of the 1D consolidometer. The tubing connection allowed water to drain by gravity from the graduated cylinder into the 1D consolidometer for filling porosity measurements. Water from the graduated cylinder flowed under gravity to fill up the consolidometer to the elevation of the visual markers, and the transparent cell made it easy to see the water level rise to the required elevation.

The consolidometer was filled from bottom to top to ensure saturation of the TDA mass for the measurements. Each TDA mass slice was filled within 24 hours—this period may not have been sufficient to ensure complete saturation of the voids in the TDA mass. Because of this, the void ratio measurements from drainable porosity presented in this article may have underestimated the values slightly. A comparison of the void ratio values from drainable porosity and those from measuring the displacement of the visual markers is presented later.

For the draining porosity, the consolidometer cell was drained by gravity into the graduated cylinder, and it was observed that draining the cell too quickly resulted in delayed drainage. Delayed drainage is a situation whereby water from preceding layers, if not allowed enough time to drain completely, seeps into lower layers while draining those layers.

Delayed drainage ultimately results in erroneous readings of draining porosity because lower layers would drain a larger volume of water, while upper layers would drain less water and the void volume in the various layers would be misrepresented. To manage delayed drainage during the draining porosity tests, a constant head container was attached to the load frame and

a flexible tubing was connected to the top of the constant head container and the ports at the bottom of the 1D consolidometer (Figure 3-7).

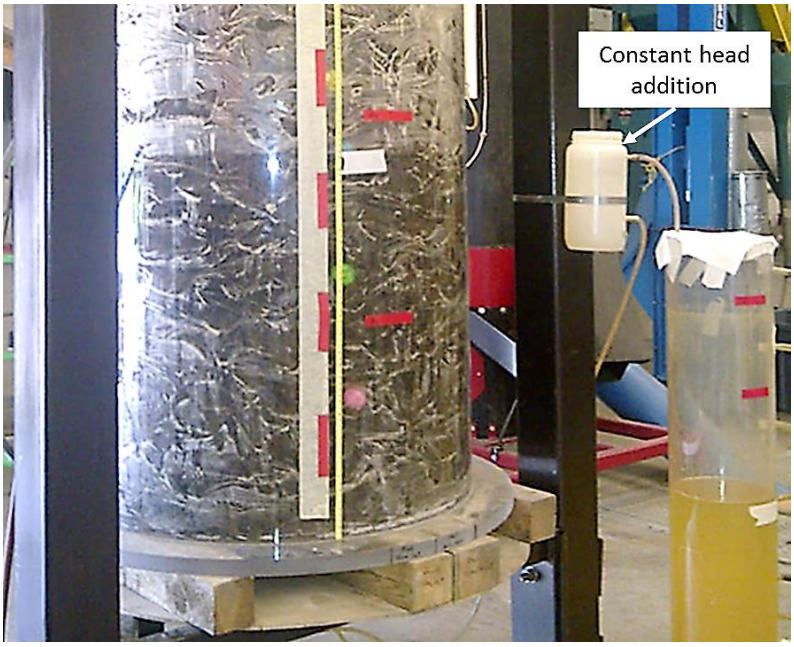

Figure 3-7: Draining porosity test in progress showing the constant head addition (container) for collecting delayed drainage during draining porosity.

The constant head container was lowered to predetermined heights—usually the height of the visual markers—and water from the 1D consolidometer drained by gravity into the constant head container through the flexible tubing. Overflow from the constant head container was collected into the graduated cylinder, and when the head of water in the 1D conslidometer was equal to that of the water inside the constant head container, the setup was left undisturbed for a few hours to collect any delayed drainage from the upper layers.

Following the drainable porosity tests, filling and draining porosity values[16] of the TDA mass slices were determined using Eq. 3-3. Corresponding void ratio values were estimated from the porosity values.

[16] The plot of the filling and draining porosity values is presented in Figure 3-16, Section 3.10.4

$$n = {}^{V_{water}}/_{V_{TDA}} \quad (3\text{-}3)$$

Where:

n = porosity

V_{water} = volume of water

V_{TDA} = volume of the TDA mass slice filled or drained

3.7 Challenge 5: Managing sidewall friction

3.7.1 Sidewall friction reduction

In the conventional 1D oedometer standard testing procedure ASTM D2435/D2435M-11, to minimize sidewall friction, height-to-specimen diameter ratios of 1:2.5 are recommended, and height-to-diameter ratios greater than 1:4 are preferred. The height to diameter ratio of the 1D consolidometer used in this study was 2.5:1. Significant sidewall friction was anticipated because of this, and methods for reducing and accounting for sidewall friction were required.

Two treatment methods for reducing sidewall friction were evaluated. Treatment 1 involved applying a layer of high-temperature grease to the inside walls of the consolidometer and placing a layer of 0.15-mm polyethylene plastic on top of the greased wall[17]. Treatment 2 involved applying two layers of the same plastic and two layers of the high temperature grease to the inside walls of the consolidometer. The grease was applied directly to the wall of the consolidometer and in between the two layers of plastic. Both treatments resulted in a reduction of over 50 % in sidewall friction as shown in the sample results for an applied stress of 112 kPa (Table 3-1) for readings from the TS cell placed beneath the TDA mass in the consolidometer. Treatment 2 achieved a slightly higher reduction and was applied in subsequent tests[18].

[17] See Figure 3-14, Section 3.10.2

[18] Sample plot of applied stress at the top and bottom of the TDA with sidewall treatment 2 is presented in Figure 4-18, Section 4.5.3, Chapter 4

Table 3-1: Effects of sidewall friction treatments at 112 kPa.

Operation	% stress reaching the bottom at 112 kPa
No sidewall treatment	46%
Treatment 1	50%
Treatment 2	54%

3.7.2 Sidewall friction evaluation

Despite applying sidewall treatments, as shown in table 3-1, it may not be possible to eliminate sidewall friction in the 1D constrained testing of a TDA mass. With this in mind, an approach that may be used to evaluate sidewall friction loss to enable a detailed evaluation of the compression behavior of the TDA mass for design was developed and is presented here. The evaluation approach presented in this study is similar to a theoretical approach that was previously developed by Beaven (2000) from the testing of municipal solid waste.

The Beaven approach relates the vertical effective stress (σ'_v) at a depth z in the cell to the internal angle of friction (ϕ') of the waste and to the interface shear friction angle (δ) between the waste and the wall of the test cell. The Beaven approach assumed that ϕ',δ and the unit weight (γ) of the waste were constant with applied stress and depth and the resulting equation was given as:

$$\sigma'_v = \frac{\gamma}{B}(1 - e^{-Bz}) + P.e^{-Bz} \qquad (3\text{-}4)$$

Where:

$B = [\frac{4(1-\sin\phi\prime).tan\delta}{d}]$

P = the applied surface stress

Although the theoretical approach by Beaven and the approach presented in this article share some similarities, the techniques that were applied to develop the resulting equations are different. In the Beaven approach, there was a reliance on the internal angle of friction of the

waste mass, additionally, the actual stress reaching the bottom of the test cell and intermediate strains within slices of the waste mass were not measured.

In addition, in the Beaven approach, the unit weight of the TDA mass was assumed to be constant. This assumption of a constant unit weight may result in errors in estimating the void ratio with applied stress and with depth. This is because the unit weight of a mass of TDA will depend on the applied stress and the resulting compression from the applied stress.

Additionally, because the applied stress in a constrained loading test of a TDA mass will vary across the thickness of the specimen as a result of sidewall friction, unit weight will not be constant throughout the specimen. As such, assuming a constant unit weight with applied stress and thickness for the TDA mass may result in errors in estimating the effects of sidewall friction and may additionally cause a misrepresentation of the void volume reduction in the TDA mass with applied stress.

The sidewall friction equation presented in this article considers intermediate slices of the TDA mass and evaluates the compression and void volume change in each slice. As such, the equation accounts for the changes in unit weight with depth across the thickness of the TDA mass and presents a range of sidewall friction angle (δ) values for various applied stress that were obtained from the test results. The sidewall evaluation equation and approach in this study are described in the following sections.

The parameters governing sidewall friction were determined using the load cell readings at the top, the intermediate strains measured from the displacement of the visual markers, and the TS cell readings beneath the TDA mass. Using these readings, it was possible to integrate applied stress with depth and to evaluate strains at any point within the TDA mass to account for sidewall friction loss. In the evaluation procedure, sidewall friction was assumed to be

analogous to the Mohr-Coulomb model, which may be used to evaluate interface shear resistance given in Eq. 3-5.

$$\tau = K_o \sigma_z \tan\delta + c_a \quad (3\text{-}5)$$

Where:

τ = shear stress

K_o = lateral "earth" pressure coefficient

σ_z = applied vertical stress

$\tan\delta$ = angle of interface shearing resistance

C_a = adhesion

It was assumed that C_a was zero, and K_{oTDA} and $\tan\delta$ were constant with depth, giving a first order decay of vertical stress with depth as follows[19]:

$$\sigma_z(z) = \sigma_z(0) exp^{(-4K_{oTDA}\tan\delta Z / D)} \quad (3\text{-}6)$$

Where:

$\sigma_z(z)$ = vertical stress at a particular depth,

$\sigma_z(0)$ = the applied vertical stress at the top

K_{oTDA} = lateral pressure coefficient for a TDA mass

δ = the interface shearing angle between the TDA mass and the walls of the test cell

Z = the depth from the applied stress

D = the diameter of the test cell

Because the applied stress at the top ($\sigma_z(0)$) and the stress reaching the bottom of the sample were known, the term $K_{oTDA}\tan\delta$ that is analogous to the parameter β for skin friction of piles was estimated from a simple root mean square error (RMSE) analysis. The parameters K_{oTDA} and $\tan\delta$ were subsequently separated and determined independently from specific individual measurements. These measurements are described in the following sections. The RMSE

[19] The derivation is presented in Section 3.10.5

analysis of top and bottom stresses in the TDA mass yielded a $K_{oTDA}tan\,\delta$ value of 0.75 for no sidewall friction treatment and 0.12 for sidewall friction treatment 2. To estimate the value of K_{oTDA}, the hoop strain was measured in the thick-walled acrylic test cylinder and this value was used with a 3D finite element (FE) model of the acrylic test cell as described in the following paragraphs. The focus of the FE modelling and independent direct shear tests completed was to determine approximate values of K_{oTDA} and $tan\,\delta$ that may separate the lumped β parameter and not for a detailed analysis of the TDA mass.

3.7.2.1 Estimation of K_{oTDA}

Three high precision strain gauges[20] were glued to the outer wall of the consolidometer 120^o apart at a height corresponding to the region of estimated maximum hoop strain upon increasing applied stress. The strain gauges were connected to a read out unit and resultant hoop strains were recorded as vertical stresses increased.

A 3D FE model was developed for the consolidometer apparatus using the software package Abaqus. The mechanical response of the acrylic cylinder was simulated using a linear elastic model for small strains in acrylic in order to estimate the value of K_{oTDA} by adjusting the horizontal earth pressure of the TDA to match the hoop strain values measured by the strain gauges on the sidewalls of the apparatus. The TDA itself was not explicitly part of the FE model except in that the outward horizontal stress applied by the vertically loaded mass of TDA was applied as a load boundary condition to the surface of the acrylic cylinder. This outward horizontal stress decreased with height along this boundary in accordance with the vertical stress distribution $\sigma_z(z)$ throughout the TDA mass and the shear stress distribution $\tau_z(z)$ along the walls of the consolidometer (Figure 3-8).

[20] See Figure 3-31, Section 3.10.6

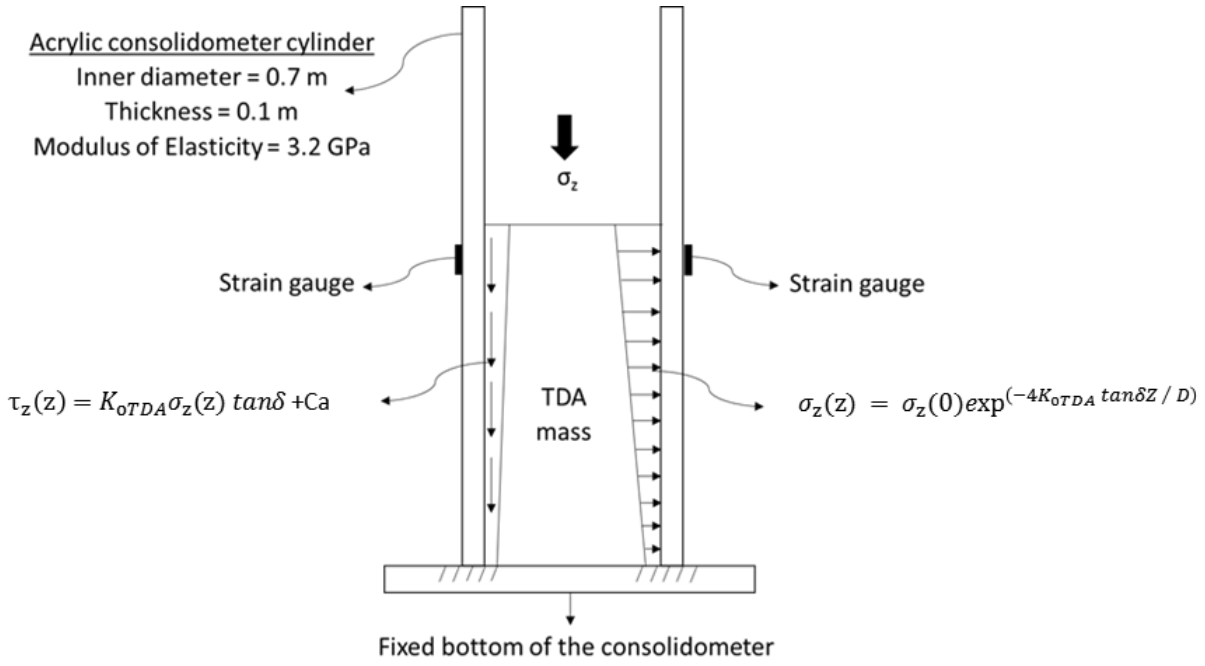

Figure 3-8: A schematic of the consolidometer cell as it was used in the 3D FE model to determine the value of K_{oTDA} for the TDA mass

The FE model was run multiple times using Eqs. 3-5 and 3-6 and the thickness of the TDA mass. The value of K_{oTDA} was varied until the hoop strain predicted by the FE model matched the observed values. The resulting best-fit value of K_{oTDA} obtained using the FE model was 0.7. It should be noted that a mass of TDA is not a perfectly homogeneous isotropic linearly elastic material and representing the lateral and shear stress from the TDA mass as a boundary condition for the FE model of the acrylic cylinder is necessarily a simplification. The FE modelling did yield a reasonable value of K_{oTDA} for the analyses. Furthermore, the value was useful for estimating the maximum stress that may be safely applied to a TDA mass in the test apparatus without the risk of damaging the acrylic cylinder.

3.7.2.2 Estimation of $tan\ \delta$

Using K_{oTDA} = 0.7, a RMSE analysis was applied to vary the value of $tan\ \delta$ in Eq. 3-6 until the calculated measurements at the bottom of the cell matched the readings from the TS cell at the bottom of the TDA mass. The estimated value of δ from this approach was between 10° to 12° for the applied stress. For an independent evaluation of $tan\ \delta$, testing was conducted in a 300

mm by 450 mm direct shear box to determine an approximate value for the interface friction angle δ between the TDA mass and the walls of the acrylic test cell with sidewall treatment 2 applied[21]. The applied normal stresses and sidewall conditions in the 1D consolidometer were simulated as closely as possible. It should be noted that the dimensions of the TDA particles (ranging from 50 mm to 305 mm) being close to the direct shear box dimensions could have resulted in edge effects between the TDA particles and the walls of the direct shear box. This may have contributed to the interface shear friction values recorded for the TDA mass and acrylic interface.

Another aspect of the direct shear test to point out is that the plastic layers were replaced and grease layers were re-applied for each test in the direct shear box. These were not done in the compression tests in the 1D consolidometer; the initial grease layers and plastic applied in the 1D consolidometer were used from start to finish of the compression tests. As such, the δ values that were determined independently in the direct shear box may have underestimated the friction values. The results from the direct shear interface friction tests are presented in Table 3-2.

Table 3-2: Results from the measurement of δ° with sidewall Treatment 2

Applied stress, σ_z, kPa	**shear stress τ, kPa**	$\boldsymbol{tan\,\delta}$	$\boldsymbol{\delta^o}$
39.4	3.8	0.01	0.7
65.3	5.9	0.04	2.3
195.0	9.4	0.03	1.8
255.0	10.9	0.03	1.7
304.4	12.1	0.03	1.7

[21] To complete the direct shear test, a piece of acrylic with the similar properties to the 1D cell and same dimensions as the direct shear box was placed in the direct shear box (see Figure 3-18) and sidewall treatment was applied to the face of the acrylic. TDA was placed on top of the acrylic and during shearing the lower portion of the shear box containing the piece of acrylic was pulled relative to the TDA to simulate sidewall friction effects during loading.

From the evaluation approach for δ as described in the preceding sections suggest that tan δ may not depend on the applied stress significantly, given the near constant values of δ° after 65.3 kPa in Table 3-2[22]. This may substantiate the premise that δ may be assumed to be constant with depth in the formulation of the sidewall evaluation strategy for evaluating stress distribution within the TDA mass presented in Eq. 3-6. The values of δ estimated from measurements in the 1D consolidometer were higher than the values from the individual direct shear tests in Table 3-2. The higher δ values may be related to the ripping of the plastic sidewall liners with increased loading, causing direct contact (sticking) of some TDA particles to the wall of the consolidometer. This may have caused non-uniform displacements along the TDA mass and wall interface, potentially increasing the sidewall friction compared with the direct shear tests in which the plastic layers were replaced for each test run and had fewer rips.

Notwithstanding, because the vertical stress applied to each slice was known and the compressive response of the TDA had been determined across a range of stresses, it was important to have a good estimate of the degree to which sidewall friction changed the vertical stress from the top to the bottom of the TDA mass. However, had the sidewall friction effect been more or less pronounced, the results in the 1D consolidometer would have still been usable as long as a good estimate of the distribution of vertical stress could be made.

3.8 Results and discussion

3.8.1 Immediate compression and creep

The progression of compression at the applied surface stress of 112 kPa and 224 kPa, simulating approximately 10 m to 25 m of waste above the drainage layer, respectively, is presented in Figure 3-9.

[22] In Figure 3-19, Section 3.10.5, the plot of δ° with applied stress is presented. The plot further shows the largely linear relationship at the higher applied stress, substantiating the assumption of a first order decay of vertical stress with depth in the formulation of the sidewall friction evaluation approach (Equation 3-6).

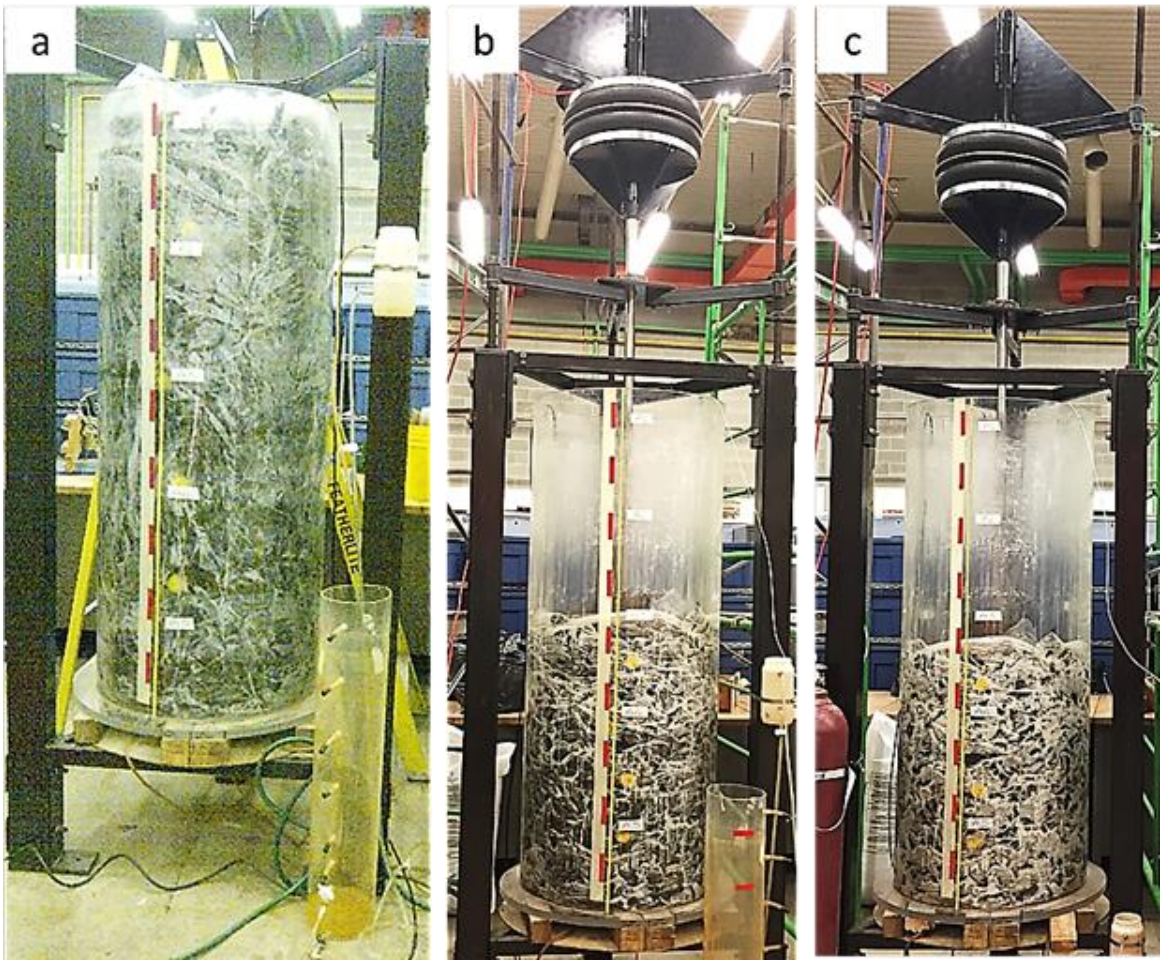

Figure 3-9: Progression of the 1D compression test: (a) no applied surface stress; (b) after applying 112 kPa surface stress; (c) after applying 224 kPa surface stress.

Compression in the TDA mass as measured periodically from the vertical displacement of the coloured visual markers is presented in Figure 3-10, where H1 to H5 are the labels for the visual markers from the topmost marker H1 to the bottom marker H5. The initial positions of the visual markers (H1 to H5) before applying the 112 kPa surface stress were H1 = 1.78 m, H2 = 1.42 m, H3 = 1.06 m, H4 = 0.72 m, and H5 = 0.32 m. At both load steps of 112 kPa and 224 kPa, there was a large immediate compression[23] followed by some creep (Figure 3-10; Table 3-3).

[23] In this article, the end of immediate compression was taken to be 24 hours after the application of the surface vertical stress. Readings after this were considered to be creep. The onset of creep was evaluated differently in Chapter 4 (Section 4.3.3.1) and was found to exceed 24 hours in layers farther from the stress

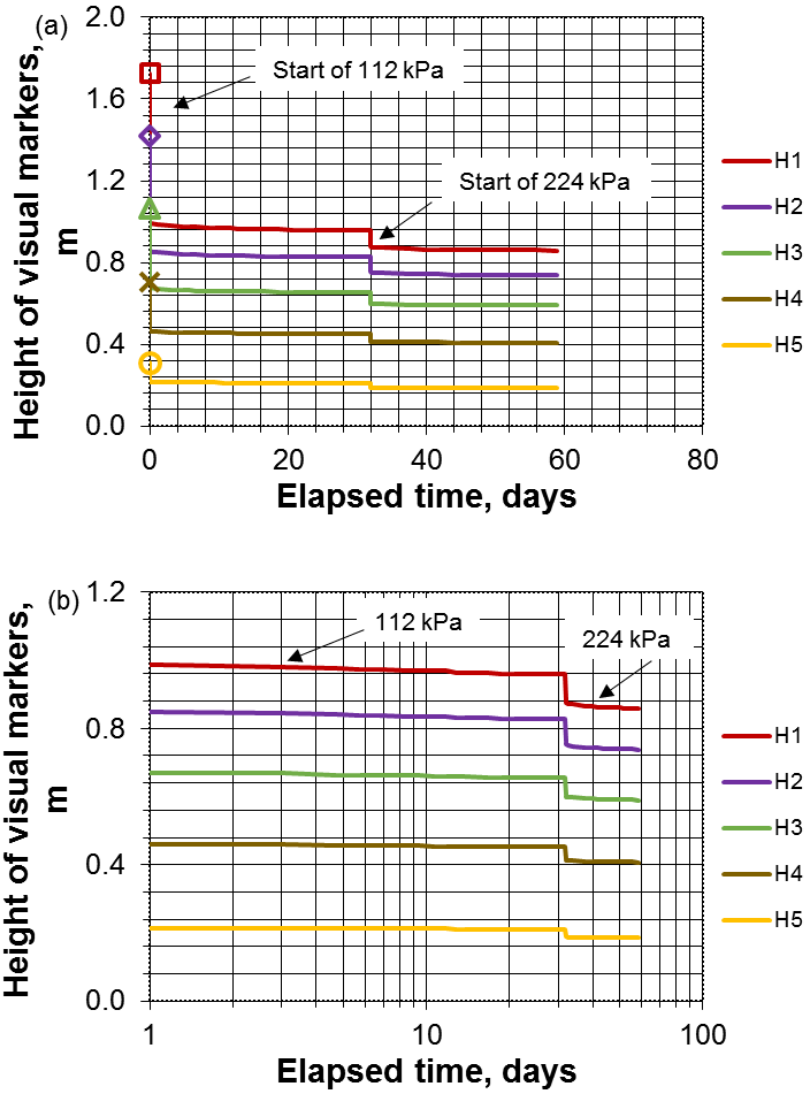

Figure 3-10: (a) Compression as change in the height of the visual markers with time at the applied surface stresses of 112 kPa and 224 kPa. H1 to H5 are the labels for the visual markers from the topmost marker H1 to the bottom marker H5. The initial positions of the visual markers (H1 to H5) before applying the 112 kPa surface stress are as follows: H1 = 1.78 m, H2 = 1.42 m, H3 = 1.06 m, H4 = 0.72 m, H5 = 0.32 m. (b) Compression plots in logarithmic scale for creep (showing data after 24 hours to the end of testing, 59 days)

Table 3-3: Immediate and time-dependent compression of the TDA mass.

Applied top stress (kPa)	Overall compression (%)	Immediate compression (%)	Time dependent compression (%)
112	44	41.5	2.5
224	Additional 10.5	7.8	2.7

The total compression at the end of the final load step of 224 kPa was approximately 55 %, and the contribution of creep to this was approximately 5 %. Immediate compression upon application of applied stress was larger at 112 kPa and reduced significantly at the 224 kPa load step. This is indicative of strain stiffening in the TDA mass with increased applied vertical stress. Strain stiffening in a TDA mass has been presented in studies by other researchers. For instance, the compression results presented by Beaven et al. (2006) and Mwai et al (2010) for different sizes and types of TDA showed reduced compression–strain stiffening at stresses from 200 kPa and greater.

3.8.2 Void ratio evaluation

Before and after creep plots of void ratio with applied stress (e-*log p* plots) for the slices in the TDA mass are presented collectively as series of tests running concurrently and are shown in Fig. 3-11a. The onset of creep was taken to be 24 hours[24] after the application of the surface vertical stress.

The void ratio in the top TDA slice (H1 to H2) decreased by approximately 57 % upon application of the initial stress of 112 kPa and further decreased by approximately 19 % when the applied stress was increased from 112 kPa (end of creep) to 224 kPa. The void ratio reduction induced by creep was approximately 10 % at 112 kPa and 8 % at 224 kPa. These were smaller than the void ratio reduction induced by immediate compression before the onset of creep.

The shapes of the e-*log p* curves in Fig. 3-11a and b suggest that there may not be a unique relationship between void ratio and applied stress for a mass of TDA as measured from constrained loading. The void ratio of a TDA mass at a particular applied stress appears to

[24] Chapter 4 (Section 4.3.3.1) contains a different evaluation approach for the onset of creep. That approach accounted for delayed compression in lower layers of TDA farther away from the applied surface stress

depend on the loading stress path taken to get to that void ratio, thus indicating that the compressive behavior of a mass of TDA under controlled conditions may be complicated and that there is need for field measurements to calibrate laboratory test results.

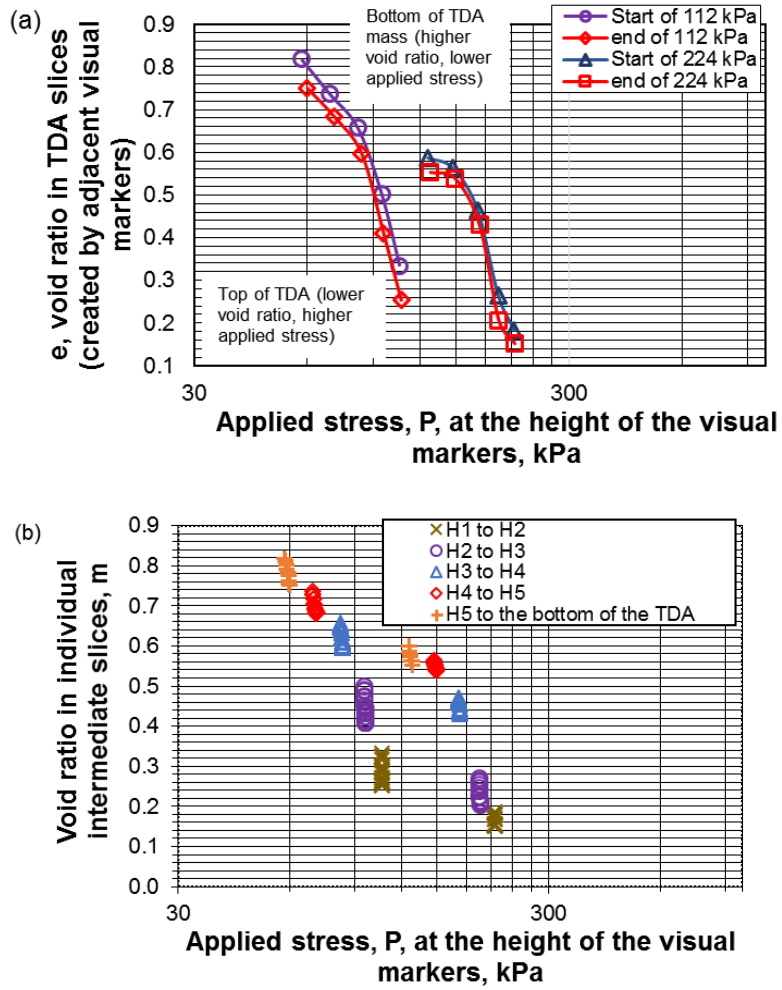

Figure 3-11: (a) e-logp curves for the entire thickness of the TDA mass, treating the slices collectively as a series of tests running concurrently. Adjacent visual markers in the test cell formed individual slices—for instance, visual markers H1 to H2 formed the topmost slice and visual marker H5 to the bottom of the cell formed the bottom slice. The applied stress in the slices were estimated using Eq. 3-6. The trend lines connecting circular markers on the plots represent the before creep values and those connecting triangular markers represent after creep values. The onset of creep in this study was taken as 24 h after the applied stress. The initial e values in the slices before the 112 kPa surface stress were H1 to H2 = 1.92, H2 to H3 = 1.92, H3 to H4 = 1.84, H4 to H5 = 1.71, and H5 to the bottom of the cell = 1.51. (b) e-log p curves for individual slices of the TDA mass at the end of creep, treating each slice as a separately run test and tracking the void ratio change in the individual slices for the applied stress. For each slice, there are two marker points indicated on the plot, indicating the void ratio values at the end of 122 kPa and 224 kPa, respectively.

3.8.3 Drainable porosity

A comparison of void ratio values estimated from the filling and draining porosities[25], and from the displacement of the visual markers is presented in Fig. 3-12.

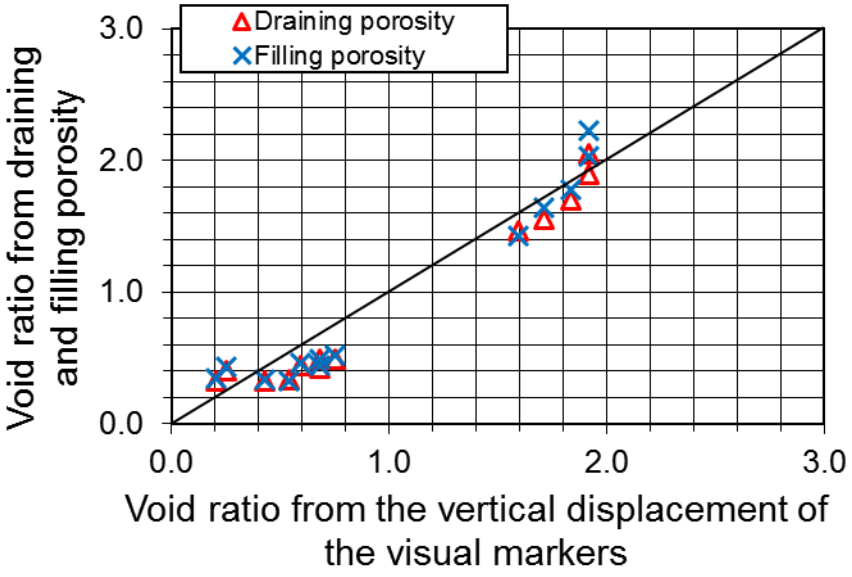

Figure 3-12: Void ratio estimated from drainable porosity versus void ratio from tracking the vertical displacement (elevation) of the visual markers.

The plot indicates some consistency between the void ratio values estimated from drainable porosity and those estimated from the displacement of the visual markers. However, the void ratio values that were estimated from drainable porosity measurements appear to be generally lower than those estimated from the displacement of the visual markers. This may be indicative of incomplete saturation of the TDA mass during the filling process for drainable porosity[26].

The void ratio results in Figure 3-12 further highlight the benefits of the primary approach, involving the use of a transparent test cell and visual markers that were employed for measuring 1D compression and void ratio in the TDA mass. Nonetheless, in the absence of a clear test cell, drainable porosity values may still be used with a good degree of reliability to estimate void

25 See Section 3.10.4 for the filling and draining porosity data
[26] The saturation of the TDA during the drainable porosity testing was not determined.

ratio change in a TDA mass in compression tests. Filling of the TDA mass should be completed over a longer period to potentially increase saturation and improve the accuracy of the measured values.

3.8.4 Implications of current findings for practice, and further completed and ongoing research work on TDA

As stated previously in this article, the performance of a mass of TDA as the drainage layer in waste disposal facilities depends on the porosity, permeability, and pore volume of the TDA mass following (1) compressive strains from overlying waste and cover materials and (2) biogeochemical clogging from leachate flowing through the drainage layer. The porosity of the TDA mass under simulated overlying waste was evaluated in this study; this was found to reduce by over 50 % from an unloaded state to about 0.26 at the maximum applied stress of 224 kPa. Although the porosity of 0.26 at an applied stress of 224 kPa—equivalent to between 20 m and 25 m of waste (Zekkos et al. 2006)—may seem low, the coefficient of vertical and horizontal permeability values of the TDA mass at a comparable porosity and applied stress have been evaluated and the results show high permeability values for the TDA mass.

The measured coefficients of the vertical and horizontal permeability of the TDA mass at an applied vertical stress of 219 kPa were 0.0079 m/s and 0.019 m/s respectively[27]. These values are higher than the regulatory requirement of 0.0001 m/s in the Western Canada jurisdiction for a landfill drainage layer. The details of the 2D permeability testing, including the equipment design and experimental strategies employed, will be presented in a companion article. In addition, a porosimeter is being used with image analysis to analyze the pore geometry of a mass of TDA under applied vertical loading to obtain parameters, such as specific surface, pore volume, and pore size distribution that may be used to evaluate the performance of a TDA mass

[27] Experimental studies and results for this are presented in Chapter 5

against biogeochemical clogging under various mass loading and flow scenarios. The findings from this study will be presented in an upcoming article[28].

3.9 Conclusions and summary

The challenges with testing large-particle-size TDA for use under large stresses imposed by overlying material have been discussed and some strategies for overcoming the challenges have been presented. The highlights of this article include the following:

(1) Laboratory testing of large-particle-sized TDA is challenging, and it unavoidably requires the use of large-sized test equipment with the capacity to apply large vertical stresses and accommodate large vertical strains.

(2) The use of air bellows that can be wound down manually made it possible to apply and sustain large applied stresses onto the test specimen while experiencing high vertical strains greater than 0.5 m.

(3) A mass of TDA with large-sized particles has an initially large void volume that reduces considerably upon loading because of a large immediate compression and some creep.

(4) Compression in a mass of TDA has been determined to be from void volume reduction, and the compression of individual solid particles may be ignored.

(5) The use of a clear, “see-through” consolidometer provided the opportunity to measure intermediate strains and void ratio in slices within the test specimen. A single test can therefore yield information regarding a range of stresses concurrently if intermediate strains in slices are measured.

(6) There is a need for unconstrained field testing of TDA to eliminate the effects of sidewall friction and to calibrate laboratory test data obtained from constrained 1D compression testing.

[28] Presented as Chapter 5

(7) It is essential to account for sidewall friction in the laboratory testing of TDA to avoid overestimating the applied stresses and void ratio throughout the test specimen. For instance, if methods for measuring and estimating sidewall friction, such as using a clear test cell, placing visual markers at intermediate levels to separate the test specimen into slices, placing a TS cell at the bottom of the specimen to account for sidewall friction loss, and using a theoretical model to estimate applied stresses in intermediate slices, were not employed, the actual applied stresses within the specimen thickness, the resulting strains, and void volume reduction may have been overestimated. Dividing the test specimen into slices and determining the applied stress and void ratio in each slice made it possible to determine the actual void ratio at an applied stress following the effects of sidewall friction.

(8) The sidewall friction evaluation approach that was presented in this article can be used to estimate stresses and strains at any point within the consolidometer, potentially eliminating the need for TS cells beneath the test specimen.

(9) Void volume reduction in a TDA mass was found to reduce significantly as applied vertical stresses increased. This confirms the strain stiffening behavior of a mass of TDA under applied stress, substantiating similar findings from previous researchers (e.g., Beaven et al. 2006; Mwai et al. 2010).

(10) Nonlinearities in the e-log p consolidation curves indicate that the 1D constrained creep compression of a mass of TDA might be complicated.

(11) Although TDA has been tested in this study, the strategies that were implemented in this study may be applicable to a wide range of highly compressible materials with initially large void volumes that would reduce significantly following compressive displacements under vertical loading.

3.10 Supplementary data for chapter

3.10.1 Solid volume compression data

As discussed in Chapter 3 – Section 3.6.3, and Chapter 4, Sections 4.2.2 and 4.3.2, presented in Figure 3-13 are the data for the solid volume compression of TDA particles under applied isotropic stresses 50 kPa, 100 kPa and 200 kPa. From Figure 3-13, following an initial elastic volume compression upon application of pressure, the total water demand in the compression cell from the PV controller was determined to be 9.19×10^{-5} ml. This was determined after eliminating data that were indicative of compression of air remaining in the system after de-airing, and/or the elastic response of the test cell and fittings (Figure 3-13). The total water demand (9.19×10^{-5} ml) after accounting for the initial (immediate) compressive response, corresponded to a total creep of 1.3 mm, over more than 90 days at the end of the final applied stress of 200 kPa.

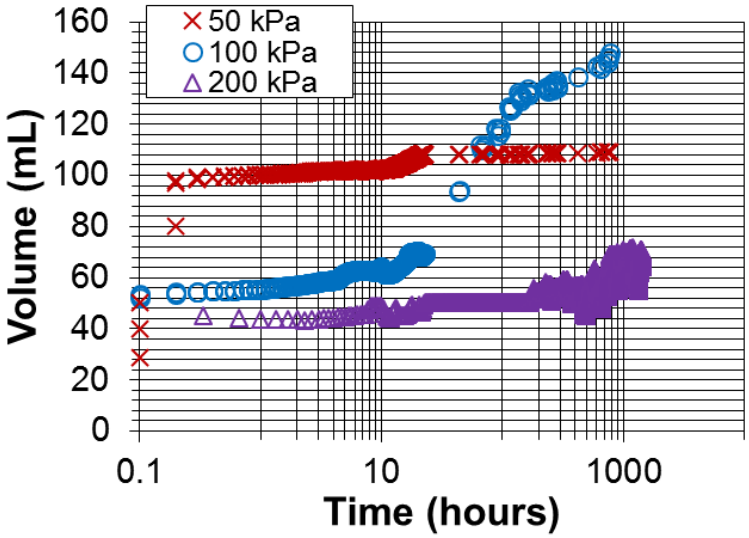

Figure 3-13: Solid volume compression of TDA particles under applied isotropic stresses, 50 kPa, 100 kPa, 200 kPa.

3.10.2 Sidewall treatment for the 1D consolidometer

As discussed in Section3.7.1, presented in Figure 3-14 are materials and details of the sidewall treatment process.

Figure 3-14: Plastic liner for sidewall treatment in 1D consolidometer, greased sidewall, grease, plastic liner and TDA in consolidometer (sidewall treatment 1 shown)

3.10.3 1D compression and creep testing steps in the consolidometer

As discussed in Section 3.6.2, the following steps were taken for the experimental work in the 1D consolidometer. The steps are a combination of the approaches in ASTM D2990-09 and ASTM D7406-07

(1) Calibrate load cell and total stress (TS) cell (Figure 3-15);

(2) Apply sidewall treatment;

(3) Place TS cell at the bottom of consolidometer;

(4) Fill up the consolidometer with known mass of TDA to a predetermined height;

(5) Place coloured balls (visual markers for compression tracking) at 120^{o} apart on top of TDA in consolidometer to mark the height of TDA of known mass;

(6) Repeat steps 4 and 5 until the consolidometer is filled with TDA;

(7) Calculate the unit weight of TDA in consolidometer at heights marked by the visual markers;

(8) Calculate the initial void ratio of TDA at heights marked by the visual markers;

(9) Place loading plate on top of the TDA, place load cell in housing and place on top of the loading plate;

(10) Positon piston rod on top of the load cell and bolt piston guide into the lower three “arms” of the load frame;

(11) Connect upper three “arms” of the load frame and mount the air bellows;

(12) Connect load cell and TS cell to read out units;

(13) Open air pressure valve to supply air into bellows for the required vertical applied stress;

(14) Measure the displacement of the visual markers at 1, 10 and 30 minutes and at 1, 2, 4, 8, 24, 48, 72, 96, 120, 144, 168 hours, then every 168 hours until the end of 1000 hours (and beyond).

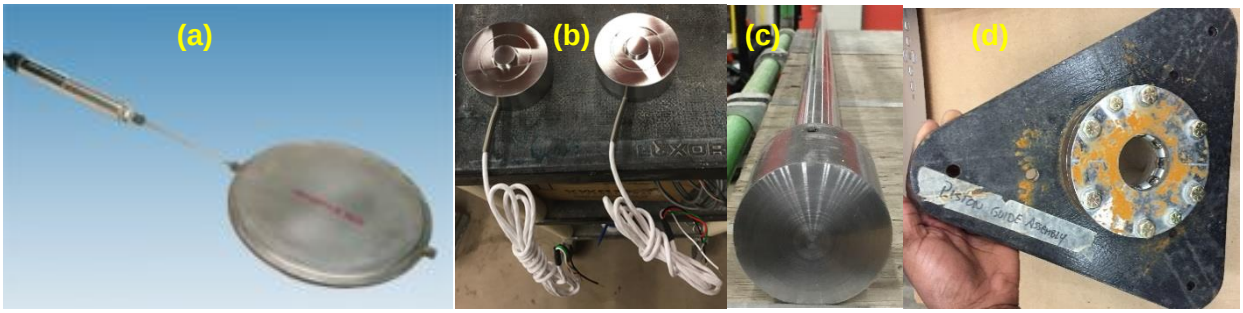

Figure 3-15: (a) Pancake type TS cell used (230 mm diameter and 11 mm thick. Stock photo – durhamgeo.com), (b) button type load cells used, (c) re-engineered piston rod with conical tip, (d) piston guide to prevent binding of the piston rod at the ends.

3.10.4 Filling and draining porosity data

As discussed in Section 3.8.3, Figure 3-16 shows the filling and draining porosity values used for the void ratio comparison in Figure 3-12, Section 3.8.3. In Figure 3-16, filling porosity values

are slightly higher than the draining porosity values. Reasons for this could be related to TDA particles or retaining some water during draining.

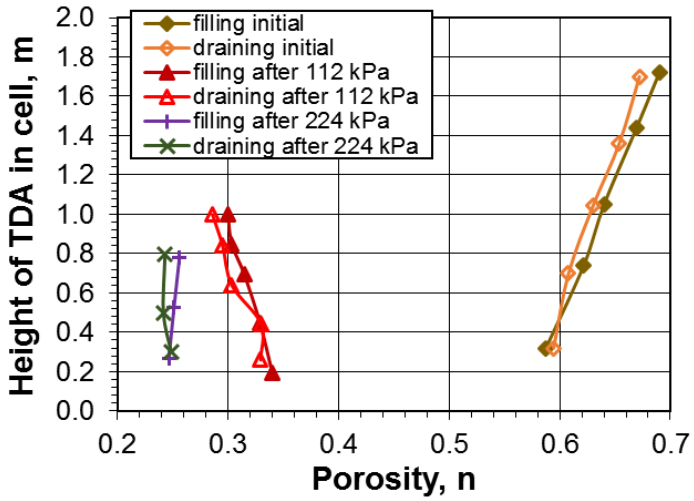

Figure 3-16: Plots of filling and draining porosities, "initial" as presented in the legend represents readings taken when the TDA was under just the weight of the loading plate and the air bellows (under less than 3 kPa of applied stress)

3.10.5 Derivation of the sidewall friction evaluation equation

As discussed in Section 3.7.2, because of sidewall friction, applied stress $\sigma_z(z)$ decreased with depth z in relation to the shear stress acting along the sidewall τ_z (Figure 3-17), hence,

$$\Delta\sigma_z / \Delta z = -\tau_z \qquad (3\text{-}7)$$

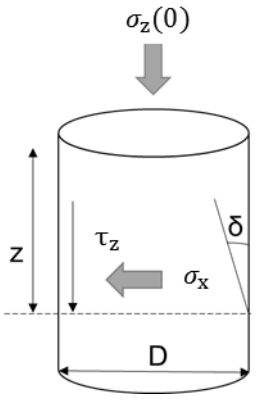

Where:

$\sigma_z(0)$ = Applied surface stress, kPa

σ_x = Lateral stress acting on the sidewall , kPa

τ_z = Shear stress from sidewall friction, kPa

z= Position/depth, m

δ = Angle of internal shearing resistance (sidewall friction angle), ^{o}

D = diameter of the test cell, m

Figure 3-17: Schematic of the 1D cell indicating parameters for determining σ_z with position (z).

If the Mohr's equation for shear stress ($\tau = \sigma_z tan\phi + c$) can be adapted, and if the apparent cohesion term (c) is ignored, and the internal friction angle ϕ is represented with the sidewall friction angle δ, the interface shear stress τ_z acting along the sidewall of the cylindrical 1D test cell can be represented as:

$$\tau_z = \frac{-(\sigma_x tan\delta)\ X\ (\pi D)z}{\pi D^2/4} \qquad (3\text{-}8)$$

Where

$(\pi D)z$ is the lateral area of the sidewall of the 1D cell, $\pi D^2/4$ is the total surface area of the cell

Substituting $\sigma_x = \sigma_z(Ko)$ (lateral stress coefficient) into Equation 3-8 gives:

$$\tau z = \frac{-(\sigma_z(Ko) tan\delta)\ X\ (\pi D)z}{\pi D^2/4} \qquad (3\text{-}9)$$

Substituting equation *3-9* into *3-7* gives:

$$\frac{\Delta\sigma_z}{\Delta z} = \frac{-(\sigma_z(Ko) tan\delta)\ X\ (\pi D)z}{\pi D^2/4} \qquad (3\text{-}10)$$

Integrating an infinitesimal change in σ_z and z:

$$\int \frac{d\sigma_z}{\sigma z} = \int -\left((Kotan\delta) * \frac{(\pi D)}{\pi D^2/4}\right) * dz$$

$$ln\ \sigma_z(z) = -\left((Kotan\delta) * \frac{4}{D}\right) * z + c \qquad (3\text{-}11)$$

When z = 0 (at the TDA surface), $\sigma_z = \sigma_z(0)$ (applied surface stress), and C = ln $\sigma_z(0)$

Substituting for C in equation 3-11 gives:

$$ln\ \sigma_z(z) = -\left((Kotan\delta) * \frac{4}{D}\right) * z + \ln \sigma_z(0) \qquad (3\text{-}12)$$

Then,

$$\sigma_z(z) = \sigma_z(0)e^{-(\frac{4Kotan\delta}{D})z}$$ *(3-13) (Equation 3-6 in Section 3.7.2)*

As discussed in 3.7.2.2, Figure 3-18 (a –c) show aspects of the direct shear testing for the estimation of $\boldsymbol{tan\ \delta}$

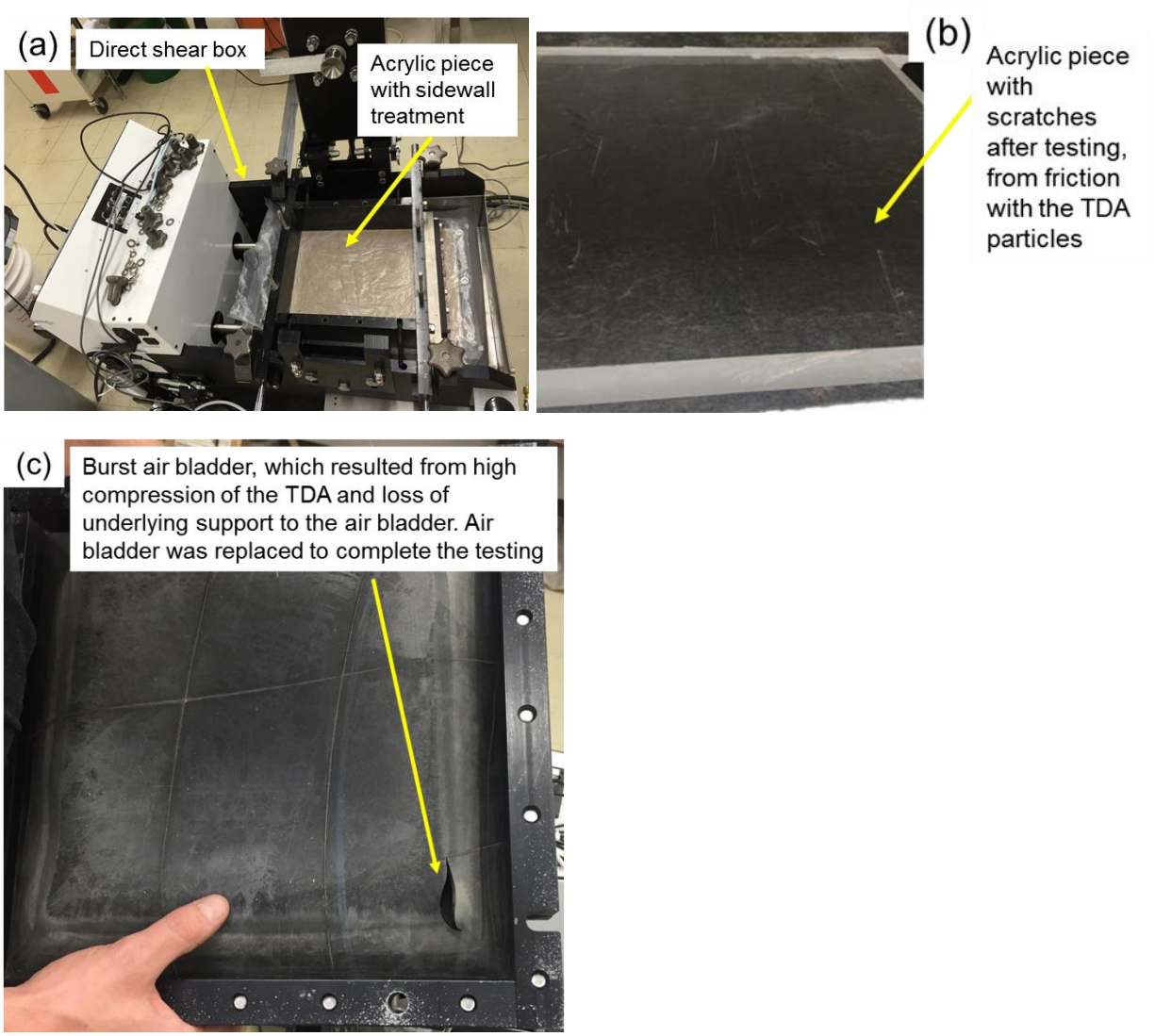

Figure 3-18: direct shear box for the testing discussed in 3.7.2.2 for the estimation of $\boldsymbol{tan\ \delta}$. (a) image shows an acrylic plate with sidewall treatment applied placed in the shear box. TDA was then placed on top of the plate and an air bladder was placed on the TDA to apply loads (b) scratches on the surface of the acrylic piece after testing from contact and friction with the TDA (c) burst air bladder which resulted from high compression of the TDA, and loss of underlying support from the TDA. This caused the air bladder to expand beyond capacity and burst. Air bladder was replaced to complete the testing.

As presented in Section 3.7.2.2, the plot of δ° with applied stress from the direct shear test is presented in Figure 3-19 below. The plot further highlights the near constant values of δ° with applied stress after 65.3 kPa as presented in Table 3-2.

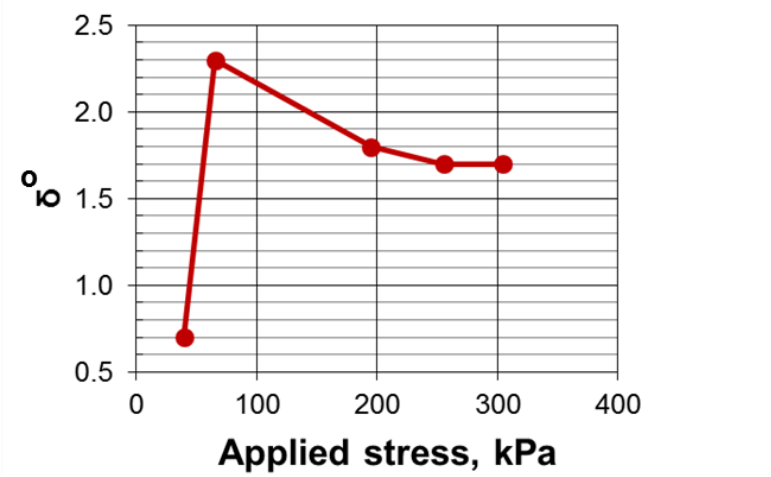

Figure 3-19: Relationship between δ° and applied stress. See also, Table 3-2, Section 3.7.2.2

3.10.6 Additional images from the laboratory testing

As discussed in Section 3.4, presented in Figure 3-20 is an image showing how the "arms" of the air bellow were manually lowered to apply loads to the TDA.

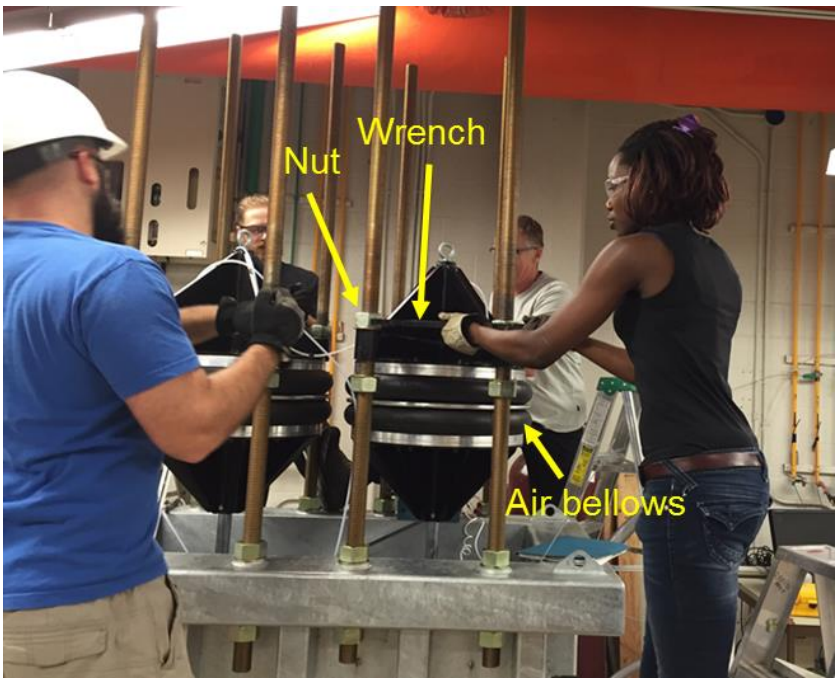

Figure 3-20: Manually lowering the air bellows to apply load to the TDA. Image here is for the test cell discussed in Chapter 5, but the same process applied to testing in the 1D cell discussed in Section 3.4. Lowering the air bellows required strong set of arms to turn the wrenches around the nuts. In this image, four strong sets of arms and muscles were needed – the strongest being those of the woman!

The strain gauges used to determine the maximum hoop strain in the 1D cell, upon increasing applied surface stress, as discussed in Section 3.7.2.1, is presented in Figure 3-21

Figure 3-21: Strain gauges used to determine the maximum hoop strain in the 1D cell, as discussed in Section 3.7.2.1

4.0 One-dimensional (1D) immediate compression and creep in large particle sized tire derived aggregate (TDA) for leachate collection and removal systems (LCRS)

Overview

Presented in this Chapter are results and discussion on void volume reduction in large particle sized TDA, from the individual and combined effects of immediate compression and creep under large sustained stresses. The effects of increased temperature – up to 58 C, applied stress, duration of sustained stresses, and loading rate on the compressive behaviour of the TDA types were also discussed.

This Chapter was accepted for publication in the Canadian Geotechnical Journal as follows:

D. Adesokan, I. Fleming and A. Hammerlindl, "One-dimensional (1D) immediate compression and creep in large particle sized Tire Derived Aggregate (TDA) for leachate collection and removal systems (LCRS)," Canadian Geotechnical Journal, manuscript ID cgj-2019-0722.R2 Accepted for publication May 25, 2020

Additional information relating to this Chapter, which were not included in the accepted manuscript are included as footnotes within the Chapter, and as supplementary data in Section 4.5.

4.1 Introduction

Modern-day engineered landfills typically have leachate collection and removal systems (LCRS) that act to control leachate mounding, and consequently reduce the build-up of excessive hydraulic head on landfill basal liner systems or subgrade of the landfill cell (Reddy and Saichek 1998; Rowe and Fleming 1998; Fleming et al., 1999; Qian et al., 2001; Warith et al., 2004; Fleming and Rowe 2004; Rowe et al., 2004; Rowe 2005; Beaven et al., 2013). The LCRS also systematically collects and removes leachate and contaminated water that would otherwise be transported into the environment. A typical LCRS consists of contiguous system of perforated leachate collection pipes, leachate collection sump(s), leachate evacuation pumps and a

drainage media. The drainage media is the channel through which infiltrating water and leachate are collected and removed from the base of the landfill into collection pipes and sumps.

TDA has been used, and studied for use, as drainage material in LCRS for over two decades, in large part for cost and environmental considerations (Hall 1991; Ahmed and Lovell 1993; Beaven 1994; Duffy 1995; Narejo and Shettima, 1995; Donovan et al., 1996; Evans 1997; Zimmerman 1997; Reddy and Saichek 1998; McIsaac and Rowe 2005; Rowe and McIsaac 2005; Beaven et al., 2006; Hudson et al., 2007; Mwai et al., 2010; Beaven et al., 2013; Adesokan et al., 2015; Adesokan et al., 2016; Adesokan et al., 2019[29]). In a Canadian context, for instance across much of western Canada, TDA is increasingly used and studied as a substitute for gravel in LCRS because good quality gravel is (a) hard to find, and (b) very expensive – the cost of a unit volume of good quality gravel can be up to 30 times the cost of the same volume of TDA.

The environmental concerns with huge stockpiles of whole and shredded scrap tires in landfills, or at tire recycling facilities also make the use of TDA in LCRS, and several other civil engineering applications very meaningful. Other civil engineering applications of TDA include reinforcement for walls, slopes and embankments; subgrade insulation for roadways and highways; lightweight backfill; daily, intermediate and final covers for landfills and basal liner protection in landfills (Manion and Humphrey 1992; Humphrey and Eaton 1993; Humphrey and Eaton 1994; Humphrey and Eaton 1995; Tweedie et al., 1998; Humphrey 1999; Reddy and Marella 2001; Moo-Young et al 2003; Dickinson and Brachman 2008; Marcotte and Fleming 2020),

[29] Chapter 3

As a polymeric composite consisting of both synthetic and natural polymers (Reddy and Marella 2001; Warith et al., 2004), TDA under applied stress is expected to undergo both immediate compression and creep – ASTM D2990-17 defines creep as times dependent compression under constant long-term static loading. Immediate compression in both large and small particle sized TDA (TDA with particle size from 50mm to over 305 mm and TDA with particle size less than 50 mm respectively) under both self-weight and applied stress has been widely studied (Hall 1991, Ahmed and Lovell 1993; Humphrey and Sandford 1993; Duffy 1995; Donovan et al., 1996; Evans 1997; Zimmerman 1997; Reddy and Saichek 1998; Tweedie et al., 1998; Humphrey et al., 2000; Moo-young et al., 2003; Warith et al., 2004; McIsaac and Rowe 2005; Rowe and McIsaac 2005; Hudson et al., 2007; Beaven et al., 2006; Il-Sang Ahn et al., 2012; Beaven et al., 2013; Yi et al., 2014; Meles et al., 2014; Meles et al., 2016). Creep in TDA under sustained applied stress has been sparsely studied; hence, understanding of its significance and contribution to void volume reduction has been limited, especially for large particle sized TDA.

Most of the limited studies on creep in TDA in the literature tested small particle sized TDA and mixtures of small particle sized TDA and sand (Tweedie et al., 1998; Youwai and Bergado 2003; Rao and Dutta, 2006; Wartman et al., 2007), only a few of those studies tested large particle sized TDA (for instance, Humphrey et al 2000). In LCRS, large particle sized TDA are preferred over small particle sized TDA because of the relatively larger void volume that is achievable within large particle sized TDA.

A large void volume is needed for long-term transmission of leachate from beneath overlying waste into leachate collection pipes and sumps; and to store biogeochemical clog as leachate permeates through the drainage layer (Reddy and Saichek 1998; Rowe and Fleming 1998; Fleming et al., 1999; Fleming and Rowe 2004; Rowe et al., 2004; Rowe 2005; McIsaac and

Rowe 2005; McIsaac and Rowe 2005; Rowe and Babcock 2007; Yu and Rowe 2012; Beaven et al., 2013).

Under applied stress, an initially large void volume is expected to undergo larger void volume reductions compared to an initially small void volume. Hence, for applications where large particle sized TDA will be buried under high stresses for extended periods, such as in LCRS – where the TDA layer will be subjected to the sustained weight of overlying waste material for long periods, it is essential to understand the contribution of both the immediate compression and creep to void volume reduction.

The response of TDA to applied stress has been found to be largely dependent on particle size, amongst several other parameters – including the shape, mode of shredding, exposed and loose wire content of the TDA particles (Hall 1991; Reddy and Saichek 1998; Warith et al., 2004; Rowe and McIsaac 2005; McIsaac and Rowe 2005; Beaven et al., 2006). Studies (such as Strenk et al., 2007) have shown a scale (particle size) dependency to the material properties of TDA; properties such as cohesion (c), compacted unit weight (γ) and secant-constrained modulus (M_{sec}) were found to decrease with increasing particle size, while friction angle (ϕ) was reported to increase with increasing particle size.

Some other studies, such as (Beaven et al., 2006; Mwai et al., 2010) have presented results indicating that the compressive response of TDA to applied stress is particle size dependent. Both Beaven's and Mwai's results showed more compression in TDA with particle sizes greater than 200 mm than in those with particle sizes smaller than that under similar applied stress. This may have been related to an initially larger void volume that is typical with larger particle sized TDA, which allows for more void volume reduction under compressive applied stress.

Overall, the results from testing small particle sized TDA have not been clearly shown to be applicable for estimating the behaviour of large particle sized TDA. Hence, size specific testing

is needed to determine the performance-related properties of large particle sized TDA, and such testing presents several challenges (Adesokan et al., 2019[30]).

In view of these, this research work studied the performance-related properties of large particle sized TDA, including immediate compression and creep, vertical and horizontal hydraulic conductivity, anisotropy in the hydraulic conductivity, and pore geometry, in relation to its use in the LCRS of waste disposal sites. A complementary article will present the 2D[31] hydraulic conductivity and the pore geometry evaluations. Presented in this article are the following aspects of the study:

- Void volume reduction from immediate compression and creep;
- Evaluation of solid volume compression in individual TDA particles and the contribution to void volume reduction;
- Effects of loading rate and elevated temperature on void volume reduction.

4.2 Materials and methods

4.2.1 The TDA

Three TDA types, sourced from two different tire processing and recycling facilities in western Canada were tested. Shercom Industries, Saskatoon SK supplied two of the TDA types described in this article as Sask TDA 1 and Sask TDA 2 (Figure 4-1 a, b); Liberty Tire, near Edmonton AB, supplied the third TDA type described here as ARMA TDA (Figure 4-1 c). Sask TDA 1 was used for the testing described as Sask TDA test 1, Sask TDA 2 was used for the testing described as Sask TDA tests 2 and 3, and ARMA TDA was used for the testing described as ARMA TDA tests 1, 2 and 3.

[30] Chapter 3
[31] Vertical and horizontal hydraulic conductivity – presented in Chapter 5

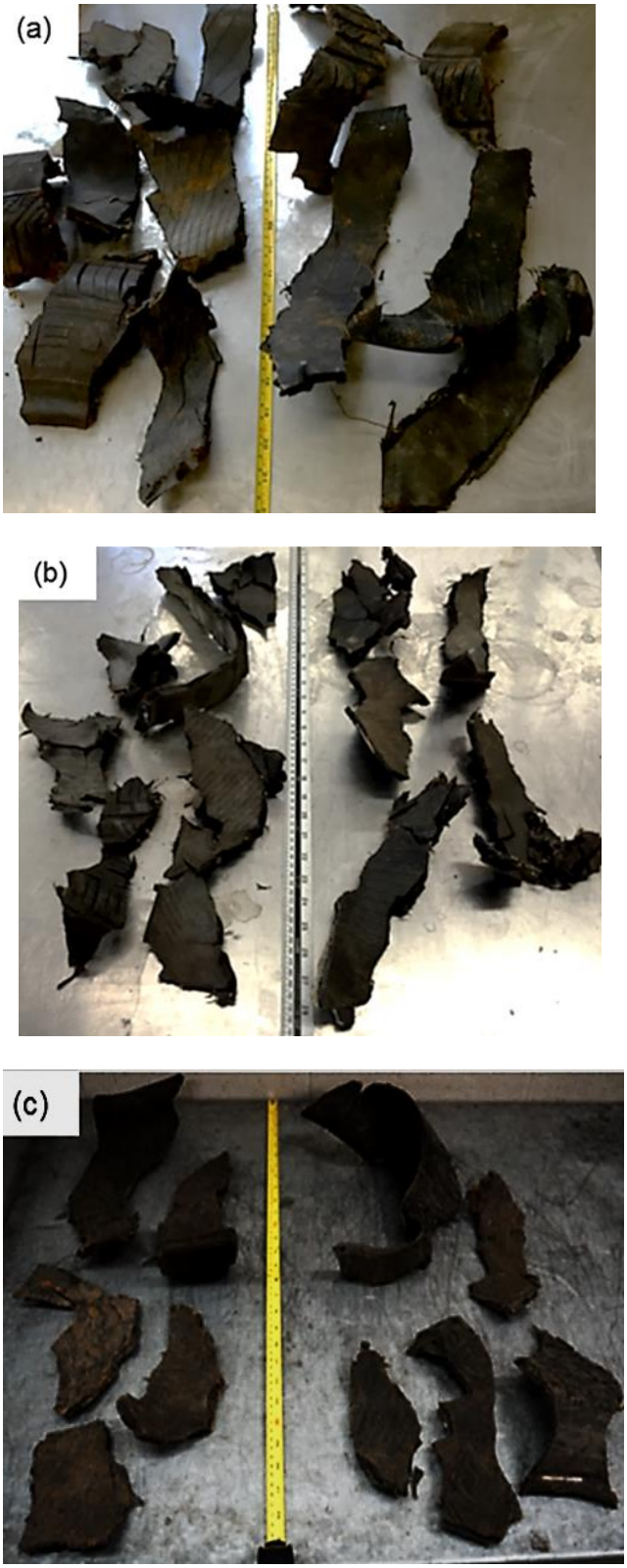

Figure 4-1: TDA types tested: (a) Sask TDA 1; (b) Sask TDA 2; (c) ARMA TDA

The TDA types (Figure 4-1) generally consisted of elongated particles that had been cleanly cut (i.e. the individual particles were fully separated from each other, and the exposed wires did not interconnect individual particles, for instance, like the “P Shred” TDA tested in McIsaac and Rowe (2005) – where the effect of exposed wire on the compressive response of TDA to applied stress was studied). The exposed wire content (loose and protruding), and particle size distribution (PSD) of the TDA particles were determined by randomly selecting a minimum of 20 kg of TDA – consisting of over 300 individual particles, and measuring the longest dimensions (length), shortest dimensions (width), and length of exposed wires with a measuring tape.

The dimensions of the TDA particles were measured manually (as opposed to with sieves) as this was determined to be a detailed way of quantifying the length of exposed wires and the actual dimensions of the TDA particles. Values from sieve analysis will depend on the orientation of the particles, and for the largely elongated TDA particles, this may not be truly representative of the particle dimensions going through or retained on the sieves.

The thickness and mass of each individual particle were also determined, and for each TDA type, PSD plots were generated using the cumulative mass percentage smaller than the length of each particle, and the cumulative mass percentage smaller than the width of each particle. The PSD plots were also presented in terms of equivalent dimension (d_{eq}) (Eq. 4-1) for direct comparison with the singular particle size dimensions typically presented for gravel.

$$d_{eq} = \sqrt{(L \times W)} \qquad (4\text{-}1)$$

Where

L = length of the TDA particle (mm);

W = width of the TDA particle (mm).

Specific gravity (G_s) was determined for each of the TDA types using the guidelines for larger particle sized aggregates presented in ASTM C127 – 12.

4.2.2 Solid volume compression

In soil mechanics, the volumetric compression of the individual mineral particles is taken to be zero. Thus, in the 1D compression (consolidation) of soils, the change in solid volume is zero and the overall volumetric strain change results only from a change in void ratio as per Eq. 4-2.

$$\Delta V/V = \Delta H/H = \Delta e/(1+e_0), \text{ and } \Delta Vs = 0 \quad (4\text{-}2)$$

Where

ΔH = change in height;

H = initial height;

Δe = change in void ratio;

e_0 = initial void ratio;

ΔV_s = change in volume of solids

TDA pieces (particles) are not solid mineral, hence in order to apply to a volume of TDA the traditional 1D compression paradigm for soils (Eq. 2-2) the authors carried out a simple experiment to determine whether or not the change in solid volume of TDA particles was minimal or negligible. Accordingly, the volumetric particle compression (change in volume of individual solid particles) under isotropic stress was measured to assess whether the overall compression of a volume of TDA may be attributed entirely to the change in void volume as for mineral soils, or whether it would be necessary to incorporate the effects of solid volume compression of the individual TDA particles.

For this, testing was completed in a large compression cell (0.6 m high, 0.3 m diameter) and every individual TDA particle was subjected to isotropic stress equal to the applied cell pressure. Given the size of this experiment, the longest TDA particles were excluded from the specimen that was tested. However, there is no reason to believe that volumetric strain under isotropic compression should be any different for those TDA particles relative to the test.

A known volume of TDA was placed in the triaxial cell and a known volume of water was added to it. Vacuum pressure was applied to the top of the cell to de-air the TDA to ensure full saturation of the particles. Using a pressure – volume (PV) controller, cell pressures (isotropic stresses) of 50 kPa, 100 kPa and 200 kPa were applied to the TDA for a total of approximately 90 days. The 50 kPa and 100 kPa stresses were sustained for a total of 30 days, and the 200 kPa stress was sustained for 60 days. The 200 kPa applied stress was sustained longer to sufficiently capture the compressive effects at that applied stress, as it was the highest and final applied stress in the study.

An increase in water demand in the compression cell from the PV controller was taken an indication of solid volume compression in the individual TDA particles. In evaluating the results[32], data were eliminated where they were indicative of compression of the small amount of air remaining in the system and/or the elastic response of the test cell and fittings.

4.2.3 Immediate compression and creep testing

Short and long duration compression testing were completed in a 1.2 m high, 0.7 m diameter 1D consolidometer, fabricated from a thick-walled clear acrylic tube (Figure 4-2). A total of six compression and creep testing was completed in the 1D consolidometer using the three TDA types. Surface stresses from 28 kPa to 300 kPa were applied to the TDA to simulate approximately 2 to 30 m of waste overlying a TDA drainage layer in a waste disposal facility (Zekkos et al., 2006). Applied load/stress was increased incrementally, and each load step was sustained for between 5 to 90 days.

Coloured lacrosse balls (at times fluorescent painted TDA pieces), spaced 120^{o} apart were placed against the sidewall of the consolidometer at various elevations for use as visual markers. Because the consolidometer is transparent, it was possible to place visual markers at

[32] Results are presented in Chapter 3, Section 3.10.1

various depths within the TDA, and track the displacement and positions of the visual markers by reading off across measuring tapes that were glued onto the outside wall of the consolidometer (Adesokan et al., 2019[33]).

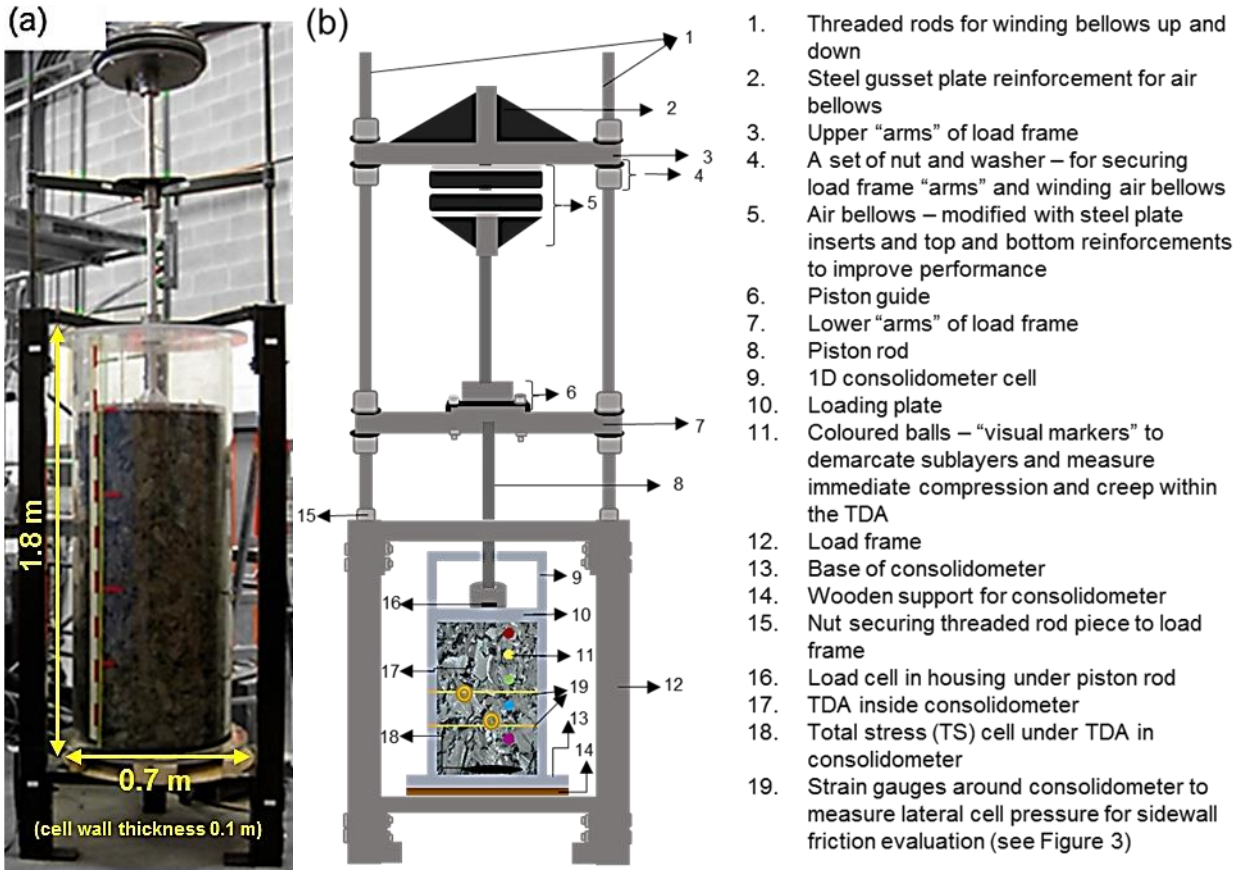

Figure 4-2: The 1D consolidometer: (a) placed on the loading frame for load application with the air bellows and loading plate in place; (b) schematic of the 1D consolidometer with description of parts (adapted from Adesokan et al (2019)[34])

The position of the visual markers within the TDA virtually divided the TDA into adjacent horizontal sublayers; hence, each testing event can be considered series of tests running simultaneously. Altogether, there were twenty three individual sublayers in all six testing events, representing twenty three distinct tests.

[33] Chapter 3
[34] Chapter 3

The mass of TDA placed in each sublayer was determined during filling up of the cell, and having measured the specific gravity (G_s), the dry unit weight of TDA in each sublayer was determined. Using these, the initial void ratio (e_0)[35] in individual sublayers was determined using Eq. 4-3. The periodic change in void ratio as testing progressed was determined using Eq. 4-2.

$$e = (G_s\gamma_w/\gamma_{dry}) - 1 \qquad (4\text{-}3)$$

Where:

G_s = specific gravity;

γ_w = the unit weight of water (kN/m^3);

γ_{dry} = the unit weight of dry TDA mass in the slices (kN/m^3)

A typical loading event in the consolidometer is presented in Figure 4-3. Loading event for Sask TDA test 3 is shown.

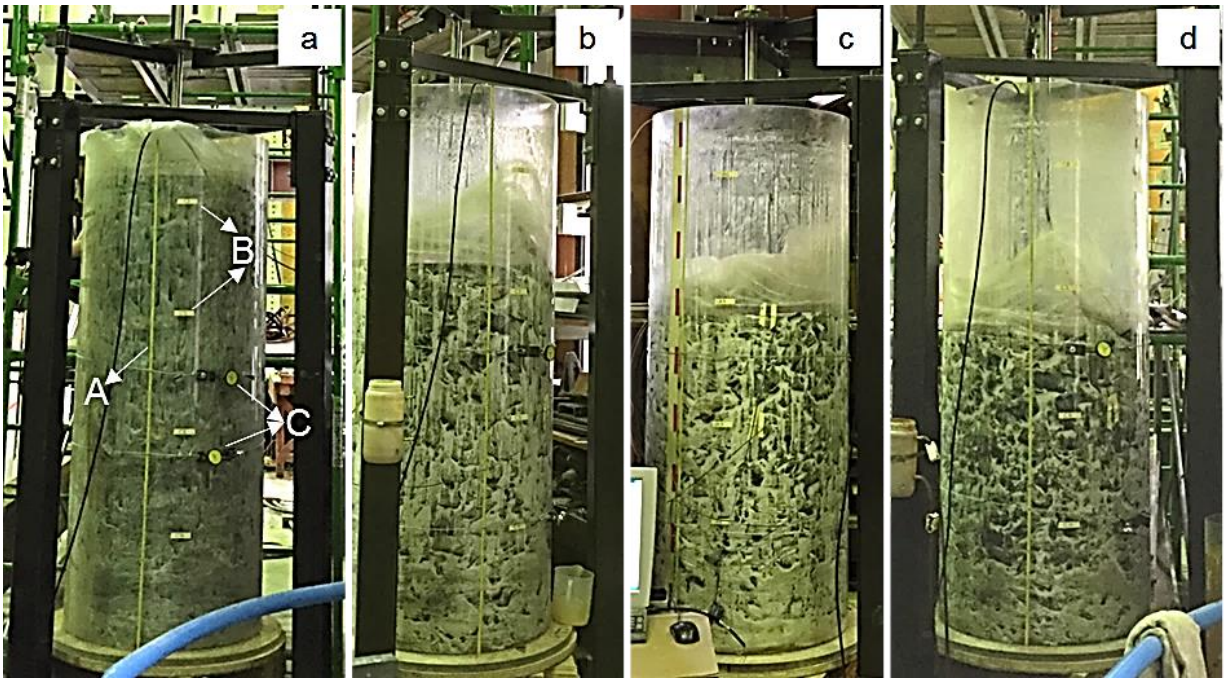

Figure 4-3: Progressive compression of TDA with incremental loading – Sask TDA test 3 shown: (a) only the loading plate on the TDA – less than 2 kPa surface stress. (A) – one of the three measuring tapes spaced 180^o apart glued onto the outside wall of the consolidometer for taking readings, (B) – marker tapes on the outside of the 1D consolidometer to mark the initial

[35] Values presented in Section 4.5.1

positions of the visual markers and the separation of the TDA into sublayers. In this loading event, there were five sublayers, (C) – strain gauges to measure lateral cell pressure for sidewall friction evaluation (see Adesokan et al. 2019[36]); (b) 28 kPa surface stress; (c) 56 kPa surface stress; (d) 112 kPa surface stress.

Figure 4-3 shows the progressive compression of TDA and individual sublayers under increased compressive loading. The four light coloured tapes at different elevations on the outside of the 1D consolidometer indicate the initial positions of the visual markers and separation of the TDA into sublayers. In this loading event, there were five sublayers. The displacement of the visual markers was periodically measured to determine the compression of the individual sublayers. Applied stress in individual sublayers was determined after accounting for sidewall friction loss as presented in Adesokan et al (2019)[37].

Measurement of drainable porosity was completed as quality check for the compression results obtained from reading the displacement of the visual markers. Both filling and draining porosities were measured. Comparative plots of porosity values from drainable porosity and those from the displacement of the visual markers are presented in Figure 4-4.

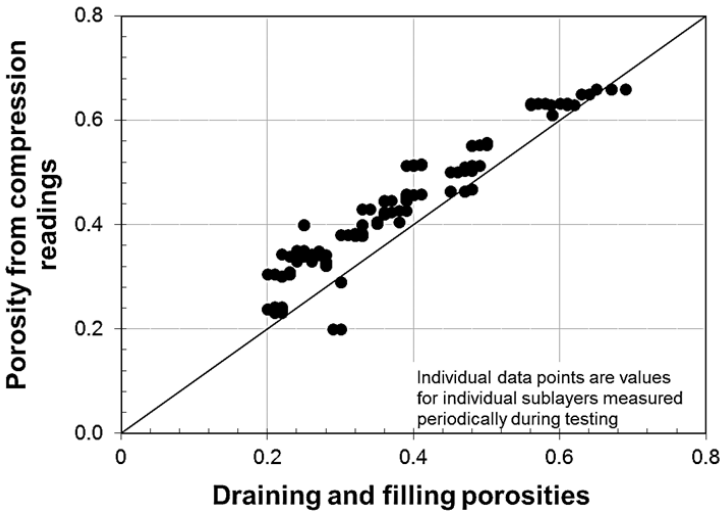

Figure 4-4: Comparative plot of porosity values from compression readings (from the visual markers) and from drainable porosity. Individual points represent corresponding porosity values at the same elapsed time and applied stress. Results for Sask TDA test 3 shown.

[36] Chapter 3
[37] Chapter 3

Figure 4-4 shows a consistency between the porosity values from drainable porosity measurements and those from the compression readings. The drainable porosity values were however generally lower than the porosity values from the compression readings, perhaps because complete saturation was not achieved during the drainable porosity measurements despite leaving the TDA for several hours to days to achieve saturation. Incomplete saturation is a common issue with drainable porosity measurements of TDA, and it typically results in an underestimation of actual porosity values (Hudson et al., 2007; Adesokan et al., 2019[38]).

The issue of incomplete saturation during drainable porosity measurements highlights the benefit of having the means (equipment and methods) for direct measurement of compression readings, such as the use of the transparent 1D consolidometer and the visual markers for tracking compression in the TDA as was used in this study. Nonetheless, in the absence of means for testing, drainable porosity measurements can still provide useful results for evaluations as presented in Figure 4-4.

Having determined the compression results from the displacement of the visual markers to be adequate, these were used throughout the study for void volume/void ratio evaluations. The design of the 1D consolidometer, modifications made to improve its performance, and testing strategies in the consolidometer – including those to account for and reduce sidewall friction loss[39], and those to measure void volume reduction, are presented in Adesokan et al (2019).

4.2.4 Effects of elevated temperature

Two aspects of temperature effects were investigated: (1) how much further void volume reduction would occur if there was surface stress on the TDA before increasing the temperature, and (2) how much compression would occur if the temperature of the TDA was increased before

[38] Chapter 3
[39] Sample plot of applied stress at the top and bottom of the TDA with sidewall treatment 2 is presented in Figure 4-18, Section 4.5.3

increasing the applied surface stress. The effects of elevated temperature was tested in a large steel compression chamber[40] (Figure 4-5), as it was not desirable to elevate the temperature of the acrylic 1D consolidometer (Figures 4-3 and 4-4), while maintaining the applied stress. Although the large steel chamber was a different shape and size, other aspects of that testing, such as the TDA tested, sidewall treatment, load application methods and applied surface stresses were generally similar to those in the acrylic 1D consolidometer.

Figure 4-5: A permeameter and consolidometer unit that was used to evaluate the effects of increased temperature on compression and void volume reduction in TDA under sustained applied stress with heating mat (A) and fiberglass insulation (and plastic to hold insulation in place) wrapped around the test cell (B).

The temperature of the TDA was increased by wrapping heating mats around the test cell and covering these with fibreglass insulation and thin plastic sheeting (Figure 4-5). The heating mats were maintained at a temperature of 58 C for 90 days. Temperature readings were taken within the TDA and in the headspace of the test cell using temperature probes. Compression readings

[40] This cell is further described in Chapter 5, as it was used primarily for the flow testing described in that Chapter

(upon loading and reloading, and relaxation upon unloading) were taken using metre long rulers placed at pre-marked locations on top of the loading plate of the test cell[41].

4.3 Results and discussion

4.3.1 The TDA types

The particle size of the TDA types ranged from a minimum of 50 mm to a maximum of less than 400 mm. The PSD curves of the three TDA types using the length, width, and average d_{eq} values are presented in Figures 4-6 (a – c). The TDA types were largely Type B – per ASTM D6270, although there were a few particles with smaller dimensions than the minimum particle size measured in any direction of a Type B TDA i.e. 75 mm. For all the TDA types, the protruding wires on the individual TDA particles were 25 mm long on less than 75% of the particles and 50 mm long on less than 20%; the loose wire content was less than 1%.

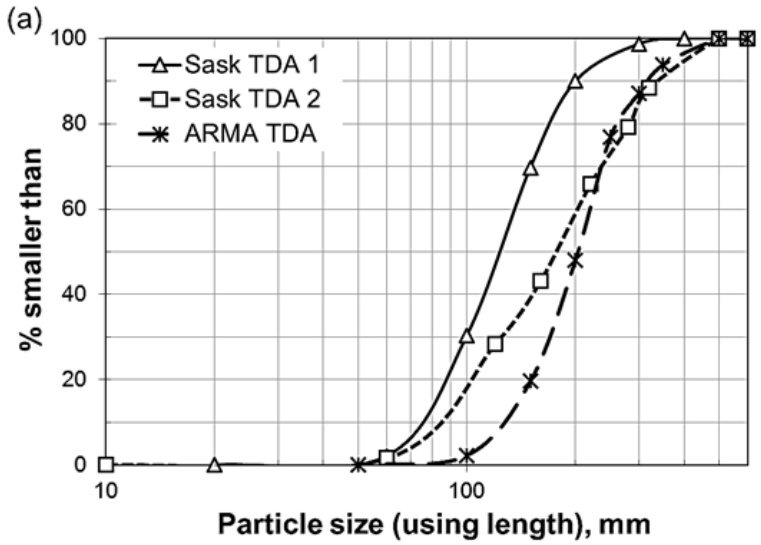

[41] Readings were taken from up to six locations on top of the loading plate (see Figure 5-32, Section 5.6.5). The average of the readings were used to determine compression in the TDA.

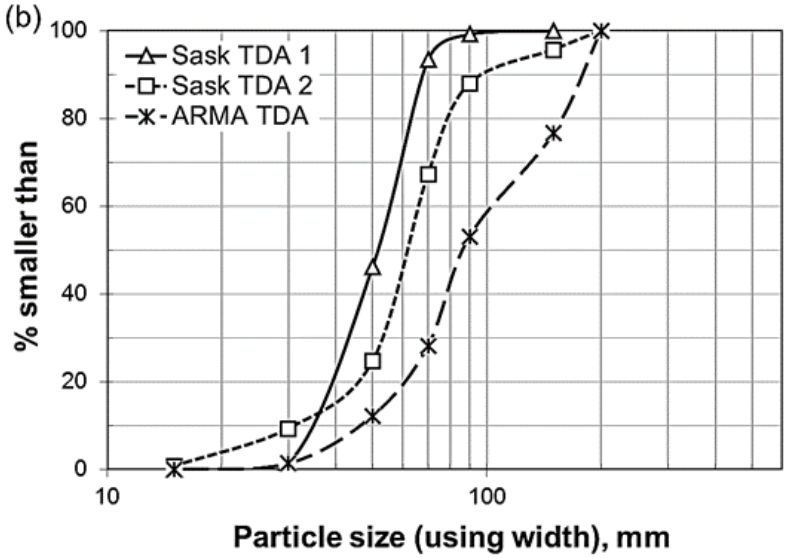

Figure 4-6: Particle size distribution of the TDA types: (a) using longest dimensions – length; (b) using shortest dimensions – width; (c) using average d_{eq} values

The average G_s of each of the TDA types was 1.27, which is in range of high G_s values in the literature (see: Geosyntec 2008). Geosyntec (2008) presented values ranging from 1.02 to 1.27, and noted that the higher values correspond to TDA with embedded wires in them. This was the case with the TDA types used in this work. The tire processing facilities from where the TDA were sourced typically remove the lightweight (high rubber) portions of the tires and recycle them into various new products (such as landscaping products, rubberized paving blocks, pads

and mats), leaving behind the heavier weight (high wire content) portions of the tires for use as TDA. Hence, TDA with relatively high G_s.

4.3.2 Solid volume compression

Following an initial elastic volume compression upon application of pressure, the total water demand in the compression cell from the PV controller was 9.19×10^{-5} ml[42], corresponding to a total creep of 1.3 mm, over more than 90 days at the end of the final applied stress of 200 kPa. Given this minimal amount of creep over the test duration, it appears that volume change in TDA under applied stress is solely from bulk void volume reduction and solid volume compression in individual particles is negligible and can be ignored. Hence, in evaluating void volume reduction in TDA under applied stress, the change in void ratio can be determined directly from the measured change in height within the TDA volume using Eq. 4-2, just as is done conventionally for soils.

4.3.3 Bulk void volume compression

4.3.3.1 Onset of creep

One of the challenges with constrained 1D compression testing of TDA is with managing and accounting for sidewall friction effects – an artefact of such testing (Olson, 1974; Adesokan et al., 2019[43]). Loss of applied surface stresses across the thickness of the TDA, and delayed immediate compression are some of the sidewall friction effects from such testing. Those effects become more prominent as the height to diameter ratio of the test cell increases, as was the case in this study with the 1D consolidometer having a relatively high height to diameter ratio of 2.5. Hence, because of sidewall friction, the sublayers in the consolidometer that were closer to

[42] See plot and data in Chapter 3, Section 3.10.1.
[43] Chapter 3

the applied surface stresses were subjected to higher stresses and higher compression, than the lower sublayers farther away from the stresses (Figure 4-7)[44].

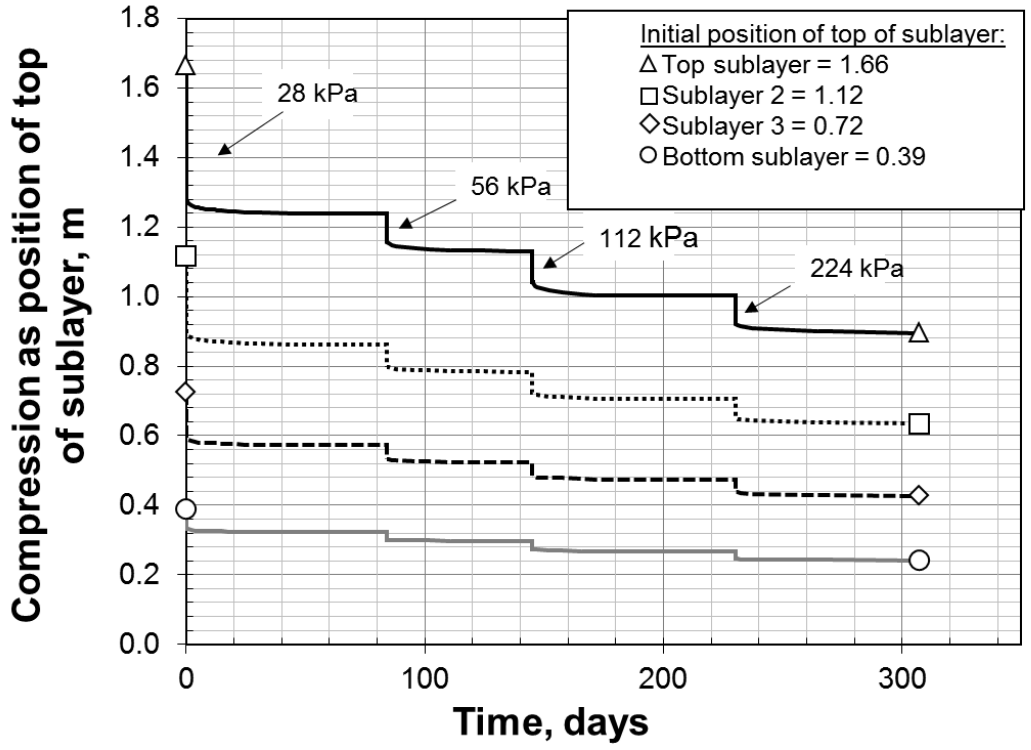

Figure 4-7: A typical compression plot showing temporally varying compression across the sublayers – with relatively higher compression in the upper sublayers than in the lower sublayers, caused by sidewall friction loss. Sask TDA test 3 shown. Sidewall friction loss was accounted for and the actual applied stress reaching each of the sublayers was determined as described in Adesokan et al (2019).

Sidewall friction also caused delayed immediate compression during the various testing events - particularly in the lower sublayers farther away from the applied surface stresses, causing immediate compression to cease sooner in the upper sublayers than in the lower sublayers. Because of this, the end of immediate compression i.e., the onset of creep varied temporally between individual sublayers, as well as with the various applied stress. The extent of delayed immediate compression and the actual onset of creep had to be determined so as not to misrepresent the delayed portions of immediate compression as creep. Delayed immediate

[44] Additional plots for all the testing events are presented in Figure 4-16, Section 4.5.2

compression and the actual onset of creep were determined from the plots of void ratio with log√time that were generated for each sublayer in each testing event and load step (Figure 4-8). The inflection points on the plots were used to identify the values of the end of immediate compression and the onset of creep in each sublayer.

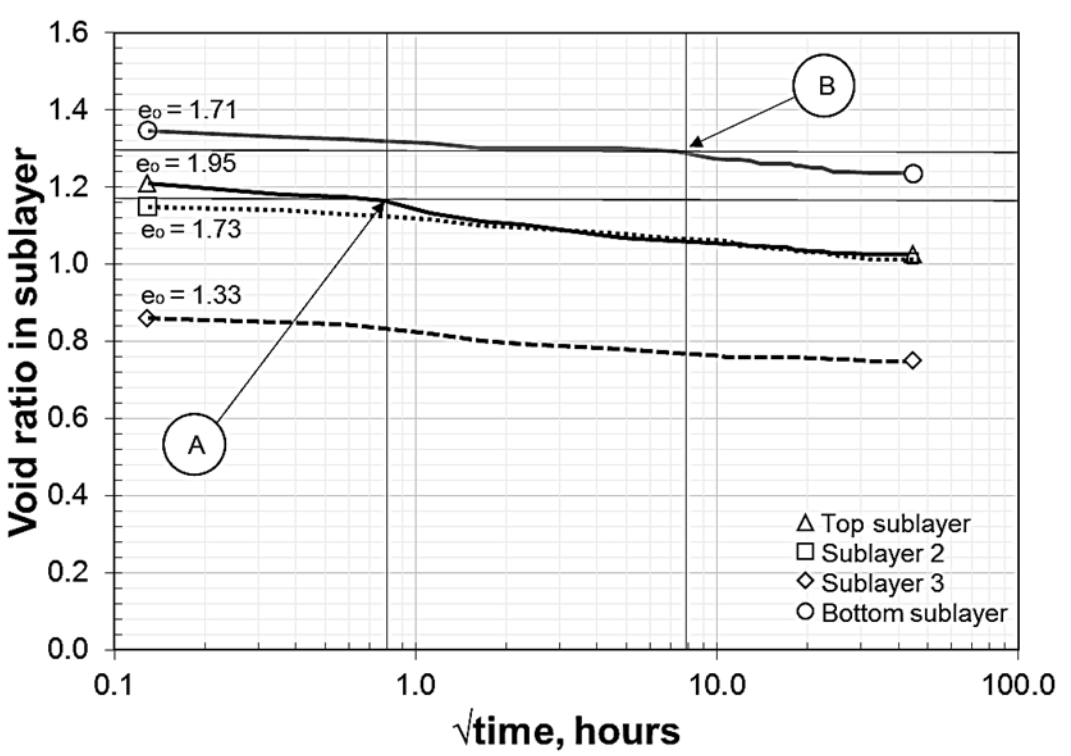

Figure 4-8: Identifying delayed immediate compression and the actual onset of creep in individual sublayers in each testing event. Sask TDA test 3 at 28 kPa from Figure 4-7 shown

For instance, in Figure 4-8, after the initial inflection point (from the initial void ratio (e_0)), at time t=0 (not shown on the log scale) to time t>0 (shown on the plot), any later distinct inflection point, identified by a significant period of no change in void ratio, was taken as the actual onset of creep. Hence, for the top sublayer in Figure 4-8, the actual onset of creep following delayed immediate compression was determined to be 0.6 hours (point A), and 53 hours for the bottom sublayer (point B).

Using the approach in Figure 4-8 the onset of creep was determined for all the sublayers, and void ratio values were determined by converting the compression readings into void ratio, using Eq.4-2. The onset of creep for the various sublayers in the testing events was found to range from less than 1 hour to over 24 hours. The shorter durations were for the upper layers closer to the applied surface stresses and the longer durations were for lower layers farther away from the applied stress.

4.3.3.2 Indexes of immediate compression and creep

Having identified the actual onset of creep, the corresponding void ratios and time for the individual sublayers were used to determine the indexes of immediate compression – C_c, and creep – C_α for each of the sublayers (Figures 4-9 and 4-10)[45], as is done conventionally for municipal solid waste (Qian et al., 2001). The respective C_c and C_α values were estimated as follows:

$$C_c = (\Delta e/\log (\sigma_1/\sigma_0)) \quad (4\text{-}4)$$

$$C_\alpha = (\Delta e/\log (t_1/t_0)) \quad (4\text{-}5)$$

Where

Δe = change in void ratio in the sublayer relative to the applied stress at the midpoint of sublayer;

σ_1 = final applied stress at the midpoint of sublayer;

σ_0 = initial applied stress at the midpoint of the sublayer;

t_1 = ending time of creep;

t_0 = starting time of creep.

The C_c values are presented here in terms of the incremental and cumulative values – $C_{c(i)}$ and $C_{c(c)}$ respectively. Although field loading in practice is cumulative, rather than incremental,

[45] The summary data for the plots are presented in Table 4-2, Section 4.5.3

evaluating both $C_{c(i)}$ and $C_{c(c)}$ provides detailed insight into the compressive behaviour of TDA, as it enables a thorough look into what is going on mechanically within the TDA. To determine $C_{c(i)}$ and $C_{c(c)}$, the following applied stress and void ratio values were calculated for each sublayer and every time step:

- $\sigma_{0\ i,j}$ Applied stress at the midpoint of sublayer i at the end of creep of load step j-1
- $e_{0\ i,j}$ Void ratio of sublayer i at the end of creep of load step j-1, before applying load step j
- $e_{1\ i,j}$ Void ratio of sublayer i at the end of immediate compression in sublayer i, during load step j
- $\sigma_{1\ i,j}$ Applied stress at the midpoint of sublayer i at the end of immediate compression in sublayer i, during load step j
- $e_{2\ i,j}$ Void ratio of sublayer i at the end of creep in sublayer i, during load step j
- $\sigma_{2\ i,j}$ Applied stress at the midpoint of sublayer i at the end of creep in sublayer i, during load step j

Using these, corresponding $C_{c(i)}$ and $C_{c(c)}$ values were determined for each sublayer (Figures 4-9 a and b). Figures 4-9 a and b show a positive relationship between the immediate compression indexes and void ratio, as both the $C_{c(i)}$ and $C_{c(c)}$ values generally increased with the corresponding void ratios. The figures also show substantial variations in C_c values for any value of void ratio, implying that the relationship between void ratio and C_c is not unique, and several factors, including the applied stress and e_0 may determine the value of C_c at any particular void ratio. Immediate compression decreased with the incremental loading, thus lower C_c values with incremental loading.

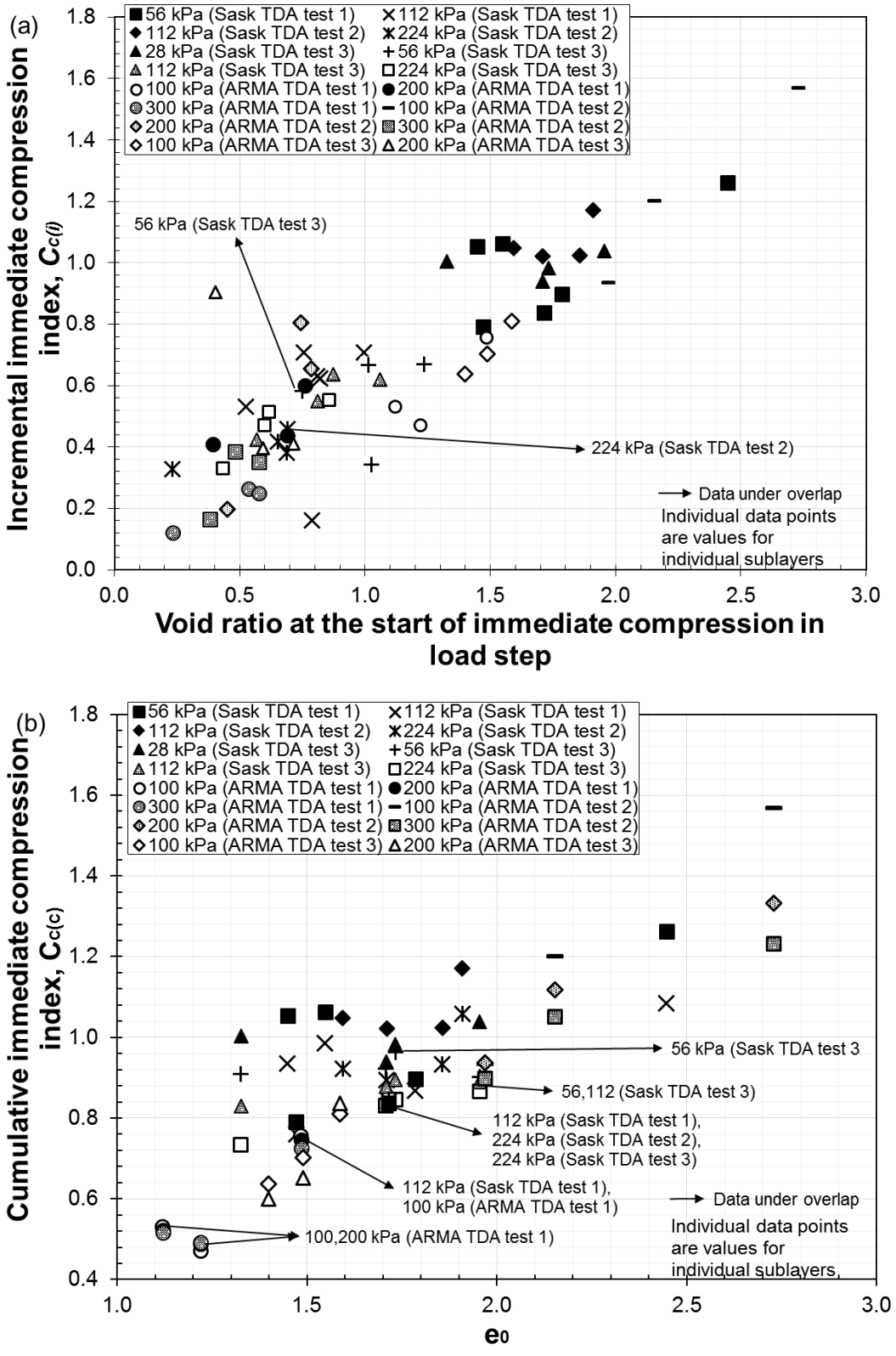

Figure 4-9: Relationship between immediate compression index (C_c) and void ratio (void ratio at the start of immediate compression in load step and e_0) for all the sublayers: (a) incremental C_c and void ratio; (b) cumulative C_c and e_0.

The C_c values in Figures 4-9a and b ranged from 0.12 to 1.57 – for $C_{c(i)}$ and 0.49 to 1.57 – for $C_{c(c)}$. Higher values of C_c indicate higher compression and lower values indicate lower compression. The values of C_c in the literature range from 0.27 to 0.8 for various particle sizes and applied stress (Geosyntec, 2008; Ghawood et al., 2017). It should however be noted that the values in the literature were not separated into C_c and C_α components as is typically done and needed in design calculations for highly compressible materials that may exhibit time dependent compression – such as municipal solid waste (Qian et al., 2001), and adapted here for TDA. Hence, comparison of the values here with those from literature is not entire.

Nonetheless, the values from the literature fall within the range of values presented here, however, some of those values are several times lower than the values here. Particle size, e_0 and applied stress are some of the factors that could influence C_c values in TDA, and higher values of these are expected to contribute to higher values of C_c – as presented in Figure 4-9b, where the $C_{c(c)}$ values increased with e_0. The particle sizes, and applied stress of the values from the literature were generally smaller than in this study – up to 3 times smaller in some cases. These could have in part contributed to the lower C_c values reported.

From Figure 4-10, C_α appeared to increase with the void ratio at the onset of creep; and as with the C_c values, there were considerable variations in the C_α values for any value of void ratio. Again, substantiating the complexities and influences of several factors in the compressive behaviour of TDA. The C_α values in Figure 4-10 range from 0.002 to 0.11. In comparison, Wartman et al (2007) reported a C_α value of 0.0074, which is in the lower end of values reported here. Higher values of C_α indicate higher compression and lower values indicate lower compression.

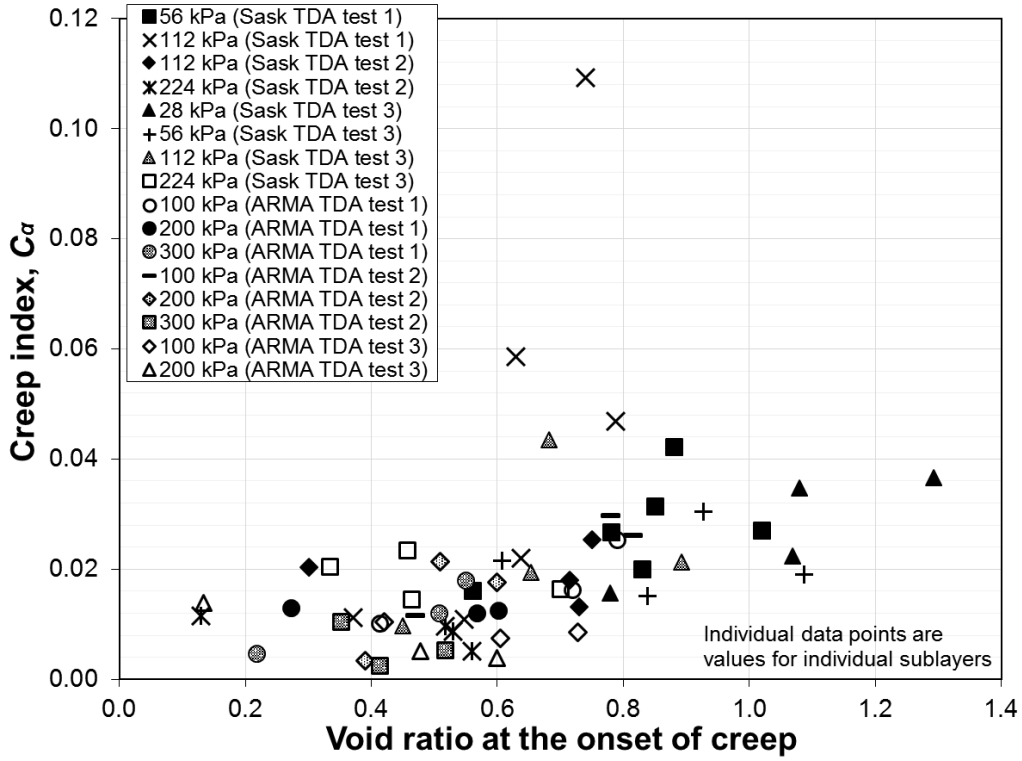

Figure 4-10: Relationship between creep index (C_α) and void ratio for all the sublayers

Factors that could affect C_α values in TDA include the applied stress, particle size, and time (the duration of sustained stresses on TDA for creep); higher values of all these are expected to contribute to higher C_α values. The particle size of TDA in the Wartman study was smaller (up to 6 times smaller) than in this study, the applied stress were lower (approximately 4 times lower), and the duration of creep much shorter – maximum 1 day. All these could have contributed in part to the lower C_c value reported. Plots of void ratio with time for all the TDA sublayers in the six testing events are presented in Figures 4-11 (a – f) (the proximity of the sublayers to the applied surface stress increases from the top sublayer to the bottom sublayer). Keeping e_0 constant within each sublayer for each testing event was very challenging, especially at the beginning for the first few testing events[46]. This however got better with time by trying different

[46] Placing visual markers in the right locations on the TDA for tracking was very difficult. Sometimes there was a need to physically enter into the cell to place the visual markers, which caused compression in lower layers. Also, sometimes, the markers moved out of place during filling of the cell when additional material was placed on top of the marker. This also affected the initial void ratio values.

methods of placing the TDA inside the consolidometer, and of placing the visual markers within the TDA to demarcate the sublayers. For each sublayer in each loading event, upon application of the surface stress, and subsequent increase in stress, there was a large void ratio reduction from immediate compression followed by some further void ratio reduction from creep. Both the immediate compression and creep decreased with incremental loading.

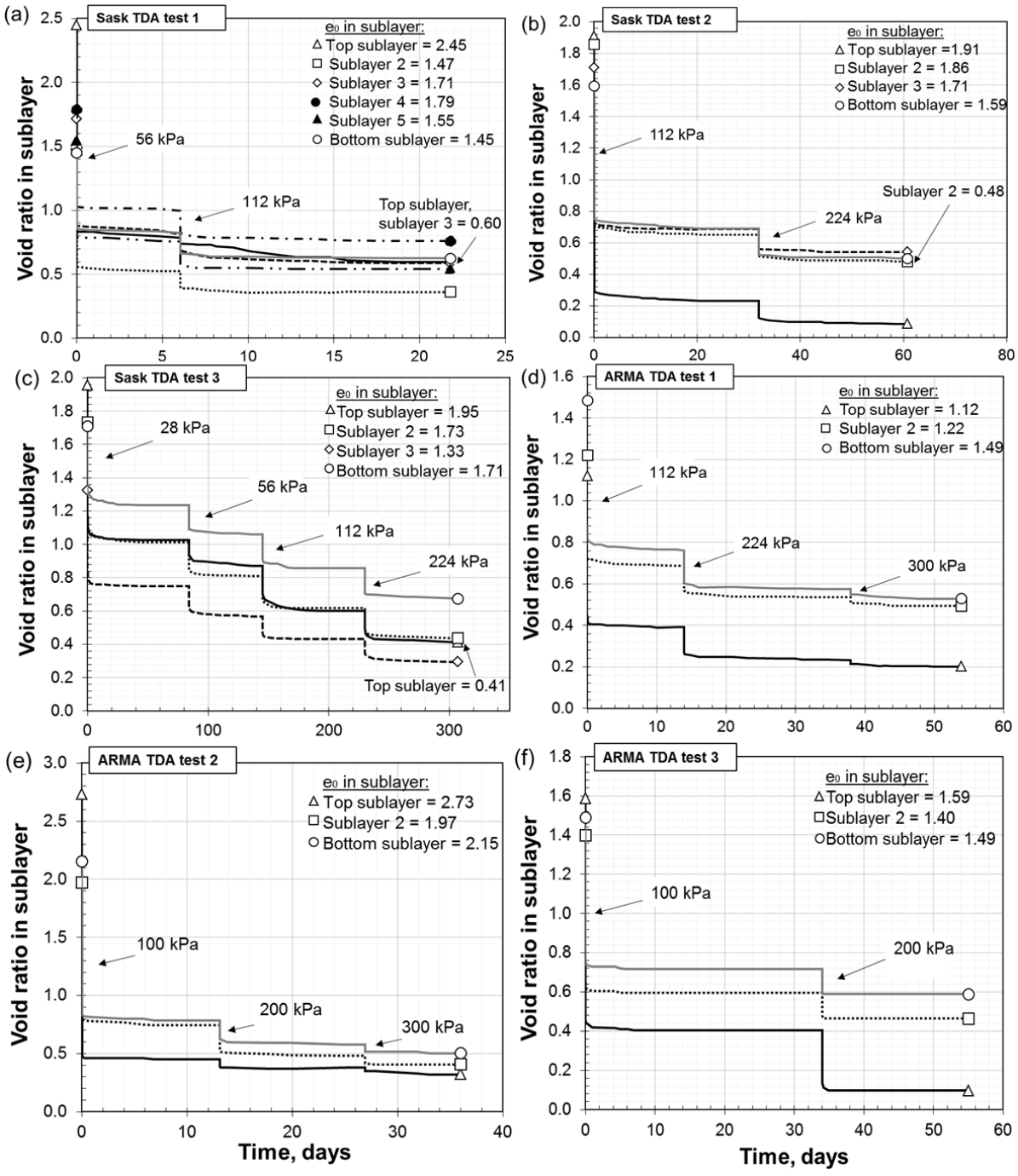

Figure 4-11: Periodic decrease in void ratio in individual sublayers under sustained incremental loading: (a) Sask TDA test 1; (b) Sask TDA test 2; (c) Sask TDA test 3; (d) ARMA TDA test 1; (e) ARMA TDA test 2; (f) ARMA TDA test 3

From Figure 4-11 (c) – the longest duration testing, creep continued for 30 to 60 days across all the sublayers; the longer durations occurred at the applied stress over 100 kPa. Thus, in order to sufficiently capture the contribution of creep to void volume reduction in TDA, applied stress on TDA should be sustained for a minimum of 30 days for lower stresses up to 100 kPa, and a minimum of 60 days for higher stresses over 100 kPa. This is in line with similar recommendations in the literature (such as Tweedie et al. 2007; Geosyntec, 2008).

Across the sublayers (Figures 4-11 (a – f)), the contribution of immediate compression to the total void volume reduction ranged from 71% to 96%, while that of creep ranged from 4% to 29% – the smaller values were mostly for the shorter duration tests at the lower applied stress. Humphrey et al (2000) noted that creep may have contributed an additional 13% to total compression in their field study consisting of a thin layer of small particle sized TDA overlaying a thicker layer of large particle sized TDA.

Although the respective results (in this study and Humphrey et al (2000)) show the contribution of creep to void volume reduction to be considerably lesser than that of immediate compression[47], not accounting for creep, or not allowing sufficient time to capture creep, may result in an underestimation of the total void volume reduction and void space within the TDA. This may consequently result in underestimating TDA void volume for several performance-related considerations, including hydraulic conductivity and biogeochemical clogging.

From (Figures 4-11 (a – f)), across the sublayers, void ratio reduction (from e_0 at the start of testing to the final void ratio at the end of testing) generally increased with e_0 - the higher the

[47] This was the case within the timeframes considered. The contribution may be substantial for longer durations, say 100 years or more

value of e_0, the higher the void ratio reduction, and vice versa. Starting with an initially high e_0 generally resulted in a relatively high final void ratio, but some sublayers, mostly the top sublayers closest to the applied stress deviated from this i.e., those sublayers started with relatively high e_0 but ended with relatively low final void ratios. It is suspected that for those sublayers, the visual markers may have moved out of place during the testing, given their close proximity to the applied surface stresses.

Compressibility (M_v) – the ratio of strain to stress, was determined for each of the sublayers and was found to decrease with incremental applied stress – an indication of strain stiffening with incremental loading (Figures 4-12 a and b). Strain stiffening is a desirable effect in TDA as this indicates that at, and beyond, certain applied stress, further void volume reduction in the TDA may become negligible. Figures 4-12 (a and b) present typical plots of incremental and cumulative compressibility in the sublayers – $M_{v(i)}$ and $M_{v(c)}$ respectively. As with the $C_{c(i)}$ and $C_{c(c)}$values discussed earlier, $M_{v(i)}$ values were determined from the start of a load step in a testing event to the end of the load step, while the $M_{v(c)}$ values were determined from the start of a testing event, cumulatively to the end of the testing event.

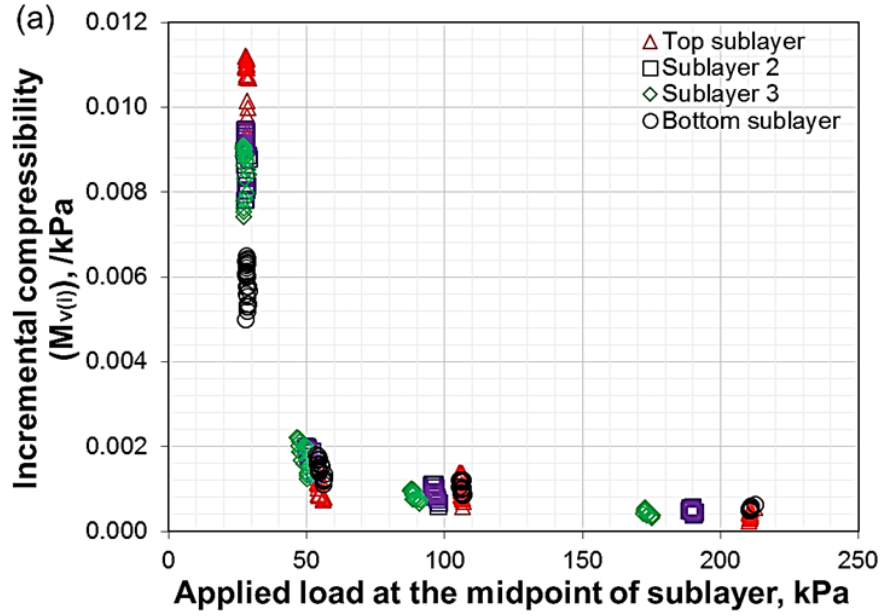

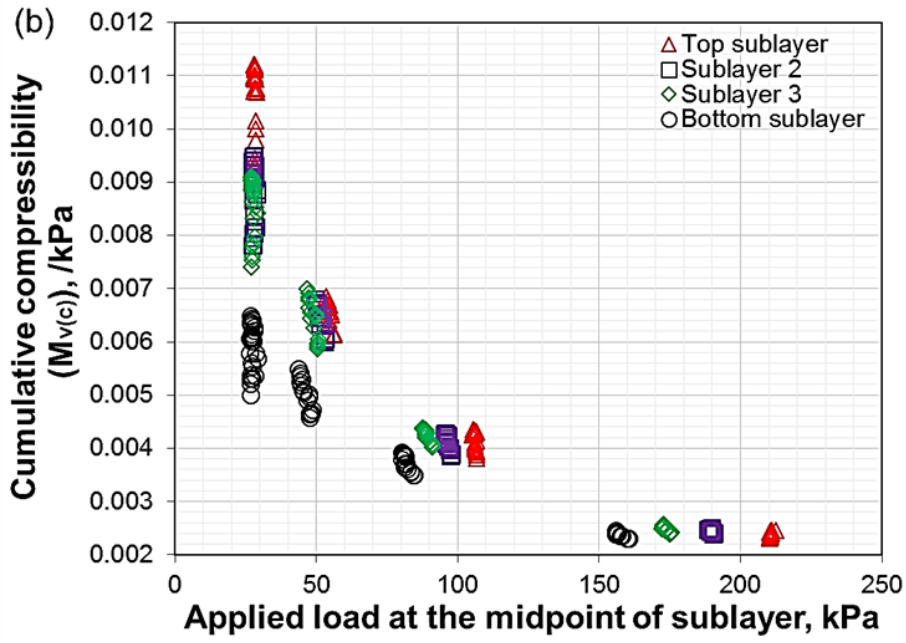

Figure 4-12: Indication of strain stiffening in TDA from plots of compressibility with applied stress – Sask TDA test 3 shown: (a) incremental compressibility with applied stress; (b) cumulative compressibility with applied stress

Conventional e *logP* plots were also generated to further investigate the relationship between void ratio and applied stress in the TDA types (Figures 4-13 (a – f)). The plots also show almost parallel lines, and a wide range of void ratio for any applied stress; implying that there may not be a unique relationship between void ratio in TDA and applied stress, and the final void ratio or void ratio at any applied stress depends partly on the e_0 (as with the C_c and C_α values). The e *logP* plots (Figures 4-13 (a – f)) also further show the void ratio reduction from creep in the individual sublayers at the various applied stress, and with incremental loading.

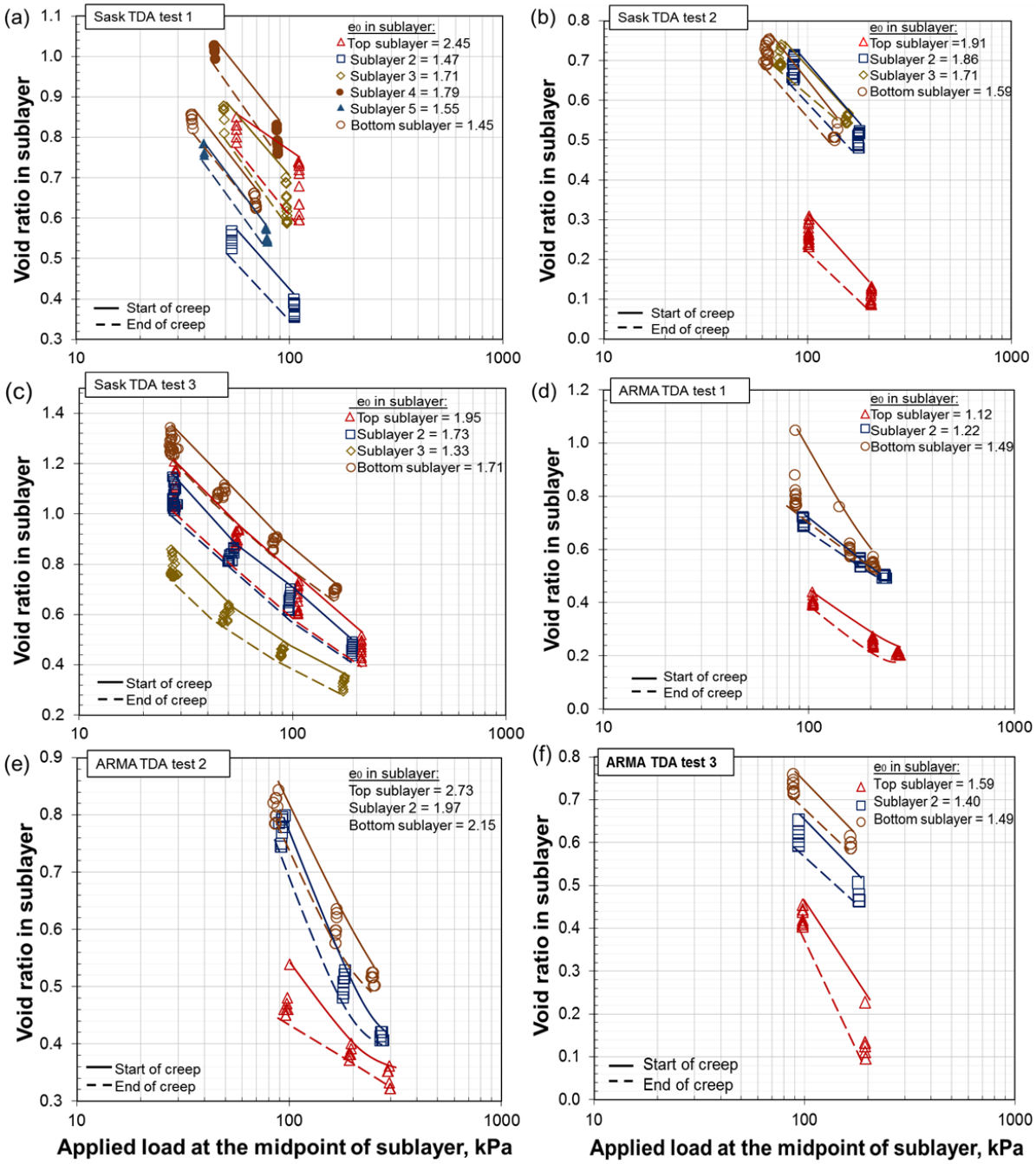

Figure 4-13: Void ratio reduction in the sublayers with applied stress – e logP plots: (a) Sask TDA test 1; (b) Sask TDA test 2; (c) Sask TDA test 3; (d) ARMA TDA test 1; (e) ARMA TDA test 2; (f) ARMA TDA test 3

Across Figures 4-13 (a – f), starting with a high e_0 generally resulted in higher void ratios throughout the testing to the end, compared to starting with a low e_0. Hence, in designing with TDA, placing at a high e_0 may be beneficial for achieving a relatively higher final void ratio than

placing at a lower e_0. Therefore, pre-compressing TDA before use may not be beneficial for maintaining the desired large void volume under applied stress in service as this reduces the e_0 at placement, and consequently may decrease the final void ratio under applied stress.

4.3.3.3 Effects of loading rate

The effect of loading rate was indicated from the analysis of data for the same TDA type with similar initial void ratios and applied stresses. For instance, from Figure 4-14 – for the top layers of Sask TDA test 2 and Sask TDA test 3, at similar e_0 values, Sask TDA test 3 had a slightly higher void ratio than Sask TDA test 2 at the final applied stress of 224 kPa.

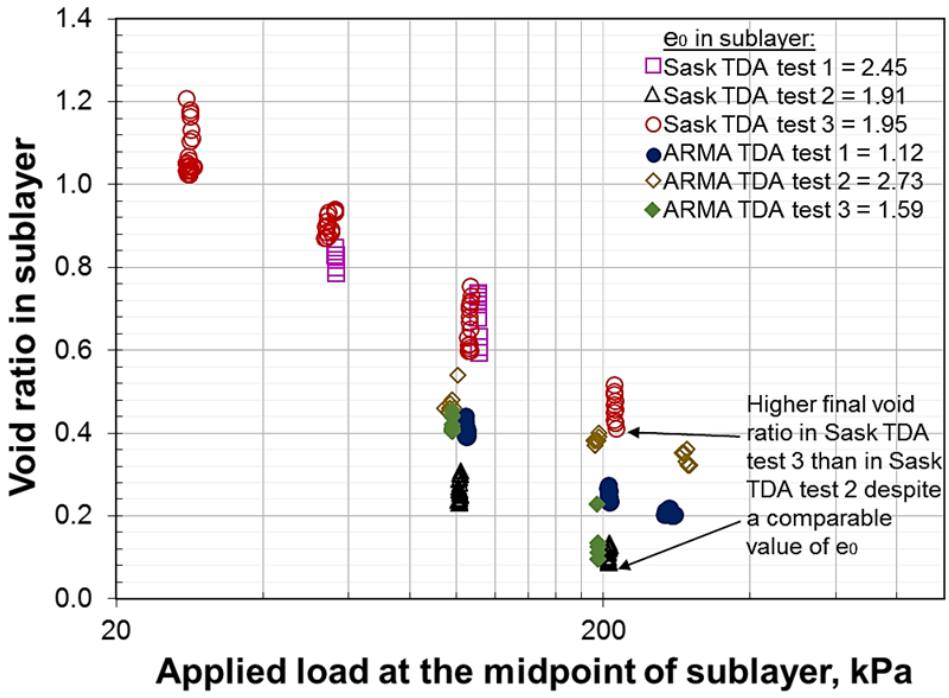

Figure 4-14: Indications that loading rate may have some control on the compressive behaviour of TDA – e logP *plots of the top sublayers of all the tests shown. (Loading rate was not measured in these testing events, but qualitatively inferred based on the increments of the applied stress. For instance, slow loading rate was inferred for smaller stress increments such as Sask TDA test 3, and fast loading rate inferred for larger stress increments such as Sask TDA test 2).*

Although the same TDA type, the two testing events differed in the loading increments to the final applied surface stress. For Sask TDA test 2, an initial surface stress of 112 kPa was applied, followed by an increase to 224 kPa (inferred as a fast loading rate), relative to Sask

TDA test 3 – where an initial surface stress of 28 kPa was applied, followed by smaller stress increments to 224 kPa (inferred as a slow loading rate). Those indications prompted further investigation into the effects of loading rate on the compressive behaviour of TDA. It was hypothesized that loading rate might represent a significant control on the final void ratio, and accordingly, two supplementary compression tests involving quick and slow loading were completed to investigate this using the same TDA type, set up at the same e_0 value of 1.8 (Figures 4-15 a and b).

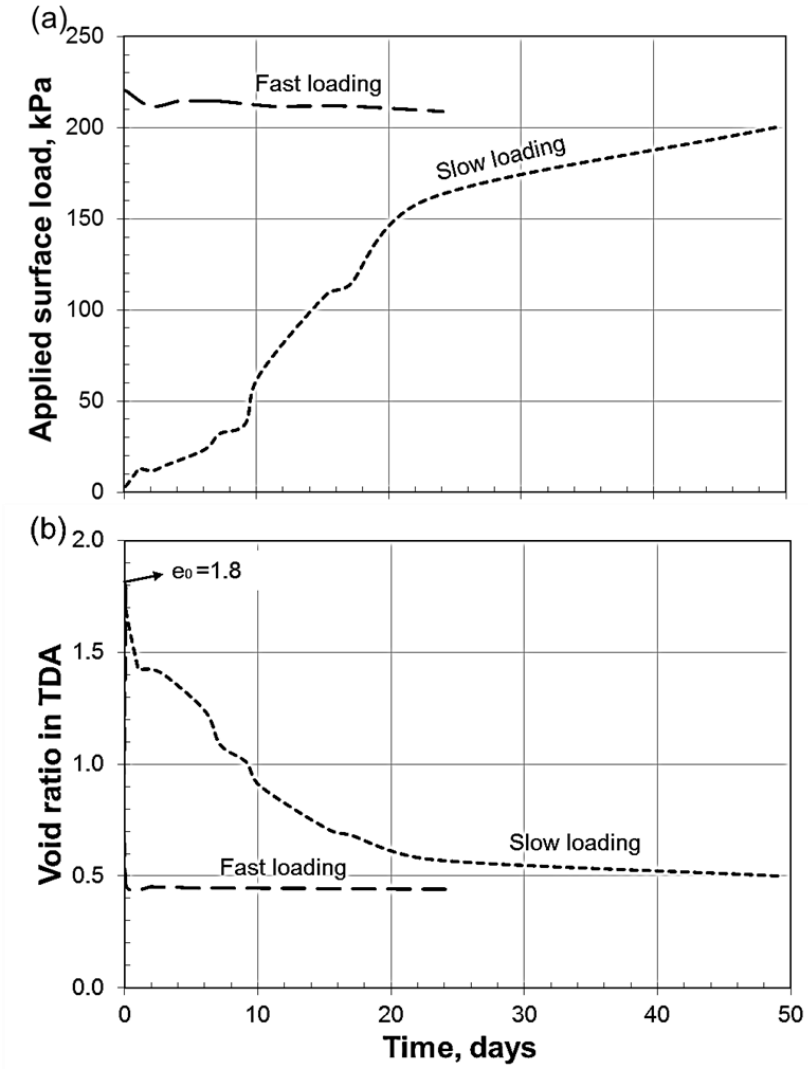

Figure 4-15: (a) Periodic increase in applied stress for fast and slow loading (the fluctuations in the applied surface stresses are from fluctuations in the building air pressure going into the air bellows, as well as imperfections with the precision of the air regulators used); (b) periodic decrease in void ratio for fast and slow loading

The results showed slightly lesser effects of loading rate on the final void ratio than had been observed initially with the Sask TDA tests 2 and 3. Both the fast and slow loading rates resulted in very similar final void ratios at the end of testing. For the slow loading, the final void ratio was 0.5 at a final applied stress of 200 kPa, while for the fast loading; the final void ratio was approximately 0.4 at an applied stress of 209 kPa. These results thus indicate that the effects of loading rate on TDA may be minimal. That minimal effect may not be significant for hydraulic conductivity concerns, but may be beneficial for pore volume considerations to store biogeochemical clog in a TDA drainage layer in a waste disposal facility. Hence, ultimately, it may be better to apply stresses to TDA in smaller stress increments, as opposed to applying larger stress increments.

4.3.3.4 Effects of increased temperature

For the first aspect of the effects of temperature investigation (up to 58 C – Section 4.2.4), no further compression was observed in the TDA after heating it up for 90 days. Similarly, for the second aspect, after unloading to 224 kPa and reloading to 375 kPa, no additional strain was observed. The observed strain was perfectly elastic as the TDA returned to its original position at the 375 kPa load step. No effects of the increased temperature was found, which is not very surprising given that rubber tires only start to thermally degrade and loose some volatile organics at a temperatures over 200 C (Williams and Besler, 1995; Seidelt et al., 2006).

4.4 Conclusions and implications for practice

Immediate compression and creep in larger particle sized TDA – with the longest dimensions greater than 50 mm, under sustained applied stress were studied. Several variables relating to the use of TDA in practice were considered in the testing and in the evaluation of the findings. The findings presented in this article are expected to improve the understanding of TDA for use in LCRS and all other applications under large sustained compressive stresses. The conclusions arrived at and their implications for practice are as follows:

- There is a need for size specific testing of TDA using particle sizes that are appropriate for an application, in order to prevent errors in estimating field performance under applied stress;
- There appears to be no volumetric strain in individual TDA particles and any compression and resulting decrease in void ratio in TDA under applied stress is essentially from the reduction of the bulk void volume within the TDA mass;
- Compressive creep contributes to void volume reduction in TDA, but its contribution is considerably lesser than that of immediate compression. Nonetheless, it is important to account for creep in TDA in order to estimate its potential effects on other performance related aspects of TDA – such as hydraulic conductivity and biogeochemical clogging.
- Pre-compressing TDA before use may not be beneficial for maintaining a large void volume under applied stress in service as the void ratio achieved at a particular stress appears to depend on the e_0;
- Strain stiffening in TDA with increased loading was observed. This is a desirable effect as it indicates that at or beyond certain applied stress, additional or incremental void volume reduction may become negligible;
- There appears to be no unique relationship between applied stress and void ratio in TDA as indicated by the considerable variation in void ratio for any applied stress, and in C_c and C_α values for any value of void ratio;
- The effect of loading rate on the final void ratio appears to be minimal. This minimal effect may not be tangible for hydraulic conductivity concerns, but may be tangible for pore volume to store biogeochemical clog in a TDA drainage layer in a waste disposal facility. Hence, there may be some benefit to slowly applying stress to TDA;

- No effects of elevated temperature, up to 58 C, was observed on compression, creep and void volume reduction in the TDA. In general, any softening of individual TDA particles that could influence bulk void volume reduction is not expected at temperatures below 200 C – the temperature at which rubber tires typically start to thermally degrade and loose some volatile organics.

4.5 Supplementary data for chapter

4.5.1 Initial measurements in sublayers for the determination of initial void ratio

As discussed in Section 4.2.3, presented in Table 4-1 are the initial measurements in individual sublayers for the determination of initial void ratio.

Table 4-1: Initial measurements in individual sublayers

Internal diameter of consolidometer (cell)		0.698	m	G_s measured	1.27		
Internal area of cell		0.383	m^2				
Sublayer ID	Description of sublayer	Mass of TDA in sublayer (kg)	Initial height of sublayer from bottom of cell (m)	Initial height of TDA in sublayer (H_0), m [A]	Initial height of solids in sublayer (H_s), m [B]	Initial void ratio in sublayer e_0 [A-B/B]	Initial dry unit weight of TDA in sublayer (γ_{dry})
Bottom sublayer	Bottom of cell to marker 5	87.4	0.44	0.44	0.18	1.45	5.08
Sublayer 5	Marker 5 to marker 4	50.6	0.71	0.26	0.10	1.55	4.98
Sublayer 4	Marker 4 to marker 3	58.5	1.04	0.34	0.12	1.79	4.40
Sublayer 3	Marker 3 to marker 2	43.0	1.28	0.24	0.09	1.71	4.58
Sublayer 2	Marker 2 to marker 1	49.2	1.53	0.25	0.10	1.47	5.04
Top sublayer	Marker 1 to top of TDA	12.7	1.62	0.09	0.03	2.45	3.61
Bottom sublayer	Bottom of cell to marker 4	60	0.32	0.32	0.12	1.59	4.80
Sublayer 3	Marker 4 to marker 3	70	0.71	0.39	0.14	1.71	4.59
Sublayer 2	Marker 3 to marker 2	60	1.06	0.35	0.12	1.86	4.36
Top sublayer	Marker 2 to top marker	120	1.78	0.72	0.25	1.91	4.28
Bottom sublayer	Bottom of cell to marker 4	70	0.39	0.39	0.14	1.71	4.60
Sublayer 3	Marker 4 to marker 3	70	0.72	0.33	0.14	1.33	5.35

Sublayer 2	Marker 3 to marker 2	70	1.12	0.39	0.14	1.73	4.55
Top sublayer	Marker 2 to top marker	90	1.66	0.55	0.19	1.95	4.21
Bottom sublayer	Bottom of cell to marker 3	83.4	0.43	0.43	0.17	1.49	5.01
Sublayer 2	Marker 3 to marker 2	89.7	0.84	0.41	0.18	1.22	5.61
Top sublayer	Marker 2 to top marker	164.9	1.55	0.72	0.34	1.12	5.87
Bottom sublayer	Bottom of cell to marker 3	65.4	0.42	0.42	0.13	2.15	3.95
Sublayer 2	Marker 3 to marker 2	71.9	0.86	0.44	0.15	1.97	4.19
Top sublayer	Marker 2 to top marker	49.3	1.24	0.38	0.10	2.73	3.34
Bottom sublayer	Bottom of cell to marker 3	74.2	0.38	0.38	0.15	1.49	5.00
Sublayer 2	Marker 3 to marker 2	71.3	0.73	0.35	0.15	1.40	5.19
Top sublayer	Marker 2 to top marker	60.5	1.05	0.32	0.12	1.59	4.81

4.5.2 Additional plots of immediate compression and creep

As discussed in Section 4.3.3, presented in Figure 4-16 are the immediate compression and creep plots for the TDA types and testing events.

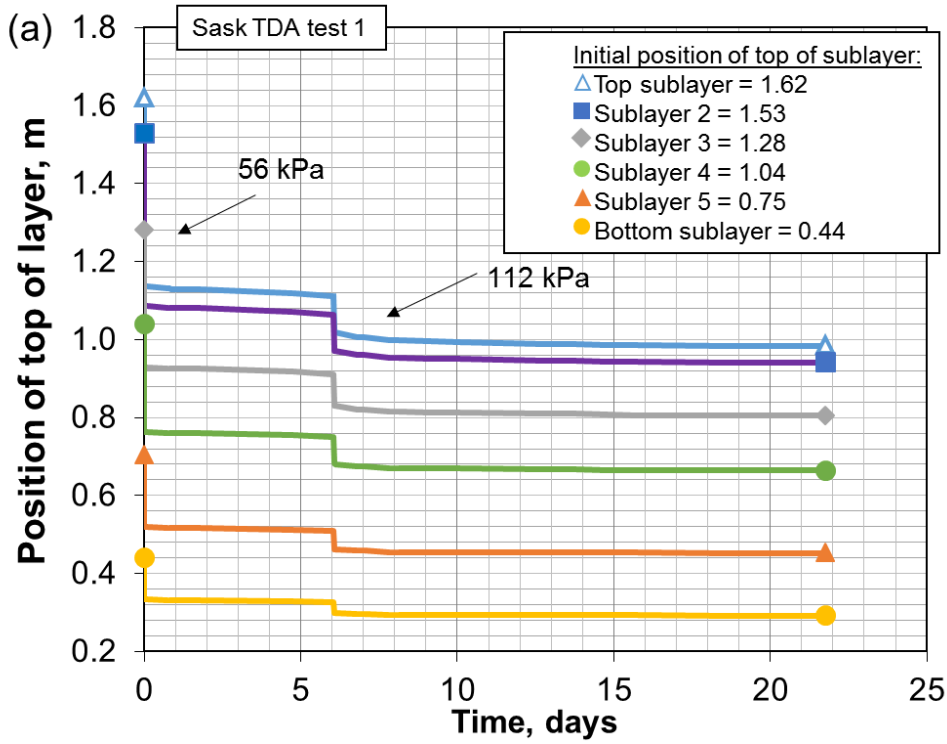

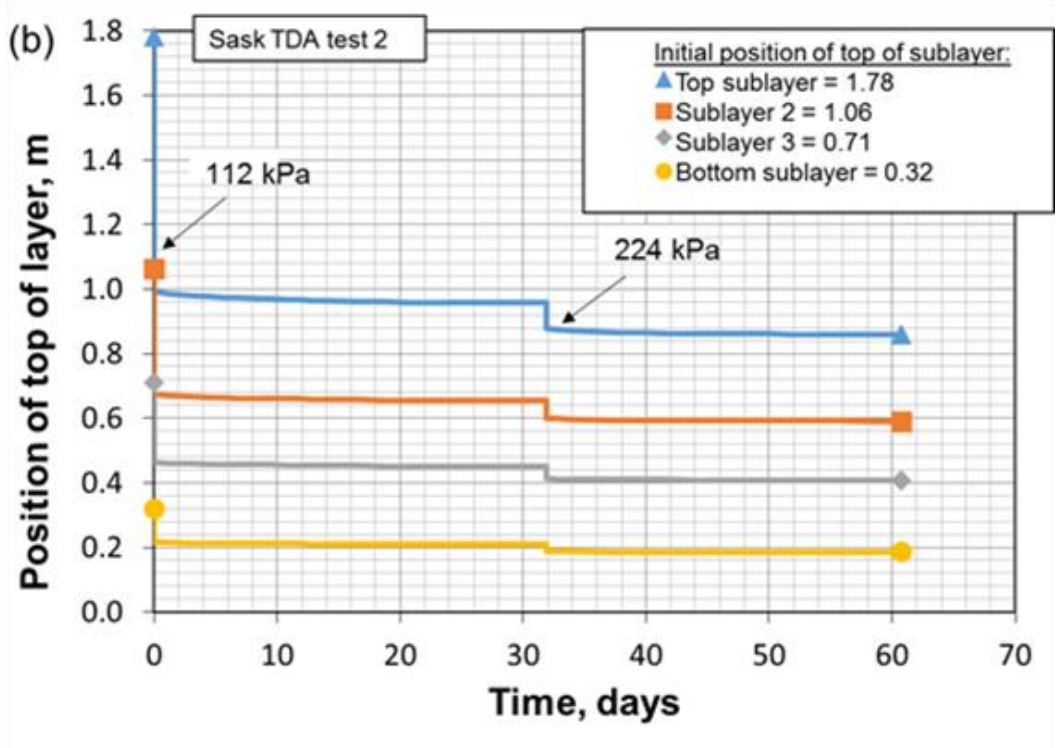
(b)
Sask TDA test 2
Initial position of top of sublayer:
Top sublayer = 1.78
Sublayer 2 = 1.06
Sublayer 3 = 0.71
Bottom sublayer = 0.32
112 kPa
224 kPa
Position of top of layer, m
Time, days
0.0
0.2
0.4
0.6
0.8
1.0
1.2
1.4
1.6
1.8
0
10
20
30
40
50
60
70

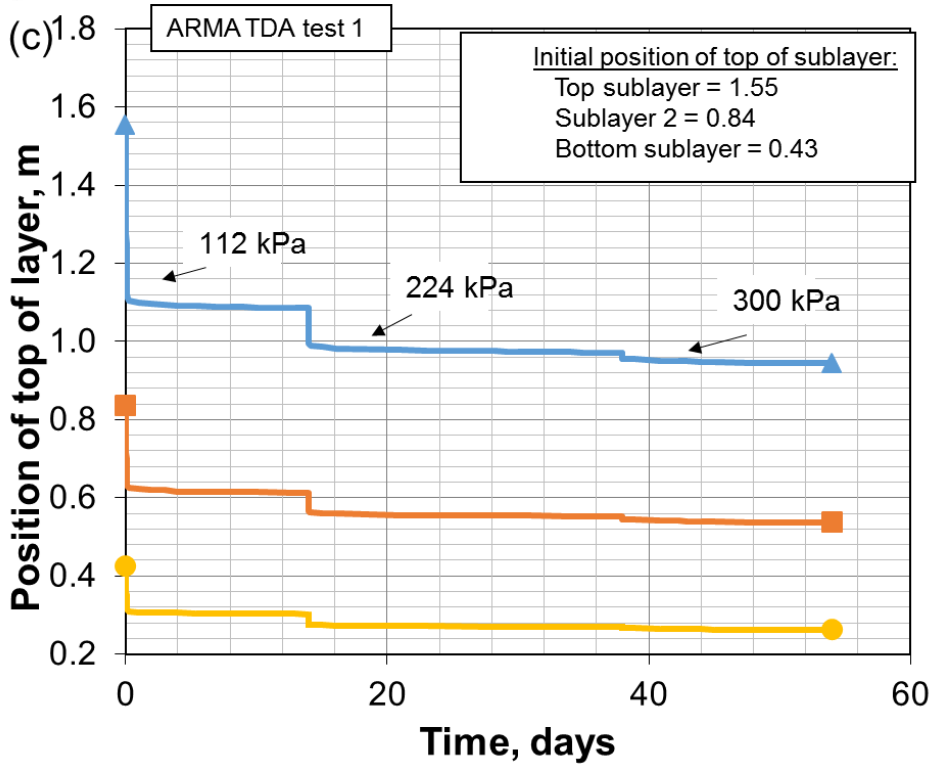
(c)
ARMA TDA test 1
Initial position of top of sublayer:
Top sublayer = 1.55
Sublayer 2 = 0.84
Bottom sublayer = 0.43
112 kPa
224 kPa
300 kPa
Position of top of layer, m
Time, days
0.2
0.4
0.6
0.8
1.0
1.2
1.4
1.6
1.8
0
20
40
60

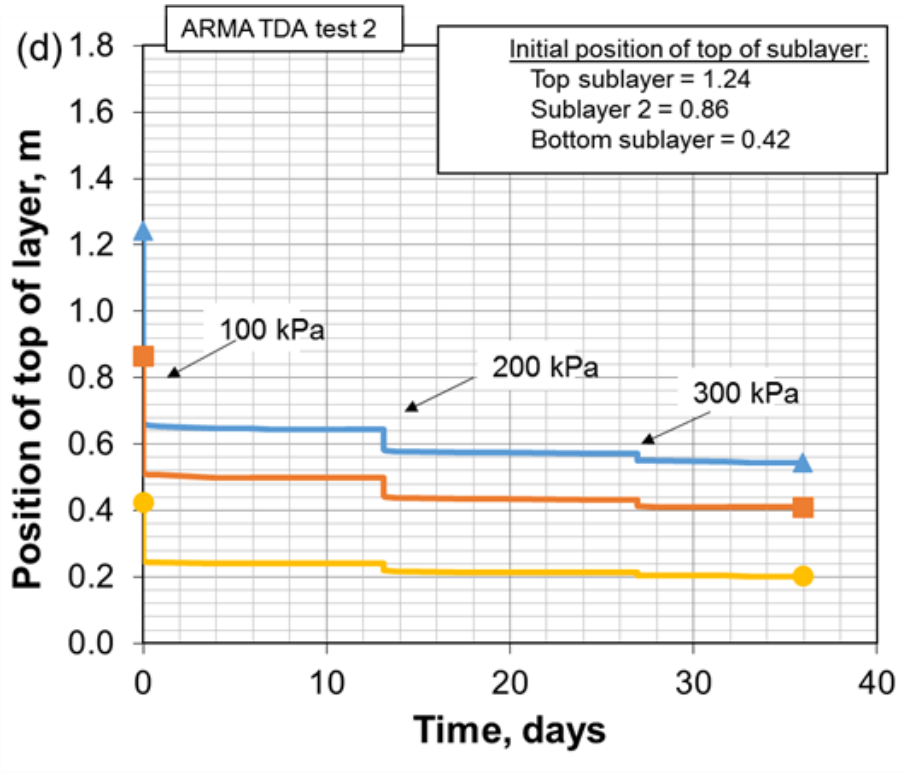

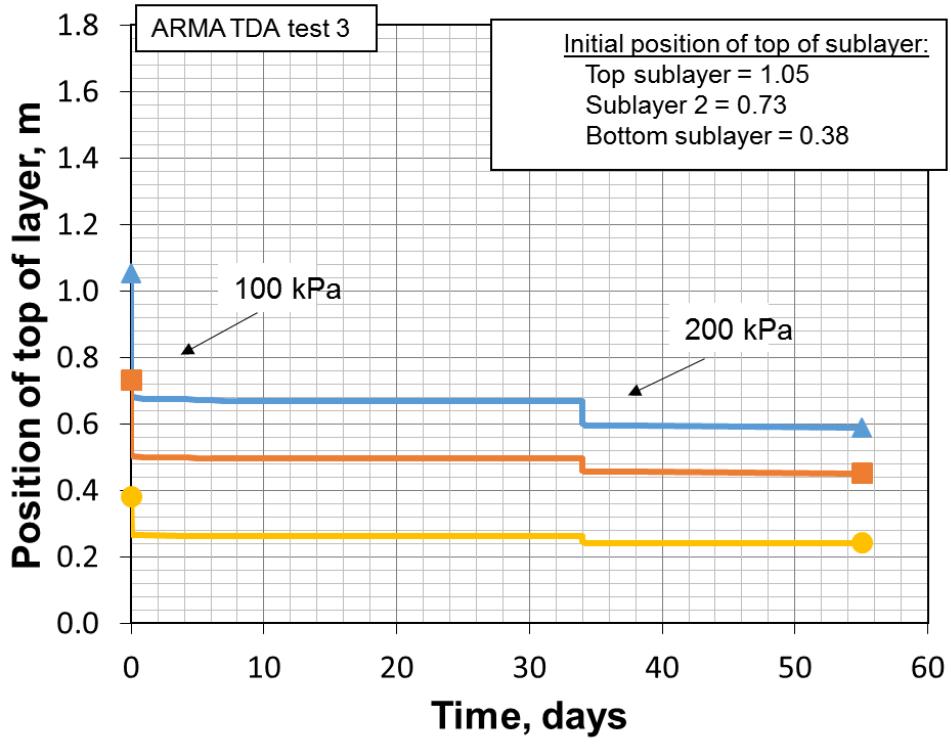

Figure 4-16: Immediate compression and creep plots for the TDA types and testing events

4.5.3 Summary compression data for all testing completed in the 1D consolidometer

From Section 4.3.3.2, presented in Table 4-2 are the summary compression data for the testing completed in the 1D cell. Values here were used to determine the C_c and C_α values in Figures 4-9 and 4-10 (Section 4.3.3.2), and the compression % plot in Figure 4-17. Sample applied load/stress at the top and bottom of the TDA are presented in Figure 4-18.

Table 4-2: Summary compression data for testing completed in the 1D cell. Values here were used to determine the C_c and C_α values in Section 4.3.3.2, and the compression % (Figure 4-17). Full compression data is available in electronic format.

TDA type	Sublayer ID	Applied surface stress, kPa	Applied stress at the midpoint of sublayer before immediate compression in load step, kPa	Applied stress at the midpoint of sublayer at the end of immediate compression in load step, kPa	Applied stress at the midpoint of sublayer at the end of creep in load step, kPa	Void ratio before immediate compression in load step (initial void ratio in load step)	Void ratio at the end of immediate compression in load step	Void ratio at the end of creep in load step	Cumulative compression in testing event ($\Delta e/1+e_0$)*100, using void ratio in sublayer at the start and end of testing), %
Sask TDA 1 - test 1	Sublayer 1	56	2.90	56.30	56.32	2.45	0.83	0.79	48.07
	Sublayer 2		3.70	53.30	53.48	1.47	0.60	0.53	38.10
	Sublayer 3		4.90	49.10	49.33	1.71	0.87	0.81	33.33
	Sublayer 4		6.20	44.20	44.51	1.83	1.02	1.00	29.25
	Sublayer 5		7.60	39.60	39.92	1.50	0.78	0.76	29.58
	Sublayer 6		9.40	34.70	35.02	1.45	0.85	0.82	25.68
	Sublayer 1	112	56.32	110.61	110.67	0.79	0.68	0.60	53.70
	Sublayer 2		53.48	104.90	105.15	0.53	0.37	0.36	44.97
	Sublayer 3		49.33	96.80	97.12	0.81	0.62	0.59	41.53
	Sublayer 4		44.51	87.53	87.83	1.00	0.79	0.76	37.75
	Sublayer 5		39.92	78.61	78.97	0.76	0.55	0.54	38.33
	Sublayer 6		35.02	69.02	69.40	0.82	0.64	0.63	33.64
Sask TDA 2 -test 2	Sublayer 1	112	4.30	101.52	101.14	4.28	0.30	0.23	76.67
	Sublayer 2		6.60	85.76	84.94	4.36	0.71	0.65	69.18
	Sublayer 3		8.20	74.50	72.84	4.59	0.73	0.69	69.81
	Sublayer 4		9.80	62.40	62.36	4.80	0.75	0.69	70.85
	Sublayer 1	224	101.14	205.98	205.68	0.23	0.13	0.09	79.41
	Sublayer 2		84.94	179.03	178.55	0.65	0.52	0.48	72.38
	Sublayer 3		72.84	158.12	157.26	0.69	0.56	0.54	72.42
	Sublayer 4		62.36	139.54	138.41	0.69	0.53	0.50	74.13
Sask TDA 2 -test 3	Sublayer 1	28	3.90	28.01	28.25	1.95	1.07	1.02	31.46
	Sublayer 2		6.00	27.58	27.81	1.73	1.08	1.01	26.36

	Sublayer 3		7.80	27.24	27.45	1.33	0.78	0.75	24.80
	Sublayer 4		9.60	26.40	27.08	1.71	1.29	1.24	17.45
	Sublayer 1	56	28.25	54.20	53.50	1.02	0.93	0.87	36.64
	Sublayer 2		27.81	50.70	49.50	1.01	0.84	0.81	33.74
	Sublayer 3		27.45	48.00	46.60	0.75	0.61	0.57	32.57
	Sublayer 4		27.08	45.10	43.50	1.24	1.09	1.06	23.96
	Sublayer 1	112	53.50	106.00	105.40	0.87	0.68	0.60	45.85
	Sublayer 2		49.50	95.90	95.70	0.81	0.65	0.62	40.84
	Sublayer 3		46.60	88.40	88.30	0.57	0.45	0.43	38.46
	Sublayer 4		43.50	81.00	81.00	1.06	0.89	0.86	31.38
	Sublayer 1	224	105.40	211.10	212.40	0.60	0.46	0.41	52.21
	Sublayer 2		95.70	189.90	189.80	0.62	0.46	0.44	47.46
	Sublayer 3		88.30	173.80	172.60	0.43	0.33	0.30	44.31
	Sublayer 4		81.00	155.80	155.70	0.86	0.70	0.68	38.14
ARMA TDA - test 1	Sublayer 1	112	4.90	104.60	104.10	1.12	0.41	0.39	34.37
	Sublayer 2		8.10	94.00	93.40	1.22	0.72	0.69	23.90
	Sublayer 3		10.40	85.60	85.80	1.49	0.79	0.76	29.13
	Sublayer 1	224	104.10	205.00	205.60	0.39	0.27	0.23	41.91
	Sublayer 2		93.40	176.70	178.00	0.69	0.57	0.54	30.75
	Sublayer 3		85.80	157.90	158.80	0.76	0.60	0.58	36.62
	Sublayer 1	300	205.60	273.60	278.00	0.23	0.22	0.20	43.33
	Sublayer 2		178.00	228.10	236.70	0.54	0.51	0.49	32.69
	Sublayer 3		158.80	201.00	208.50	0.58	0.55	0.53	38.51
ARMA TDA - test 2	Sublayer 1	100	3.40	94.00	96.10	2.73	0.47	0.45	61.12
	Sublayer 2		5.00	93.70	91.30	1.97	0.78	0.75	41.25
	Sublayer 3		6.70	87.80	85.70	2.15	0.82	0.79	43.33
	Sublayer 1	200	96.10	194.80	191.40	0.45	0.39	0.38	62.97
	Sublayer 2		91.30	179.60	178.60	0.75	0.51	0.48	50.10
	Sublayer 3		85.70	165.00	164.30	0.79	0.60	0.58	49.94
	Sublayer 1	300	191.40	290.10	300.70	0.38	0.35	0.32	64.55
	Sublayer 2		178.60	267.60	277.20	0.48	0.41	0.41	52.63
	Sublayer 3		164.30	243.00	251.60	0.58	0.52	0.50	52.32
ARMA TDA - test 3	Sublayer 1	100	3.60	97.60	97.60	1.59	0.42	0.40	45.71
	Sublayer 2		5.20	92.10	92.10	1.40	0.61	0.59	33.56
	Sublayer 3		7.10	85.80	86.00	1.49	0.73	0.72	31.10
	Sublayer 1	200	97.60	194.40	194.60	0.40	0.13	0.10	57.62
	Sublayer 2		92.10	180.80	181.20	0.59	0.48	0.46	38.97
	Sublayer 3		86.00	164.70	165.40	0.72	0.60	0.59	36.16

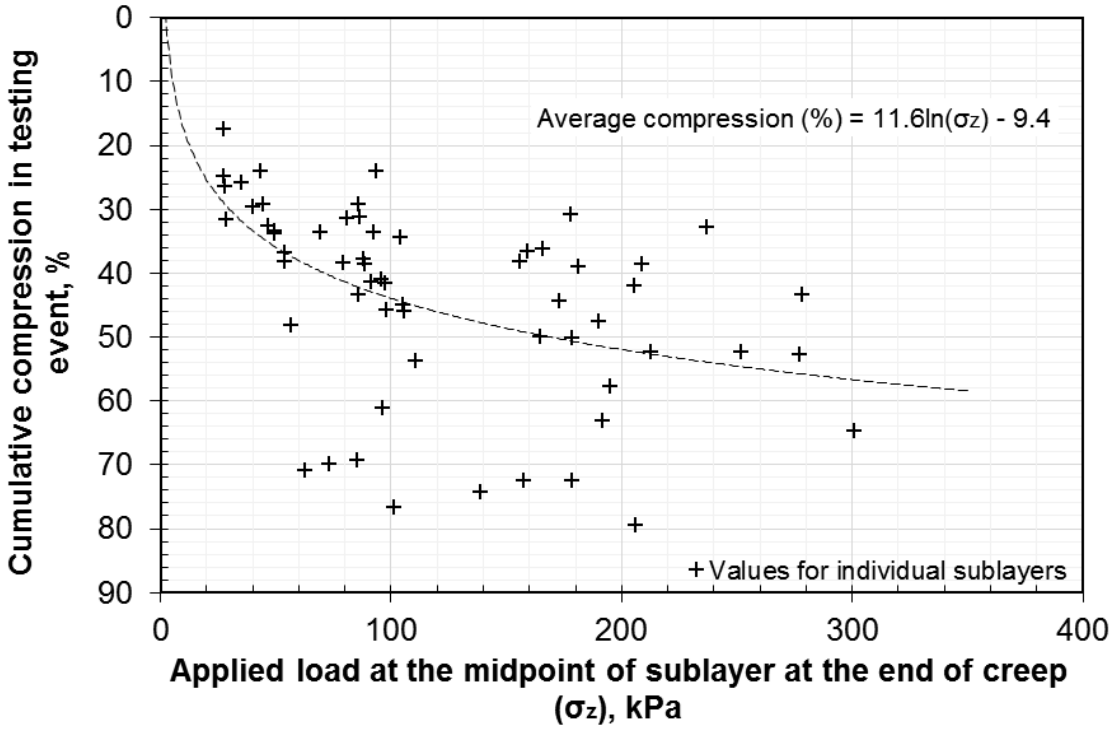

Figure 4-17: Relationship between compression and applied stress in the TDA types for all testing completed in the 1D cell (using values in Table 4-2)

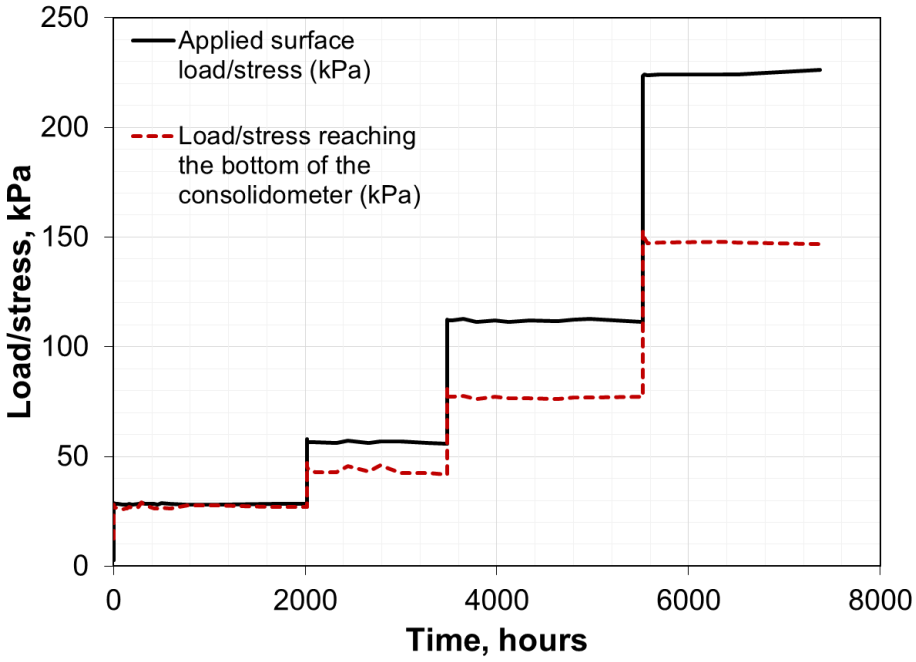

Figure 4-18: Applied load/stress at the top of the TDA determined from the load cell measurements and load/stress at the bottom of the TDA determined from the TS cell measurements. Test data for Sask TDA are shown, however values measured were similar for the other testing in the 1D cell.

5.0 Hydraulic Conductivity of Tire Derived Aggregate for Leachate Collection and Removal

Overview

Presented in this Chapter are the results and discussion on the vertical and horizontal hydraulic conductivity of large particle sized TDA for use as drainage material in landfill LCRS. Two of the TDA types in this Chapter (Sask TDA and ARMA TDA double pass, were studied in Chapter 4 as Sask TDA 1 and ARMA TDA respectively). Also presented are details of a porosimetry evaluation that was carried out to look within the fabrics of the TDA under applied stress to assess the geometry of voids and TDA particles under applied stress, to validate the results from the flow measurements. The porosimetry evaluation was used to determine the specific surface area of TDA under applied stress. This was used in the formulation of pressure and hydraulic conductivity functions to address sidewall friction effects in the flow data. The details of a consolidometer and permeameter that was used for vertical and horizontal flow testing, as well as the experimental methodologies employed are also presented in this Chapter.

This Chapter was submitted to Environmental Geotechnics as follows:

D. Adesokan, I. Fleming and A. Hammerlindl, "Hydraulic Conductivity of Tire Derived Aggregate for Leachate Collection and Removal," Environmental Geotechnics Journal, Submitted August 2, 2020.

Additional information relating to this Chapter, which were not included in the submitted manuscript are included as footnotes within the Chapter, and as supplementary data in Section 5.6.

5.1 Introduction

Vertical hydraulic conductivity of tire derived aggregate (TDA) for use in landfill leachate collection and removal systems (LCRS) has been widely measured. Studies (such as Hall 1991; Ahmed and Lovell, 1993; Beaven, 1994; Duffy, 1995; Donovan et al. 1996; Evans, 1997; Zimmerman, 1997; Reddy and Saichek, 1998; Reddy and Marella, 2001; Warith et al. 2004;

Hudson et al. 2007; Beaven et al. 2007; Beaven et al. 2013, Mwai 2016) have all shown that regardless of the differences in the particle size, shape and wire content of the TDA, the vertical hydraulic conductivity of TDA can exceed commonly prescribed regulatory limits for drainage materials in LCRS. Horizontal hydraulic conductivity of TDA, on the other hand, has been sparsely measured.

In drainage applications, such as in the LCRS of waste disposal facilities, vertical hydraulic conductivity is needed to evaluate the flow of leachate into the drainage layer. However, horizontal hydraulic conductivity is needed to evaluate the lateral flow of leachate from the drainage layer into collection pipes, sumps and leachate pond. The higher the horizontal hydraulic conductivity, the faster the drainage layer can remove leachate to keep the leachate mound within acceptable service conditions.

When TDA is used as the drainage material in LCRS, its hydraulic conductivity is expected to decrease because of void volume reduction from immediate compression and creep under increased and sustained loading imposed by the overlying waste (Hall, 1991; Beaven, 1994; Duffy, 1995; Narejo and Shettima, 1995; Reddy and Saichek, 1998; Warith et al. 2004; Beaven et al. 2007; Hudson et al. 2007). In addition, biogeochemical clogging from permeating leachate is also expected to decrease the hydraulic conductivity of a drainage layer over time (Rowe and Fleming 1998; Fleming et al. 1999; Cooke et al. 1999; McIsaac et al. 2000; Rowe et al. 2000a, b; Cooke et al. 2001; Qian et al. 2002; Cooke et al. 2005; Cooke and Rowe, 2008 a, b; Fleming and Rowe, 2004; Rowe et al. 2004; Rowe, 2005; Rowe and McIsaac, 2005; McIsaac and Rowe, 2005; Rowe and Babcock, 2007; Yu and Rowe, 2012; Beaven et al. 2013; Rowe and Yu, 2013, Mwai 2016). Both the vertical and horizontal hydraulic conductivity of TDA are expected to decrease under compression, creep and biogeochemical clogging.

Studies have reported values of the vertical hydraulic conductivity of TDA under applied stress (Hall 1991; Beaven, 1994; Duffy, 1995; Donovan et al. 1996; Evans, 1997; Zimmerman, 1997; Reddy and Saichek, 1998; Warith et al. 2004; Hudson et al. 2007; Beaven et al. 2007; Mwai et al. 2010, Mwai 2016). Some vertical hydraulic conductivity values for large particle sized TDA (TDA with particle size over 50 mm) are presented in Table 5-1.

Table 5-1: Some vertical hydraulic conductivity values for large particle sized TDA[48]

TDA description /particle size	Applied surface stress, kPa	Vertical hydraulic conductivity (m/s)	Author	Year
Whole light truck and passenger tires	Not stated	>0.7 to 0.025	Beaven	1994
Nominal size 76.2 mm	60	0.13	Warith et al	2004
Nominal size 76.2 mm	330	0.0067		
101.6 mm x 50.8 mm x 10.2 mm	150	0.007	Rowe and McIsaac	2005
127 mm x 40.6 mm x 10.2 mm		0.02		
Nominal size 200 mm	100	0.01	Hudson et al	2007
	400	0.001		
PLTT- 125 minus (D60= 90 mm, D10 = 50 mm)	~350	0.016	Mwai	2016
OTR- 125 minus (D60= 95 mm, D10 = 55 mm)		0.027		
MTT- 125 minus (D60= 100 mm, D10 = 48 mm)		0.011		
PLTT + OTR- 125 minus (D60= 95 mm, D10 = 53 mm)		0.006		

Vertical hydraulic conductivity values of TDA as affected by biogeochemical clogging have also been reported (Rowe and McIsaac, 2005; McIsaac and Rowe, 2005; Beaven et al. 2013, Mwai 2016). Very few studies have looked at the horizontal hydraulic conductivity of TDA under applied stress or evaluated anisotropy in the hydraulic conductivity of TDA; particularly large particle sized TDA.

[48] Table 2-1, Chapter 2

The study by Beaven et al (2013) is one of the few to have set out to measure horizontal hydraulic conductivity in large particle sized TDA under sustained loading, however, the hydraulic conductivity measurements in the study were completed at constant volume and not at constant applied stress. Hence, some stress relaxation may have also occurred prior to completing the flow measurements that may have had some effects on the results. In addition, the testing was completed as part of a biogeochemical clogging evaluation of TDA, and the direct effects of compression were not separated from those of clogging. While clogging was deemed to have had little effect in that study, evaluating these effects independently will allow the implications of each to be evaluated for different landfill conditions.

In the Beaven et al (2013), TDA was compressed, held in place at constant volume, and then turned sideways to have its ends facing upwards and its top facing sideways. Leachate was introduced into the TDA from the new top to bottom to simulate horizontal flow. It is not clear, if the TDA was held at constant volume after allowing some time for time dependent compression (creep), or if the TDA was held in place right after compression. If the contribution of creep was not captured in the constant volume approach, then creep-induced strain and the void volume reduction from creep, which could be up to 29% of the total void volume reduction (Adesokan et al. 2020)[49] would not have been captured. Consequently, a higher void volume and consequently a higher hydraulic conductivity would have been measured in the TDA.

The horizontal hydraulic conductivity of TDA, particularly large particle sized ones with particle sizes from over 50 mm under sustained loading thus remains largely unknown. A knowledge of both the horizontal and vertical hydraulic conductivity, as well as the anisotropy in the hydraulic conductivity, is needed to adequately evaluate the service life of a TDA drainage layer in waste disposal facilities.

[49] Chapter 4, Section 4.3.3.2

Testing of the permeability or hydraulic conductivity of highly permeable materials is very challenging, as it requires a sufficient length in the direction of flow such that the potential gradient may be measured with reasonable precision, whilst preventing preferential flow along the walls of the test cell. In addition, for highly compressible materials such as TDA, sidewall friction during vertical compression causes a decrease in applied stress with depth (thickness of the TDA) (ASTM D6270-98). This results in higher compression in the upper layers of TDA closer to the applied surface stress than in the lower layers farther away from the stress (Beaven, 1994; Warith et al. 2004; Adesokan et al. 2019[50]; Adesokan et al. 2020[51]).

The non-uniform compression created by sidewall friction loss results in horizontal “layering” in the TDA (Figure 5-1), and a variation in void ratio and permeability/hydraulic conductivity across the TDA thickness. In such, or any, horizontally layered system (Figure 5-1), the equivalent horizontal flow (hydraulic conductivity/permeability) is always greater than the equivalent vertical flow, as the arithmetic mean of the total flow in the horizontal direction is always higher than the harmonic mean of the flow in the vertical direction (Figure 5-1) (see e.g., Bear 1972; Freeze and Cherry, 1979; Das, 1983; Domenico and Schwartz, 1997). This creates anisotropy in the flows, even if the material were isotropic.

[50] Chapter 3
[51] Chapter 4

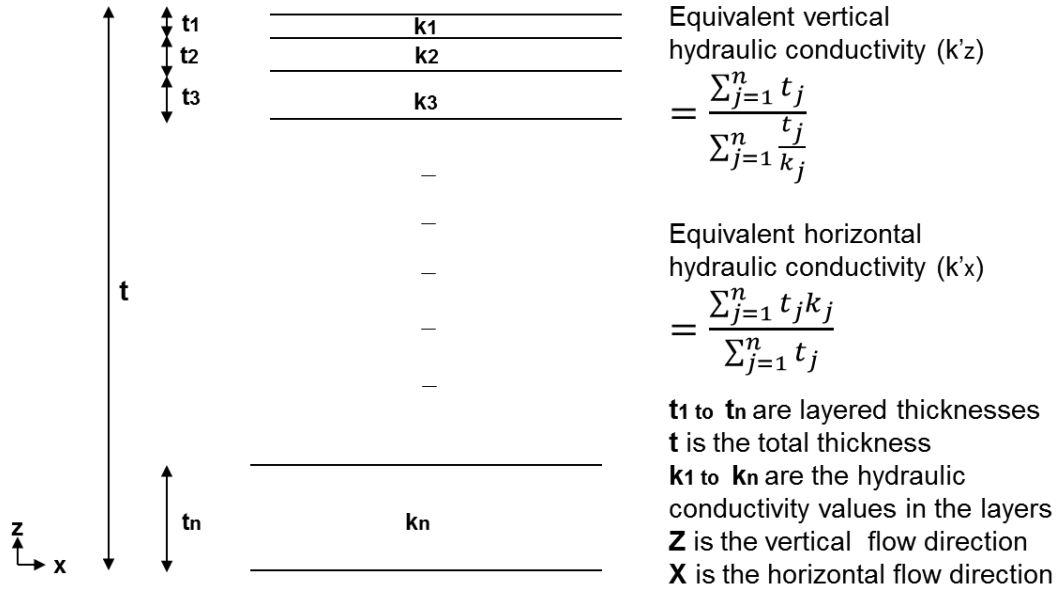

Figure 5-1: Schematic of layered heterogeneity (Redrawn from Freeze and Cherry, 1979). For TDA, because of sidewall friction loss, there is higher compression, lower void ratio and lower hydraulic conductivity closer to the applied surface stress, relative to the layers farther away from the applied stress. This creates compression (sidewall friction) induced layering across the TDA thickness, which may be conceptualized as layered heterogeneity like the schematic.

Compression (sidewall friction) induced horizontal layering in TDA, and resulting anisotropy, may not reflect the actual fabric anisotropy created by the shape, preferred orientation, and alignment of the TDA particles. Generally, large particle sized TDA, such as tested in this study, have elongated flat shapes that cause the TDA particles to largely align horizontally. This horizontal alignment is expected to inherently create fabric anisotropy in the TDA, potentially causing higher flows in the horizontal direction than in the vertical direction.

Sidewall friction induced layering is an artifact of constrained loading tests (Olson 1986; Sarsby and Vickers 1986), and will not occur in under field conditions in practice. Thus, its effects need to be accounted for, in order to adequately evaluate the performance-related properties of TDA for design. Despite all efforts to minimize sidewall friction in constrained loading tests, it can still

occur considerably (Beaven, 1994; Warith et al. 2004; Adesokan et al., 2019[52]), as was the case in the testing presented here.

Two approaches were applied to address sidewall friction effects in the data. The first approach (presented in Section 5.4) involved determining the equivalent values of air permeability (and hydraulic conductivity) within the TDA, using the known flow rates and pressure (and hydraulic head) readings at the inlet and exit ports alone, ignoring all other readings in between. This way, the non-uniform effects, gradients, and head losses created by sidewall friction across the TDA thickness are ignored. The average applied stress within the TDA was also determined, so as to correlate the equivalent air permeability and hydraulic conductivity values to the average applied stress within the TDA, and not the applied surface stress.

The second approach (presented in Section 5.6.4) involved formulating pressure distribution and hydraulic conductivity analytical forms, which were used to determine the vertical distribution of both vertical and horizontal hydraulic conductivity at any point across the thickness of the TDA. With the analytical forms, values were determined for portions where data was inconsistently low or non-existent because TDA partially or completely blocked the measurement ports. The vertical distribution of applied stress was also determined for correlation with the corresponding values of vertical and horizontal hydraulic conductivity across the thickness of the TDA. From the vertical distribution of hydraulic conductivity, equivalent values of vertical and horizontal hydraulic conductivity were determined using the corresponding relations in Figure 5-1.

Another challenge in the permeability/hydraulic conductivity testing of TDA is deciding the flow medium to use, for instance, choosing between water and air. There are several drawbacks to using water as the permeant fluid, which may affect the results of intrinsic permeability

[52] Chapter 3, Section 3.7.1

measured with water. One of such drawbacks is that it is very difficult to achieve complete saturation in such testing (Long et al. 1988), and that becomes even more difficult for materials such as TDA (with voids within individual particles) (Adesokan et al. 2019[53]). Access to interstitial voids within particles, and the time required establishing pressure and flow equilibrium are also slower with water than with air, since water is more viscous than air (Long et al. 1988; Wells et al. 2006; Wells et al. 2007; Huang et al. 2015; Huang et al. 2016). In addition, dissolved air released from solution during measurements may block the passage of water through the voids of the material, resulting in incorrect measurements (Long et al. 1988).

Because of the drawbacks to using water as permeant fluid, which are overcome by using air, it has been stated that measurements with air might reflect the true intrinsic permeability of porous materials (Long et al. 1988). In view of this, air was used as the primary permeant fluid to determine air/intrinsic permeability values, which were then converted into hydraulic conductivity values using empirical relations. To compare the hydraulic conductivity values determined directly with those estimated from air permeability, water was introduced at the final load step after completing the measurements with air.

This paper presents the equipment design, laboratory testing, and results of the vertical and horizontal hydraulic conductivity of large particle sized TDA under applied surface stress up to 375 kPa – equivalent to 30 m to 40 m of overlying landfill waste (Zekkos et al. 2006) on a TDA drainage layer. This is perhaps the first study on TDA where hydraulic conductivity is being estimated from air permeability; the authors do not know of any such study in the published literature. Hence, the testing and analytical approach presented here are essentially novel for TDA.

[53] Chapter 3

5.1.1 Theory

The flow of fluids through a porous material can be evaluated using Darcy's equations of flow – Equation 1 (for air as flow medium) and Equation 2 (for water as flow medium) (Freeze and Cherry, 1979):

$dP/dl = -(\mu q)/K_a$ *5-1*

$dh/dl = -(q)/k$ *5-2*

Where,

dP is the pressure differential (for air flow) (Pa)

dl is the change in length in the direction of flow (m)

μ is the dynamic viscosity of air (Pas)

q is the discharge velocity of the fluid in the direction of flow (m/s)

K_a is the intrinsic permeability as determined from air permeability (m^2)

dh is the change in total head (m)

k is the hydraulic conductivity (m/s).

Darcy's equations of flow (Equations 5-1 and 5-2) are generally accepted to be valid for laminar flows, that is: Reynold's number (Re) values from <1 to 10 (Equation 3) (Bear, 1972). A transitional flow range (nonlinear laminar or unsteady laminar flow) is accepted to exist for 10<Re<1000 and turbulent flows for Re ≥1000 (Bear, 1972).

$Re = (\rho q d_{30})/\mu$ *5-3*

Where,

ρ is the density of the fluid (kg/m^3)

q is the discharge velocity in the direction of flow (m/s)

d_{30}[54] is the characteristic pore dimension – in this case, the diameter of 30% smaller than the longest dimensions of each TDA type

μ is the dynamic viscosity of the fluid (kg/ms)

When Darcy's law does not apply, correctional parameters, such as Forcheimer's second order term relating to inertia – given as $\beta\rho(q^2)$ (Zeng and Grigg, 2006) can be added to the basic Darcy's flow equations to account for the non-linearity and unsteadiness in the flows. The modified Darcy's equations of flow are as follows (Zeng and Grigg, 2006):

$$dP/dl = -((\mu q)/K_a) - \beta\rho(q^2) \qquad 5\text{-}4$$

$$dh/dl = -((q)/k) - \beta\rho(q^2) \qquad 5\text{-}5$$

Where,

β is Forchheimer's constant

q is the discharge velocity in the direction of flow (m/s)

ρ is the density of the fluid (kg/m^3).

By representing Equations 5-4 and 5-5 in terms of the linear equation (Y = mX + C), the vertical axis is dP/dl (or dh/dl) (for all the flow rates per test), and the horizontal axis is $\rho(q^2)$. Then, the slope of the linear plot is the term β, and from the value of the intercepts, K_a and k are determined from $-(\mu q)/K_a$ and $-(q)/k$ respectively in Equations 5-4 and 5-5.

For a dry porous material, with the assumption that air permeability measurements represent true intrinsic permeability (Long et al, 1988), hydraulic conductivity values can be estimated directly from air permeability as follows (Freeze and Cherry, 1979):

[54] The d_{30} value was used (instead of d_{50} – which is commonly used for coarse materials, or d_{10} – effective diameter, for finer materials, such as sandy soils, whether uniform or more well-graded), so as to consider the average of the d_{50} and d_{10} values. The Reynolds number calculated using either of d_{10} or d_{50} still resulted in non-Darcian flows, requiring correction for inertia, as with the outcome of using d_{30}, so it did not really matter which of the three values was used. Using d_{30} was ultimately taking the average of the d_{50} and d_{10}.

$k = (K_a \rho g)/\mu$ *5-6*

Where,

k is the hydraulic conductivity (m/s)

K_a is the intrinsic permeability as determined from air permeability (m^2)

ρ is the density of water (kg/m^3)

g is the acceleration due to gravity (m/s^2)

μ is the dynamic viscosity of water (kg/ms).

Initial void ratio (e_0) in the TDA can be determined as for solid minerals as follows:

$e_0 = (G_s \gamma_w / \gamma_{dry}) - 1$ *5-7*

Where,

e = void ratio (initial void ratio e_0 in this case)

G_s = specific gravity;

γ_w = the unit weight of water (kN/m^3);

γ_{dry} = the unit weight of dry TDA in test cell (kN/m^3)

The change in void ratio can be determined as for solid mineral particles as follows (Adesokan et al. 2019[55]; Adesokan et al. 2020[56]):

$\Delta V/V = \Delta H/H = \Delta e/(1+e_0)$, and $\Delta Vs = 0$ *5-8*

Where,

ΔH = change in height of TDA;

H = initial height;

Δe = change in void ratio;

e_0 = initial void ratio;

[55] Chapter 3
[56] Chapter 4

ΔV_s = change in volume of solids

5.2 Materials

5.2.1 TDA

TDA was sourced from tire recycling facilities in Saskatchewan and Alberta, Canada for the study. The TDA from Saskatchewan is presented here as Sask TDA and those from Alberta as ARMA TDA single pass and ARMA double pass – relative to the number of shredding passes used to reduce the whole tires into small sizes. Particle size distribution (PSD) was determined for the TDA types by randomly selecting a minimum of 20 kg of TDA – consisting of over 300 particles, and measuring the longest dimension (length), shortest dimension (width) with a measuring tape. The mass of individual particles was determined, and PSD plots were generated using the cumulative mass percentage smaller than the length and width of each particle (Figure 1 a, b). The PSD plots were also generated in terms of the equivalent dimension (deq) – given as √ (length x width) (Figure 1 c), in order to compare directly with the singular particle size dimensions typically presented for gravel.

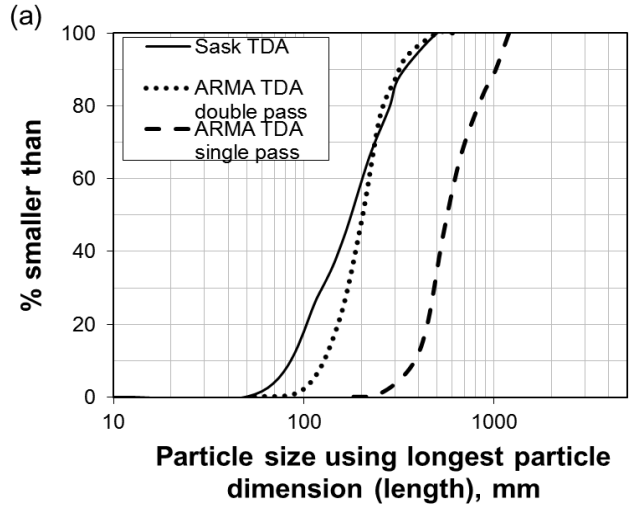

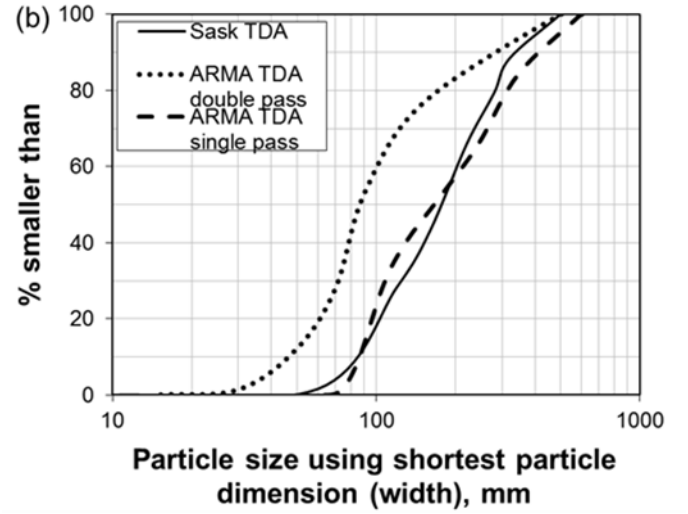

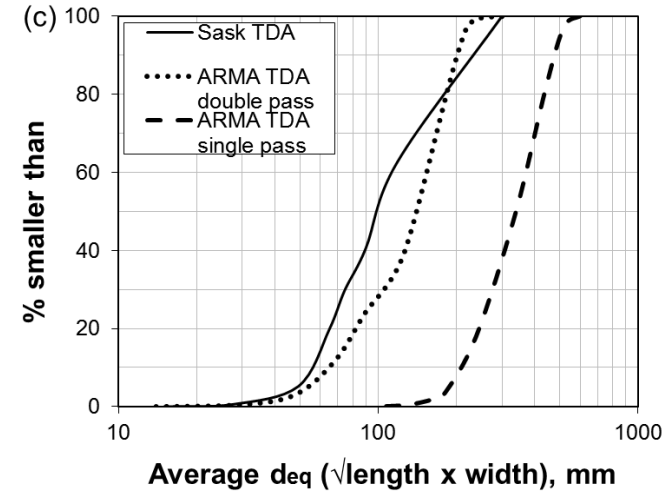

Figure 5-2: PSD plots of the TDA types (a) using the length of particles; (b) using the width of particles; (c) using the average d_{eq}

The specific gravity (G_s) of the TDA types, determined using the guidelines for larger particle sized aggregates in ASTM C127 – 12, was 1.27. Although this value is at the high end of G_s values in the literature – for instance, Geosyntec (2008) presented values ranging from 1.02 to 1.27, it is typical for TDA with embedded wires in them (Geosyntec, 2008), as was the case with the TDA types tested in this work.

5.2.2 Equipment

5.2.2.1 Consolidometer and permeameter for vertical and horizontal flows

A large sized 1 m x 0.6 m x 1.2 m, consolidometer and permeameter (2D cell) (Figure 5-3) was custom-built to complete both horizontal and vertical flow testing of large particle sized TDA under sustained loading.

Figure 5-3: The consolidometer and permeameter (2D cell)

The 2D cell and loading plate were fabricated from mild steel. The 2D cell weighs approximately 8 kN, and the loading plate weighs approximately 1 kN. The loading plate contains housings for load cells to be placed in direct contact with air bellows for applied surface stress measurements (Figure 5-4). The loading plate also has forty eight 12.7 mm diameter holes for outflow of fluids during vertical flow testing (Figure 5-4).

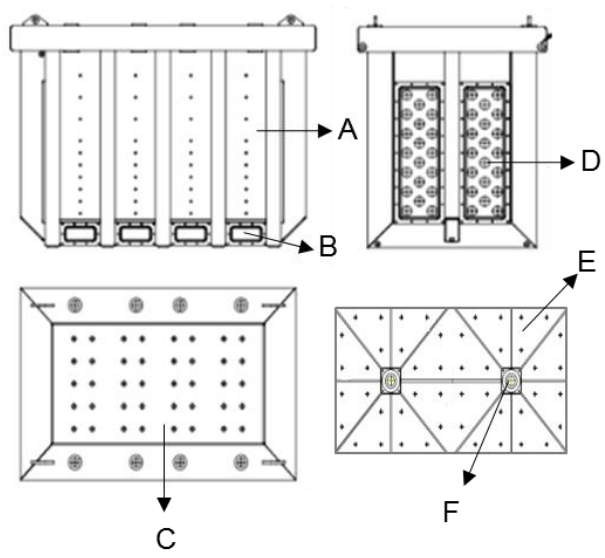

A – front panel of the cell with four vertical columns of measurement ports and ten ports in each column. Ports are spaced farther apart in the top half in anticipation of compression past those ports under large applied loads
B – bottom flange with four holes connecting to a false bottom of the cell (with holes for introducing vertical flow - see "C")
C – false bottom of the cell with holes for introducing vertical flow
D – holes at the ends of cell for introducing horizontal flow
E – loading plate with holes for vertical flow outlet
F – load cell housing

Figure 5-4: Flow parts of the 2D cell

On the front panel of the cell, there are four vertical columns of measurement ports, with each column containing ten ports for measuring gauge pressure during air permeability testing and hydraulic head during hydraulic conductivity testing (Figure 5-4). On each end of the cell, there are twenty 50 mm diameter holes for introducing horizontal flow into the cell (Figure 5-4). At the bottom flange on the front panel of the cell, there are four similar sized holes that connect to the space below a false bottom with holes for introducing vertical flow into the cell (Figure 5-4). Plastic "cookies" were used to cover the holes at the ends of the cell before loading with TDA to provide a smooth flush surface along the inner wall of the cell during loading in order to decrease excessive friction along the end walls of the cell during compression of TDA (Figure 5-5). The plastic cookies were removed for the horizontal flow tests to allow for the introduction and flow of fluids through the cell, and were replaced for the vertical flow tests.

Gasket fittings were placed around the holes and steel plate facings were bolted into place to cover the holes (Figure 5-5). The steel plate facings each have six holes with connectors to attach hoses to distribute fluid evenly for horizontal flow testing (Figure 5-5).

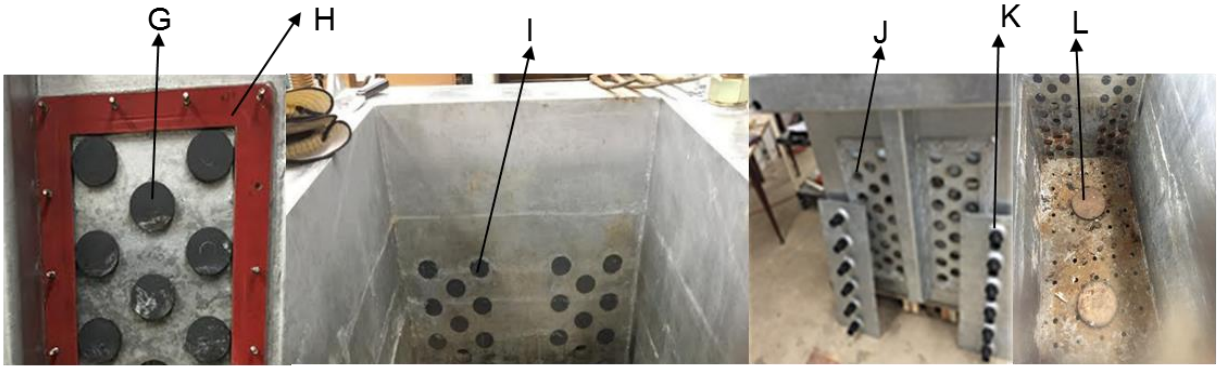

G – plastic “cookies” in place before filling the cell
H – gasket to ensure tight seal around facing
I – flush sidewall created on the inside of the cell with the plastic cookies in place
J – plastic cookies removed for horizontal flow testing
K – steel plate facings with holes with connectors to attach hoses for horizontal flow testing
L – removable circular platforms for placing total stress (TS) cells on the false bottom to measure applied stress reaching the bottom of the cell

Figure 5-5: Additional parts of the 2D cell

5.2.2.2 Compression cell for porosimetry evaluation

A compression cell (Figure 5-6) was fabricated for use in a complementary porosimetry evaluation. The porosimetry evaluation was completed to look within the fabric of TDA to assess particle orientation void geometry, and pore size following compression under sustained applied stress. From the porosimetry evaluation, the specific surface area of TDA as a function of void ratio was also determined for use in the formulation of pressure and hydraulic conductivity distribution forms for addressing sidewall friction effects in the data (see Sections 5.6.3, 5.6.4).

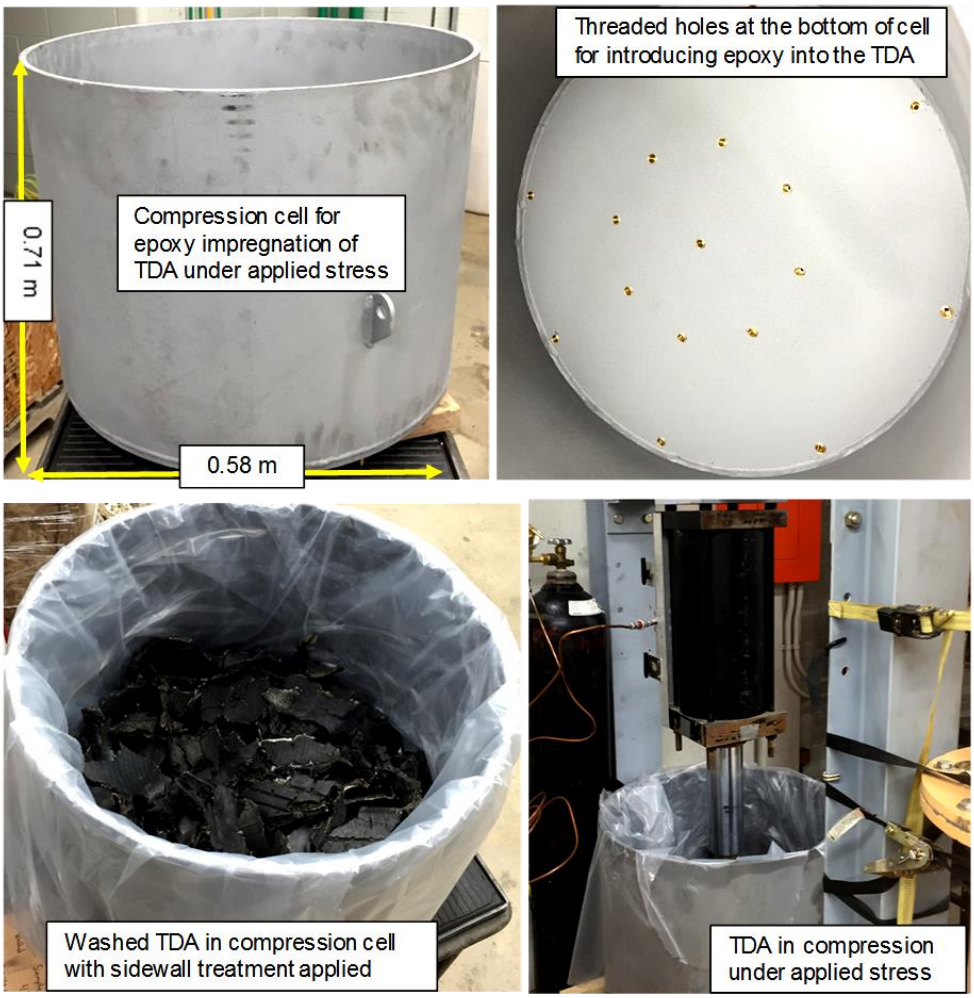

Figure 5-6: Compression cell for complementary porosimetry evaluation

5.3 Experimental methods

5.3.1 Horizontal and vertical flow measurements

For the vertical flow tests, inflow was introduced through the holes at the bottom flange of the cell and outflow was at the top of the cell through the holes in the loading plate and the clearance between the loading plate and the walls of the cell. For horizontal flow tests, the steel cover plates on the ends of the cell were removed to take out the cookie plugs from the holes, and then the fittings for the steel manifold facing, and the hoses and tubing for the flows were all connected. One end of the hoses were attached to the connectors on the steel plate and the other ends connected to flow measurement systems.

To leak proof the test cell to ensure accurate measurements, holes in the test cell not used for inlet or outlet flows, or for head measurements were completely plugged or sealed during testing. Holes in the loading plate were plugged tightly with rubber plugs and the base of the plugs sealed with silicon to leak proof the cell for horizontal flows. The clearance between the loading plate and the walls of the cell were also plugged with flexible tubing (Figure 5-7 (a)), then silicon was applied (Figure 5-7 (b)) and smoothed into place over and around the tubing to ensure good sealing around the loading plate (Figure 5-7 (c)). The silicon for sealing the openings was allowed a minimum of 12 hours to set before commencing testing.

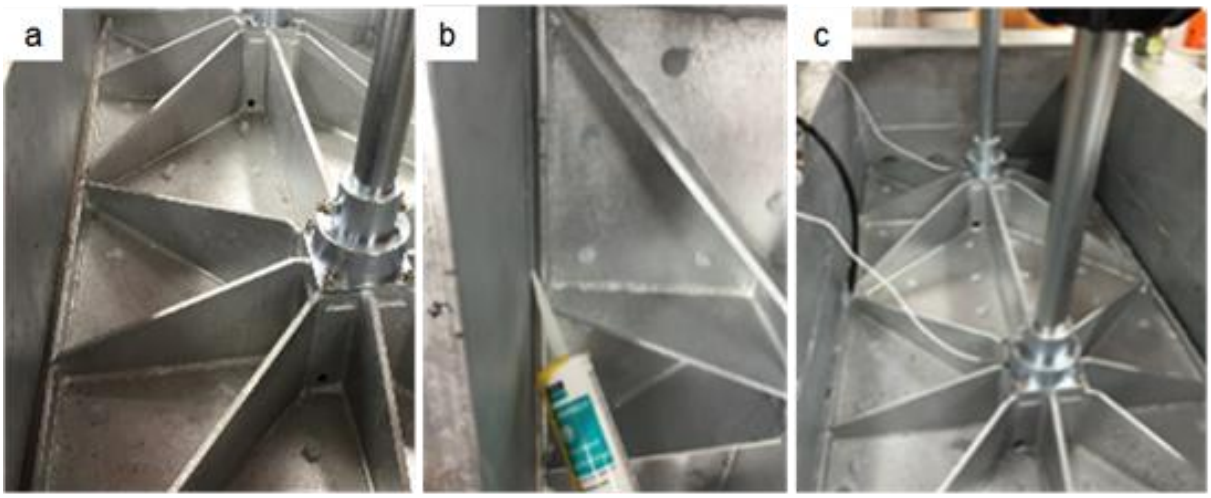

Figure 5-7: sealing of the openings within and around the loading plate to complete horizontal flow measurements (a) clearance between the loading plate and the walls of the cell plugged with flexible tubing; (b) silicon applied and smoothed over the tubing to ensure good sealing around the loading plate;(c) silicon left to set before commencing testing

Before taking head readings (pressure or hydraulic), the measurement ports were pierced through with a long 3 mm diameter steel needle to break through the layers of plastic sheeting treatment that had been applied for minimizing sidewall friction along the sidewalls of the cell. As the TDA compressed under the applied stress, the loading plate and top of the TDA moved beyond the uppermost ports, hence those ports were shut out for the remainder of the test.

Before loading up the cell with TDA, two pancake type VW total stress (TS) cells manufactured by DurhamGeo Slope Indicator (DGSI) were placed at the bottom of the cell (Figure 5-5) to measure applied stress reaching the bottom of the TDA in order to account for inevitable sidewall friction loss (Adesokan et al. 2019[57]). Sidewall friction treatment consisting of two layers of high temperature grease and two layers of 2 mm thick plastic sheeting was applied prior to loading up the cell with TDA (Adesokan et al. 2019[58]), and the holes on the ends of the cell were plugged with the plastic cookies.

Surface stresses of 56, 112, 224, 250 and 375 kPa were applied[59] to the TDA to simulate from approximately 5 m to 40 m of waste (Zekkos et al. 2006) above a TDA drainage layer. Because of logistical constraints, the 56 kPa applied stress was only applied to the Sask TDA, and only 250 kPa was applied to ARMA TDA single pass. Compression of TDA was measured using meter long rulers placed at pre-marked locations on top of the loading plate[60]. The flow measurements were completed at the end of creep for each applied stress.

5.3.1.1 Air permeability measurements

For both vertical and horizontal flows, three blowers that could deliver a combined flow rate of up to 0.24 m^3/s in free air were used to supply airflow into the 2D cell. Inlet and outlet flow rate were measured using calibrated Pitot tube assemblies attached to a flow measurement system consisting of 30 mm PVC pipe with a 90° bend. One end of flow hoses were connected to the measurement system and the other ends connected to the 2D cell (Figure 5-3)[61]. Gauge pressure within the TDA during testing was measured using large sized custom-made water manometers that were connected to the measurement ports on the front panel of the 2D cell

[57] Chapter 3
[58] Chapter 3
[59] See Figure 5-31, Section 5.6.5 for the load cells placed within a housing on the loading plate under the piston rod
[60] See Figure 5-32, Section 5.6.5
[61] See additional images and schematics of the setup in Section 5.6.5

(Figures 5-3). Flow was left to stabilize before taking readings, typically after approximately 5 to 10 minutes.

Three airflow rates for high, medium and low flows (corresponding to the number of blowers placed in parallel) were completed per testing cycle for each applied surface stress. For all the TDA types, the vertical airflow rates ranged from 0.08 m^3/s – with three blowers, to 0.02 m^3/s – with one blower, horizontal airflow rates ranged from 0.07 m^3/s – with three blowers, to 0.02 m^3/s – with one blower.

5.3.1.2 Hydraulic conductivity measurements

Water was introduced into the TDA at the final applied surface stress of 375 kPa (for Sask TDA and ARMA TDA double pass. Water-based testing was not completed at the final applied surface stress of 250 kPa for ARMA TDA single pass, because of logistical constraints). Water-based testing was done at the final applied stress to compare the hydraulic conductivity of the TDA types from both air and water measurements. For each of the vertical and horizontal hydraulic conductivity measurements[62], a minimum of four flow rates was measured. The flow rates ranged from 0.00063 m^3/s to 0.00097 m^3/s for vertical flows and from 0.00017 m^3/s to 0.00032 m^3/s for the horizontal flows.

The flow rates were determined both manually and electronically. The manual approach involved collecting the effluent from the cell into a large graduated clear cylinder and using a stopwatch to estimate the flow time. The electronic measurements were taken with a Rosemount 8732 integral mount magnetic flow reader (Figure 5-8) to check the accuracy of the manually obtained flow measurements. The readings obtained with the magnetic flow reader were found to be consistent with the readings from the manual measurements within a 5% error margin. Hydraulic head was measured using large sized standpipe piezometers (Figure 5-8).

[62] See additional images and schematics of the setup in Section 5.6.5

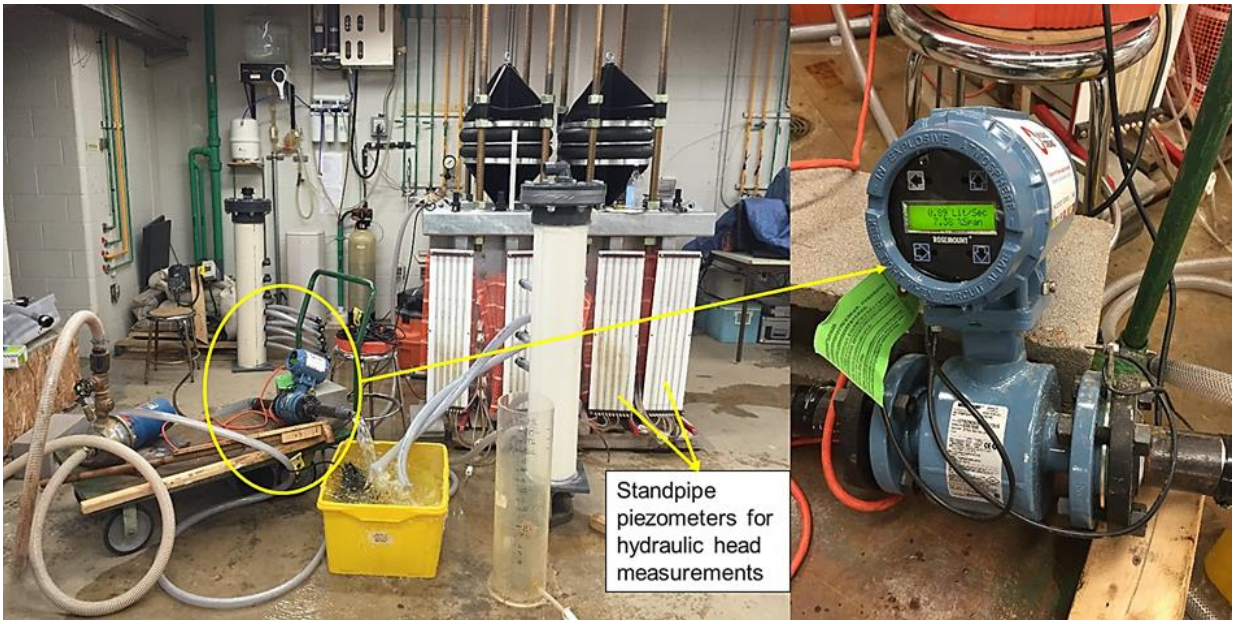

Figure 5-8: A magnetic flow reader in place to check the accuracy of the manually obtained flow measurements

5.3.1.3 Porosimetry evaluation

For the complementary porosimetry evaluation, sidewall friction treatment consisting of two layers of high temperature grease and two layers of 2 mm thick plastic sheeting (Adesokan et al. 2019[63]) was applied to the compression cell before filling with TDA. Sask TDA[64] was used in the study. The TDA was washed and dried prior use to remove loose particles (see Section 5.6.3), and a 60 kN hydraulic unit was used to apply approximately 224 kPa of stress to the TDA. A mixture of epoxy resin, hardener and fluorescent yellow dye – to make the voids more identifiable for mapping, was used for the impregnation. While under sustained loading, the epoxy mixture was pumped into the TDA using a peristaltic pump (Figure 5-9 (a)).

The epoxied TDA was left to set and solidify under the applied stress for several days (Figure 5-9 (b)). The applied stress was removed after the TDA was completely solidified. The solidified

[63] Chapter 3
[64] Presented as Sask TDA 2 in Chapter 4

epoxied TDA (Figure 5-9 (c)) was cut vertically into 0.025 m thick slices using a water jet cutter with Garnet 80 mesh spec sand[65].

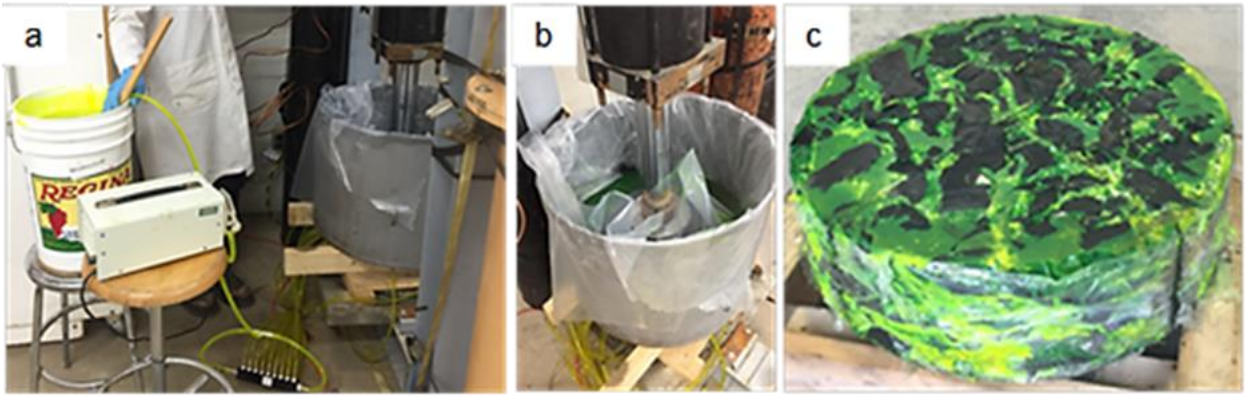

Figure 5-9: Porosimetry evaluation to look within the fabric of TDA, and to determine the specific surface area of TDA as a function of void ratio used in sidewall friction evaluation approach 2 (see Sections 1, 5.4 and 5.6.4). Sask TDA was used in the evaluation (a) TDA compressed under an applied stress of 224 kPa being pumped full with a mixture of epoxy resin, hardener and florescent yellow dye; (b) impregnated TDA left to set under the sustained applied stress; (c) solidified epoxied TDA extruded for thin sectioning and analysis[66].

5.4 Results and discussion

Figure 5-10 shows typical applied surface stress at the top of the TDA (determined from the load cell readings), and the stress reaching the bottom of the TDA (determined from the TS cell readings). The difference in the top and bottom readings shows the loss of applied surface stress to sidewall friction. The average stress in the TDA at an applied stress were determined from the average of the top and bottom stresses[67] (Figure 5-10).

[65] See Section 5.6.3 for images of the thin sectioning process
[66] See Section 5.6.3 for more on the porosimetry evaluation and analysis.
[67] Equation 5-14 – Section 5.6.4, and Equation 3-13 – Section 3.10.5, can also be used to determine the distribution of applied stress across the TDA, and from this, the average value of applied stress in the TDA can be determined.

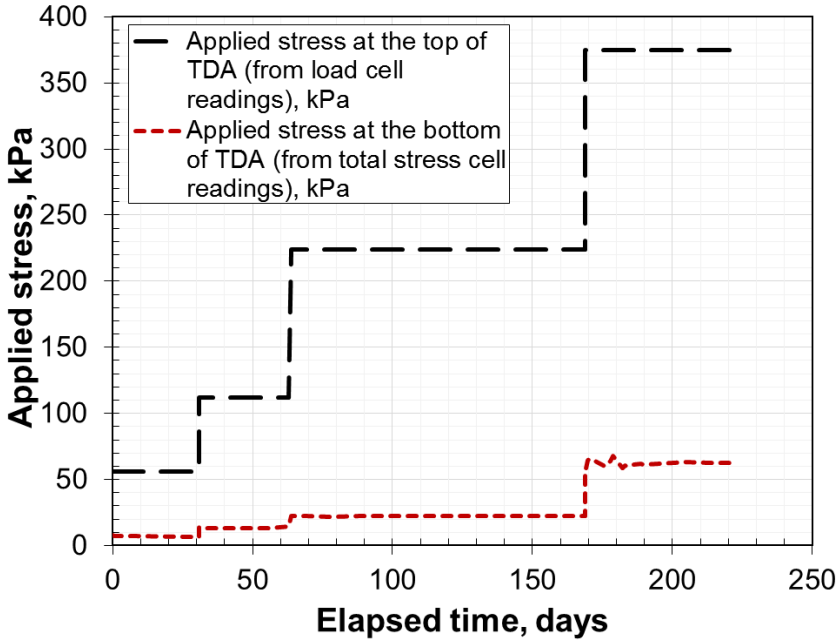

Figure 5-10: Applied stress at the top and bottom of TDA in the 2D cell during testing showing considerably lower applied stress at the bottom of TDA than at the top – caused by sidewall friction loss, even though sidewall treatment had been applied to the cell. Results for Sask TDA shown.

Typical vertical flow data for measurements with air and water are shown in Figures 5-11 (a) and (b) respectively[68]. In Figures 5-11 (a) and (b), out of the ten measurement ports in each vertical column, only seven were available for readings, as the upper three had been shut out because TDA had compressed beyond those ports.

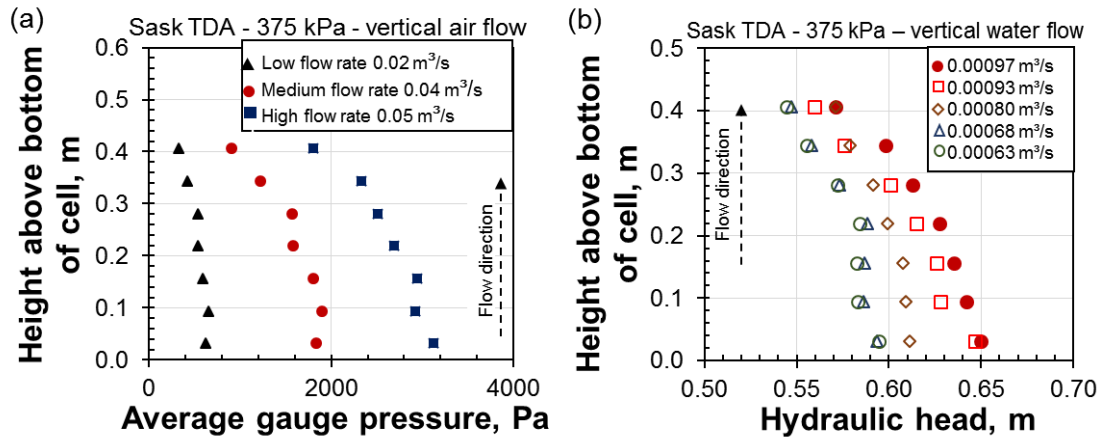

[68] Vertical flow plots for all the TDA types are presented in Section 5.6.1

Figure 5-11: Typical vertical flow data. Values for Sask TDA at the 375 kPa applied surface stress shown. Each data point represents the average of readings from the four vertical columns of ports at the same height. The TDA here had been compressed from an initial height of 1 m; (a) measurements with air; (b) measurements with water

Figures (5-11 (a) and (b)) show the vertical flow gradients increasing upwards, indicating that the air permeability (Figure 5-11 (a)), and hydraulic conductivity (Figure 5-11 (b)) of the TDA decreased closer to the applied stress – an effect of sidewall friction, which caused layers of TDA closer to the applied stress to compress more than layers farther away from it.

To address sidewall friction effects in the data, the approach used here involved assuming a uniform distribution of applied stress and compression across the TDA thickness, by "ignoring", as much as possible, the sidewall friction effects, and non-uniform distribution of gradient so created (Figure 5-12). Accordingly, for measurements with both air and water, the vertical flow gradients at each flow rate were determined using only the inlet and outlet readings, and the vertical distance between them, ignoring all other values in between (Figure 5-12).

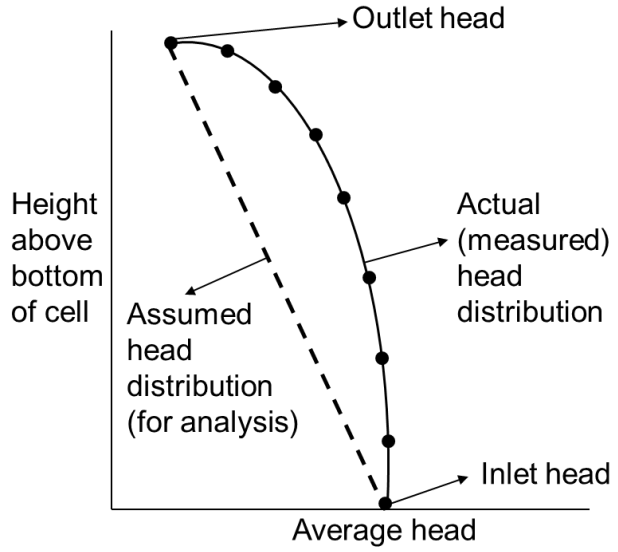

Figure 5-12: Schematic of approach used in the analysis to "ignore" the non-distribution of gradient created by sidewall friction effects across the TDA thickness, and assume a uniform distribution of gradient.

For instance, for vertical flow gradient for measurements with air (Figure 5-11 (a)), at the low flow rate, the inlet pressure was 625 Pa at a height of 0.03, and the outlet pressure was 325 Pa at a height of 0.41. Then the dP at that flow rate was calculated as 625 - 325 = 300 Pa, and dl was calculated as 0.41 - 0.03 = 0.38. Thus, the pressure gradient (dP/dl) was 789.4 Pa/m. A limitation with this approach is that sidewall friction effects still exists in the data. Thus, the vertical hydraulic conductivity determined may be relatively lower than without sidewall friction effects (in the field), likewise, the horizontal hydraulic conductivity may be relatively lower than without sidewall friction effects.

Another approach for addressing sidewall friction effects in the flow data, presented in Section 5.6.4, involved using formulated pressure and hydraulic distribution forms to determine equivalent vertical and horizontal hydraulic conductivity values. In that approach, discrete values of gradients and hydraulic conductivity were determined using the head measurements taken at adjacent ports and the distance between the ports. From these, equivalent hydraulic conductivity values were determined to calibrate the estimated distribution of hydraulic conductivity generated using the formulated pressure and hydraulic distribution forms.

A limitation with the approach is that some relationships in the analytical forms (such as specific surface area vs. void ratio) had only been determined at one applied stress. Hence, the change in such relationship with applied stress was not factored into the analysis. In addition, there may be some limitations with some of the assumptions used in the formulation of the analytical forms. For instance, the Kozeny-Carman relation (see Das, 1983; Carrier III, 2003; Chapuis and Aubertin, 2003) was used in the formulation of the hydraulic conductivity forms was formulated for solid mineral particles. There may be limitations to applying the relation to highly compressible and highly permeable materials, such as TDA.

Ultimately, for any sidewall friction evaluation approach, the results from field studies (under unconstrained loading conditions) are needed to calibrate the results from laboratory testing. The data from such field studies will also be useful for validating and updating any assumptions made in the formulation of sidewall friction analytical forms.

The Re values for all the vertical flow measurements fell within the transitional nonlinear laminar flow range[69]. Hence, correction for inertia was needed, and this was done using Equations 5-4 and 5-5, as described in Section 5.1. The vertical flow gradients determined were used to generate linear plots (Figures 5-13 to 5-15), to determine vertical air permeability and hydraulic conductivity values[70], with consideration for inertia, for all the TDA types.

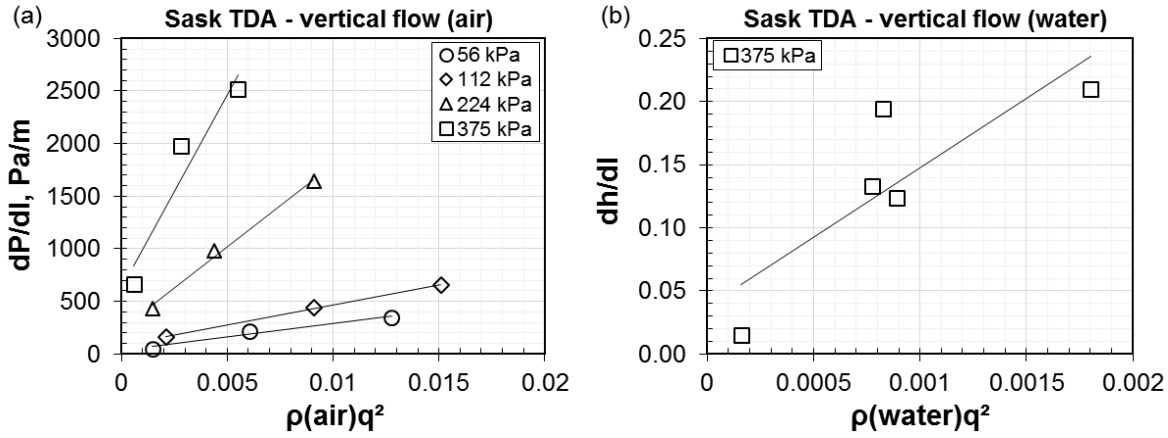

Figure 5-13: Determination of vertical air permeability and hydraulic conductivity with consideration for inertia for Sask TDA (a) air permeability; (b) hydraulic conductivity

[69] See Section 5.6.1 for a summary of Reynolds values.
[70] The vertical flow plots for all the TDA types are presented in Section 5.6.1

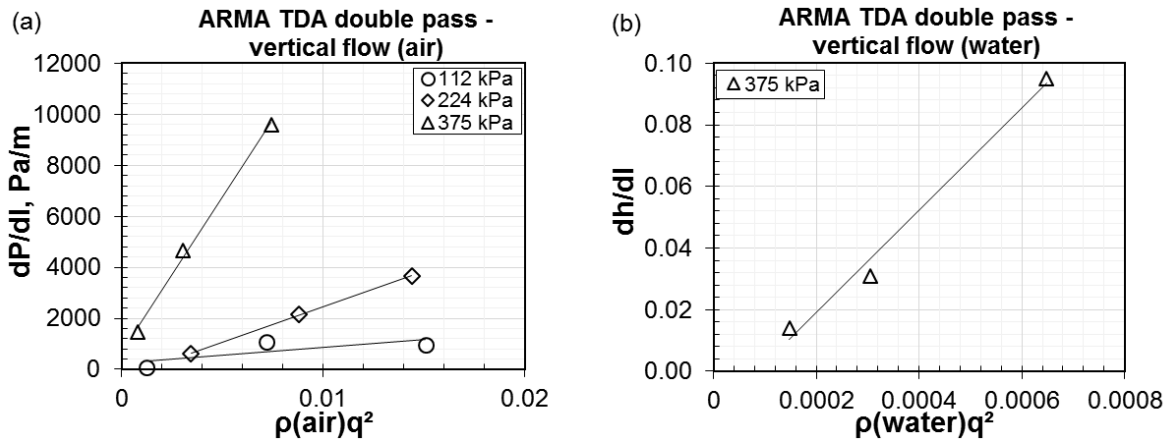

Figure 5-14: Determination of vertical air permeability and hydraulic conductivity with consideration for inertia for ARMA TDA double pass (a) air permeability; (b) hydraulic conductivity

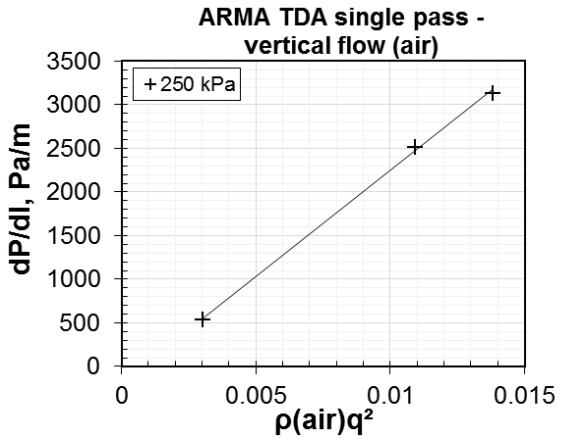

Figure 5-15: Determination of vertical air permeability with consideration for inertia for ARMA TDA single pass

Presented in Figures 5-16 (a) and (b) are typical horizontal flow data[71] for measurements with air and water respectively, at the final applied surface stress. The horizontal flow gradients at each flow rate were determined using only the inlet and outlet readings, as with the vertical flow gradients.

[71] Horizontal flow plots for all the TDA types are presented in Section 5.6.1

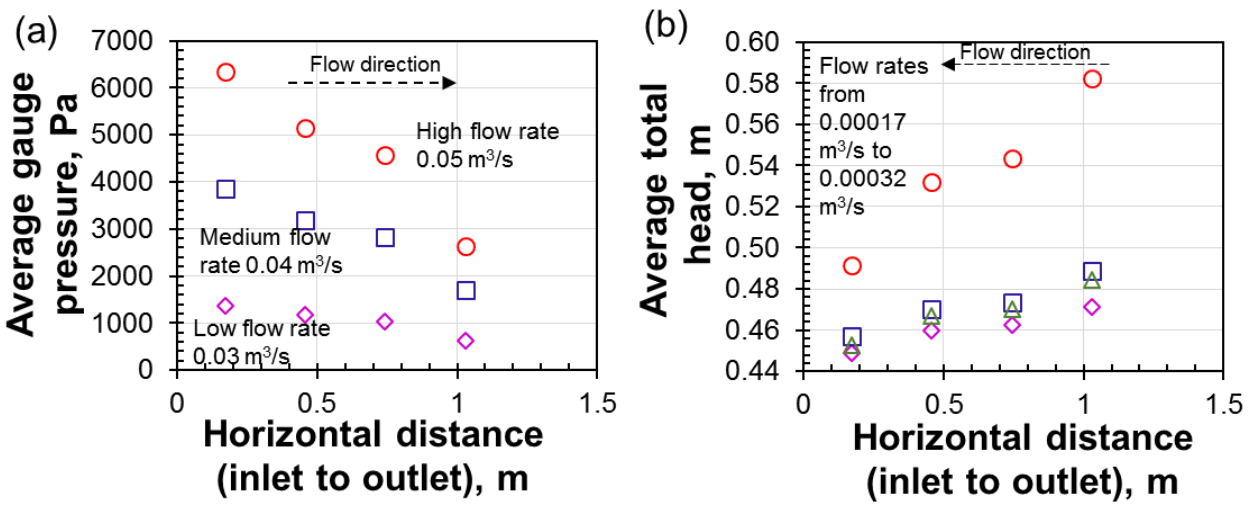

Figure 5-16: Typical horizontal flow data. Values for Sask TDA at the 375 kPa applied surface stress shown. Each data point represents the average of readings from the four vertical columns of ports at the same height; (a) measurements with air; (b) measurements with water.

The Re values for all the horizontal flows[72] were also within the transitional nonlinear laminar flow range, and inertia effects were corrected for using Equations 5-4 and 5-5. The horizontal flow gradients determined were used to generate the linear plots (Figures 5-17 to 5-19), for the determination of horizontal air permeability and hydraulic conductivity values with consideration for inertia (Section 5.1).

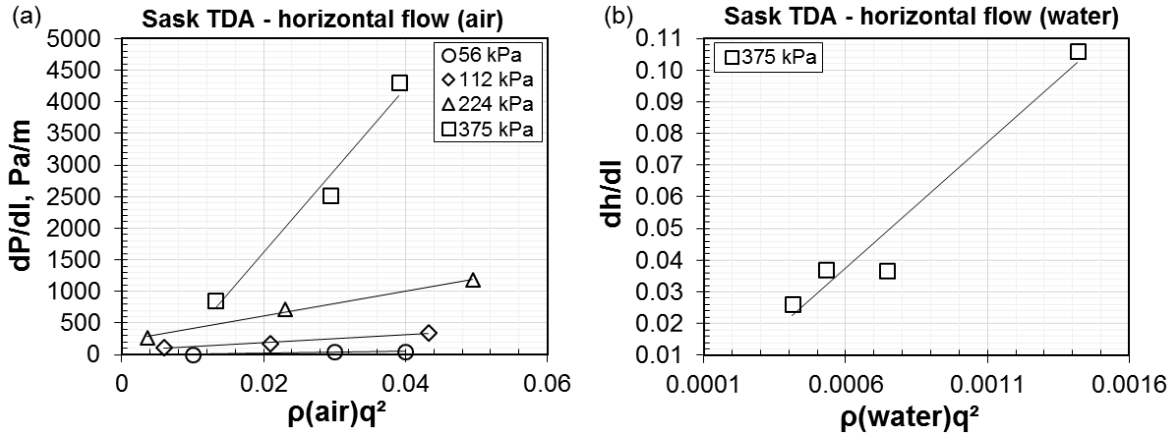

Figure 5-17: Determination of horizontal air permeability and hydraulic conductivity with consideration for inertia for Sask TDA (a) air permeability; (b) hydraulic conductivity

[72] The Re values are presented in Section 5.6.1

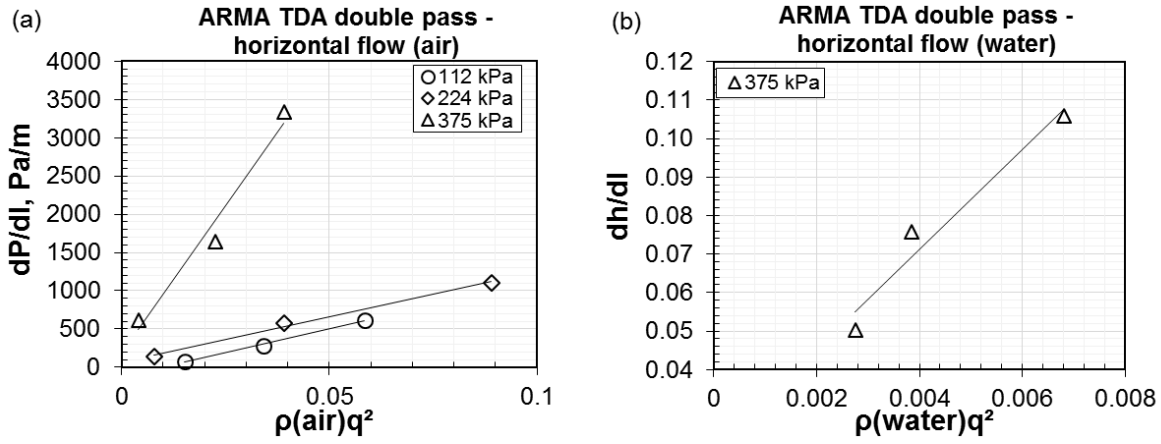

Figure 5-18: Determination of horizontal air permeability and hydraulic conductivity with consideration for inertia for ARMA TDA double pass (a) air permeability; (b) hydraulic conductivity

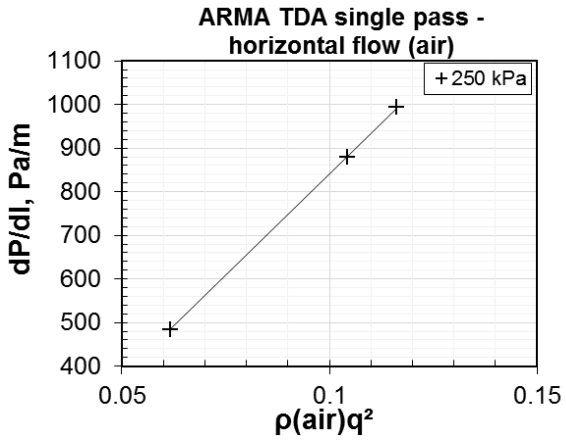

Figure 5-19: Determination of horizontal air permeability with consideration for inertia for ARMA TDA single pass

Since the TDA was dry during the measurements with air, the air permeability values were taken to represent the intrinsic permeability of the TDA (see Sections 5.0, 5.1). Accordingly, the air permeability values were converted directly to hydraulic conductivity using Equation 5-6. The hydraulic conductivity values determined from the air permeability measurements are presented in Table 5-2a; those obtained directly (at the final applied surface stress) are presented in Table 5-5-2b. The values of fluid constants used in the estimations are presented in Table 5-2c.

Table 5-2a: Equivalent vertical and horizontal hydraulic conductivity values from measurements with air.

TDA type	Applied surface stress, kPa	Average applied stress in TDA, kPa	Height of waste relative to applied surface stress (Zekkos et al. 2006), m	Initial void ratio (e_0) in TDA	Void ratio in TDA at the end of creep in load step	Equivalent horizontal hydraulic conductivity, m/s [A]	Equivalent vertical hydraulic conductivity, m/s [B]	Anisotropy in the hydraulic conductivity [B/A]
Sask TDA	56	32	5 to 6	2.19	0.99	3.77	0.38	10
	112	63	10 to 15		0.74	0.32	0.15	2
	224	123	20 to 25		0.52	0.10	0.04	2
	375	219	30 to 40		0.41	0.02	0.01	2
ARMA TDA double pass	112	53	10 to 15	2.09	0.65	0.35	0.05	7
	224	134	20 to 25		0.44	0.19	0.04	5
	375	210	30 to 40		0.34	0.03	0.01	2
ARMA TDA single pass	250	140	22 to 27	N/A	N/A	0.50	0.09	6

Table 5-2b: Equivalent vertical and horizontal hydraulic conductivity values from measurements with water – at the final applied stress (375 kPa).

TDA type	Applied surface stress, kPa	Equivalent horizontal hydraulic conductivity, m/s [A]	Equivalent vertical hydraulic conductivity, m/s [B]	Anisotropy in the hydraulic conductivity [B/A]
Sask TDA	375	0.07	0.03	2
ARMA TDA double pass	375	0.11	0.04	3

Table 5-2c: Values of parameters used in the flow equations

Parameter	Value
Average water temperature, ^oC	15
Average air temperature, ^oC	32
ρ(water) @ 15 ^oC, kg/m^3	999.1
ρ(air) @ 15 ^oC, kg/m^3	1.225
ρ(air) @ 32 ^oC, kg/m^3	1.131
μ(air) @ 32 ^oC, kg/ms	0.000019
μ(water) @15 ^oC, kg/ms	0.0012

The vertical hydraulic conductivity values in Tables 5-2 a, b are comparable to those in the literature for similar applied stress (Section 1.0). For all the applied stresses, the vertical and horizontal hydraulic conductivity of the TDA types (Table 5-2 a) were higher than 0.0001 m/s – the typical minimum stipulation for landfill drainage layers (Duffy, 1995; Narejo and Shettima, 1995; Warith et al. 2004). The values are also comparable to the typical range of 0.001 to 10 m/s for gravel – which has been conventionally used as drainage material in LCRS (Fleming and Rowe, 2004; McIsaac and Rowe, 2005; Rowe and McIsaac, 2005). Thus, further showing that large particle-sized TDA can be a suitable alternative to gravel in constructing the leachate collection and drainage layers in landfills (Hudson et al. 2007; Beaven et al. 2007; Mwai et al. 2010; Beaven et al. 2013; Mwai 2016; Adesokan et al. 2019; Adesokan et al. 2020; Marcotte and Fleming, 2020).

Anisotropy in the hydraulic conductivity generally decreased with the applied stress (Table 5-2 a). For Sask TDA, anisotropy was initially high at the applied surface stress of 56 kPa, but decreased to 2 at 112 kPa, and remained constant afterwards up to 375 kPa (Table 5-2 a). For ARMA TDA double pass, anisotropy decreased from 7 at the applied surface stress of 112 kPa, and also to 2 at 375 kPa (Table 5-2 a).

For ARMA TDA single pass, the anisotropy was 6 at an applied surface stress of 250 kPa. From these results, the anisotropy under applied stress appears to be material dependent, given the higher value for ARMA TDA double pass than Sask TDA at similar applied stress. This is perhaps not surprising as the ARMA TDA double pass particles were larger in length and width, but the same in thickness as the Sask TDA particles.

Although anisotropy in the hydraulic conductivity of the TDA types from the water and air based measurements were generally consistent (Tables 5-2a and 5-2b), the average vertical and horizontal hydraulic conductivity values from the measurements with water (Table 5-2b) were

somewhat higher than those from measurements with air (Table 5-2a). Given the large sized voids within the TDA (Figure 5-20), the large flows through, and the general difficulty of measuring the hydraulic conductivity of such highly permeable materials, the disparity in values is considered within reason. Similar disparity in values has been reported for fine grained soils with relatively smaller sized voids than tested in this work (Huang et al. 2016). Possible specific reasons for the disparity in values in this work include the inability of water to fully access the smaller/interstitial voids within individual TDA particles within the timeframe of the testing, coupled with preferential flow along the walls of the test cell.

Qualitative (visual) assessment of the particle geometry, and void sizes in the TDA thin section slices, from the porosimetry evaluation (Figure 5-20)[73], shows that the voids remained large under high applied surface stresses – 224 kPa in this instance (equivalent to 20 m – 25 m of waste (Zekkos et al. 2006)). There however does not appear to be significantly more elongated voids in the horizontal direction than in the vertical direction, as might have been expected in relation to the largely horizontal alignment of large particle-sized TDA. The initial void ratio of TDA in the porosimetry assessment (Equation 5-7) was 1.72; the final void ratio (Equation 5-8) was 0.2.

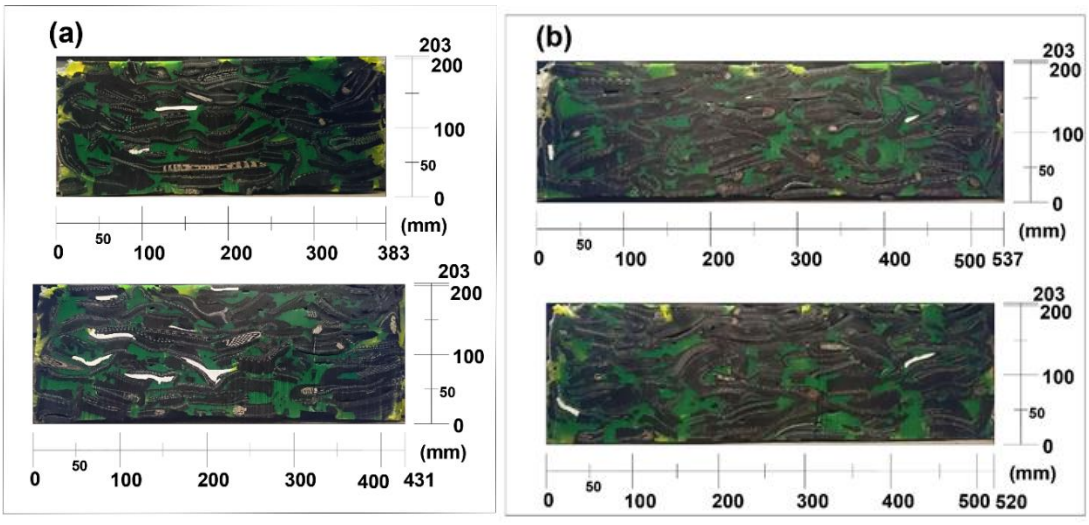

[73] Additional thin section images are presented in Section 5.6.3.2

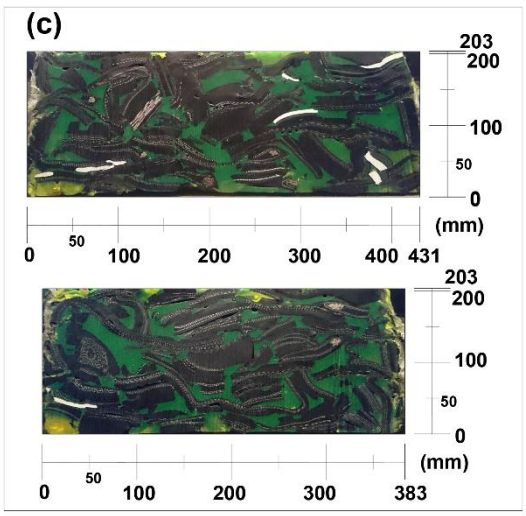

Figure 5-20: Some thin section slices of TDA from various portions of the epoxied TDA mass for the assessment of voids and particles under 224 kPa applied stress. The dark coloured portions are TDA pieces and the light coloured (greenish yellow) portions are the voids. Sask TDA was used in the porosimetry evaluation (a) slices from the right end; (b) slices from the middle; (c) slices from the left end. (Additional thin section images are presented in Section 5.6.3.2)

Although the hydraulic conductivity values for the various TDA types are sufficiently high for use in LCRS, biogeochemical clogging over time is expected to decrease these values as leachate permeates through the drainage layer, and this requires detailed investigation.

5.5 Conclusions and implications for practice

It is very difficult to measure the hydraulic conductivity of very coarse, highly compressible and highly permeable materials like large particle sized TDA. The high flow velocities through the voids of the TDA may result in non-Darcian flows, requiring correction for inertia. Likewise, because of sidewall friction during testing, vertical stress may be significantly higher at the top of the TDA than at the bottom, with correspondingly lower void ratio and permeability in the upper portion of the TDA than at the bottom. Thus requiring methods to account for the effects of sidewall friction loss on the inherent properties of TDA that may influence fluid flow. Both sidewall friction and inertia effects were accounted for in the analysis and discussion of results.

Because of the several drawbacks to using water as permeant fluid in determining the permeability/hydraulic conductivity of porous materials, air was used as the primary permeant

fluid to determine intrinsic permeability/air permeability values. From these, hydraulic conductivity values were determined. Direct measurement of hydraulic conductivity (with water) was completed at the final applied surface stress, and values obtained were compared with the hydraulic conductivity values estimated indirectly (from air permeability measurements). The results from the direct and indirect measurements were found to be generally consistent.

At all the applied stresses, for all the TDA types, the average vertical and horizontal hydraulic conductivity were higher than 0.001 m/s, which is comparable to the typical range of values for gravel used in LCRS, and meets, and exceeds the common recommendation of 0.0001 m /s for the hydraulic conductivity of drainage layers in LCRS. Anisotropy in the hydraulic conductivity of the TDA types was found to decrease with applied stress, and seemed to be dependent on the TDA type.

Overall, the results from this study show that the hydraulic conductivity of TDA can be determined effectively using air as the permeant fluid, and the high hydraulic conductivity values measured show that large particle sized TDA can be used as a suitable substitute for gravel for constructing the drainage layer of landfills. The effects of biogeochemical clogging on the hydraulic conductivity however need to be considered.

There is also a need to complete field measurements of air permeability or hydraulic conductivity to determine values under unconstrained loading conditions where sidewall friction effects are non-existent. The results from those measurements will be useful for calibrating laboratory testing results obtained under constrained loading conditions with sidewall friction effects. The results presented in this paper are expected to provide some further guidance on constructing a landfill drainage layer with large particle sized TDA.

5.6 Supplementary data for chapter

5.6.1 Summary Re values and flow plots for all the TDA types

As discussed in Section 5.4, presented in Table 5-3 are the Range of Re values for horizontal and vertical air and water flows for the TDA types. Full data is available in electronic format

Table 5-3: Range of Re values for horizontal and vertical air and water flows for the TDA types.

TDA type	Applied stress kPa	Flow medium	Flow direction	Range of specific discharge (m/s) (min to max)	Range of Re values (corresponding min to max specific discharge)
Sask TDA	56	air	horizontal	0.07 to 0.19	315 to 825
	112	air	horizontal	0.07 to 0.21	311 to 909
	224	air	horizontal	0.06 to 0.21	242 to 914
	375	air	horizontal	0.11 to 0.21	463 to 926
	375	water	horizontal	0.00064 to 0.0012	39 to 72
	56	air	vertical	0.03 to 0.10	128 to 441
	112	air	vertical	0.04 to 0.12	185 to 509
	224	air	vertical	0.03 to 0.09	114 to 385
	375	air	vertical	0.02 to 0.09	97 to 410
	375	water	vertical	0.00069 to 0.0014	42 to 84
ARMA TDA double pass	112	air	horizontal	0.11 to 0.23	497 to 976
	224	air	horizontal	0.08 to 0.28	356 to 1203
	375	air	horizontal	0.06 to 0.18	258 to 797
	375	water	horizontal	0.0017 to 0.0020	101 to 119
	112	air	vertical	0.03 to 0.11	142 to 496
	224	air	vertical	0.05 to 0.11	236 to 484
	375	air	vertical	0.03 to 0.08	114 to 347
	375	water	vertical	0.0004 to 0.0006	33 to 49
ARMA TDA single pass	250	air	horizontal	0.23 to 0.32	1004 to 1380
	250	air	vertical	0.07 to 0.11	296 to 476

The Reynolds numbers were generally higher for the testing completed with air, indicating more inertia effects and more turbulent-like flows when air is used as flow medium, even for similar void structures in a porous media.

As discussed in Section 5.4, the vertical and horizontal flow plots for testing with air and water for all the TDA types at the various applied stress are presented in Figures 5-21.

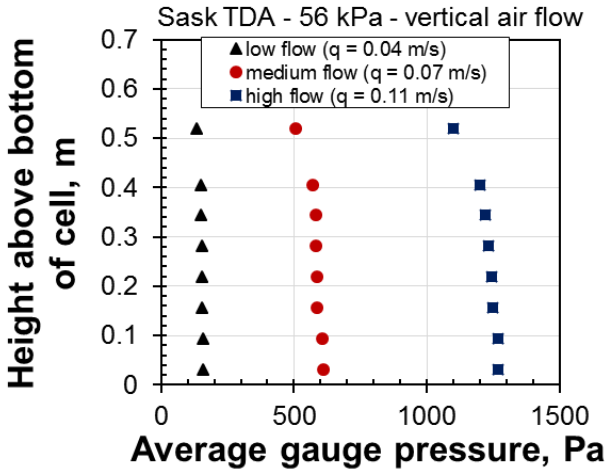
Sask TDA - 56 kPa - vertical air flow
low flow (q = 0.04 m/s)
medium flow (q = 0.07 m/s)
high flow (q = 0.11 m/s)
Height above bottom of cell, m
Average gauge pressure, Pa

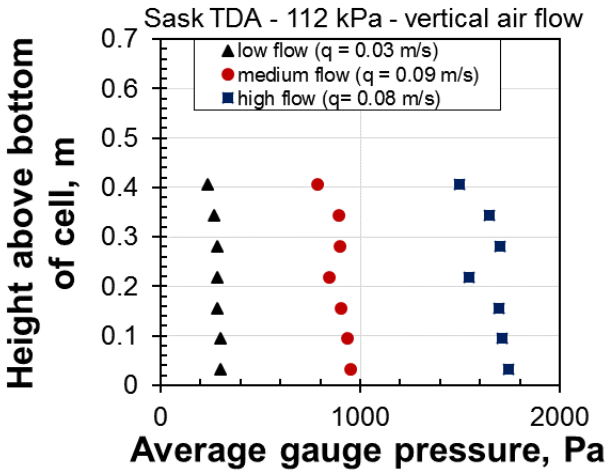
Sask TDA - 112 kPa - vertical air flow
low flow (q = 0.03 m/s)
medium flow (q = 0.09 m/s)
high flow (q= 0.08 m/s)
Height above bottom of cell, m
Average gauge pressure, Pa

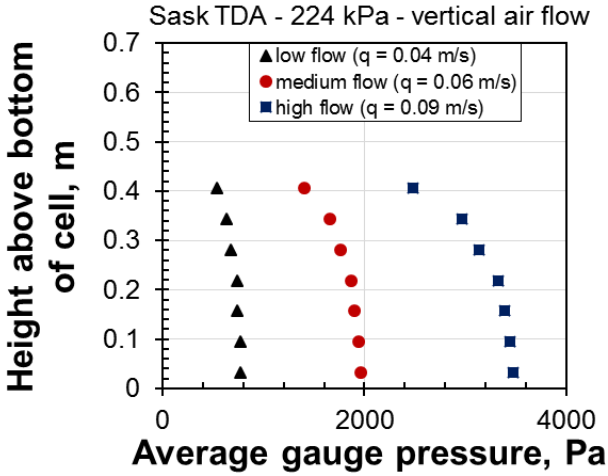
Sask TDA - 224 kPa - vertical air flow
low flow (q = 0.04 m/s)
medium flow (q = 0.06 m/s)
high flow (q = 0.09 m/s)
Height above bottom of cell, m
Average gauge pressure, Pa

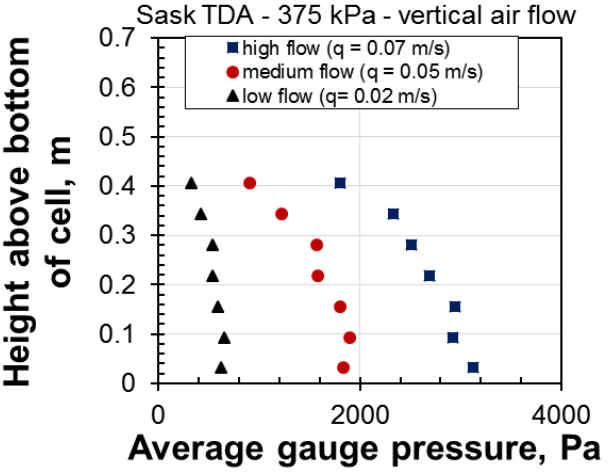
Sask TDA - 375 kPa - vertical air flow
high flow (q = 0.07 m/s)
medium flow (q = 0.05 m/s)
low flow (q= 0.02 m/s)
Height above bottom of cell, m
Average gauge pressure, Pa

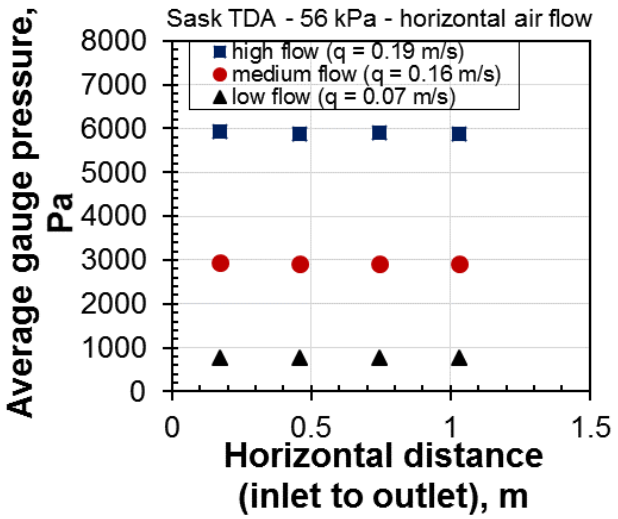
Sask TDA - 56 kPa - horizontal air flow
high flow (q = 0.19 m/s)
medium flow (q = 0.16 m/s)
low flow (q = 0.07 m/s)
Average gauge pressure, Pa
Horizontal distance (inlet to outlet), m

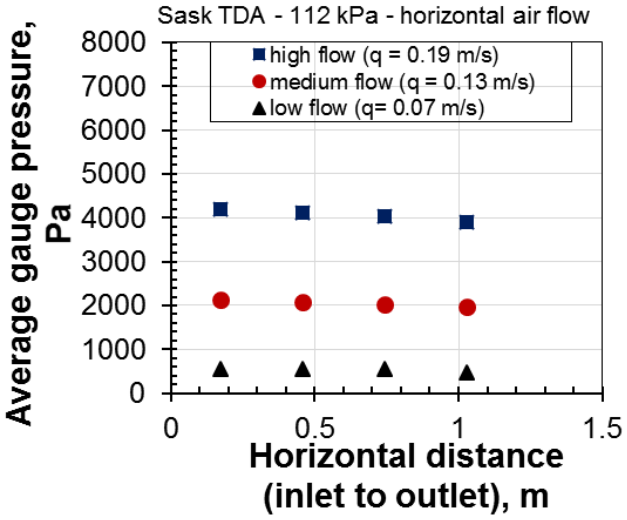
Sask TDA - 112 kPa - horizontal air flow
high flow (q = 0.19 m/s)
medium flow (q = 0.13 m/s)
low flow (q= 0.07 m/s)
Average gauge pressure, Pa
Horizontal distance (inlet to outlet), m

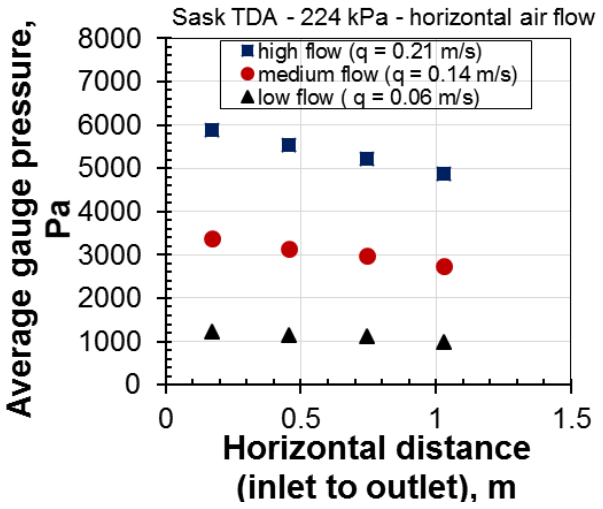
Sask TDA - 224 kPa - horizontal air flow
high flow (q = 0.21 m/s)
medium flow (q = 0.14 m/s)
low flow (q = 0.06 m/s)
Average gauge pressure, Pa
Horizontal distance (inlet to outlet), m

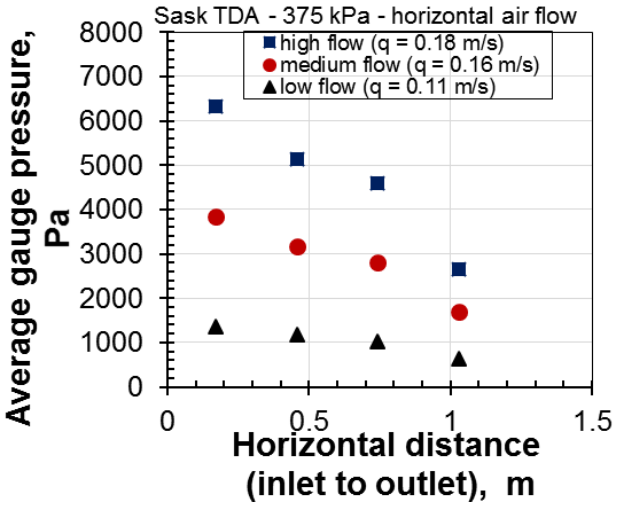
Sask TDA - 375 kPa - horizontal air flow
high flow (q = 0.18 m/s)
medium flow (q = 0.16 m/s)
low flow (q = 0.11 m/s)
Average gauge pressure, Pa
Horizontal distance (inlet to outlet), m

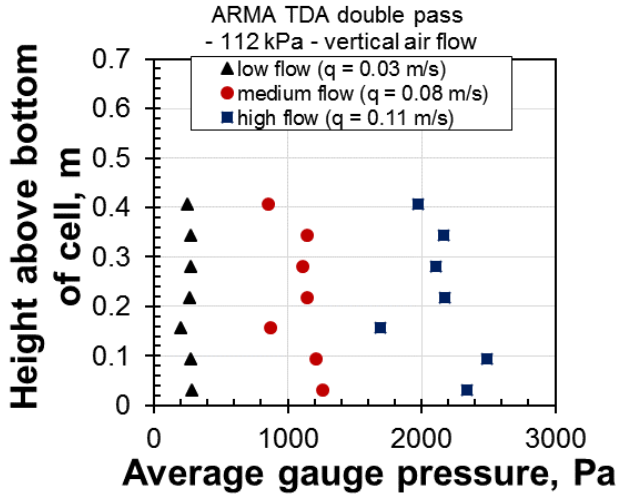
ARMA TDA double pass - 112 kPa - vertical air flow
low flow (q = 0.03 m/s)
medium flow (q = 0.08 m/s)
high flow (q = 0.11 m/s)
Height above bottom of cell, m
Average gauge pressure, Pa

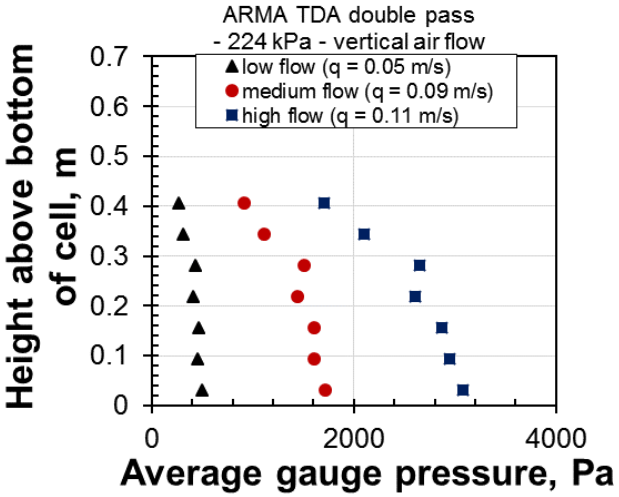
ARMA TDA double pass - 224 kPa - vertical air flow
low flow (q = 0.05 m/s)
medium flow (q = 0.09 m/s)
high flow (q = 0.11 m/s)
Height above bottom of cell, m
Average gauge pressure, Pa

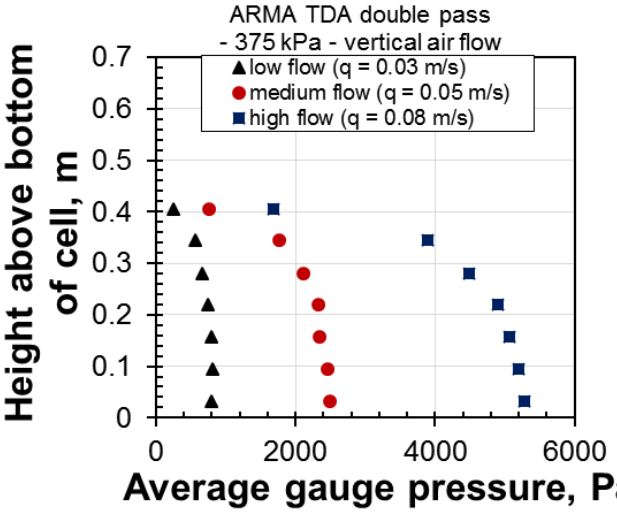
ARMA TDA double pass - 375 kPa - vertical air flow
low flow (q = 0.03 m/s)
medium flow (q = 0.05 m/s)
high flow (q = 0.08 m/s)
Height above bottom of cell, m
Average gauge pressure, Pa

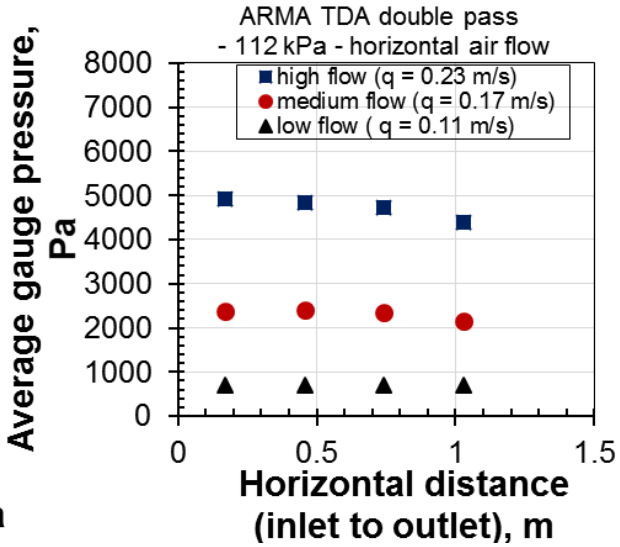
ARMA TDA double pass - 112 kPa - horizontal air flow
high flow (q = 0.23 m/s)
medium flow (q = 0.17 m/s)
low flow (q = 0.11 m/s)
Average gauge pressure, Pa
Horizontal distance (inlet to outlet), m

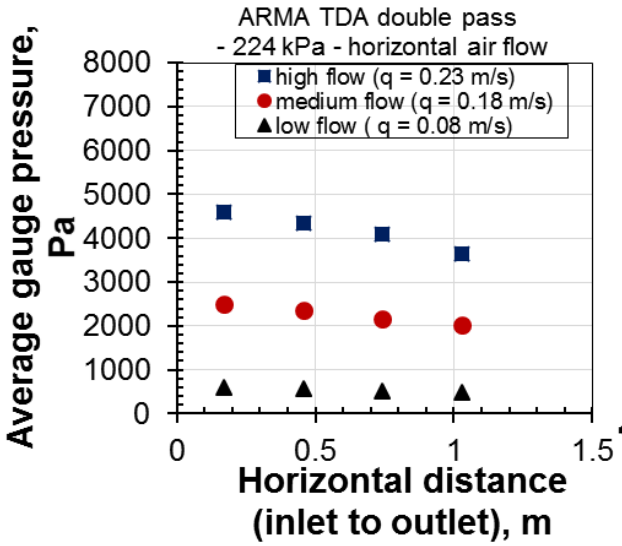
ARMA TDA double pass
- 224 kPa - horizontal air flow
high flow (q = 0.23 m/s)
medium flow (q = 0.18 m/s)
low flow (q = 0.08 m/s)
Average gauge pressure, Pa
Horizontal distance (inlet to outlet), m

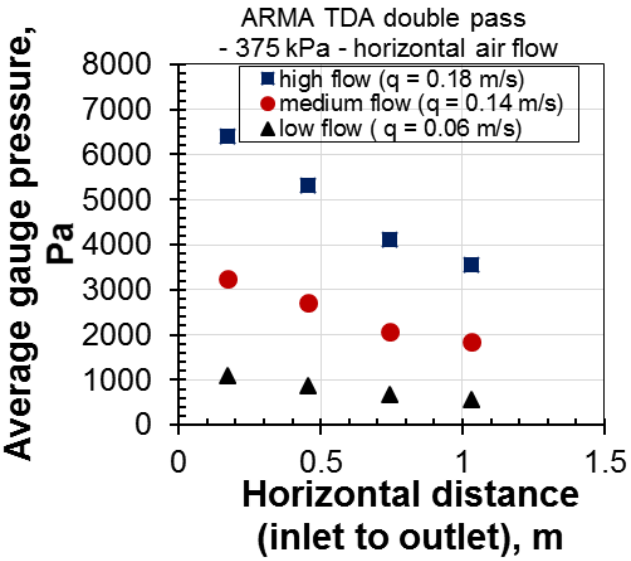
ARMA TDA double pass
- 375 kPa - horizontal air flow
high flow (q = 0.18 m/s)
medium flow (q = 0.14 m/s)
low flow (q = 0.06 m/s)
Average gauge pressure, Pa
Horizontal distance (inlet to outlet), m

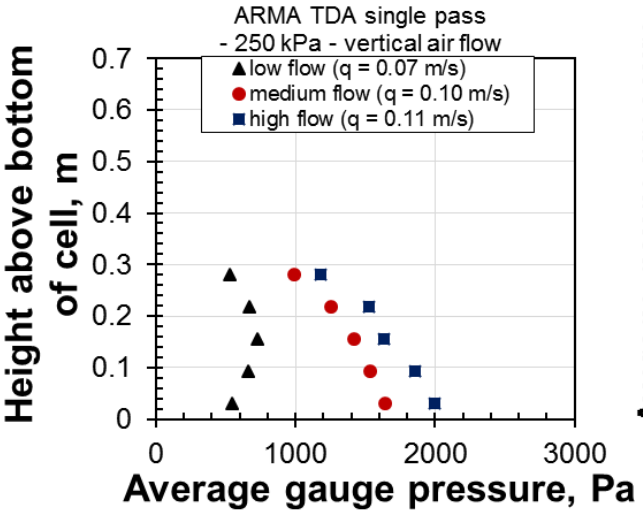
ARMA TDA single pass
- 250 kPa - vertical air flow
low flow (q = 0.07 m/s)
medium flow (q = 0.10 m/s)
high flow (q = 0.11 m/s)
Height above bottom of cell, m
Average gauge pressure, Pa

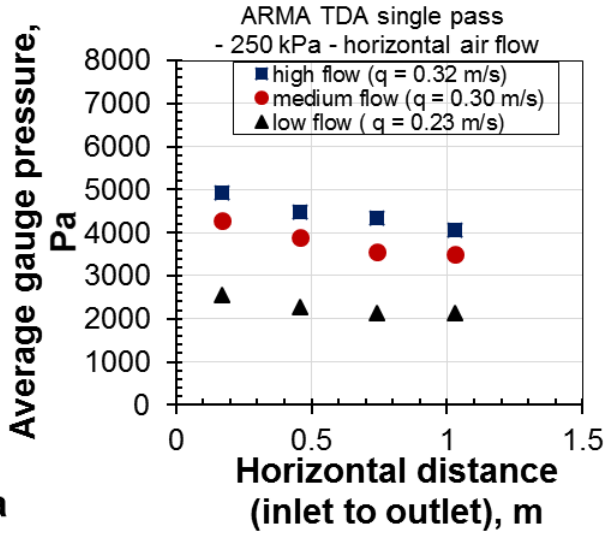
ARMA TDA single pass
- 250 kPa - horizontal air flow
high flow (q = 0.32 m/s)
medium flow (q = 0.30 m/s)
low flow (q = 0.23 m/s)
Average gauge pressure, Pa
Horizontal distance (inlet to outlet), m

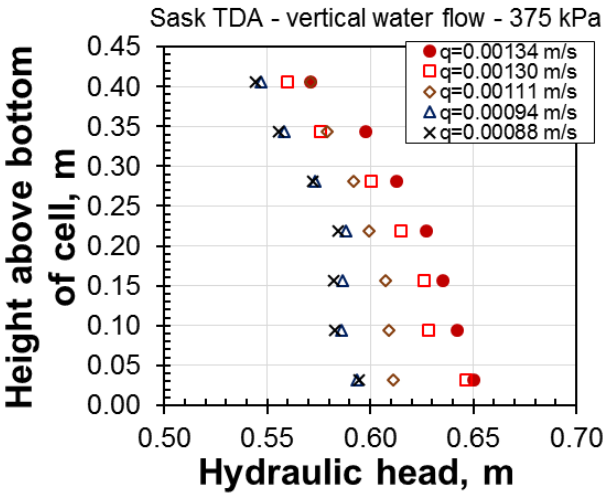
Sask TDA - vertical water flow - 375 kPa
q=0.00134 m/s
q=0.00130 m/s
q=0.00111 m/s
q=0.00094 m/s
q=0.00088 m/s
Height above bottom of cell, m
Hydraulic head, m

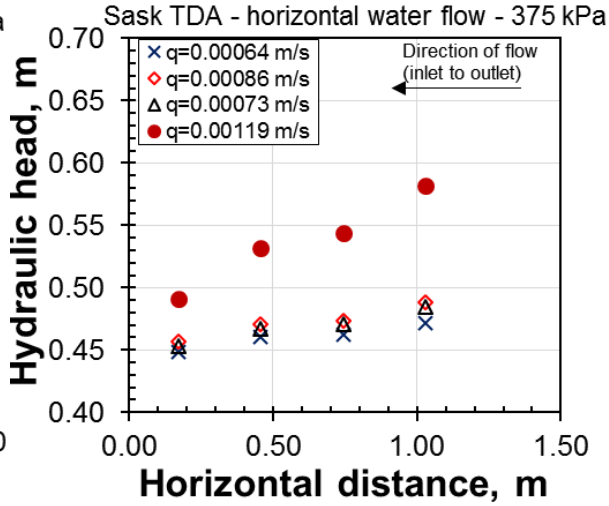
Sask TDA - horizontal water flow - 375 kPa
q=0.00064 m/s
q=0.00086 m/s
q=0.00073 m/s
q=0.00119 m/s
Direction of flow (inlet to outlet)
Hydraulic head, m
Horizontal distance, m

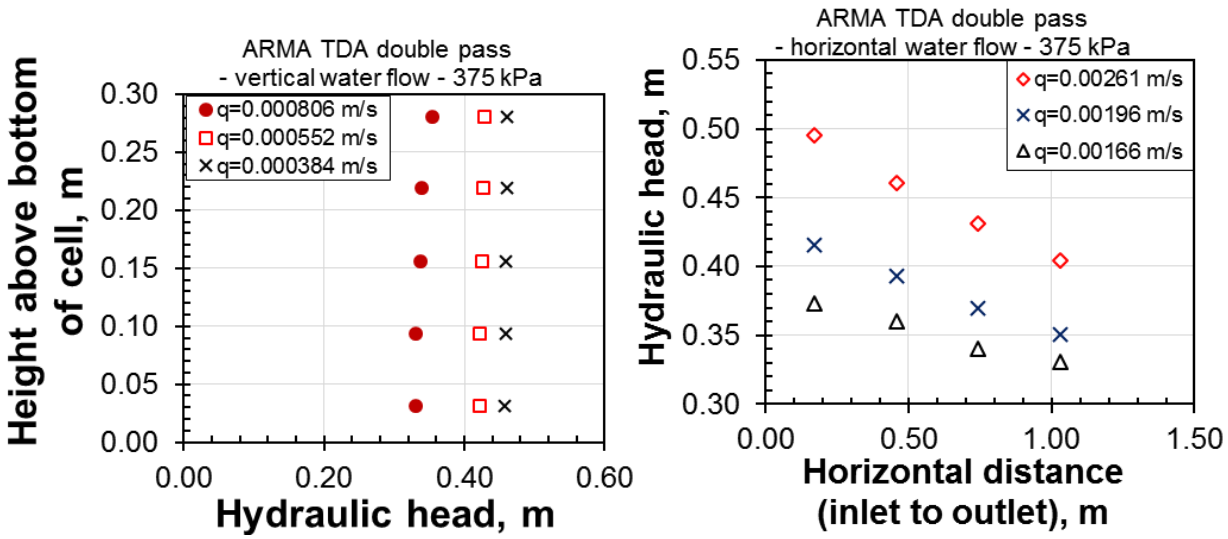

Figure 5-21: Vertical and horizontal flow plots for testing with air and water for all the TDA types at the various applied stress

5.6.2 Compression data for testing completed in the 2D cell

As presented in Section 5-4 – Table 5-2 (a),Table 5-4 contains a summary of the compression results for testing completed in the 2D cell in Table 5-2(a).

Table 5-4: Summary compression data for testing completed in the 2D cell (compression readings were not taken for ARMA TDA single pass). Full compression data is available in electronic format.

TDA type	Applied surface stress, kPa	Average stress in TDA[74]	Initial void ratio (at the start of testing event), e_0 [A]	Void ratio at the end of creep in load step [B]	Average compression $(\Delta e/1+e_0)*100$ [(A-B)/(1+A)] (%)
Sask TDA	56	31.60	2.2	0.99	37.81
	112	63.23		0.74	45.63
	224	123.11		0.52	52.50
	375	218.87		0.41	55.94
ARMA TDA double pass	112	52.86	2.1	0.65	48.44
	224	134.41		0.44	55.00
	375	209.65		0.34	58.13

[74] See Section 5.4

Presented in Table 5-5 are the initial measurements for testing completed in the 2D cell for the compression results in Table 5-2 (a)), Section 5-4, and Table 5-4 (Section 5.6.2 above)

Table 5-5: Initial measurements for testing completed in the 2D cell. Internal area of cell 0.72 = m^2, Gs measured = 1.27

	Total mass (kg)	Height (m)	Volume (m^3)	γ (kg/m^3)	Initial void ratio, e_0	Porosity, n
Sask TDA	290.0	1.00	0.72	402.78	2.15	0.68
ARMA TDA double pass	296.7	1.00	0.72	412.08	2.08	0.68

A plot of the compression results in Table 5-4 is presented in Figure 5-22. Figure 5-22 further shows the importance of the initial void ratio on the void ratio of TDA at any applied stress, as starting with a higher void ratio (Sask TDA) resulted in higher void ratios throughout the testing event than starting with a lower initial void ratio (ARMA TDA double pass). This finding is similar to the findings from testing in the 1D cell (Chapter 4). Figure 5-22 also shows variations in void ratio values for any value of applied stress, as with the findings in Chapter 4.

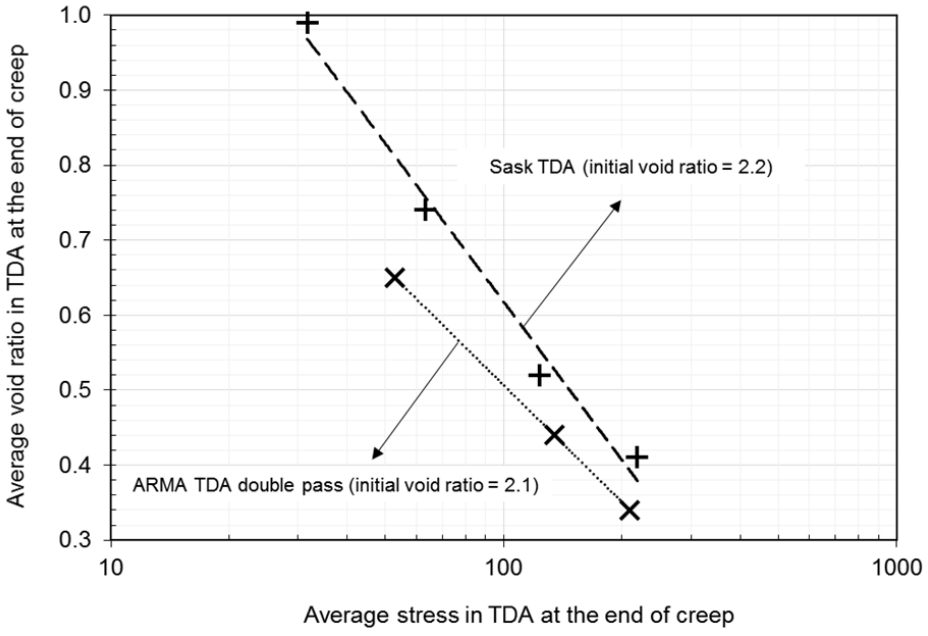

Figure 5-22: Relationship between void ratio and applied stress (e logP plots) from testing completed in the the 2D cell. Compression readings were not taken for ARMA TDA single pass (Additional details of the TDA types are presented in Section 5.2.1).

Compression of TDA in the 2D cell was generally lower than in the 1D cell at similar applied stresses and initial void ratios, because sidewall friction loss was higher in the 2D cell than in the 1D cell. Even with similar sidewall treatments in both cells, there were still considerable differences in the applied stress reaching the bottom of the cells. For instance, at 224 kPa, in the 1D cell, the bottom stress was approximately 150 kPa (Figure 4-18, Section 4.5.3), while in the 2D cell, at that applied stress, the bottom stress was less than 50 kPa (Figure 5-10, Section 5.4). The variation in compression values in the two cells highlights the need to evaluate sidewall friction loss in the laboratory testing of TDA as this will enable accurate evaluation of void ratio and compression, relative to the applied stress. In addition, it is recommended to evaluate sidewall friction loss independently for individual testing units.

5.6.3 Specific surface area mapping

5.6.3.1 TDA used for the porosimetry evaluation

As discussed in Sections 5.2.2.2 and 5.3.1.3, presented in Figure 5-23 are images of the TDA type that was used in the porosimetry evaluation – Sask TDA, same as Sask TDA 2 in Chapter 4 (Figure 4-1).

(a)

Figure 5-23: (a) Unwashed, (b) washed for epoxy impregnation/cold mounting

5.6.3.2 Thin section images from porosimetry evaluation

As discussed in Sections 5.2.2.2, 5.3.1.3 and 5.4, presented in Figure 5-24 (a – c) are additional images of the epoxy impregnation process.

Figure 5-24(a): Epoxy impregnation process under approximately 224 kPa of applied stress. TDA thin section slices below

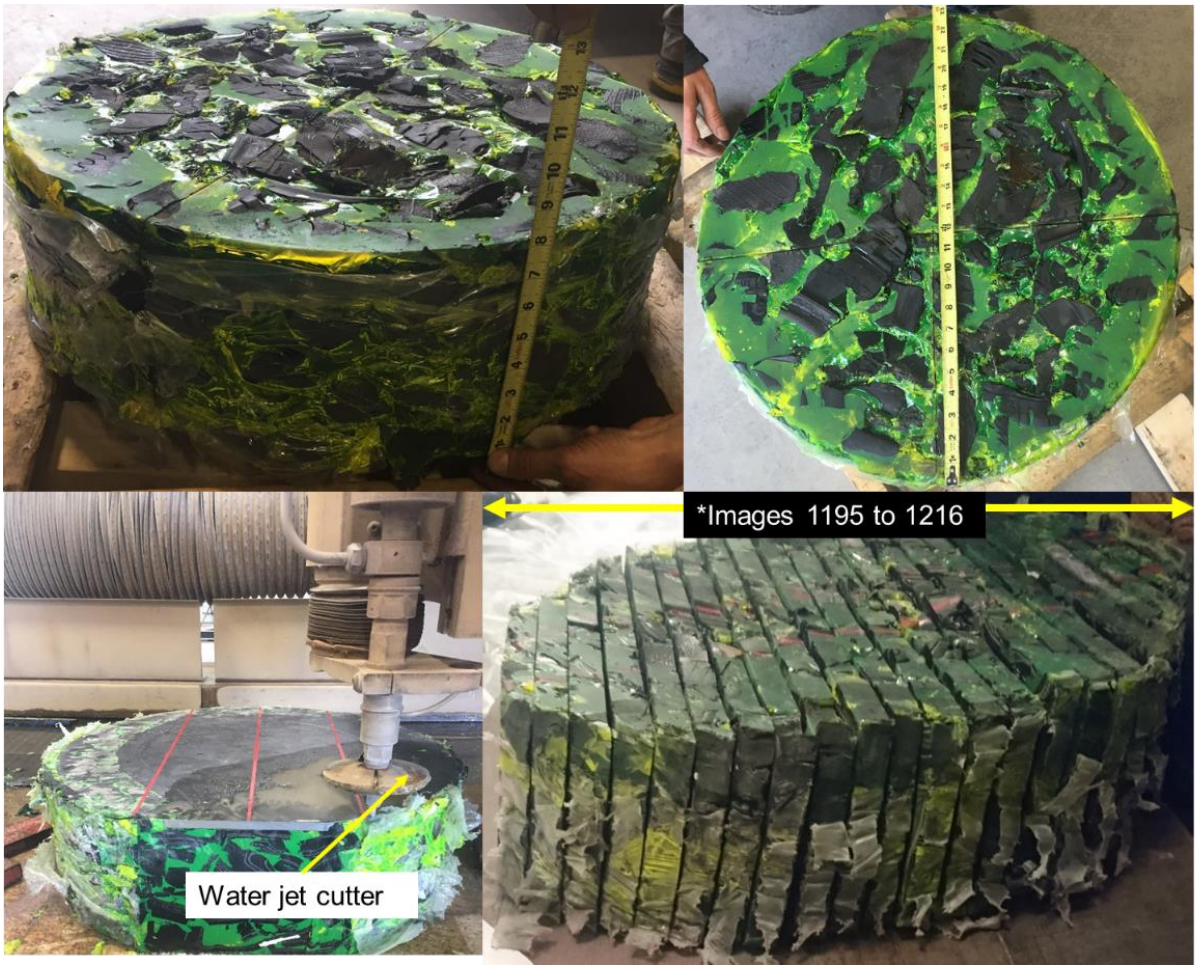

*Figure 5-24(b): Epoxied TDA thin sectioned into 0.025 m slices using a water jet cutter with Garnet 80 mesh spec sand. *See Figure 5-25(c)*

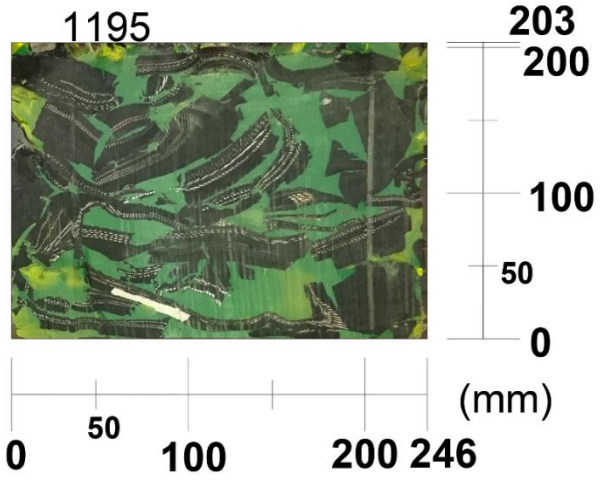

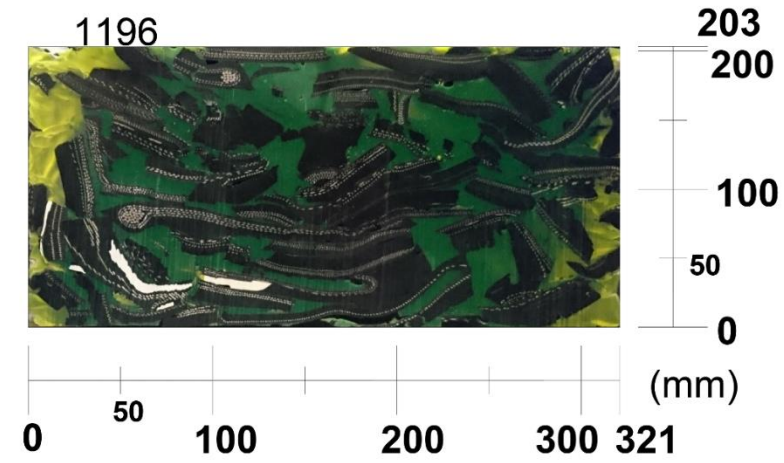
1196
203
200
100
50
0
(mm)
0
50
100
200
300
321


1197
203
200
100
50
0
(mm)
0
50
100
200
300
383

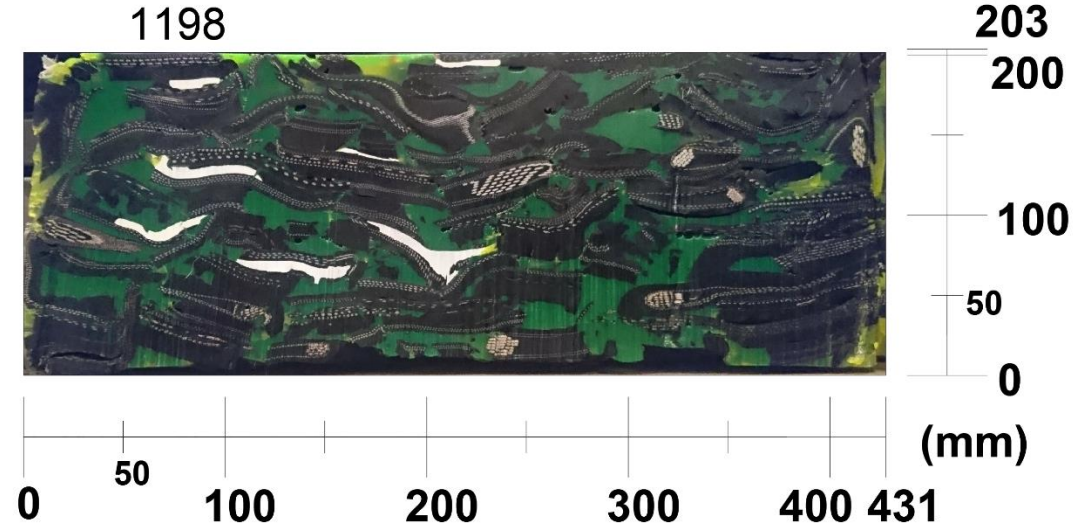
1198
203
200
100
50
0
(mm)
0
50
100
200
300
400
431

1199

203
200
100
50
0
(mm)
0 50 100 200 300 400 468

1200

203
200
100
50
0
(mm)
0 50 100 200 300 400 459

1201

203
200
100
50
0
(mm)
0 50 100 200 300 400 498

1202

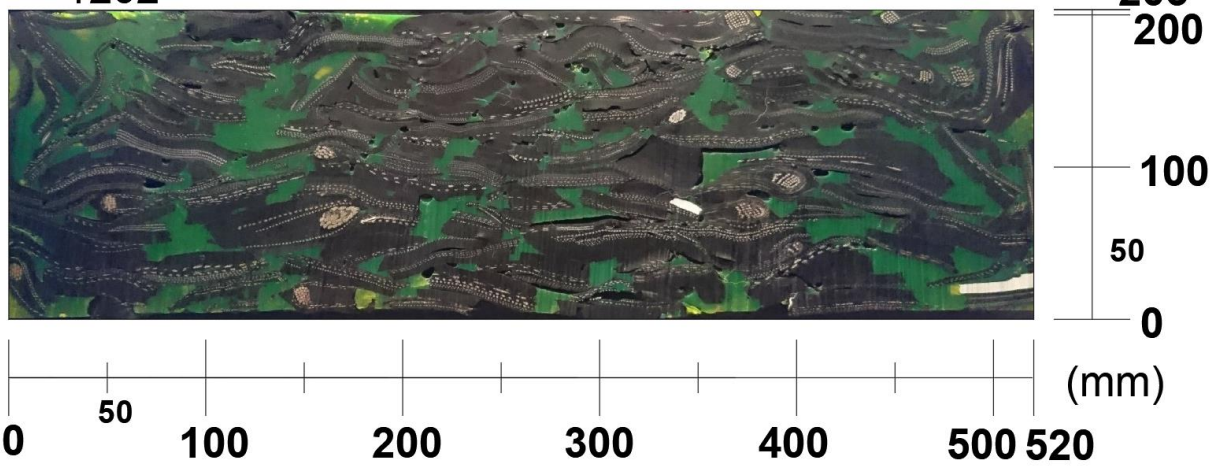

1203

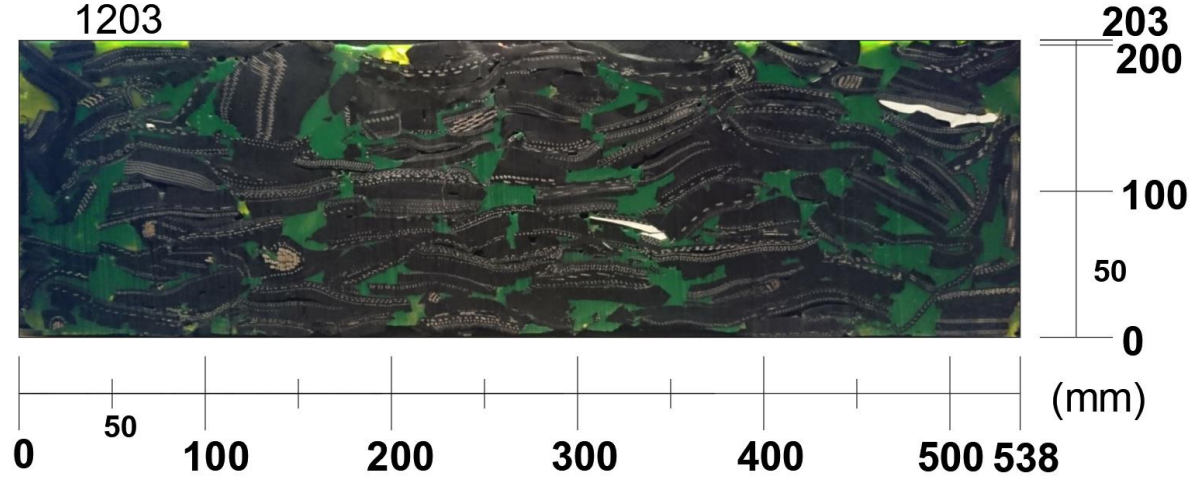

1204

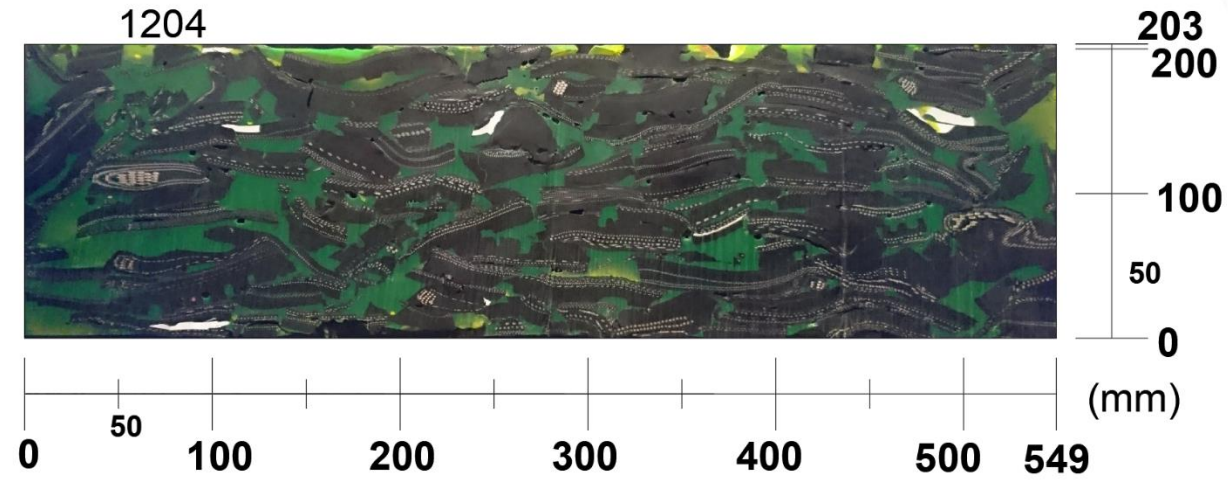

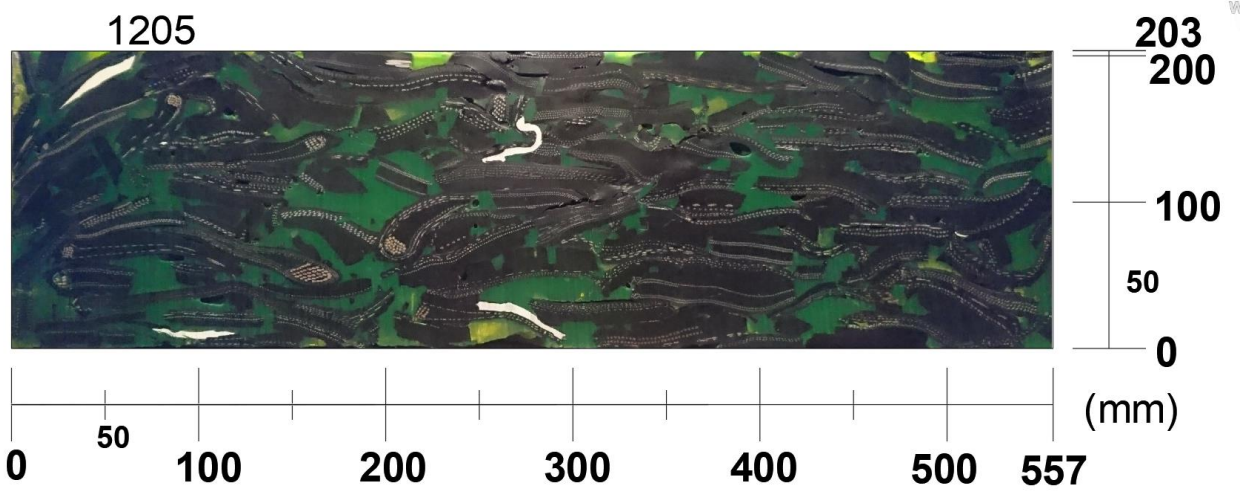
1205
203
200
100
50
0
(mm)
0
50
100
200
300
400
500
557

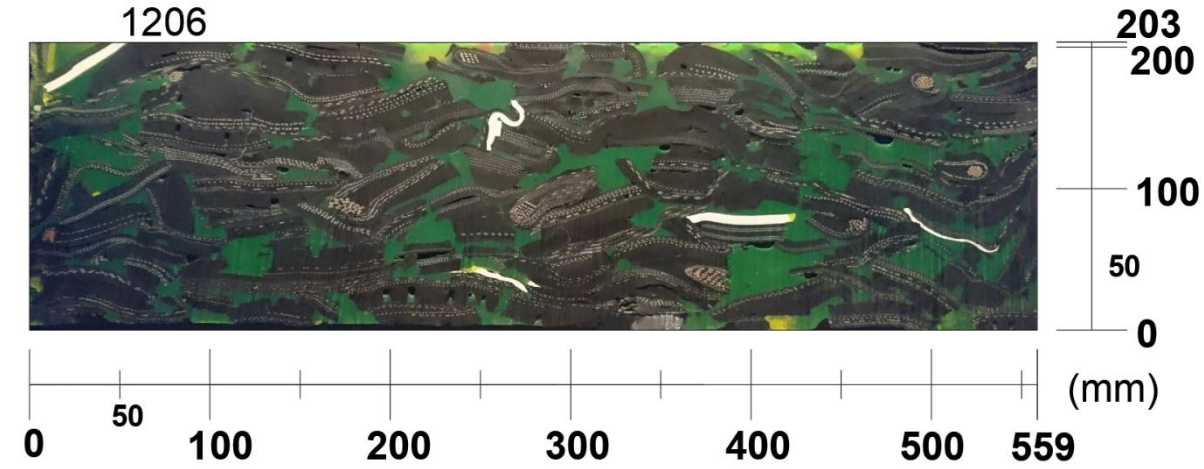
1206
203
200
100
50
0
(mm)
0
50
100
200
300
400
500
559

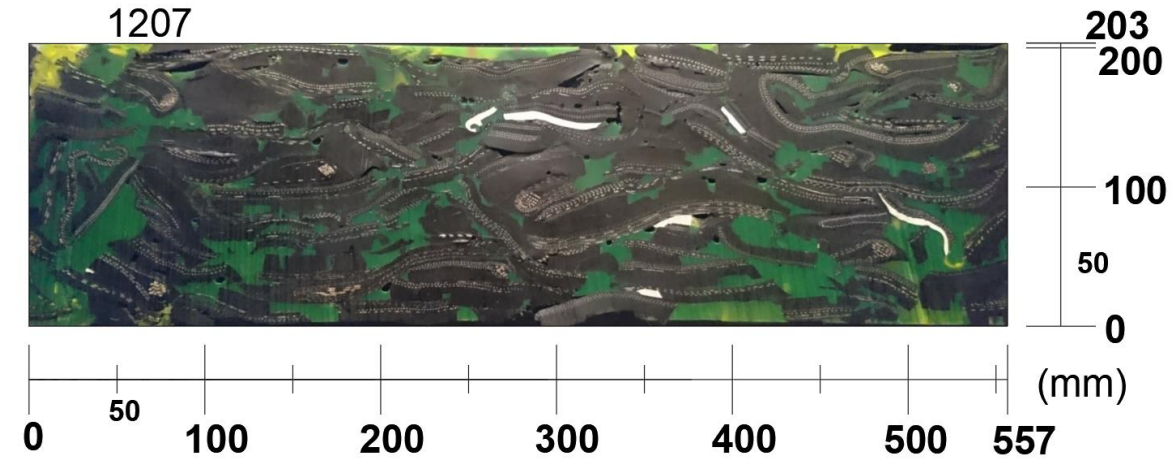
1207
203
200
100
50
0
(mm)
0
50
100
200
300
400
500
557

1208

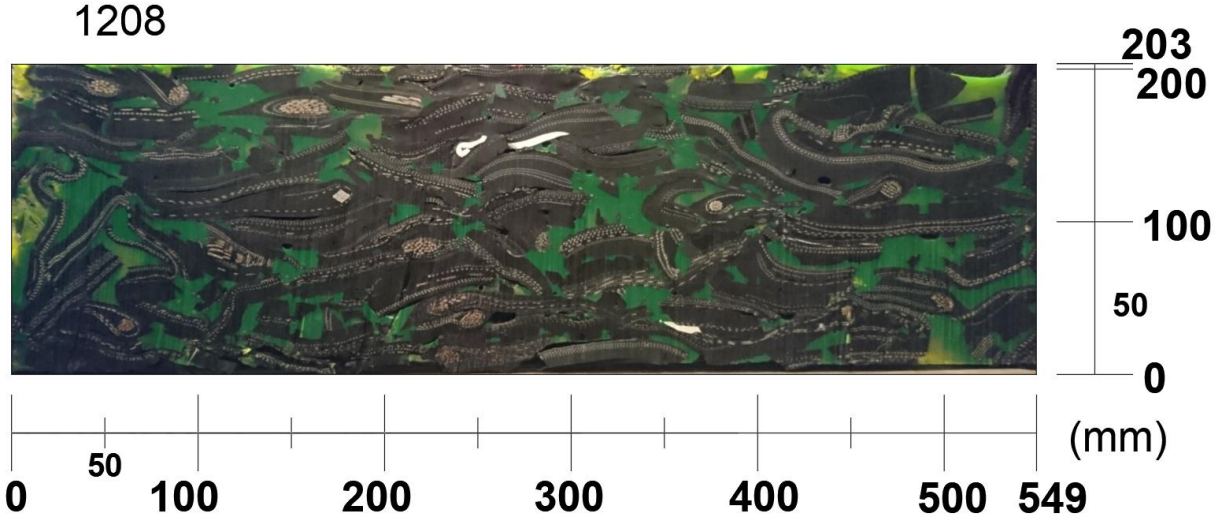

1209

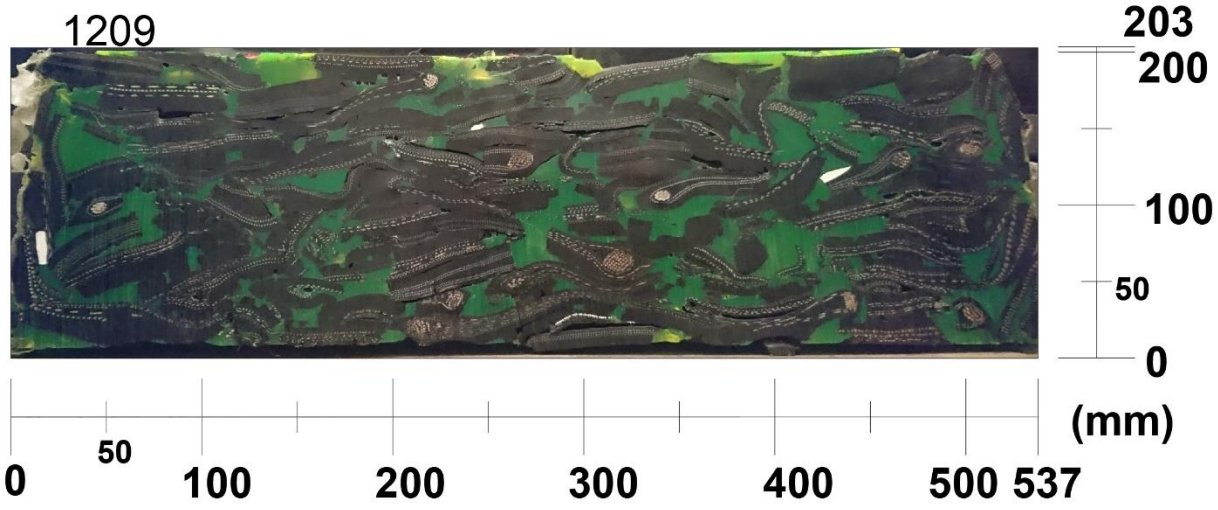

1210

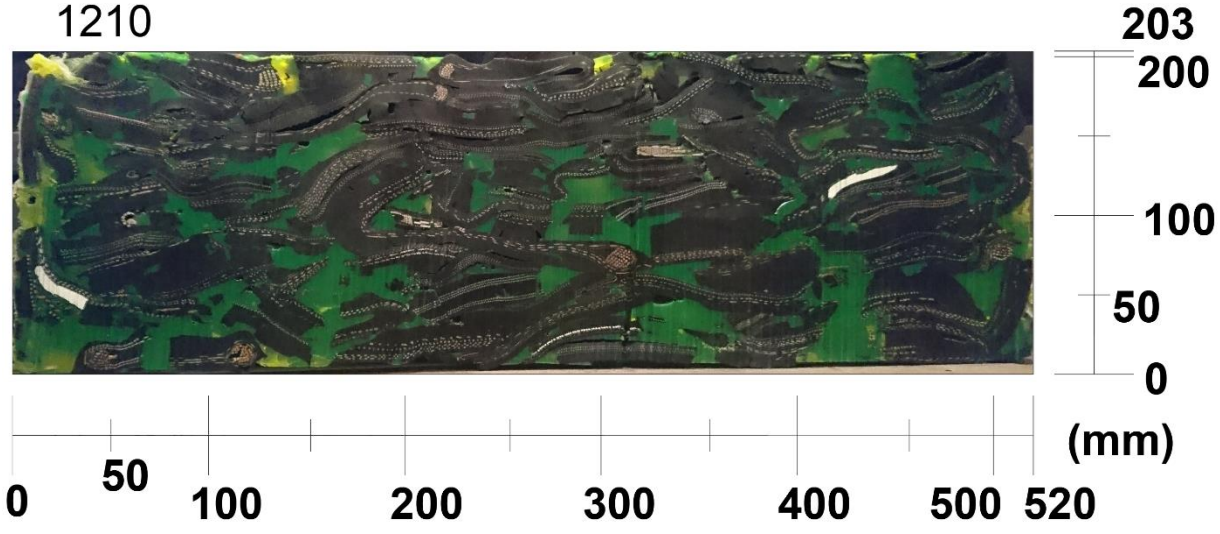

1211

1212

1213

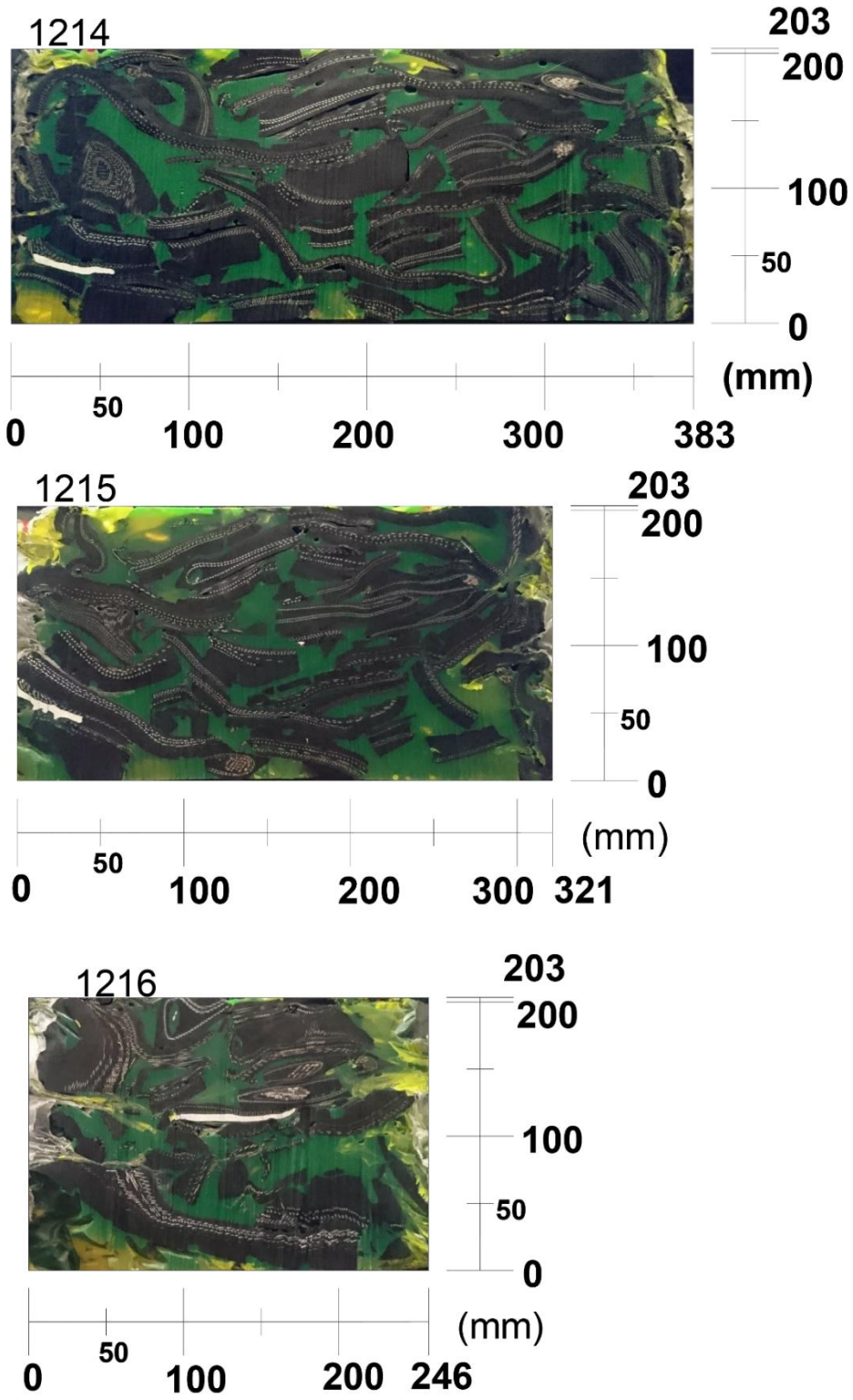

Figure 5-24(c): Thin section slices of TDA for specific surface area and void ratio analysis (Table 5-6). The dark portions are the TDA pieces and the light coloured (greenish yellow) portions are the voids

5.6.3.3 Analysis of thin section images using Image J

Presented in Figure 5-25 is the process used to map the geometry of voids and TDA particles within the TDA thin sections, using Image J – an image processing application. The voids and solids geometry was used to determine specific surface area and void ratio in the TDA (Table 5-6, Figure 5-26) for use in formulating functional equations for an alternative sidewall friction approach discussed in Sections 5.1 and 5.4. Derivations of the equations are presented in Section 5.6.4

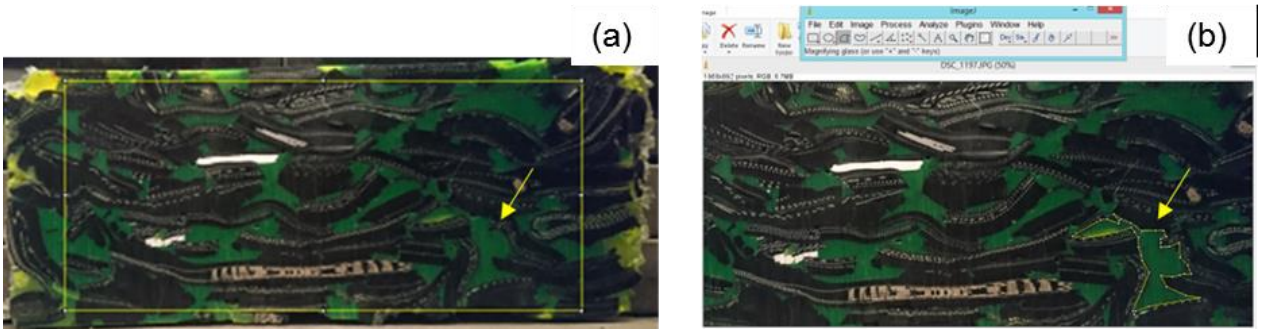

Figure 5-25: Mapping the geometry of voids and TDA particles within the thin sections using Image J. (a) a light coloured box is used to isolate edge effects and highlight a region to map on a thin sectioned slice of TDA. The light coloured arrow points to the void to be mapped in this instance; (b) the target void is mapped by manually clicking around its peripheries to isolate the void for evaluation. The perimeter and area of the selected voids was calculated using the "Analyze" function in Image J. This process was repeated for every void and TDA solids within each thin section. The results of the analyses are presented in Table 5-6.

Presented in Table 5-6 are the results of the voids and solids geometry mapping process. The results in Table 5-6 were used to plot Figure 5-26 to determine the relationship between specifc surface area and void ratio for use in the functional forms that were formulated (see Section 5.6.4) to address sidewall friction effects in the flow data.

The results from the porosimetry evaluation can also be used in existing biogeochemical clogging models to evaluate clogging in TDA under applied stress. It is however recommended to complete similar specific surface area evaluations under additional applied stresses, especially those greater than 224 kPa, which was studied in this work. This will enable clogging

evaluations to be carried out for TDA under overlying waste thicknesses greater than 25 m of overlying waste (Zekkos et al. 2006).

Table 5-6: Results from the analysis of the thin sections using ImageJ (see Figure 5-25). (Results from mapping images 1201 to 1208 – Figure 5-24(c) were excluded from Table 5-6 as they were inconsistent with the other results)

Thin section ID (thin section images in Figure 5-23)	Total area of image [T]	Correction factor (image dimension/ actual dimension), m	Corrected perimeter of TDA solids in image [P]	Corrected area of TDA solids in image [A]	Specific surface area of TDA solids in image, /m [P/A]	Porosity (in thin section) [C] = (1-(A/T))	Void ratio (in thin section) [V] = C/(1-C)
1195	263856	2894	14949	195052	221.79	0.26	0.35
1196	328434	2874	19920	253569	225.78	0.23	0.30
1197	328434	2680	19920	253569	210.50	0.23	0.30
1198	145392	1596	8631	125690	109.60	0.14	0.16
1199	118314	1379	10316	101855	139.71	0.14	0.16
1200	117369	1294	10988	103551	137.34	0.12	0.13
1209	113460	1216	9762	99598	119.21	0.12	0.14
1210	121485	1262	9166	107503	107.61	0.12	0.13
1211	123778	1325	9256	108844	112.69	0.12	0.14
1212	134506	1428	6697	118436	80.75	0.12	0.14
1213	142209	1548	9824	121214	125.42	0.15	0.17
1214	164012	1849	9236	138686	123.12	0.15	0.18
1215	206504	2292	10802	164917	150.14	0.20	0.25
1216	277400	3055	11933	212493	171.56	0.23	0.31

From Table 5-6, the average void ratio in the TDA is 0.2, at an applied stress of approximately 224 kPa. The initial void ratio of TDA in the porosimeter was 1.7. The final void ratio of 0.2 is a little lower than those measured for similar initial void ratios, and applied stress in the other tests completed in this research work (testing in the 1D consolidometer, and in the 2D cell). The reason for the lower final void ratio may be related to the voids mapping process. For instance, portions in the images that were voids may have been inadvertently mapped as solids, especially for areas with interparticle contact.

The lower final void ratio may also be because generally smaller particle sized TDA were used in the porosimetry evaluation (Figure 5-23), than in the other tests (Chapters 3, 4, 5). The

particles used in the porosimetry evaluation were generally smaller because of the smaller size of the compression cell (Figure 5-6), which had the maximum diameter that could fit within the frame of the load application unit used.

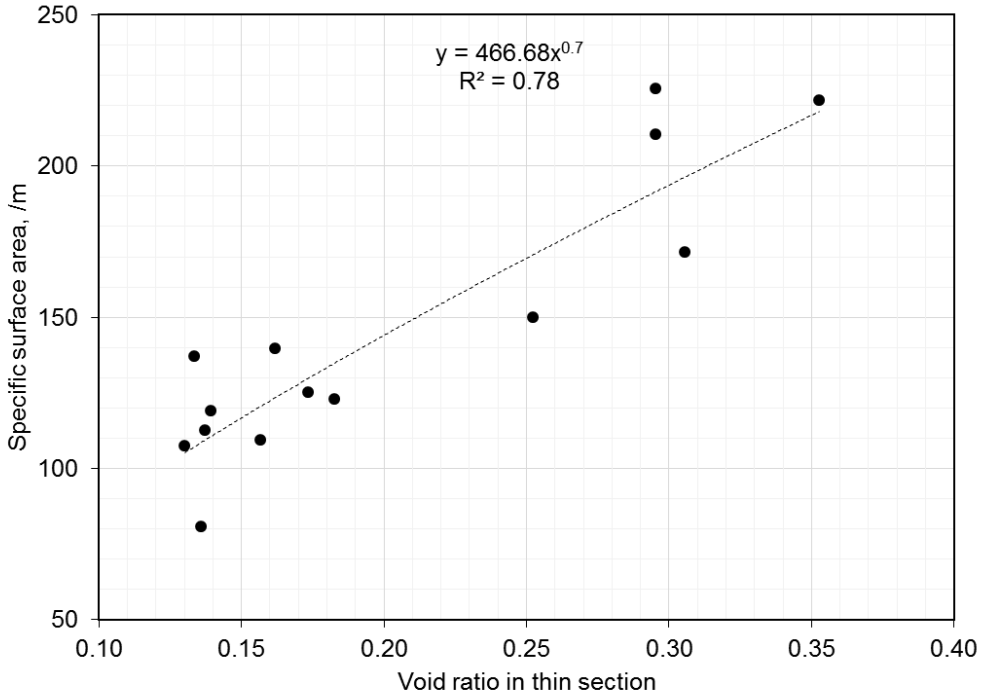

Figure 5-26: Relationship between specific surface area and void ratio in thin sections (data in Table 5-6, images of thin sections in Figure 5-24 (c))

Figure 5-26 shows the relationship between specific surface area and void ratio in the thin sections. This was used in the formulation of the hydraulic conductivity function to address sidewall friction effects in the laboratory data (see Section 5.6.4).

5.6.4 Determining the functional forms of pressure and hydraulic conductivity distribution for addressing sidewall friction effects in the flow data (approach #2 for addressing sidewall friction effects in the data)

As discussed in Sections 5.1 and 5.4, functional forms of pressure and hydraulic conductivity were formulated for use in determining the vertical distribution of both vertical and horizontal hydraulic conductivity to address sidewall friction effects in the flow data. The functional form of vertical hydraulic conductivity $k_z(z)$ was first determined and then inserted into the pressure

distribution form P(z). Knowing $k_z(z)$ and P(z), the vertical distribution of horizontal hydraulic conductivity $k_x(z)$ across the TDA thickness was determined.

5.6.4.1 Deriving the functional form of $k_z(z)$

The functional form of $k_z(z)$ was derived by incorporating into the Kozeny Carman relation for hydraulic conductivity (Equation 5-20) – see Das (1983), Carrier III (2003), Chapuis and Aubertin (2003), a series of relations that had been determined from previous and complementary laboratory testing and analysis completed in this study. The relations used in the derivation of $k_z(z)$ are as follows:

(1) Applied stress as a function of height ($\sigma_z = f(z)$);

(2) Void ratio as a function of applied stress $e = f(\sigma_z)$);

(3) Void ratio as a function of height e = f(z)) ;

(4) Vertical hydraulic conductivity as a function of void ratio (e) and specific surface (S) k = f(e, S_s));

(5) Specific surface (S_s) as a function of void ratio (e) ($S_s = f(e)$).

(1) Determining applied stress as a function of position i.e. $\sigma_z = f(z)$

A schematic of the 2D test cell indicating parameters for determining $\sigma_z = f(z)$ is presented in Figure 5-27. The relationship between σ_z and z had been determined for the 1D cell (Section 3.10.5), this was determined for the 2D test cell as follows:

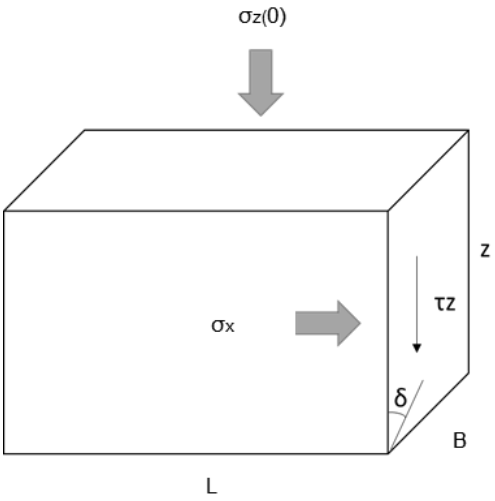

Where:

$\sigma_z(0)$ = Applied surface stress, kPa

σ_x = Lateral stress acting on the sidewall , kPa

τ_z = Shear stress from sidewall friction, kPa

z= Position/depth, m

δ = Angle of internal shearing resistance (sidewall friction angle)

L = length of the test cell, m

B = breadth of the test cell, m

Figure 5-27: Schematic of 2D test cell indicating parameters for determining $\sigma_z = f(z)$

Because of sidewall friction, applied surface stress $\sigma_z(0)$ decreased with depth z in relation to the shear stress acting along the sidewall τ_z (Figure 5-27).

Hence,

$$\Delta\sigma_z / \Delta z = -\tau_z \qquad (5\text{-}9)$$

If the Mohr's equation for shear stress (Equation 5-10) can be adapted, then, ignoring the apparent cohesion (c) term, and representing the internal friction angle ϕ as the sidewall friction angle δ, the interface shear stress τ_z acting along the sidewall of the 2D test cell can be represented as Equation 5-11.

$$\tau = \sigma_z \tan\phi + c \qquad (5\text{-}10)$$

$$\tau_z = \frac{-(\sigma_x \tan\delta) \times (2(L+B))z}{LB} \qquad (5\text{-}11)$$

Where

$2(L+B)z$ is the lateral area of the sidewalls of the 2D cell, LB is the total surface area of the cell

Substituting $\sigma_x = \sigma_z(K_0)$ (lateral stress coefficient) into Equation 5-11 gives:

$$\tau_z = \frac{-(\sigma_z K o t a n \delta) \text{ X } (2(L+B))z}{LB} \qquad (5\text{-}12)$$

Substituting Equation 5-12 into 5-9 gives:

$$\frac{\Delta\sigma_z}{\Delta dz} = \frac{-(\sigma_z K o t a n \delta) \text{ X } (2(L+B))z}{LB} \qquad (5\text{-}13)$$

Integrating an infinitesimal change in σ_z and z gives

$$\int \frac{d\sigma_z}{\sigma_z} = \int - \left((K o t a n \delta) * \frac{(L+B)*2}{LB} \right) * dz$$

$$\ln \sigma_z(z) = - \left((K o t a n \delta) * \frac{(L+B)*2}{LB} \right) * z + c$$

When z = 0, $\sigma_z = \sigma_z(0)$ and $C = \ln \sigma_z(0)$

$$\ln \sigma_z(z) = - \left((K o t a n \delta) * \frac{2(L+B)}{LB} \right) * z + \ln \sigma_z(0)$$

$$\sigma_z(z) = e^{-((K o t a n \delta)*2(L+B)/LB)*z} + e^{\ln \sigma_z(z)}$$

$$\sigma_z(z) = \sigma_z(0) e^{-(\frac{2 K o t a n \delta (L+B)}{LB})z} \qquad (5\text{-}14)$$

Equation 5-14 was used to determine the vertical distribution of applied stress across the TDA thickness in the 2D cell as used in Figure 5-30(b). A similar relation was determined for the 1D cell (Equation 3-13, Section 3.10.5).

(2, 3) Void ratio as a function of applied stress ($e = f(\sigma_z)$), and void ratio as a function of height ($e = f(z)$)

From the e*logP* plots of the 1D compression tests in Chapters 3 and 4, the relationship between void ratio and applied stress (e and $\sigma_z(z)$) in TDA can be described using the consolidation equation for soils (Das, 1983) as follows:

$$e_z = e_0 - C_c \log \sigma_z(z)/\sigma_z(0) \qquad (5\text{-}15)$$

Where,

e_z is the void ratio with applied vertical stress

e_0 is the initial void ratio

C_c is the slope of the e-*log* σ_z curve

$\sigma_z(z)$ is the applied vertical stress, kPa

$\sigma_z(0)$ is the initial applied vertical stress, kPa

Representing Equation 5-14 in terms of its constants and variables gives:

$$\sigma_z(z) = Ae^{-Gz} \qquad (5\text{-}16)$$

Where:

$A = \sigma_z(0)$

$G = 2K_0 \tan\delta(L+B)/LB$

Substituting Equation 5-16 into 5-15 gives:

$$e_z = e_0 - C_c \log Ae^{-Gz}/A \qquad (5\text{-}17)$$

Let:

$e_0 = C$, and $C_c = D$

Then Equation 5-17 becomes:

$$e_z = C - D\log Ae^{-Gz}/A$$

Then,

$$e_z = C - D\log e^{-Gz} \qquad (5\text{-}18)$$

Using the following relation:

$\log e^x = e \log x = x$

Equation 5-18 then becomes:

$e_z = C - (D)(-Gz)$

Then,

$e_z = C + (DGz)$ *(5-19)*

(4) Vertical hydraulic conductivity as a function of void ratio and specific surface ($k_z(z) = f(e,S)$)

The Kozeny-Carman equation (Das, 1983; Carrier III, 2003; Chapuis and Aubertin, 2003) was represented for this as follows:

$k_z(z) = (\gamma/\mu)(1/C_{k-c})(1/S_s^2)((e_z^3/(1+e_z))$ *(5-20)*

Where:

$k_z(z)$ is the hydraulic conductivity, m/s

γ is the unit weight of permeant, N/m^3

μ is the viscosity of permeant, Ns/m^2

C_{k-c} is the Kozeny – Carman empirical coefficient

S_s is the specific surface area, /m

e_z is the void ratio with applied vertical stress

For simplicity, let,

$(\gamma/\mu)(1/C_{k-c}) = \omega$

Then,

$k_z(z) = \omega(e_z^3)/S_s^2(1+e_z)$ *(5-21)*

(5) Specific surface as a function of void ratio ($S_s = f(e)$)

The relationship between specific surface (S_s) and void ratio (e) had been determined in Figure 5-26 as follows:

$S_s = 466.68\ e_z^{0.7}$ *(5-22)*

$S_s = 466.68\ e_z^{1}$

Then,

$S_s = Fe_z$, where F=466.68

And

$S_s^2 = (Fe_z)^2$ *(5-23)*

Substituting Equation 5-23 into 5-21 gives $k_z(z)$ in terms of e_z

$k_z(z) = \omega(e_z^3)/ (Fe_z)^2(1+e_z)$ *(5-24)*

Then,

$k_z(z) = \omega(e_z)/ F^2(1+e_z)$ *(5-25)*

Substituting Equation 5-19 into 5-25 gives the functional form of $k_z(z)$ as follows:

$k_z(z) = \omega(C+DGZ)/ F^2(1+C+DGZ)$ *(5-26)*

Equation 5-26 was used to determine the continuous distribution of $k_z(z)$ at any point across the thickness of the TDA, not just at the points where readings had been taken from the measurement ports (i.e. discrete points). The $k_z(z)$ values generated were used to determine the corresponding values of $k_z(x)$ to evaluate anisotropy.

The terms D, F, and the $C_{k\text{-}c}$ term embedded in ω were determined by varying the parameters, while matching the equivalent k_z (determined from the harmonic mean of $k_z(z)$ values estimated using Equation 5-26), to the equivalent k_z determined from the laboratory measurements. The harmonic mean of $k_z(z)$ was determined as for a layered system, based on the premise that sidewall friction created apparent horizontal layering in the TDA (see Section 5-1).
The data matching was done by minimizing the RMSE and normalized error between the estimated data and the measured laboratory data, while varying the values of the unknown parameters. Data solver in Microsoft Excel was used for this process.

Deriving the functional form of P(z)

Using Equations 5-1 and 5-6, the flow equation for air permeability was represented as follows:

$dP = (-A/k_z(z))dz$ *(5-27)*

Where,

dP is the differential pressure

A is $q\mu_a\rho_w g/\mu_w$

q is the discharge velocity, m/s

μ_a is the dynamic viscosity of air, kg/ms

ρ_w is the density of water, kg/m^3

g is the acceleration due to gravity, m/s^2

μ_w is the dynamic viscosity of water, kg/ms

dz is the change in length in flow direction, m

$k_z(z)$ is the hydraulic conductivity (m/s)

Substituting for $k_z(z)$ (i.e. Equation 5-26) in Equation 5-27 gives:

$$dP = - AF^2/ \omega ((1/C+DGZ)+1))dz \quad (5\text{-}28)$$

Integrating dP gives:

$$P(z) = - AF^2/ \omega [(1/DG)\ln (C+DGZ) + Z] + \text{Constant} \quad (5\text{-}29)$$

$$\text{When } P(z) = 0;\ \text{Constant} = AF^2/ \omega [(1/DG) \ln(C)] \quad (5\text{-}30)$$

Hence,

$$P(z) = - AF^2/ \omega [(1/DG)\ln (C+DGZ) + Z]+ AF^2/ \omega [(1/DG) \ln(C)] \quad (5\text{-}31)$$

Rearranging 5-31 gives the functional form of P(z)

$$P(z) = AF^2/ \omega [(\ln(C)/DG] - AF^2/ \omega [(1/DG)\ln (C+DGZ) + Z] \quad (5\text{-}32)$$

Data generated using the P(z) function (Equation 5-32) was fit to the laboratory P(z) data (Figure 5-28). During the fitting process, the values of the unknown parameters $C_{k\text{-}c}$, $D(C_c)$ and F were determined. The unknown parameters were determined concurrently for the $k_z(z)$ form, as they are the same. Presented in Figure 5-27 is an example of the estimated data fitted to the measured laboratory data. Values of the unknown parameters used in the fitting process for all the evaluations are presented in Table 5-7.

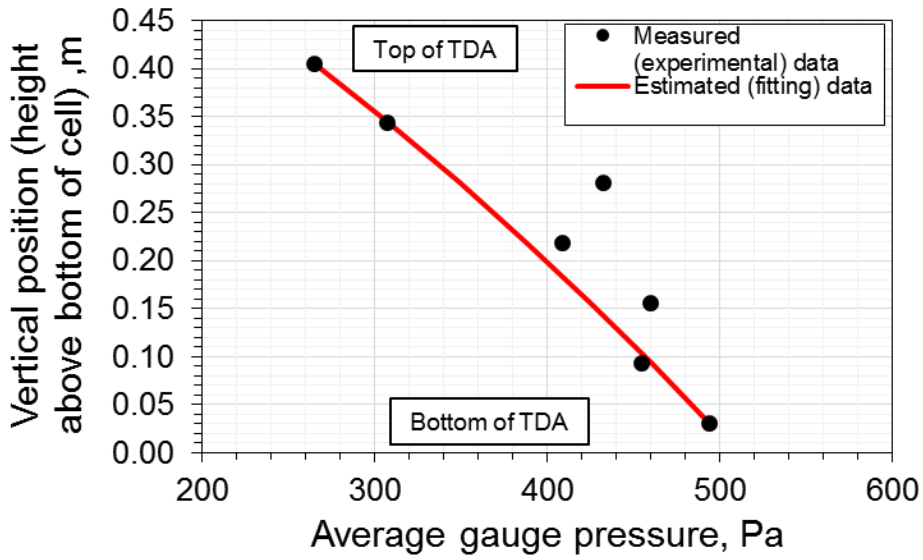

Figure 5-28: Typical plot of measured and estimated P(z). Data for low flow (q = 0.054 m/s) at 224 kPa for ARMA TDA double pass shown.

Determining the distribution of $k_x(z)$

The distribution of $k_x(z)$ was determined by initially assuming an isotropic condition where the $k_z(z)$ and $k_x(z)$ values were the same. Then, anisotropy was gradually introduced by varying the $k_x(z)$ values until the estimated equivalent k_x matched the measured the equivalent k_x and the discharge velocity q (m/s) from the laboratory data. The equivalent k_x were determined from the arithmetic mean of $k_x(z)$ values across the entire TDA thickness, as for a layered system – see Section 5-1. For simplicity, inertia effects were not considered in the formulation of the $k_z(z)$ function, but correction values were applied to the estimated data afterwards they were generated.

Correction values for inertia were determined from the equivalent k_z and k_x values from the laboratory data and afterwards applied to the estimated equivalent k_z and k_x values determined using the functional forms. To determine the correction values, the head measurements at adjacent ports and the distance between the ports were used to determine discrete values of gradients and discrete values of hydraulic conductivity (see Figure 5-1). From these, equivalent k_z and k_x values were determined from the laboratory data (Figure 5-29). Equivalent k_z and k_x

values without inertia effects were determined using Equations 5-1 and 5-2, and those with inertia effects were determined using Equations 5-4 and 5-5. The ratio of values with inertia to those without inertia was used as the correction values for inertia. Presented in Figure 5-29 are the values with and without inertia that were used to determine the correction values for inertia that were applied to the estimated equivalent k_z and k_x values.

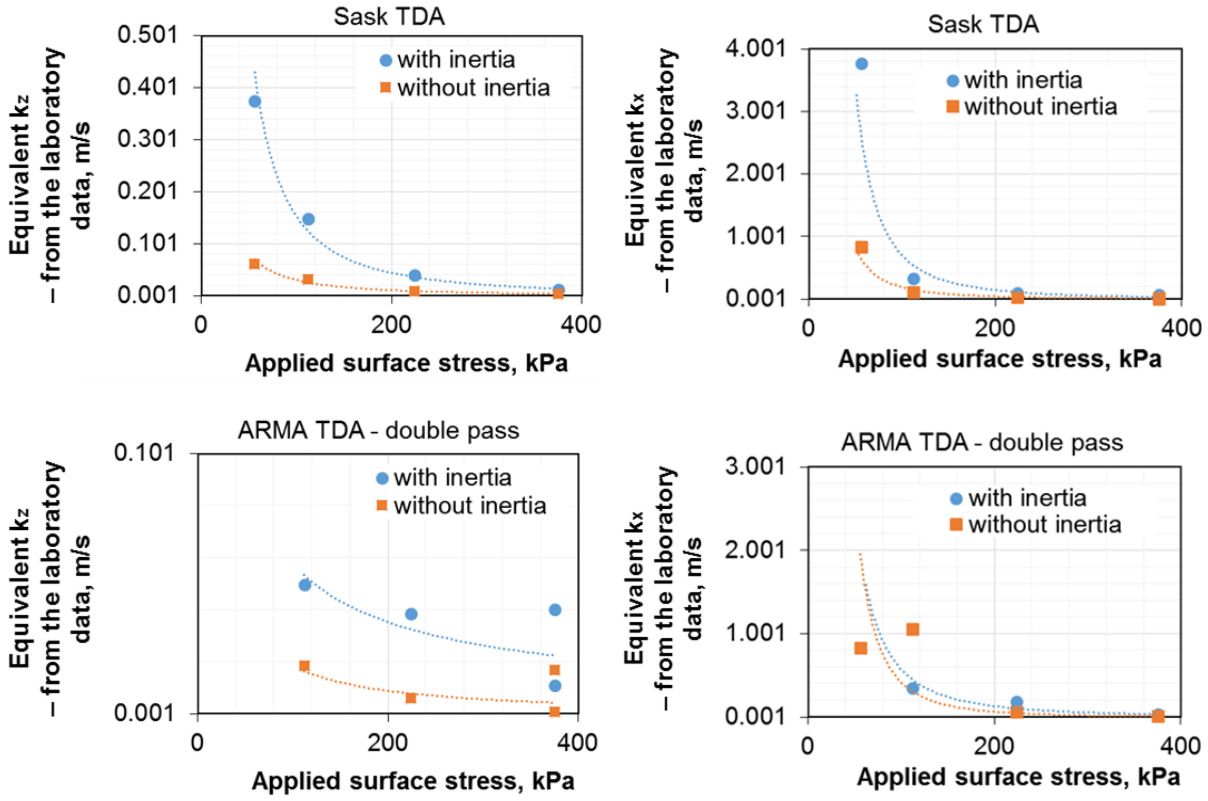

Figure 5-29: Values with and without inertia for Sask TDA and ARMA TDA double pass used to determine the correction values for inertia that were applied to the equivalent k_z and k_x values determined using the functional forms. For ARMA TDA single pass at the 250 kPa applied surface stress, the equivalent k_z with the inertia consideration was 0.09 m/s, and that without inertia consideration was 0.02 m/s, the equivalent k_x with inertia consideration was 0.50 m/s, without inertia consideration was 0.06 m/s. These values for ARMA TDA were used to correct for inertia in the equivalent k_z and k_x values.

The equivalent values of k_z and k_x with inertia were up to 5 times greater than those without considering inertia, thus indicating that hydraulic conductivity may be grossly underestimated if laminar flow is assumed, when the flow is not, and inertia effects are not considered. Inertia effects appeared to generally decrease with applied stress. This is perhaps because as void

volume within the TDA becomes smaller under increased applied stress and compression, the velocity of flows through the voids also becomes smaller, reducing the inertia effects. Presented in Figure 5-30 (a) are plots of $k_z(z)$ and $k_x(z)$ with depth across the TDA thickness, as determined using the formulated functional forms (Section 5.6.4.1). Corresponding plots of $k_z(z)$ and $k_x(z)$ with applied stress are presented afterwards in Figure 5-30 (b). Presented in Table 5-7 are the values of the unknown parameters – $C_{k\text{-}c}$, $D(C_c)$ and F used in the functional forms to estimate $k_z(z)$ and $k_x(z)$ in Figures 5-30 (a, b).

Table 5-7: Values of the $C_{k\text{-}c}$, $D(C_c)$ and F parameters used in the functional forms. Full data available in electronic format

TDA Type	Applied stress kPa	Flow type	Fitting parameters		
			$C_{k\text{-}c}$	$D(C_c)$	F
Sask TDA	56	High	4613.7	-0.4	41.9
		Medium	4431.8	-0.4	38.8
		Low	3711.0	-0.4	29.9
	112	High	3775.9	-0.3	42.2
		Medium	3556.7	-0.4	41.5
		Low	4223.5	-0.4	29.4
	224	High	4182.8	-0.5	78.8
		Medium	4097.2	-0.5	72.2
		Low	3620.4	-0.5	65.2
	375	High	4685.4	-0.5	84.3
		Medium	4619.4	-0.7	91.1
		Low	4509.2	-0.7	80.6
ARMA TDA double pass	112	High	3776.0	-0.4	52.9
		Medium	3776.3	-0.4	47.3
		Low	3775.8	-0.3	29.5
	224	High	3749.4	-0.6	80.2
		Medium	3749.2	-0.6	68.0
		Low	3752.4	-0.6	46.7
	375	High	4999.6	-0.5	93.3
		Medium	4999.6	-0.5	83.1
		Low	4999.5	-0.5	68.0
ARMA TDA single pass	250	High	4999.4	-0.7	57.4
		Medium	4457.7	-0.6	55.2
		Low	4258.0	-0.2	27.0

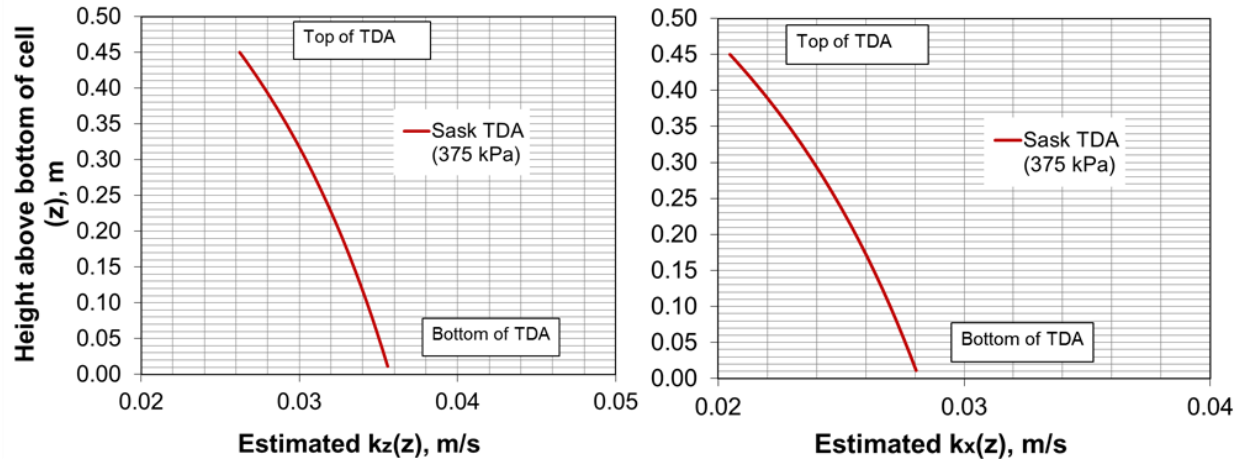
Height above bottom of cell (z), m
Top of TDA
Sask TDA (375 kPa)
Bottom of TDA
Estimated kz(z), m/s
Estimated kx(z), m/s

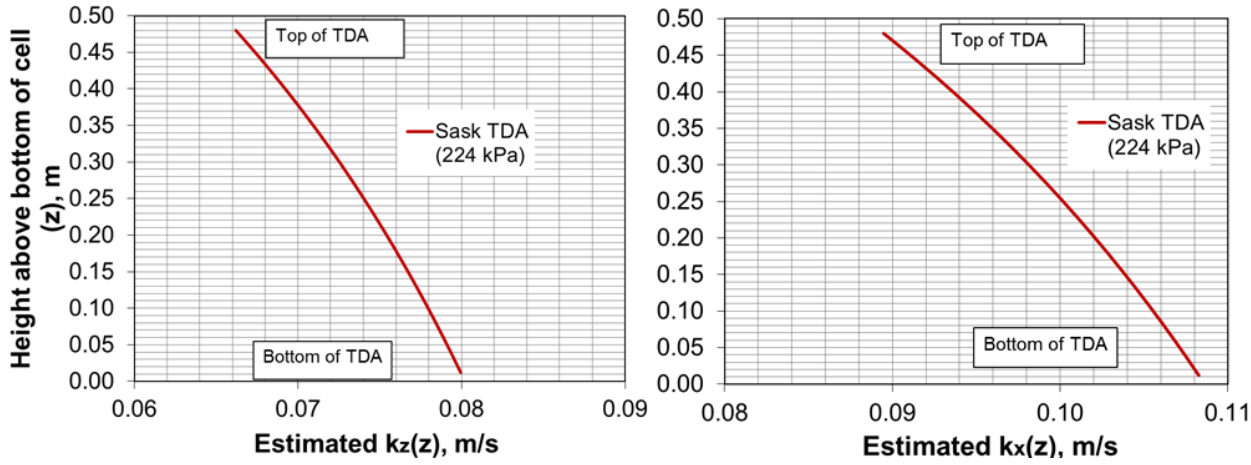
Height above bottom of cell (z), m
Top of TDA
Sask TDA (224 kPa)
Bottom of TDA
Estimated kz(z), m/s
Estimated kx(z), m/s

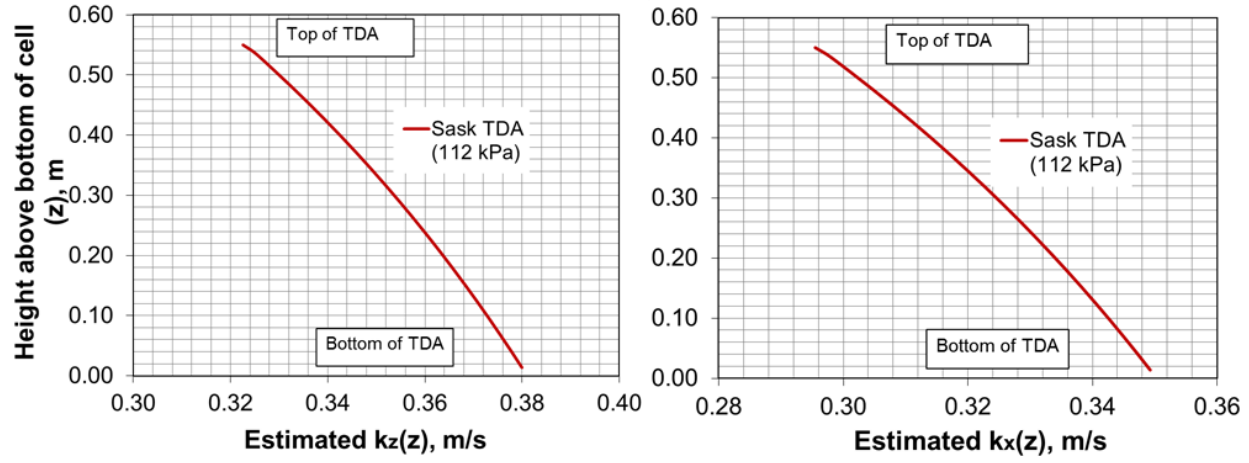
Height above bottom of cell (z), m
Top of TDA
Sask TDA (112 kPa)
Bottom of TDA
Estimated kz(z), m/s
Estimated kx(z), m/s

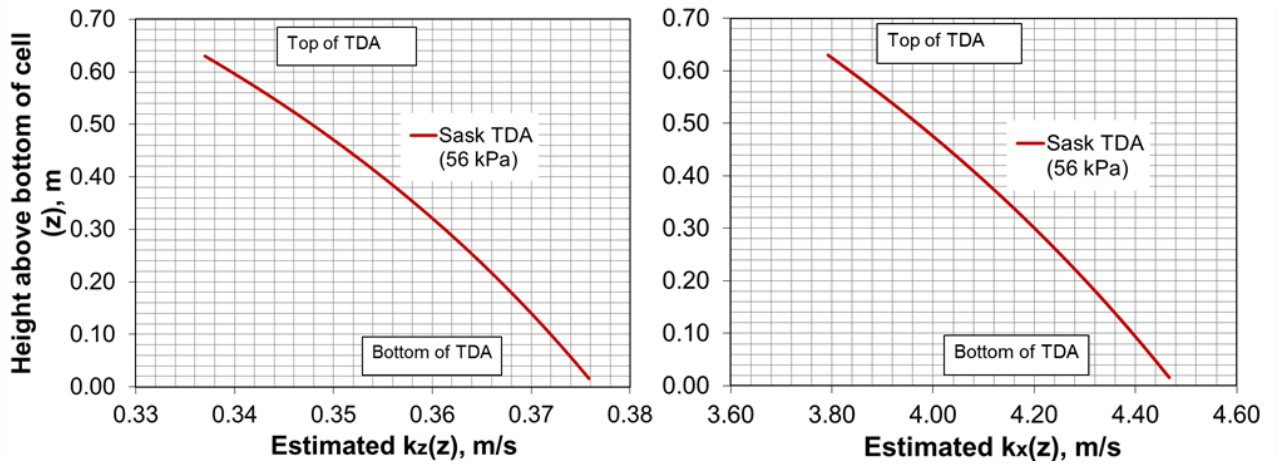
Height above bottom of cell (z), m
0.70
0.60
0.50
0.40
0.30
0.20
0.10
0.00
Top of TDA
Sask TDA (56 kPa)
Bottom of TDA
0.33
0.34
0.35
0.36
0.37
0.38
Estimated kz(z), m/s
3.60
3.80
4.00
4.20
4.40
4.60
Estimated kx(z), m/s

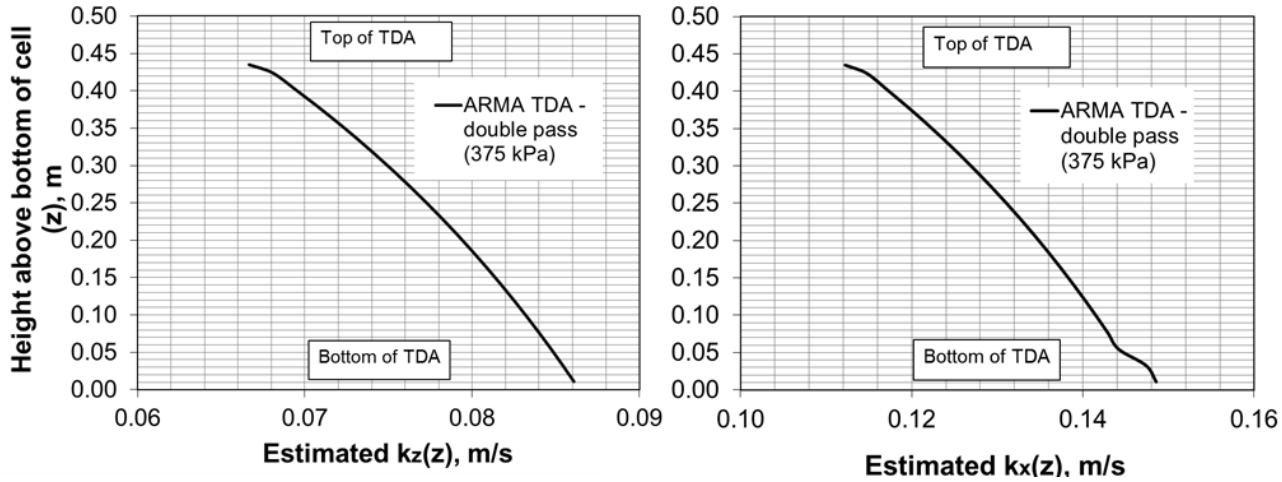
Height above bottom of cell (z), m
0.50
0.45
0.40
0.35
0.30
0.25
0.20
0.15
0.10
0.05
0.00
Top of TDA
ARMA TDA - double pass (375 kPa)
Bottom of TDA
0.06
0.07
0.08
0.09
Estimated kz(z), m/s
0.10
0.12
0.14
0.16
Estimated kx(z), m/s

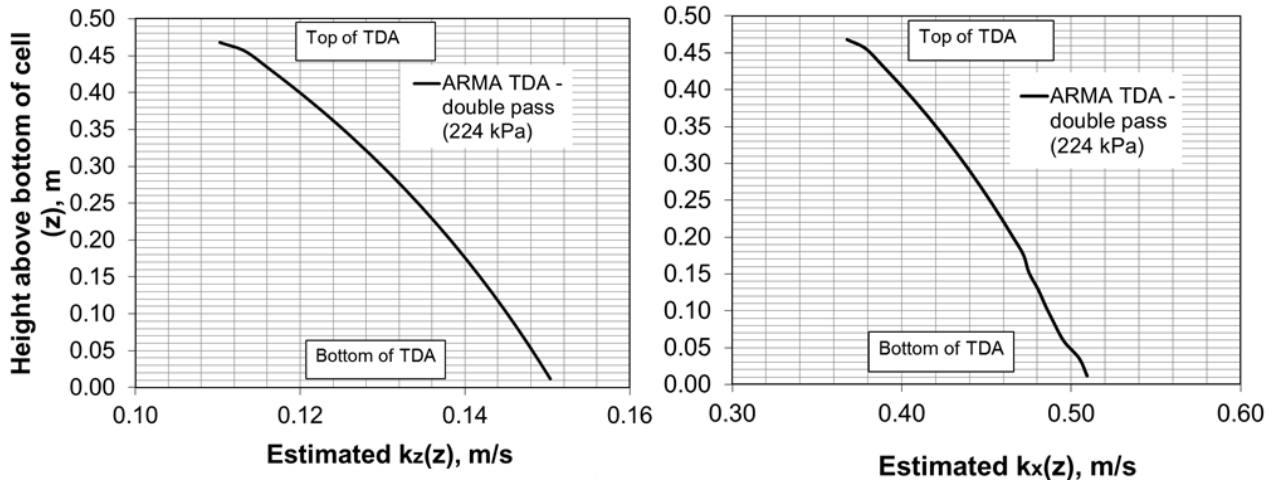
Height above bottom of cell (z), m
0.50
0.45
0.40
0.35
0.30
0.25
0.20
0.15
0.10
0.05
0.00
Top of TDA
ARMA TDA - double pass (224 kPa)
Bottom of TDA
0.10
0.12
0.14
0.16
Estimated kz(z), m/s
0.30
0.40
0.50
0.60
Estimated kx(z), m/s

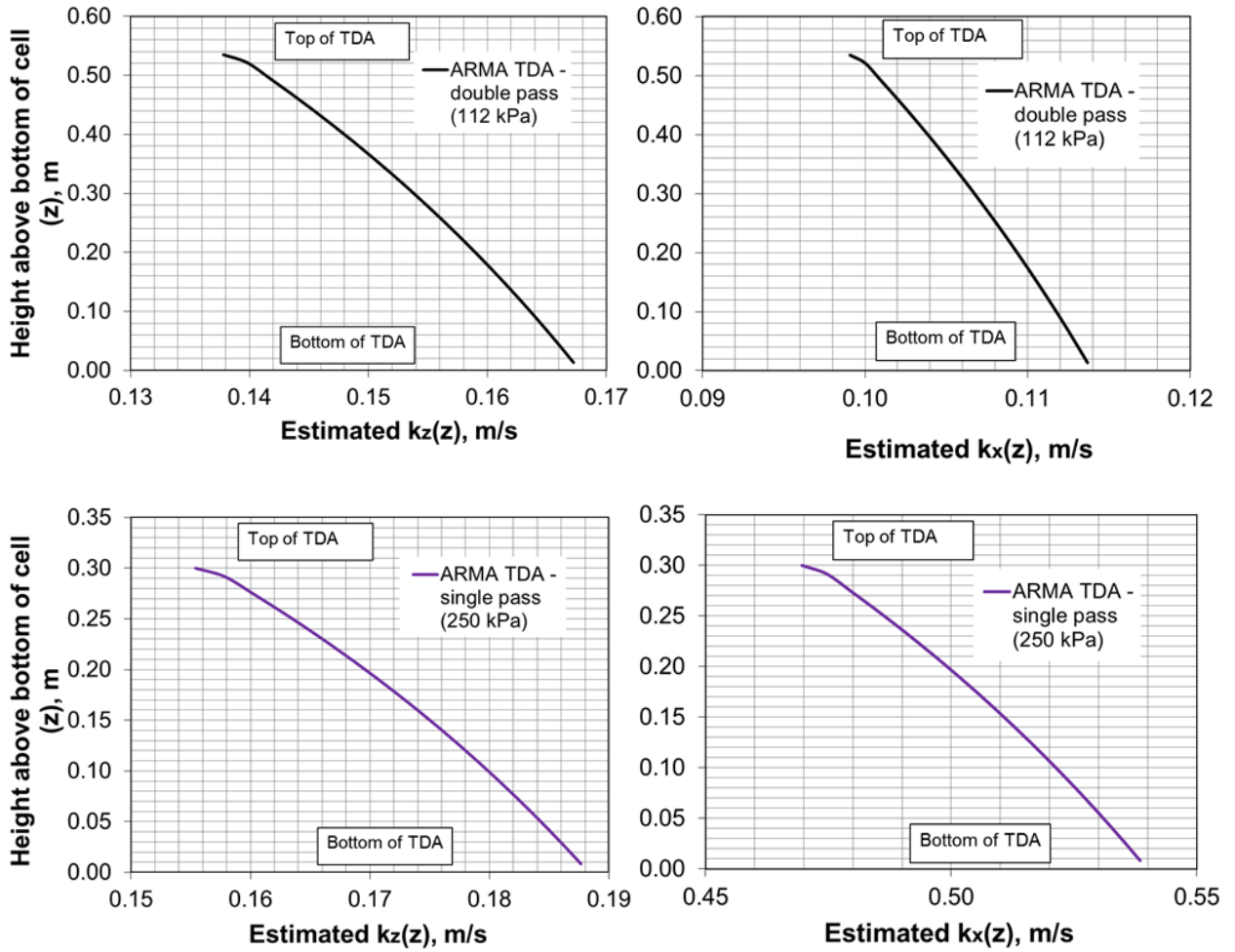

Figure 5-30 (a): The distribution of $k_z(z)$ and $k_x(z)$ – as determined using the functional forms, vs. height – across the TDA thickness.

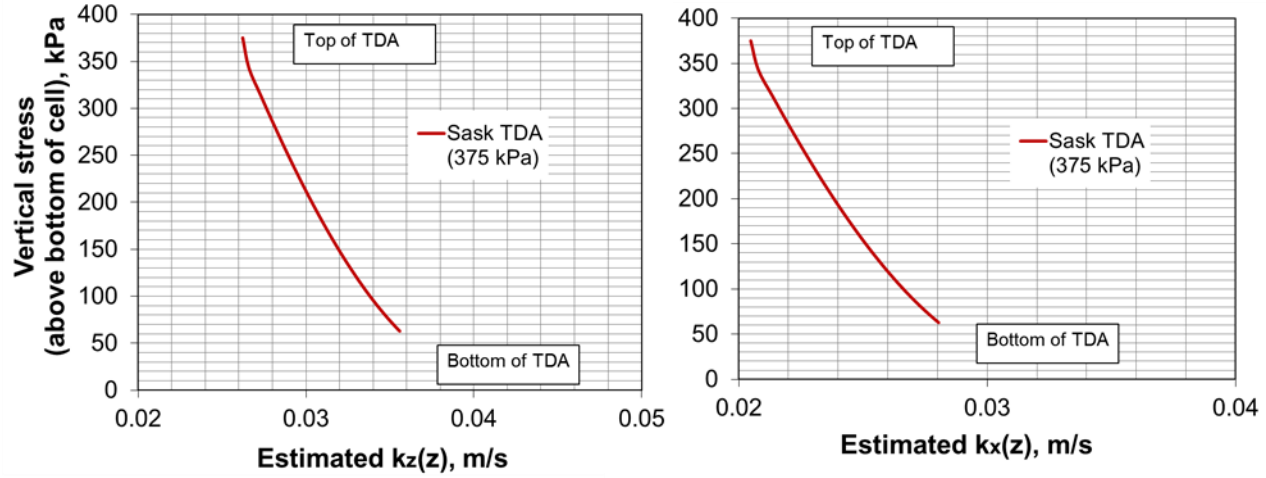

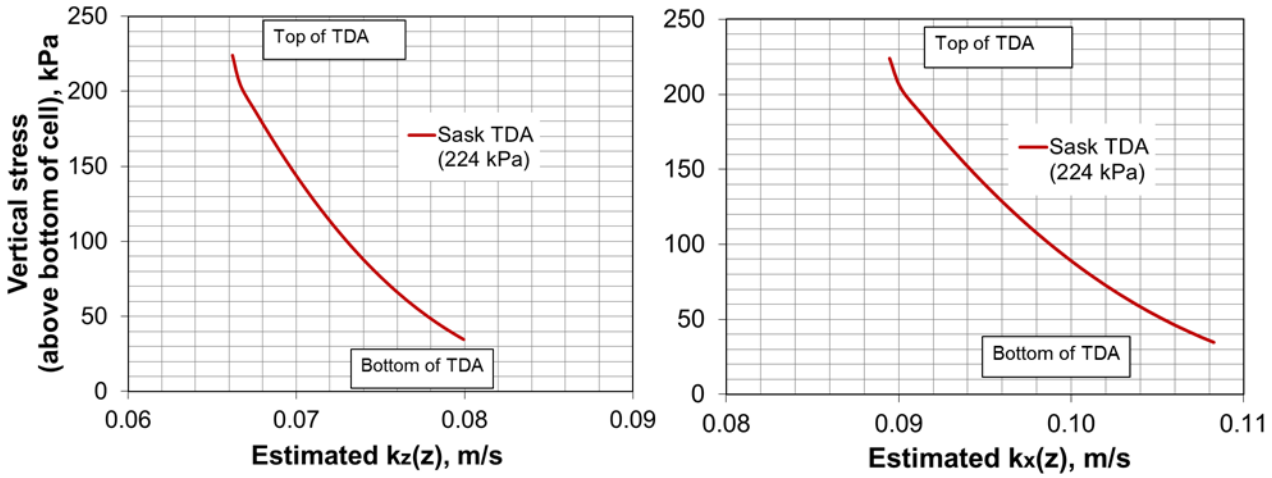
Vertical stress (above bottom of cell), kPa
250
200
150
100
50
0
Top of TDA
Sask TDA (224 kPa)
Bottom of TDA
0.06
0.07
0.08
0.09
Estimated kz(z), m/s
0.08
0.09
0.10
0.11
Estimated kx(z), m/s

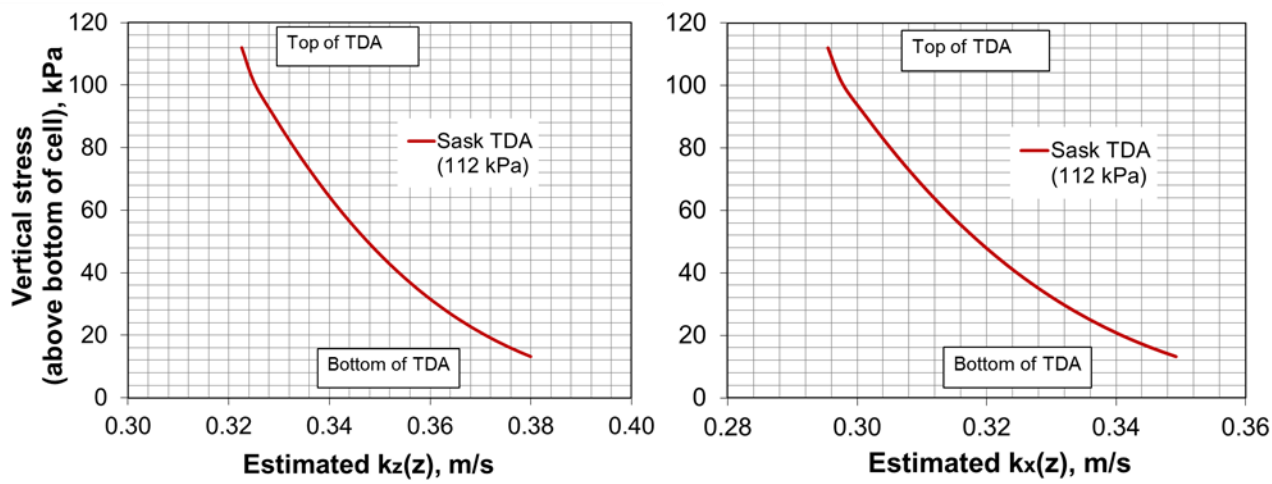
Vertical stress (above bottom of cell), kPa
120
100
80
60
40
20
0
Top of TDA
Sask TDA (112 kPa)
Bottom of TDA
0.30
0.32
0.34
0.36
0.38
0.40
Estimated kz(z), m/s
0.28
0.30
0.32
0.34
0.36
Estimated kx(z), m/s

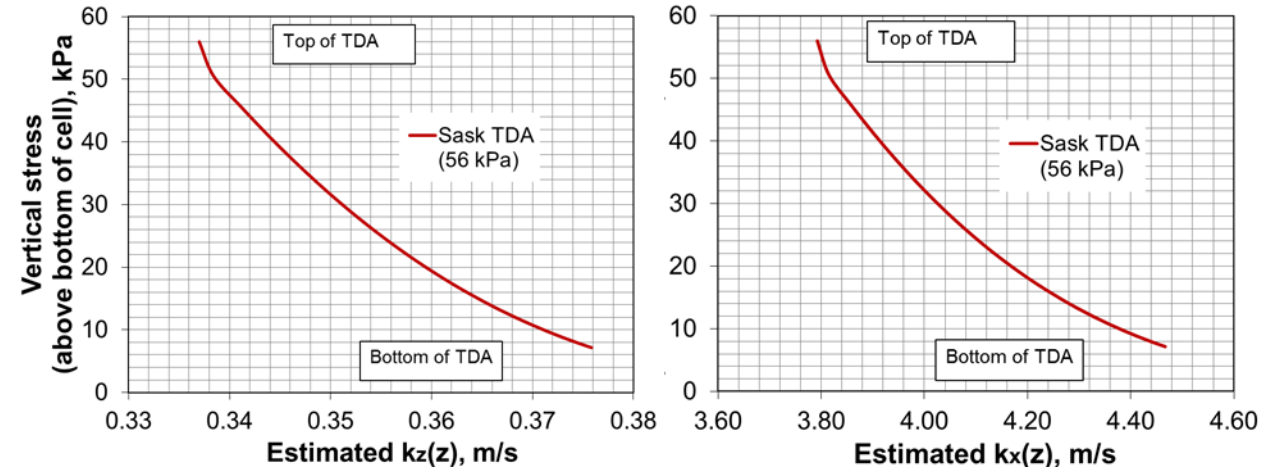
Vertical stress (above bottom of cell), kPa
60
50
40
30
20
10
0
Top of TDA
Sask TDA (56 kPa)
Bottom of TDA
0.33
0.34
0.35
0.36
0.37
0.38
Estimated kz(z), m/s
3.60
3.80
4.00
4.20
4.40
4.60
Estimated kx(z), m/s

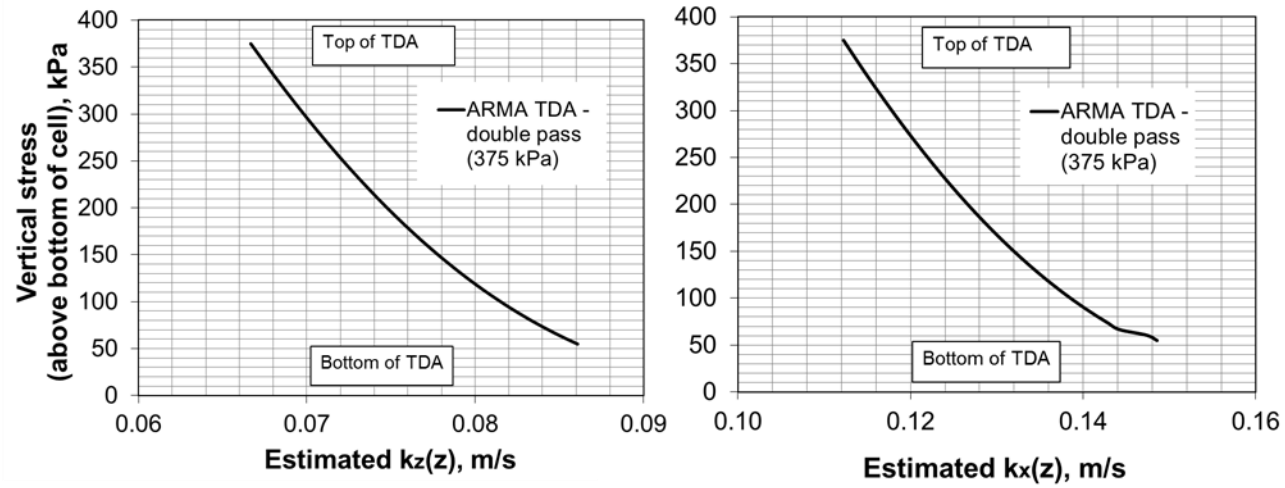
Vertical stress (above bottom of cell), kPa
Top of TDA
ARMA TDA - double pass (375 kPa)
Bottom of TDA
Estimated kz(z), m/s
Estimated kx(z), m/s

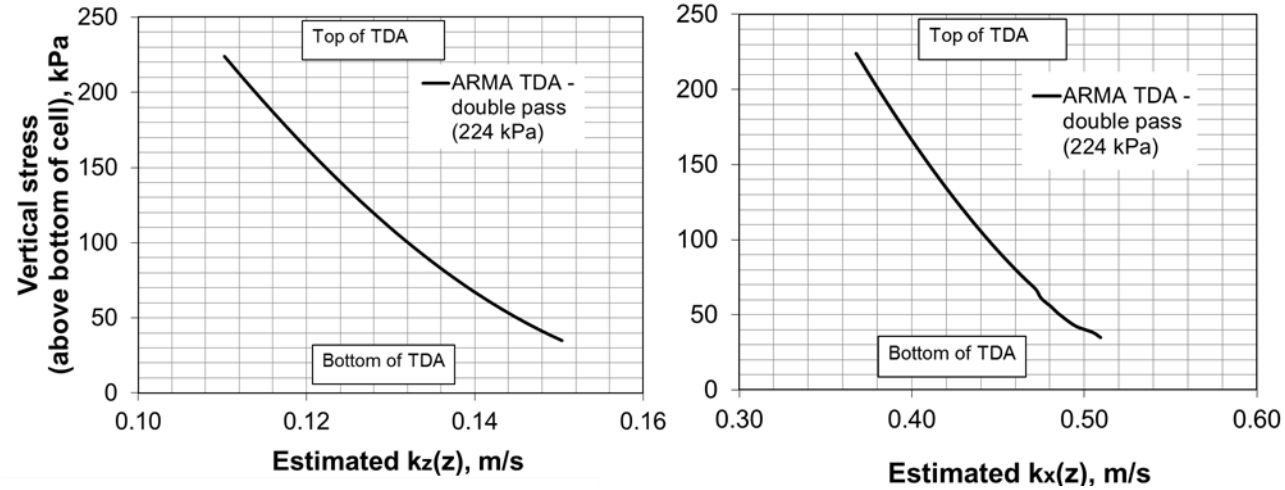
Vertical stress (above bottom of cell), kPa
Top of TDA
ARMA TDA - double pass (224 kPa)
Bottom of TDA
Estimated kz(z), m/s
Estimated kx(z), m/s

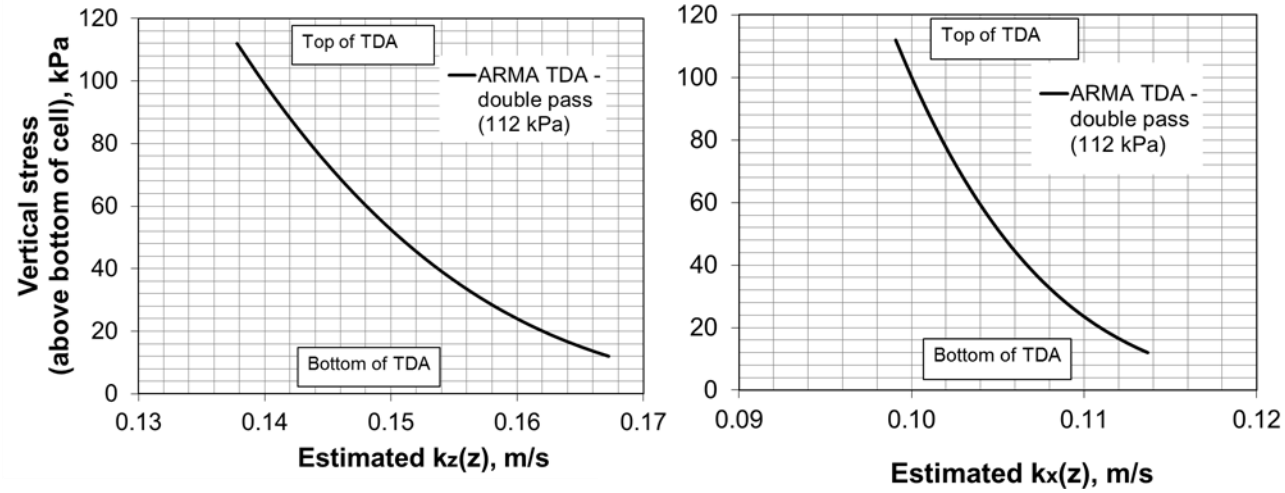
Vertical stress (above bottom of cell), kPa
Top of TDA
ARMA TDA - double pass (112 kPa)
Bottom of TDA
Estimated kz(z), m/s
Estimated kx(z), m/s

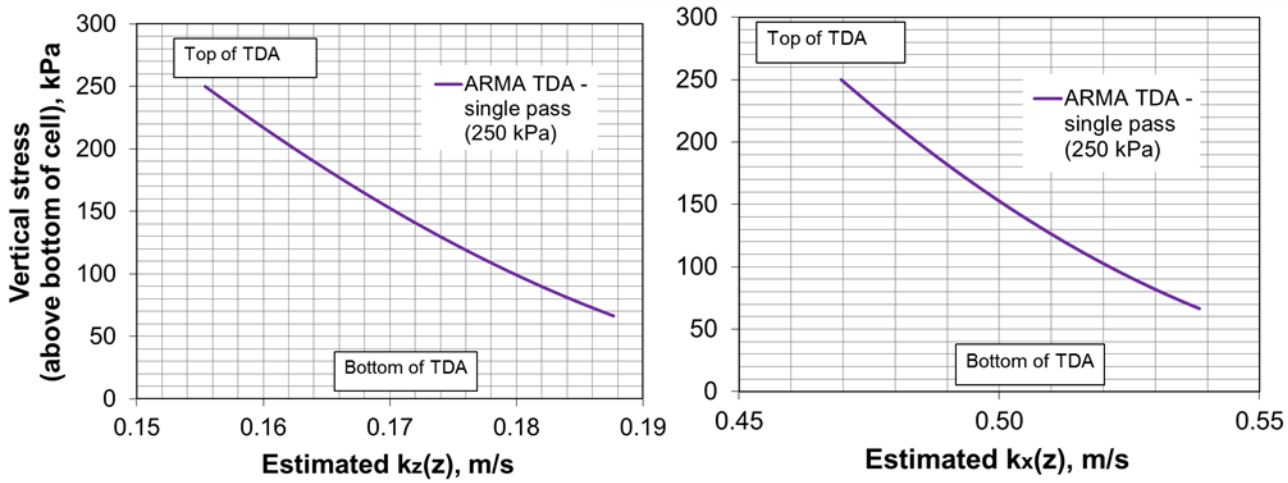

Figure 5-30 (b): The distribution of $k_z(z)$ and $k_x(z)$ – as determined using the functional forms, vs. corresponding applied vertical stress distribution – determined using Equation 5-14.

In Figures 5-30 (a and b) the values of $k_z(z)$ and $k_x(z)$ at a specific height and applied stress depend on the applied surface stress. Using the $k_z(z)$ and $k_x(z)$ distribution, for each applied surface stress, equivalent k_z values were determined from the harmonic mean of the $k_z(z)$ distribution, and equivalent k_x values were determined from the arithmetic mean of the $k_x(z)$ distribution (Table 5-8).

Table 5-8: Equivalent k_z and k_x, and corresponding anisotropy after correcting for inertia

TDA type	Applied surface stress, kPa	Average applied stress in TDA	Initial void ratio in TDA	Void ratio in TDA at the end of creep in load step	Corrected estimated equivalent k_z, m/s	Corrected estimated equivalent k_x, m/s	Anisotropy in the hydraulic conductivity k_x/k_z
Sask TDA	56	32	2.19	0.99	0.36	4.16	12
	112	63		0.74	0.30	0.32	1
	224	123		0.52	0.08	0.10	1
	375	219		0.41	0.03	0.02	1
ARMA TDA double pass	112	53	2.09	0.65	0.33	0.52	2
	224	134		0.44	0.11	0.30	3
	375	210		0.34	0.02	0.05	2
ARMA TDA single pass	250	140	N/A	N/A	0.30	0.50	2

The equivalent k_z and k_x values and corresponding anisotropy presented in Table 5-8 are slightly different from those presented in Table 5-2 (a) – Section 5.4, which were determined using a different approach. The anisotropy values in Table 5-2 (a) were generally higher than those presented here in Table 5-8.

The variations may be related to the data set used to determine the equivalent values. In the approach in Section 5.4, only the entry and exit values were used to determine equivalent values, while in the approach presented here, the full vertical distribution of $k_z(z)$ and $k_x(z)$ were used to determine the equivalent values. In addition, in the approach presented here, the TDA was treated like a layered system (see Section 1.0). Thus, after determining average values of the $k_z(z)$ and $k_x(z)$ distributions for all flow rates at an applied surface stress, equivalent k_z values were determined from the harmonic mean of the $k_z(z)$ distribution, and equivalent k_x values were determined from the arithmetic mean of the $k_x(z)$ distribution.

On the other hand, in Section 5.4, the equivalent k_z and k_x values were determined entirely from the arithmetic mean of the k_z and k_x values for all the flow rates. The differences in determining the mean values may have contributed to the variations in the equivalent k_z and k_x values from both approaches.

Summary of the P(z), $k_z(z)$ and $k_x(z)$ determination and estimations

- Formulated $k_z(z)$ and P(z) functions was to determine the vertical distribution of hydraulic conductivity and pressure values across the TDA thickness (Equation 5-32).
- Used normalized error and RMSE methods to match the estimated P(z) values to the measured laboratory values of P(z) (Figure 5-28). The matching was done by minimizing both normalized error and RMSE between the measured and estimated P(z) values, while varying the values of unknown parameters – Ck-c, D(Cc) and F in the formulated $k_z(z)$ and P(z) functions. Values for the unknown parameters are presented in Table 5-7.

- Values of tanδ in the functions were determined by generating the vertical distribution of applied stress (using Equation 5-14). The applied stress distribution was validated by matching the stress at the bottom to the value measured from the TS cell (see Sections 5.2 and 5.3).
- To verify the $k_z(z)$ distribution generated using the formulated functional form, equivalent k_z was determined (from the harmonic mean of the $k_z(z)$ values) and matched to the equivalent k_z from the laboratory $k_z(z)$ values.
- Knowing $k_z(z)$ at any vertical point (Figure 5-30), corresponding $k_x(z)$ at any vertical point was determined (Figure 5-30) by assuming the same relative change in $k_x(z)$ from top to bottom of the TDA as with $k_z(z)$ i.e. the difference between $k_x(z)$ at the top and that at the bottom was the same as that for $k_z(z)$. For instance, say at the bottom $k_z(z)$ was 0.001 and 0.0001 at the top, the same 10 times difference from top to bottom was assumed for $k_z(z)$. An isotropic condition was initially assumed, where the $k_z(z)$ and $k_x(z)$ values were the same, and then anisotropy was gradually introduced by varying the $k_x(z)$ values until the arithmetic mean of the estimated $k_x(z)$ values (across the thickness of the TDA) matched the measured discharge velocity q (m/s), and the arithmetic mean of $k_x(z)$ values from the laboratory measurements.
- The estimated $k_z(z)$ and $k_x(z)$ values determined using the functional forms were corrected for inertia (see Figure 5-29). From these equivalent k_z, k_x and corresponding anisotropy that were corrected for inertia were determined (Table 5-8).

5.6.5 Additional images from laboratory testing with the 2D cell

As discussed in Section 5.3.1, presented in Figure 5-31 are images of the load cell placed under the piston rod to measure the surface load applied to the TDA.

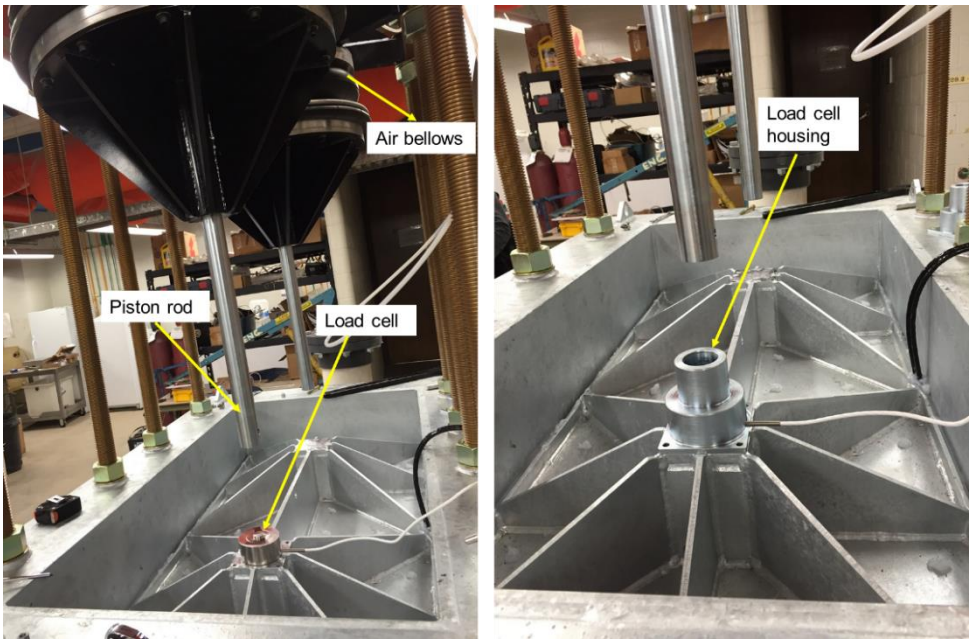

Figure 5-31: Images of the load cell placed under the piston rod to measure the surface load applied to the TDA.

Presented in Figure 5-32 is an image of a meter rule placed at pre-marked locations above the loading plate to measure compression in the TDA in the 2D cell (discussed in Section 5.3.1).

The thickness of the loading plate was subtracted from the readings.

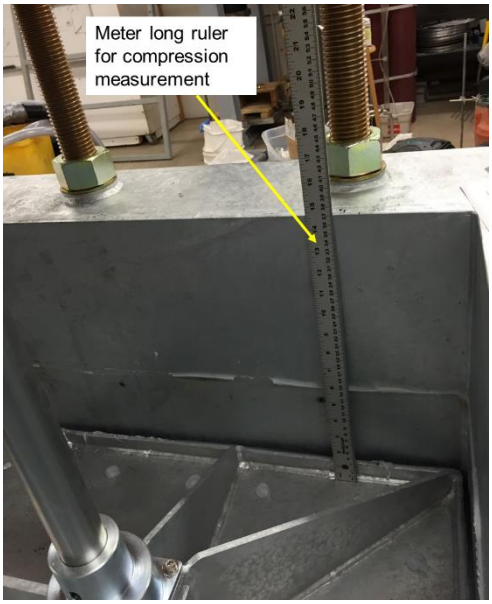

Figure 5-32: Meter rule placed at pre-marked locations above the loading plate to measure compression in the TDA in the 2D cell. The thickness of the loading plate was subtracted from the readings

Presented in Figures 5-33 (a, b) to 5-36 (a, b) are additional images for the air permeability and hydraulic conductivity measurements discussed in Section 5.3.

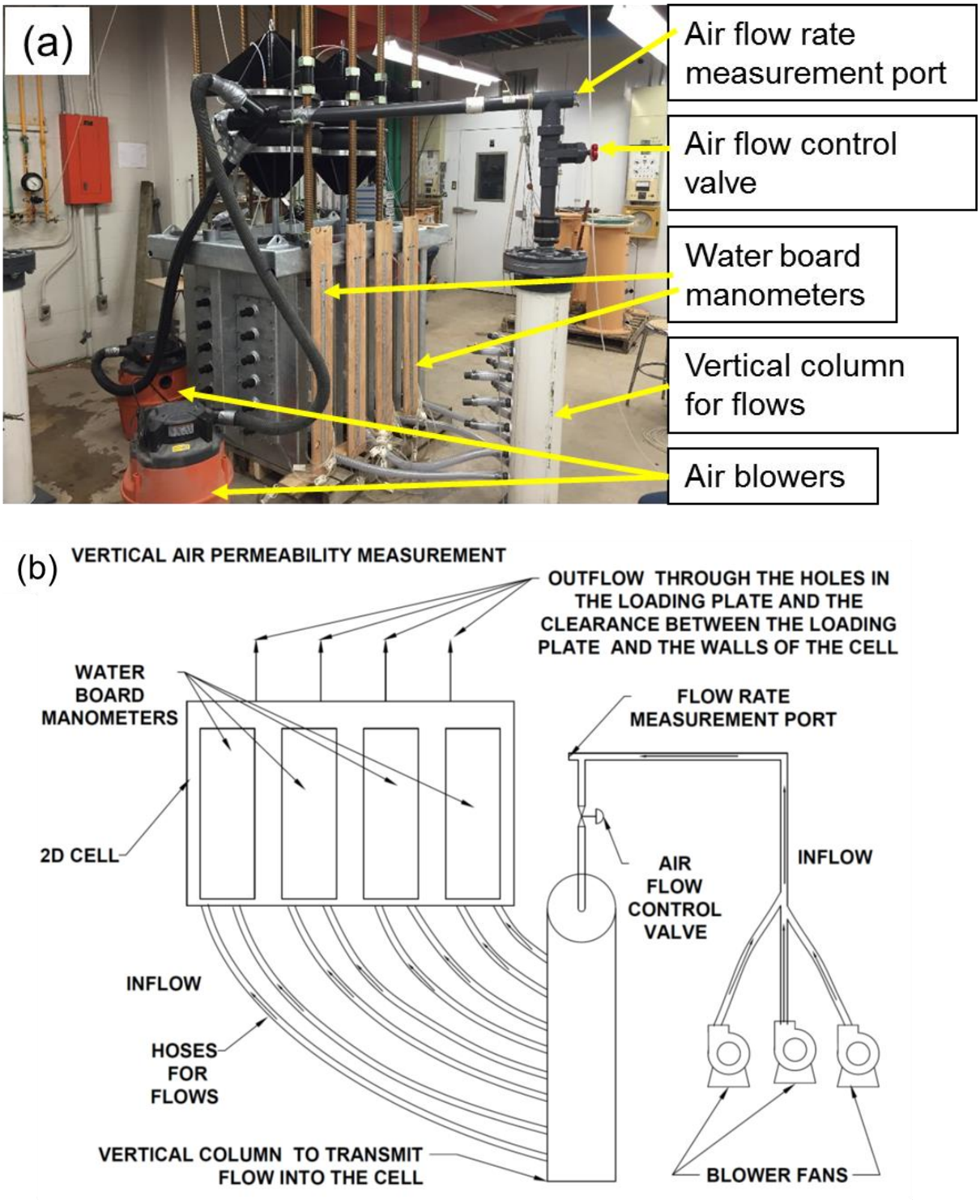

Figure 5-33: (a) Laboratory setup for vertical air permeability measurement (b) Schematic of the laboratory setup

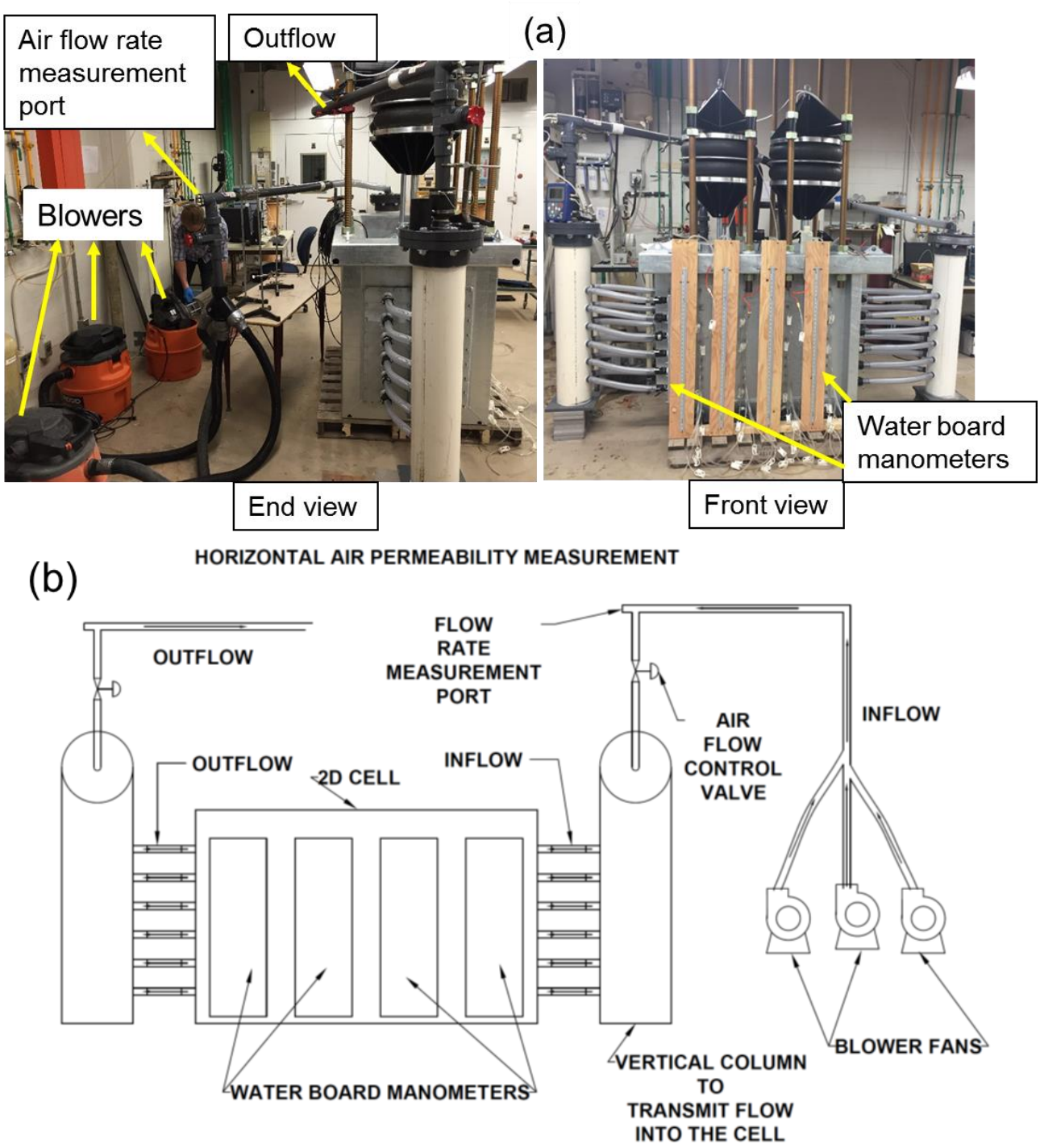

Figure 5-34: (a) Laboratory setup for horizontal air permeability measurement (b) Schematic of the laboratory setup

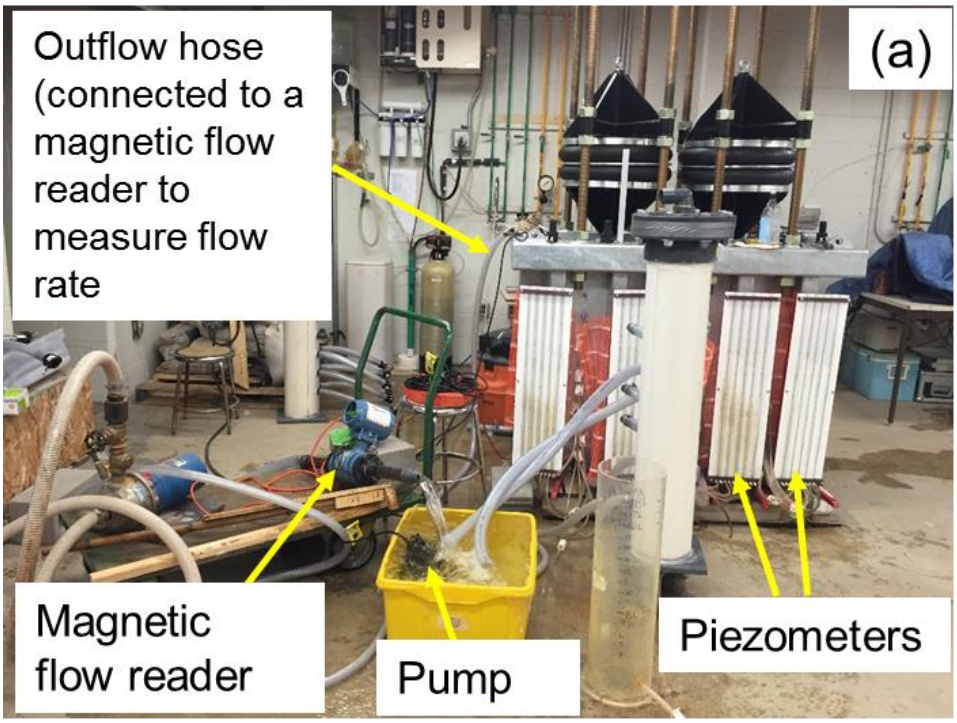

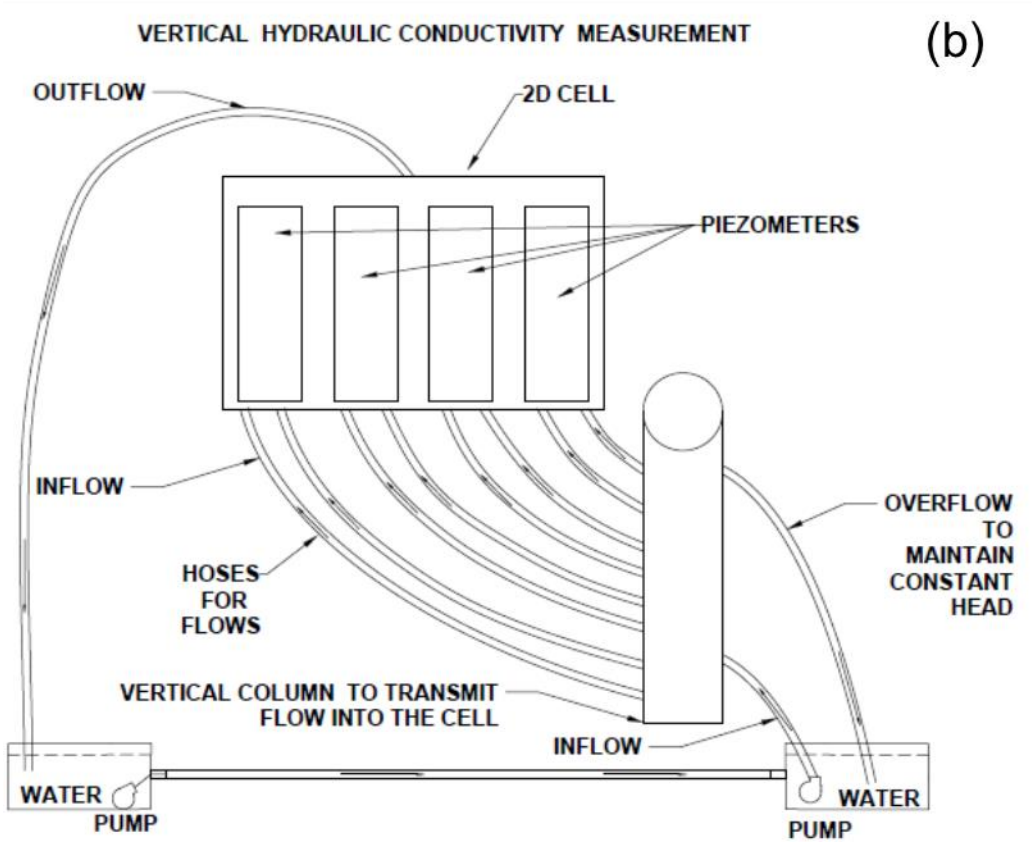

Figure 5-35: (a) Laboratory setup for vertical hydraulic conductivity measurement (b) Schematic of the laboratory setup

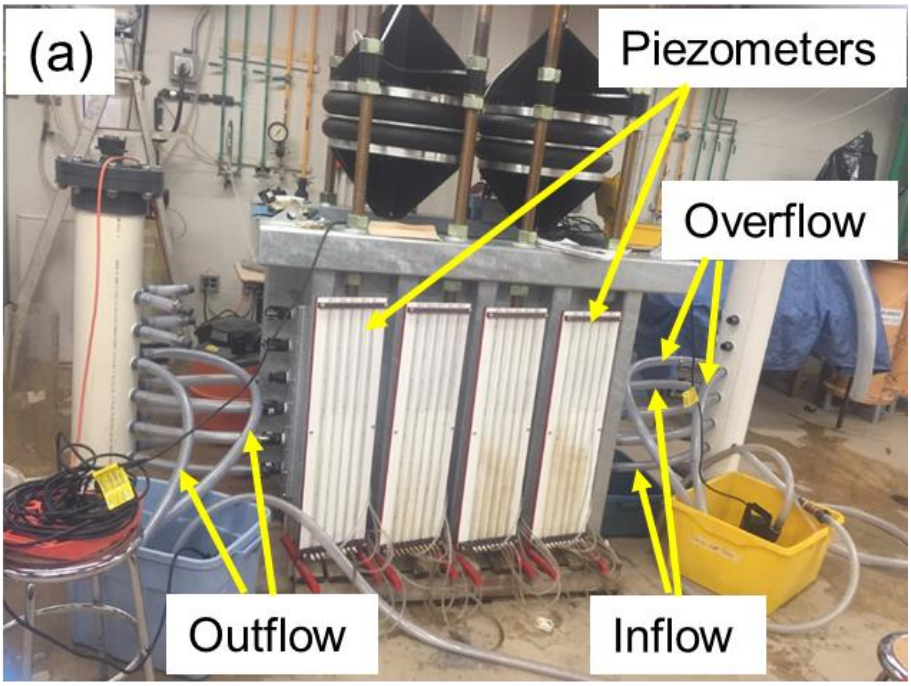

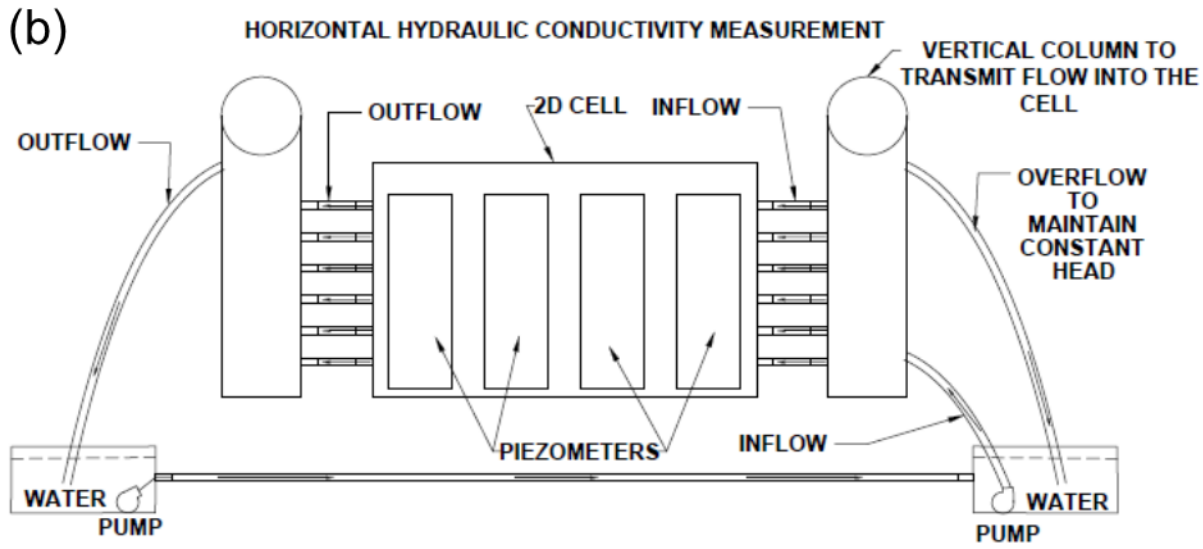

Figure 5-36: (a) Laboratory setup for horizontal hydraulic conductivity measurement (b) Schematic of the laboratory setup

6.0 Design Guidance

In this section, some practical uses of the compression, void ratio, and hydraulic conductivity values from this work are presented in the form of design charts that can be used to determine the maximum leachate head (H_{max}) in a TDA drainage layer in service. Regulations, such as in Saskatchewan (Chapter 1, Section 1.1), stipulate an H_{max} of 0.3 m, and a drainage layer thickness ≥ 0.3 m, ideally, the leachate head must not exceed the thickness of the drainage layer. Various closed form analytical relationships have been developed over the years to estimate the H_{max} in a granular drainage layer. One of such relations, the Giroud and Houlihan (1995) approach for steady state conditions (Eq. 6-1) was applied in this *Design Guidance* to determine the approximate values of H_{max} in a drainage layer constructed with large particle sized TDA.

Using the Giroud and Houlihan (1995) approach, H_{max} can be determined as follows:

$$H_{max} = (\sqrt{}\ (((\tan 2\beta + 4q_i/k) - \tan\beta)/2\cos\beta)\ L)\ \cos\beta \qquad (6\text{-}1)$$

Where,

H_{max} is the maximum head;

tan β is the slope towards the leachate collection pipes;

q_i is the average infiltration into the drainage layer from the overlying waste;

k is the hydraulic conductivity of the drainage media;

L is the horizontal length of the drainage path into leachate collection pipes.

The physical representation of parameters in Eq. 6-1 are presented in Figure 6-1.

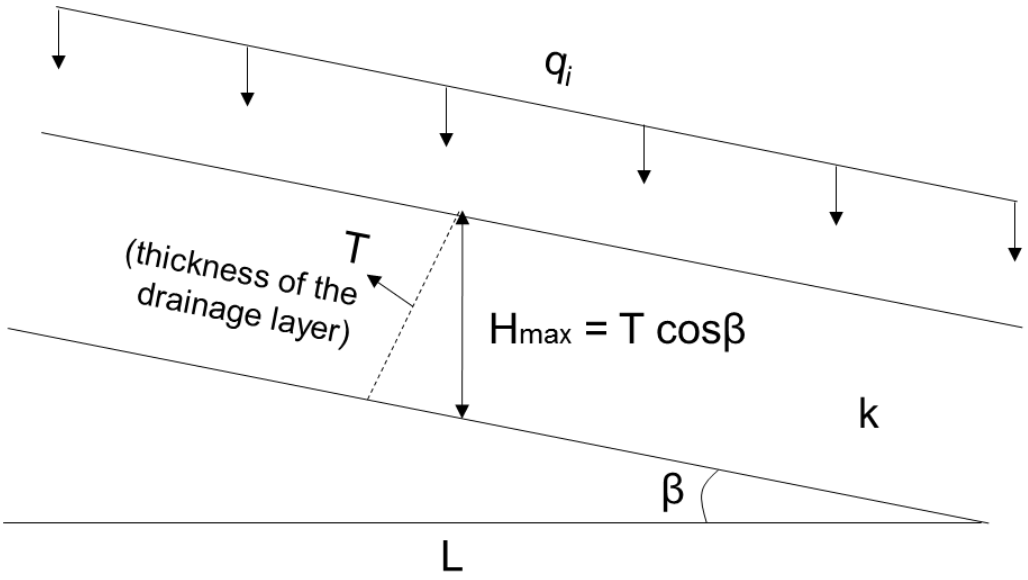

Figure 6-1: Schematic showing the various parameters in the Giroud and Houlihan (1995) approach for determining H_{max} in a landfill drainage layer above a basal liner

Equation 6-1, as with other approaches for estimating H_{max} (see: Qian et al, 2001. pp.280-281), were developed for granular materials that do not compress under applied stress. To apply those approaches to a TDA drainage layer, consideration has to be made for compression of the TDA layer under applied stress. Thus, using the immediate compression and creep values in this work, a chart is presented in Section 6-2 to determine the initial thickness of TDA that may be used to meet the stipulated thickness of the drainage layer and H_{max}. The horizontal hydraulic conductivity values determined in this work were used for the values of k in Equation 6-1 to develop charts of H_{max} for various values of L, tanβ and q_i.

6.1 Guidance charts for compression (%) of a TDA drainage layer

The relationship between average compression (%) in TDA and applied surface stresses can be represented as follows:

Average compression in TDA (%) = 9.23ln (σ_z) + 8.26 (Figure 6-2) *(6-2)*

Where,

Average compression in TDA (%) = ($\Delta e/1+e_o$);

e_o = the initial void ratio in a sublayer in a testing event (Figure 6-3);

$\Delta e = e_o$ – final void ratio in the sublayer at the end of the testing event (Figure 6-3);

σ_z = applied surface stress, kPa.

Compression and void ratio data from testing completed in the 2D cell (Figure 6-2) were used to determine Eq. 6-2. Compression data[75] from the 2D cell were used as they correlate directly with the measurements of hydraulic conductivity completed in the cell, which will be used in this design guidance (Table 6-1). It should however be noted that compression in TDA (as in Figure 6-2), and void ratio after creep (as in Figure 6-3) are highly dependent on the initial void ratio[76]. To create Figures 6-2 to 6-4 for use in the design guidance, the values for Sask TDA and ARMA TDA double pass were combined, given the similarities in their initial void ratio values, and final void ratio with applied stress. The initial void ratio for Sask TDA was 2.2, while that for ARMA TDA was 2.1, at similar applied stresses, the difference in void ratio values between the two TDA types was less than 0.2 (Figure 6-3). Values for ARMA TDA single pass were not used as although hydraulic conductivity measurements were completed for the TDA, compression measurements were not completed.

The compression values from testing completed in the 1D consolidometer –the immediate compression and creep indexes (C_c and C_α respectively in Chapter 4) can equally be used to determine the average compression values. A plot of average compression (%) vs. applied stress, using the void ratio values for all the sublayers in the 1D compression testing is presented in Chapter 4, Section 4.5.3. This can also be used to estimate average compression in the TDA.

[75] See Section 5.6.2 for the compression data for testing completed in the 2D cell
[76] See Chapters 4 and 5

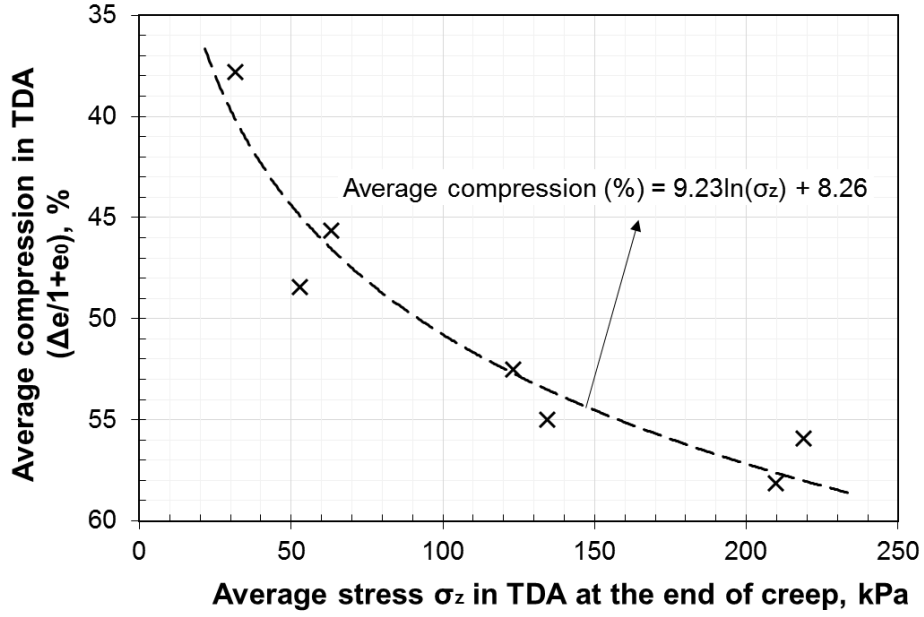

Figure 6-2: Relationship between average compression (%) and average applied stress in TDA using values from testing completed in the 2D cell (See Chapter 5, Section 5.6.2 for data). Note: compression in TDA is dependent on the initial void ratio as well as the applied stress – See Chapter 4

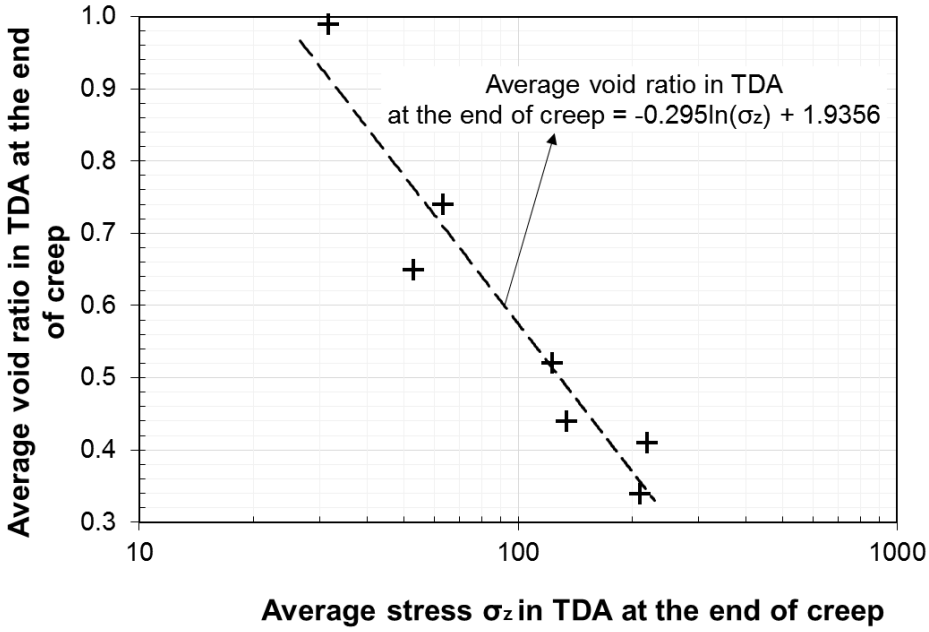

Figure 6-3: Relationship between void ratio and applied stress (e logP*) from testing completed in the 2D cell. This is also Figure 5-22 in Chapter 5 – Section 5.6.2. The data for Sask TDA and ARMA TDA double pass were combined here in Figure 6-3 for use in the design guidance, given the closeness in the initial and final void ratio values for the two TDA types. *Final void ratio in TDA is dependent on the initial void ratio as well as the applied stress – See Chapter 4.*

Although the applied surface stress in the 2D cell was up to 375 kPa, the average stress in TDA at that applied surface stress was only up to 218 kPa (Figure 6-3). Average stress in the TDA was determined from the average of the top and bottom stresses (from the load cell readings at the top of the TDA and the TS cell at the bottom of the TDA, respectively)[77]. To determine the average compression and hydraulic conductivity values at stress values ≥ 375 kPa (e.g. 375, 500 and 800 kPa in Table 6-1), known relationships from the 2D testing (Figures 6-2, 6-3 and 6-4) were applied. The steps taken are as follows:

- the relationship in Figure 6-2 was used to estimate compression (%) relative to the applied stress;
- the relationship in Figure 6-3 was used to estimate the void ratio values at the applied stress;
- the relationship in Figure 6-4 was used to estimate the hydraulic conductivity values corresponding to the void ratio values at the applied stress.

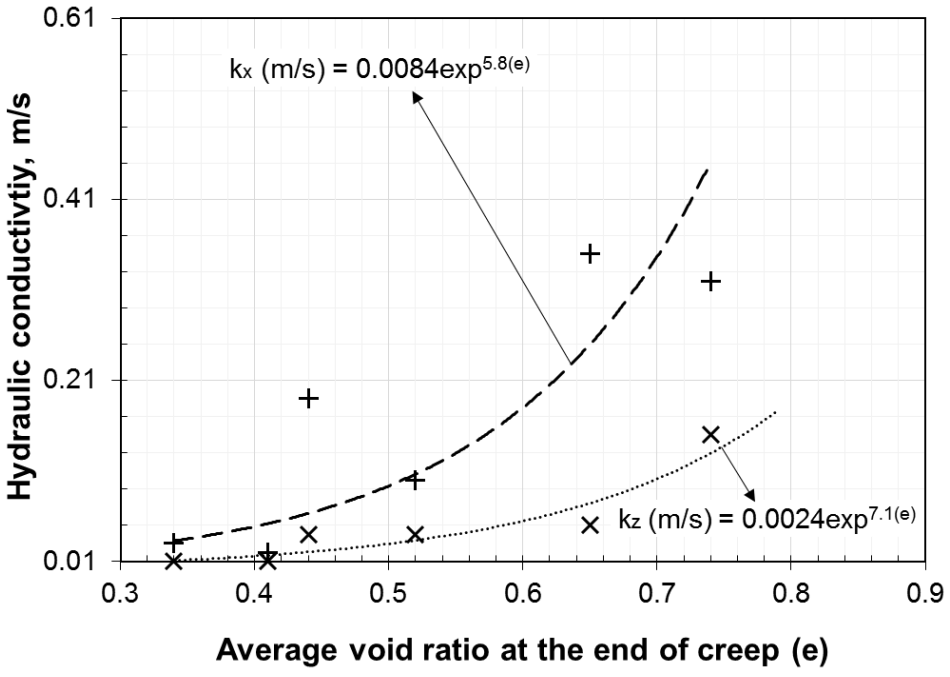

[77] See Chapter 5.

Figure 6-4: Relationship between hydraulic conductivity and void ratio – from measurements in the 2D cell (see Figure 6-3). The hydraulic conductivity values here are from Table 5-2(a), values in Table 5-8 can also be used.

Compression of initial TDA thicknesses of 1 m, 1.5 m and 2 m were considered for the design guidance in Table 6-1. Table 6-1 can be used in combination with the H_{max} charts (Figures 6-6 (a-f)) to select suitable design parameters for constructing a landfill drainage layer with TDA.

Table 6-1: Initial and final thicknesses, applied stress, and hydraulic conductivity values that may be used for design.

Average stress in TDA	Equivalent height of waste (using the range of unit weights in Zekkos et al., 2006), m	Average % compression Figure 6-2 ($\Delta e/1+e_0$)	Thickness of TDA layer after compression (from initial values of 1 m to 2 m)			Hydraulic conductivity, m/s (Table 5-2a[78] – average of values & Figure 6-4 – for 375, 500, 800 kPa)	
			1 m	1.5 m	2 m	k_z	k_x
32	2 to 3	37.8	0.62	0.93	1.24	0.20	1.14
63	5 to 8	45.6	0.54	0.82	1.09	0.12	0.57
123	8 to 12	52.5	0.48	0.71	0.95	0.05	0.15
219	18 to 23	55.9	0.44	0.66	0.88	0.01	0.03
375	30 to 40	63.0	0.37	0.56	0.74	0.01	0.03
500	40 to 53	65.6	0.34	0.52	0.69	0.006	0.02
800	70 to 85	70.0	0.30	0.45	0.60	0.003	0.01

6.2 Guidance charts for (H_{max}) in a TDA drainage layer

After determining approximate values of H_{max} using Eq. 6-1, a steady state finite element numerical modeling with SEEP/W (GEOSLOPE.com) was completed to validate the results. The numerical modelling showed that Eq. 6-1 underestimated the H_{max} values when a specified thickness of the drainage layer was exceeded. This is because the Eq. 6-1 assumes that the thickness of the drainage layer increases as the head of leachate increases. Thus, when the thickness should have transitioned into the lower hydraulic conductivity zone of the overlying waste (Fleming, 2011 measured 3 x10^{-9} m/s), Eq. 6-1 continues to assume the higher hydraulic

[78] Values in Table 5-8 can also be used.

conductivity values of the drainage layer throughout the apparently extended thickness, underestimating the H_{max} in the drainage layer.

As an example, for the model in Figure 6-5 with a specified thickness of 0.5 m, L = 30 m, tanβ = 1% and q_i = 0.1 m/year (3.17 x 10^{-9} m/s), when k (m/s) was > 0.000001 m/s, H_{max} remained within the thickness of the drainage layer (Figure 6-5 a) and the values from the numerical modeling matched those from Eq. 6-1. However, when k (m/s) was < 0.000001 m/s, H_{max} exceeded the thickness of the drainage layer (Figure 6-5 b) and the values from the numerical modelling were considerably greater than those from Eq. 6-1 in some cases. For instance, at k (m/s) = 0.000001, H_{max} was 3.05 m for numerical modeling (Figure 6-5 b) and 1.55 m with Eq. 6-1.

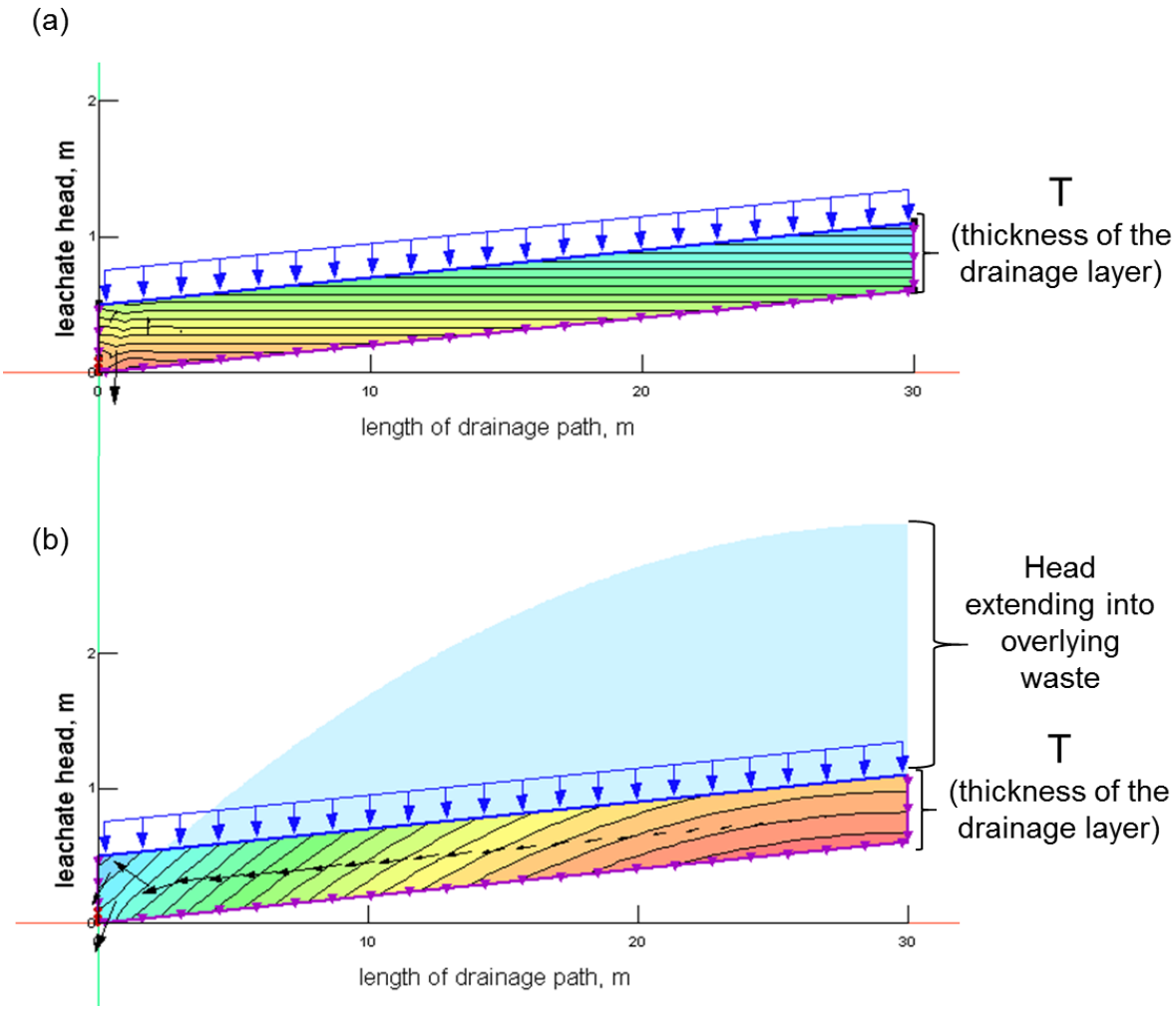

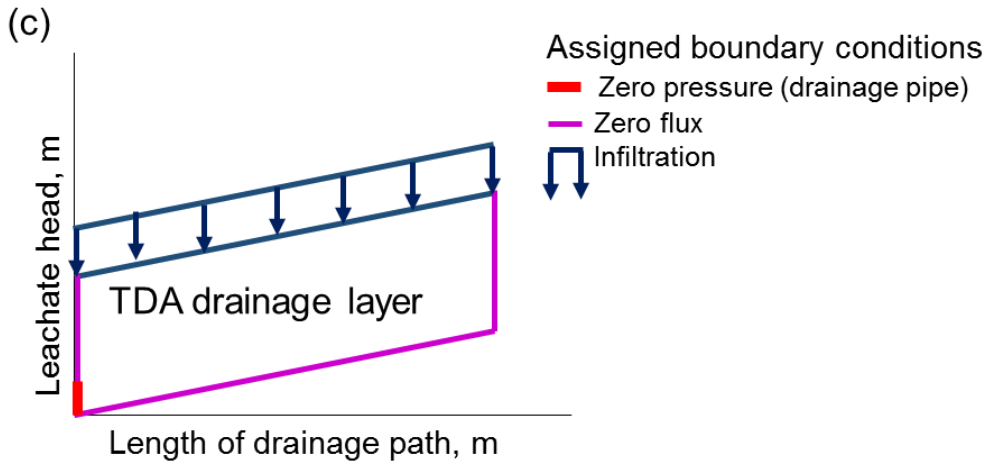

Figure 6-5: Numerical modeling of H_{max} for high and low values of k m/s at specified values of T, L, q_i and tanβ (a) k m/s >0.000001; (b) k m/s <0.000001; (c) boundary conditions used in the finite element modelling.

Hence, for a conservative approach, the values from the numerical modeling were used to correct the H_{max} values from Eq. 6-1 when the head exceeded the specified thickness of 0.5 m that was used in the modeling. The H_{max} values determined from Eq. 6-1 as corrected with the numerical modeling are presented in Figures 6-6 (a-f). Figures 6-6 (a-f) are for:

- vertical infiltration rate q_i = 0.1 m/yr (3.17 x 10^{-9} m/s) and 1 m/yr (3.17 x 10^{-8} m/s) – for landfill conditions without and with leachate recirculation respectively;
- slope angle to drainage pipes = 1%, 2 % and 5%;
- length of drainage path L = 10 m, 20 m and 30 m. Simulations of L values > 30 m are not presented as pipe spacing in excess of 30 m is considered by the author to be poor design practice. The shorter the drainage path, the better, as excessively long drainage paths may result in longer drainage times for the transmission of leachate into collection pipes.
- horizontal hydraulic conductivity k_x = 0.01 m/s to 0.000001 m/s.

(a)

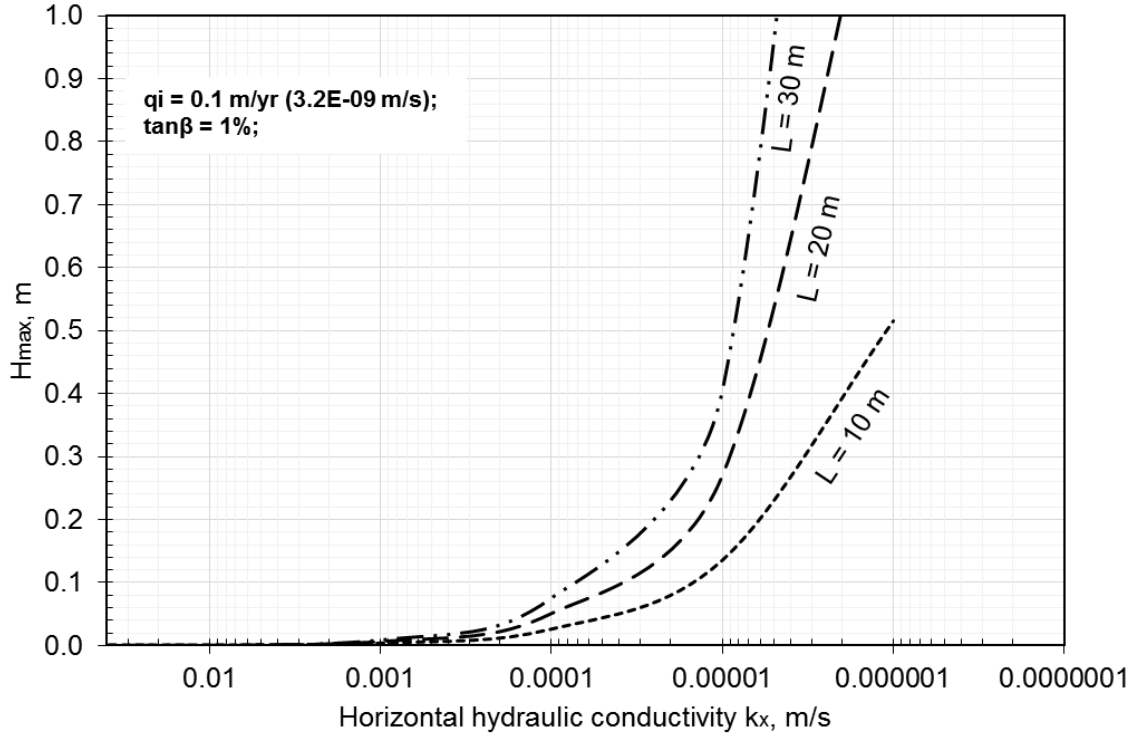
qi = 0.1 m/yr (3.2E-09 m/s);
tanβ = 1%;
L = 30 m
L = 20 m
L = 10 m
Hmax, m
1.0
0.9
0.8
0.7
0.6
0.5
0.4
0.3
0.2
0.1
0.0
0.01
0.001
0.0001
0.00001
0.000001
0.0000001
Horizontal hydraulic conductivity kx, m/s

(b)

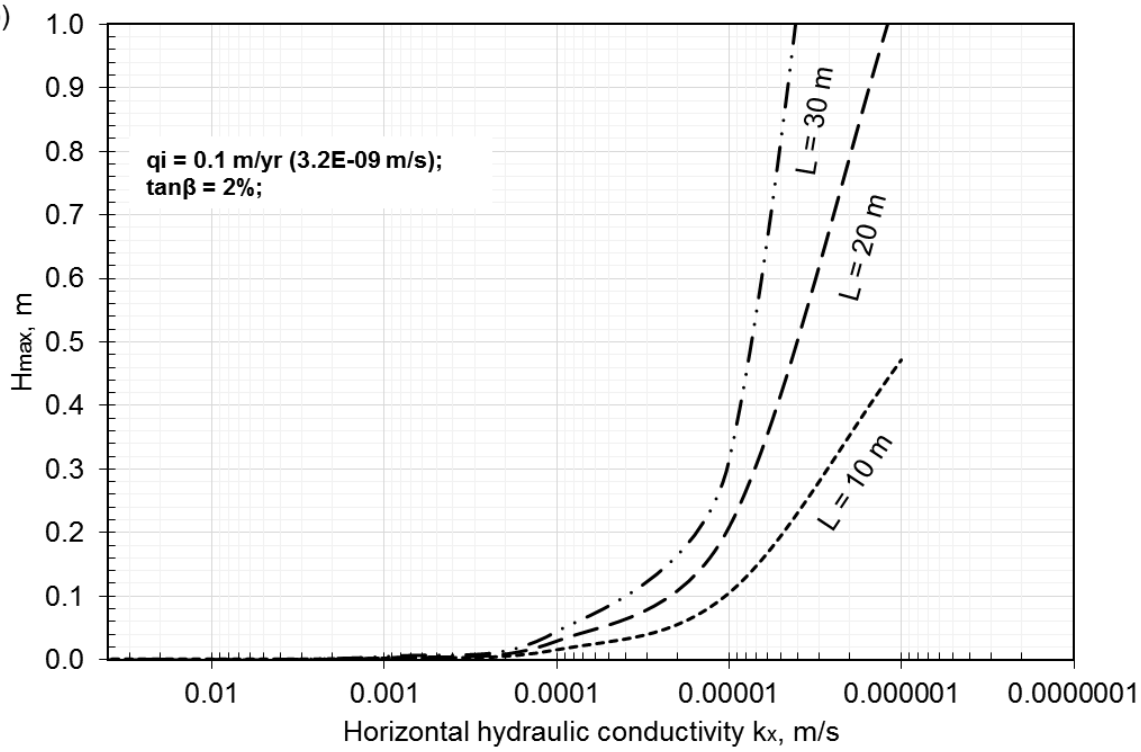
qi = 0.1 m/yr (3.2E-09 m/s);
tanβ = 2%;
L = 30 m
L = 20 m
L = 10 m
Hmax, m
1.0
0.9
0.8
0.7
0.6
0.5
0.4
0.3
0.2
0.1
0.0
0.01
0.001
0.0001
0.00001
0.000001
0.0000001
Horizontal hydraulic conductivity kx, m/s

(c)

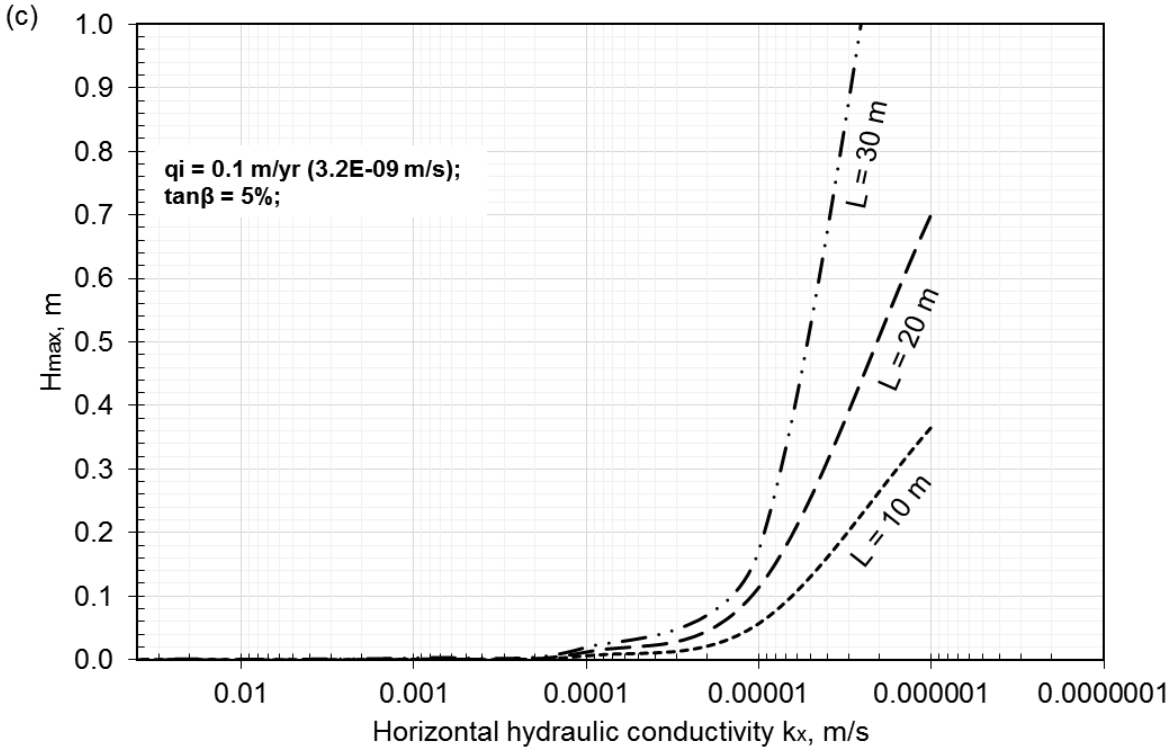
qi = 0.1 m/yr (3.2E-09 m/s);
tanβ = 5%;
L = 30 m
L = 20 m
L = 10 m
Hmax, m
1.0
0.9
0.8
0.7
0.6
0.5
0.4
0.3
0.2
0.1
0.0
0.01
0.001
0.0001
0.00001
0.000001
0.0000001
Horizontal hydraulic conductivity kx, m/s

(d)

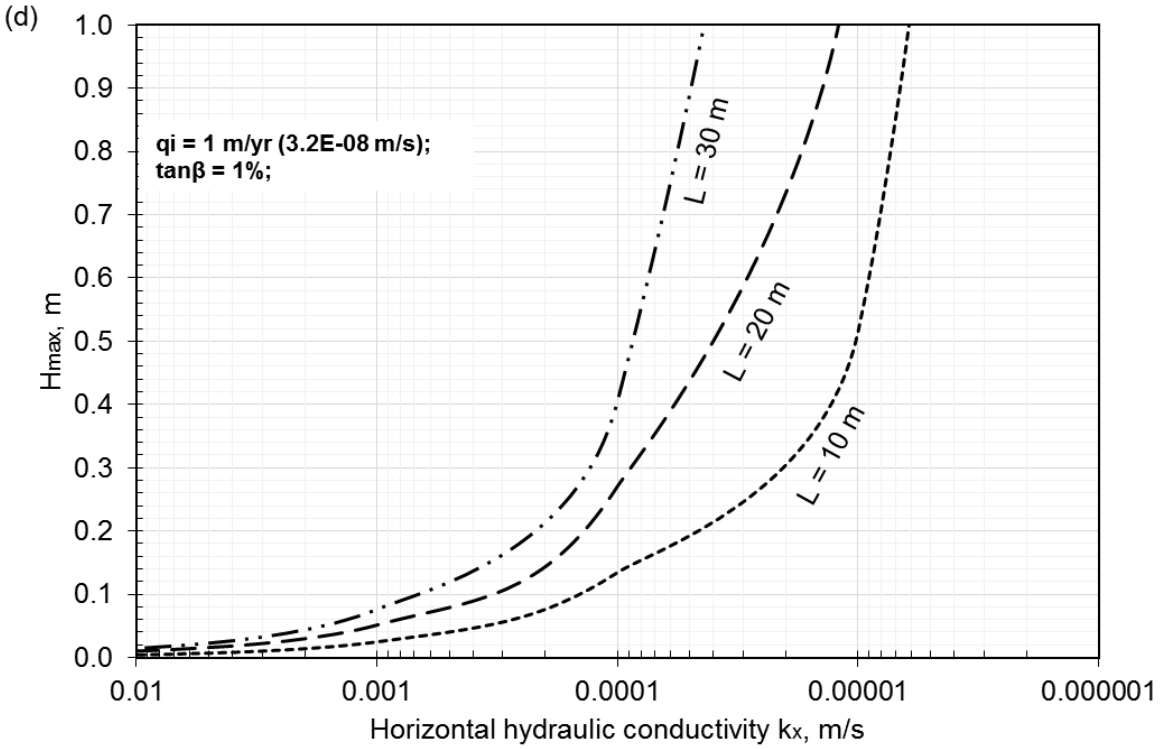
qi = 1 m/yr (3.2E-08 m/s);
tanβ = 1%;
L = 30 m
L = 20 m
L = 10 m
Hmax, m
1.0
0.9
0.8
0.7
0.6
0.5
0.4
0.3
0.2
0.1
0.0
0.01
0.001
0.0001
0.00001
0.000001
Horizontal hydraulic conductivity kx, m/s

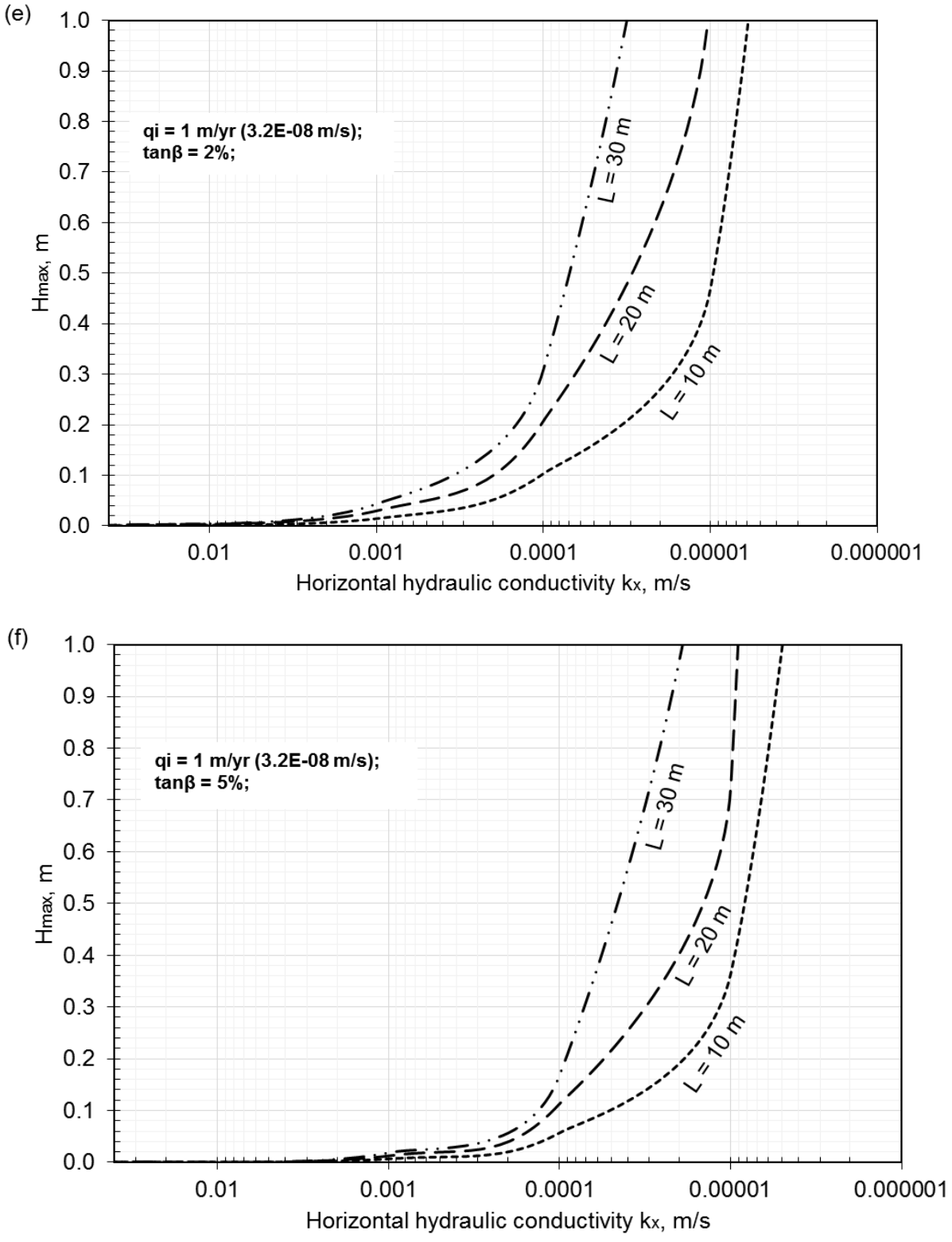

Figure 6-6(a – f): Variation of maximum head (H_{max}) on basal liner with horizontal hydraulic conductivity of drainage media. H_{max} values beyond 1 m were not included, as those values excessively exceed typical regulatory limits.

From Figures 6-6 (a-f), it is evident that H_{max} in a TDA drainage layer can easily be maintained less than 0.3 m for hydraulic conductivity values >0.00001 m/s, and increasing tanβ or decreasing L results in relatively lower values of $H_{max.}$ On the other hand, hydraulic conductivity values <0.00001 m/s will be problematic for the performance of the drainage layer especially for high values of qi and L, and low values of tanβ.

The contribution of biogeochemical clogging to the void volume and hydraulic conductivity reduction needs to be determined in order to adequately evaluate the design parameters for the drainage layer. In a design example presented at the end of this section, a hypothetical decrease in hydraulic conductivity of up to three orders of magnitude is used to evaluate suitable design parameters for a heavily clogged TDA drainage layer, using reported values for clogged granular drainage layers. Rowe and Fleming (1998) reported a decrease in hydraulic conductivity of up to two orders of magnitude for a clogged gravel drainage layer.

The values of H_{max} presented in Figures 6-6 (a-f) can be used for an initial evaluation of design parameters (as presented in the example at the end of this section). Once the design parameters have been narrowed down, more precise estimations of H_{max} can be made using the modified Giroud's equation in Giroud and Houlihan (2005) (Qian et al, 2001. pp.280-281), the McEnroe's 1993 method or other methods (Qian et al, 2001. pp. 281), in combination with numerical simulations. Other values of the design parameters can also be considered for additional evaluation of various scenarios.

The H_{max} values in Figures 6-6 (a-f) can be used to select a suitable initial thickness of TDA (using Table 6-1), or a suitable initial thickness of TDA can be selected and the compression and H_{max} values determined. The value of hydraulic conductivity selected for the design will depend on the maximum expected height of waste on the TDA drainage layer (as presented in Table 6-1).

Example

For an expected maximum height of waste of 30 m – 40 m over a landfill drainage layer constructed using large particle sized TDA,

(1) what is the expected hydraulic conductivity to determine the lateral flow of leachate into collection pipes under the maximum height of waste?
(2) for a vertical infiltration rate q_i of 0.1 m/yr (3.2×10^{-9} m/s), and using the expected hydraulic conductivity under the maximum height of waste, what are the design parameters – length of drainage path L, and slope angle to drainage pipes tanβ, to ensure that the maximum head of leachate in the drainage layer (H_{max}) does not exceed a regulatory limit of 0.3 m?
(3) assuming biogeochemical clogging results in a reduction in the hydraulic conductivity up to three orders of magnitude, what are the design parameters to ensure that H_{max} does not exceed a regulatory limit of 0.3 m?
(4) for the selected design parameters in "2" and "3", what is the recommended initial thickness of TDA to meet the regulatory thickness requirement of ≥ 0.3 m and regulatory limit of H_{max}?

Solution

(1) From Table 6-1, horizontal hydraulic conductivity k_x is relevant for lateral flow, and at 375 kPa (30 m – 40 m of waste), k_x = 0.03 m/s;
(2) For k_x = 0.03 m/s, and q_i = 0.1 m/yr (3.2×10^{-9} m/s)
    - Using Figure 6-6(a), with a 1% slope, the value of H_{max} is <0.04 m for all values of L
    - Using Figure 6-6(b), with a 2% slope, the value of H_{max} is <0.02 m for all values of L

- Using Figure 6-6(c), with a 5% slope, the value of H_{max} is <0.02 m for all values of L

Therefore, any combination of slope angle (>1%) and length of drainage pipe (≤30m) (Figures 6-6 a-c) can be used. However, further evaluation of biogeochemical clogging effects in "3" below will further determine suitable parameters.

(3) For k_x = 0.00001 m/s, and q_i = 0.1 m/yr (3.2×10^{-9} m/s)

- Using Figure 6-6(a), with a 1% slope,
  - H_{max} is <0.3 m for L = 10 m; 0.3 m for L = 20 m; and just over 0.3 m for L = 30 m
- Using Figure 6-6(b), with a 2% slope,
  - H_{max} is <0.3 m for L = 10 m and 20 m; and at 0.3 m for L = 30 m
- Using Figure 6-6(c), with a 5% slope,
  - H_{max} is <0.3 m for all values of L

Therefore, for the design situation in question, with consideration for biogeochemical clogging, suitable combination of parameters can be a 1% slope with L = 10 m; 2% slope with L = 20 m; 5% slope with L= 30 m. The slope selected will depend on the existing natural gradient of the site and how much earthwork is needed to increase the slope angle.

(4) From Table 6-1, at 375 kPa (30 m to 40 m of waste), the average compression is approximately 63%. Thus, a suitable initial thickness of TDA in this instance will be 1.5 m, for a thickness after compression of 0.56 m.

– An initial thickness of 1 m can be used, but the thickness of the TDA layer after compression will only be 0.37 m. In this example, this was the minimum regulatory stipulation so a somewhat larger initial thickness would ensure compliance;

– An initial thickness of 2 m can also be used, for a thickness after compression of 0.74 m; however, to keep the thickness of the drainage layer to a minimum in order to maximize air space, and perhaps for monetary savings on the TDA material, an initial thickness of 1.5 m is suitable.

7.0 Conclusions

The goal of the research work was *"to gain a better understanding of the immediate and time dependent performance-related properties of TDA for use as drainage medium in the LCRS of engineered landfills and other waste disposal facilities*". This, and the research objectives, have been met in the preceding chapters. This chapter presents a summary of the key findings and their implication for practice, some practical design guidance for constructing a landfill drainage layer with TDA, and some recommendations on the direction of future work.

7.1 Summary of key findings and implications of practice

The function of a TDA drainage layer in a landfill is to rapidly collect and transmit infiltrating leachate into collection pipes for removal from the base of the landfill to keep leachate mound (hydraulic head) on basal liners to a minimum. The higher the head leachate over basal liners, the higher the potential for leachate and contaminants to go through the liner. The performance of a TDA drainage layer therefore depends on maintaining sufficient void volume and hydraulic conductivity (1) under large applied stress from the weight of the overlying waste, and (2) following biogeochemical clogging, to effectively remove leachate from the base of the landfill. Evaluation of biogeochemical clogging was outside the scope of the research work. Nonetheless, parameters that may be used to model biogeochemical clogging, such as void ratio and specific surface area, under applied stress have been determined. These parameters may be used in simple mass-balance approaches (Rowe and Fleming, 1998), or in elaborate numerical models such as BioClog (Rowe and Yu, 2013) to evaluate biogeochemical clogging in TDA drainage layers.

The following are some of the key observations and performance-related findings from the research study, and their relevance for practice:

- Laboratory testing of large-particle-sized TDA (particle size over 50 mm) unavoidably requires the use of large-sized test equipment that can accommodate large vertical stresses and strains. In such equipment, sidewall friction loss will be significant, with over 40% of the applied stress not reaching the bottom of the test cell (Chapters 2, 3, 5). The resultant effect of this is an overestimation of the applied stresses and void ratio throughout the TDA. Sidewall friction loss needs to be accounted for in order to properly assess the void volume of TDA under applied stress for field conditions where sidewall friction loss will not occur. Several approaches were implemented to account for sidewall friction loss during testing (Chapter 3). The approaches implemented enabled adequate evaluation of the performance related properties of the TDA types;

- TDA being a polymeric composite may be expected to undergo both immediate compression and creep. Both immediate compression and creep were found to contribute to void volume reduction in TDA, but the contribution of creep was considerably lesser than that of immediate compression. The contribution of creep to the total void volume reduction ranged from 4% to 29% (Chapter 4). This contribution is comparable to the 17% that was observed by Humphrey et al. (2000) in a field study of large particle sized TDA for a roadway construction project. The higher values of creep were observed in the longer duration tests, and at the higher applied stress (Chapter 4). The contribution of immediate compression ranged from 71% to 96%. Despite the lower contribution of creep relative to that of immediate compression, it is not adequate to neglect creep. The additional void volume reduction from creep is needed to evaluate total void volume in the TDA under applied stress for hydraulic conductivity and biogeochemical clogging evaluations. Hence, sufficient time should be allowed to capture creep in determining void volume reduction in TDA under applied stress. Some of the findings on creep in this research work differ from those in Wartman et al. (2007), another of the few studies in the literature to have looked

at creep in TDA (albeit tire chips and mixtures of tire chips and sand). In the Wartman study, creep in TDA was stated to have occurred initially from pore volume reduction, and as the TDA aged under applied stress with time, solid particle compression dominated the creep phenomenon. The study also stated that creep in TDA can be determined in the first five days of the experiment and long duration tests may not be needed in practice. In this study, solid volume compression in individual TDA particles was found to be negligible, and therefore did not contribute to void volume reduction in the bulk volume of TDA. In addition, unlike the Wartman study, creep was found to continue considerably over five days (Chapter 4), thus highlighting the need for sufficient time to capture creep. The immediate compression and creep curves in this study were found to be similar to the initial strain, primary and secondary stages in Figure 2-3 Chapter 2, however, the total strain in the secondary stage was more constant with time;

- Strain stiffening behaviour was observed in the TDA with increased applied stress, implying that at and beyond certain applied stress, void volume reduction may become negligible (Chapters 3, 4). The cause of strain stiffening in TDA may be related to inter particle movement, friction and bending, which is initially high under applied stress but gradually reduces as areal contact between particles increase and space for further inter particle movement reduces. The restriction of inter particle movement then causes a reduction in the compression of the TDA. In order to determine the “ultimate applied stress” where further compression may become negligible because of strain stiffening, the void ratio values in this study were projected to higher applied stress beyond those covered in the study. Corresponding values of vertical and horizontal hydraulic conductivity values for the projected applied stress and void ratios were also estimated. An ultimate applied stress was not determined, at least not within reasonable values of applied stress, nonetheless, the projections indicate that at 800 kPa, void ratio reduces

to 0.01, and beyond that, void ratio becomes considerably less than 0.01. Projections of the hydraulic conductivity values show that at void ratios of 0.01, the vertical and horizontal hydraulic conductivity can be as high as 0.003 and 0.01 m/s respectively (Table 6-1). Thus implying that void ratio alone is not sufficient for evaluating the performance of a TDA drainage layer, as even at considerably low void ratios, adequate flows can still be maintained in a TDA drainage layer;

- The final void ratio achieved/void ratio at a particular stress appears to depend considerably on the initial void ratio, as well as the applied stress (Chapters 4, 5). This is perhaps related to the strain stiffening behaviour, and because as areal contact between particles and inter particle friction becomes so high under applied stress particle re-arrangement is mostly bending and not inter particle shearing. Given the apparent dependence of void ratio at any applied stress on the initial void ratio, pre-compressing TDA before use may not be beneficial for maintaining a large void volume in service as this will reduce the initial void ratio, and consequently the void ratio under applied stress. Any approach that can increase the final void volume in TDA under applied stress is better;
- There were wide variations in void ratio, immediate compression and creep indexes (C_c and C_α respectively) for any value of applied stress, indicating that there may not be a unique relationship between applied stress and void ratio in TDA (Chapter 4). Nonetheless, the values of C_c and C_α appeared to increase with the corresponding initial void ratio values (void ratio at the start of the testing event and void ratio at the start of creep respectively). The C_c values ranged from 0.12 to 1.57 corresponding to void ratio values of 0.3 to 2.7 respectively, and the C_α values ranged from 0.002 to 0.11 corresponding to void ratio values of 0.5 to 0.7 respectively (Chapter 4). Higher values of C_c relate to higher immediate compression and higher values of C_α relate to higher values of creep. Similar variations in void ratio, C_c and C_α with applied stress have been

reported for highly compressible materials that exhibit time dependent compression, such as municipal solid waste (Qian et al. 2011). The variations reported for solid waste were stated to be dependent on the type, composition and organic content of the waste, amongst other factors (Qian et al. 2011). On the contrary, the TDA types tested in this work were similar in composition, as the scrap tire portions used to produce the TDA types are generally similar. Typically, the tire portions with high rubber content are removed and recycled and portions with high wire content are left behind for use as TDA. Thus, the reasons for the variations in the void ratio, C_c and C_α values relative to applied stress for the TDA types in this work does not appear to be expressly related to the TDA composition, unlike with solid waste. The reasons for the variations are not clear, and may be an indication of a complex compressive behaviour, or may potentially be related to parameters outside of those investigated in this work;

- The effect of loading rate was found to be minor (Chapter 4), as the difference in void ratio achieved from a slow loading rate (approximately 4 kPa/day) and that from a faster loading rate (approximately 8 kPa/day) was only 0.1. Although minimal, the resulting difference in void ratio may be tangible for void volume to store eventual biogeochemical clog. Hence, applying loads/stress to TDA in small increments may be ultimately beneficial;
- Temperatures at the bottom of landfills can often exceed 40 C (Rowe, 2005), thus it was necessary to investigate the effect of elevated temperatures over 40 C on the compressive behaviour of TDA (Chapter 4). No effects of elevated temperature, up to 58 C, was observed on the immediate compression, creep and void volume reduction in TDA. Heating up the TDA before applying stress did not induce more compression or creep; neither did heating up the TDA after applying stress (Chapter 4). It is not surprising that no effect of temperature was found at the temperature studied because

rubber tires only start to thermally degrade and loose some volatiles at temperatures over 200 C (Chapter 4);

- The voids in TDA remained large under high applied surface stresses – 224 kPa (equivalent to 20 m – 25 m of waste (Zekkos et al. 2006)), and there does not appear to be significantly more elongated voids in the horizontal direction than in the vertical direction, as might have been expected in relation to the largely horizontal alignment of large particle sized TDA (Chapter 5);
- The mean vertical and horizontal hydraulic conductivity of the TDA types at all the applied stress up to 375 kPa (30 – 40 m of overlying waste), after correcting for inertia, and accounting for sidewall friction loss, were higher than 0.01 m/s (Chapter 5). This is comparable to the typical range of values for gravel used in LCRS (Fleming and Rowe, 2004), and exceeds the typical stipulation of 0.0001 m/s for the hydraulic conductivity of drainage layers in LCRS (see: Duffy, 1995; Narejo and Shettima, 1995; Warith et al. 2004; *Standards for Landfills in Alberta,* 2010 – which is used in Saskatchewan). The stipulation for hydraulic conductivity however does not typically factor in biogeochemical clogging. A minimum hydraulic conductivity of 0.01 m/s before clogging is recommended for any drainage layer. This value was met by all the TDA types evaluated in both the vertical and horizontal directions. Anisotropy in the hydraulic conductivity decreased with the applied surface stress, from as high as 7 at 56 kPa, to 2 at the final applied stress, across the three TDA types tested (Chapter 5). Visual examination of TDA thin section slices from a porosimetry evaluation to look within the fabrics of the TDA (Chapter 5), correlated reasonably with the anisotropy value of 2 measured at the 224 kPa surface stress for the TDA type used in the evaluation. Thus substantiating the results from the flow measurements. Anisotropy under applied stress appeared to be material dependent, as it was higher for the TDA type with particles that were larger in length and width, but the same in thickness as others, under similar applied stress (Chapter 5). The

anisotropy values provided in this research work will enable better evaluations of flows and maximum head (Chapter 6) in the design, assessment and construction of a landfill drainage layer with large-particle sized TDA.

Ultimately, this study has shown that despite a considerable amount of immediate compression, followed by some creep, large voids remain present in large particle sized TDA under high stresses to maintain sufficiently large flows. Thus making large particle sized TDA an adequate, economically and environmentally beneficial substitute for gravel in landfill LCRS. The findings and design guidance presented in this research work are expected to provide guidance on designing with large particle sized TDA as drainage material for leachate transmission in waste disposal applications. The testing approaches and analytical procedures implemented can be applied to similar laboratory evaluations of highly compressible materials that undergo large strains under applied stress, or materials where applied stress and sidewall friction significantly affect material properties.

7.2 Recommendations for future work

Three areas are recommended for future work as follows:

(1) Unconstrained compression testing of TDA, preferably under actual field conditions should be completed to eliminate the effects of sidewall friction and to calibrate laboratory test data obtained from the constrained 1D compression laboratory testing;

(2) Measurement or modelling of biogeochemical clogging under applied stress simulating various landfill conditions should be completed to evaluate void volume reduction from the individual and combined effects of biogeochemical clogging.

(3) Measurement of the specific surface area should be completed under additional applied stresses, especially at high applied stresses, over the 224 kPa that was applied in this work. This will enable clogging evaluations to be carried out for TDA under overlying waste thicknesses greater than 25 m – Zekkos et al. 2006. The data obtained can also

be used in the hydraulic conductivity and pressure distribution forms presented in Chapter 5, Section 5.6.4. to address sidewall friction effects in the flow data. Future measurements of specific surface area should also be done using test cells with similar geometry to that for the flow testing to avoid differences in TDA packing orientations and sidewall friction effects, which may result in different compression profiles, surface area, voids and volume parameters.

References

Adesokan D, Fleming I and Hammerlindl A (2020) One-dimensional (1D) immediate compression and creep in large particle sized Tire Derived Aggregate (TDA) for leachate collection and removal systems (LCRS). Canadian Geotechnical Journal 'in press'.

Adesokan D, Fleming I, Hammerlindl A et al. (2019) Strategies for one dimensional (1d) compression testing of large-particle-sized tire derived aggregate. Geotechnical Testing Journal 42(5): 1336-1358, https://doi.org/10.1520/GTJ20170091.

Adesokan, D., and Fleming, I. 2016. Compression and creep of Tire Derived Aggregate (TDA) under applied load. In Proceedings of the 69th Canadian Geotechnical Conference - GeoVancouver 2016, Vancouver, Canada, October 2-5, 2016.

Adesokan, D., Fleming, I., and Stevens, D. 2015. Assessing performance of tire derived aggregate for use in landfill drainage. In Proceedings of the 14th Global Joint Seminar on Geo-Environmental Engineering – Geo-Environmental Engineering, Concordia University Montreal, Canada, May 21-22, 2015.

Adesokan, D., Fleming, I., Hammerlindl, A., and McDougall, J. (2019). Strategies for one dimensional (1d) compression testing of large-particle-sized tire derived aggregate. Geotechnical Testing Journal, 42(5): 1336-1358. doi:10.1520/GTJ20170091.

Ahmed, I. and Lovell, C. W. 1993. Tire chips as permeable aggregate in landfills. In Proceedings of the 1st Annual Great Lakes Geotechnical/Geoenvironmental Conference, Toledo Section of the American Society of Civil Engineers, Toledo, USA, pp. 83-90.

Ahn, I., Cheng, L., Fox, P. J., Wright, J., Patenaude, S., and Fujii, B. 2015. Material properties of large-size tire derived aggregate for civil engineering applications. Journal of Materials in Civil Engineering, 27(9). Available from

https://ascelibrary.org/doi/10.1061/(ASCE)MT.1943-5533.0001225 [last accessed February 5, 2020].

ASTM C127-12: Standard Test Method for Relative Density (Specific Gravity) and Absorption of Coarse Aggregate, ASTM International, West Conshohocken, PA, 2012, www.astm.org

ASTM D2435 / D2435M - 11: Standard Test Methods for One-Dimensional Consolidation Properties of Soils Using Incremental Loading, ASTM International, West Conshohocken, PA, 2011, www.astm.org

ASTM D2990-09: Standard Test Methods for Tensile, Compressive, and Flexural Creep and Creep Rupture of Plastics, ASTM International, West Conshohocken, PA, 2009, www.astm.org

ASTM D6270-08: Standard Practice for Use of Scrap Tires in Civil Engineering Applications, ASTM International, West Conshohocken, PA, 2008, www.astm.org

ASTM D7406-07: Standard Test Method for Time-Dependent (Creep) Deformation Under Constant Pressure for Geosynthetic Drainage Products, ASTM International, West Conshohocken, PA, 2007, www.astm.org

ASTM D7361-07: Standard Test Method for Accelerated Compressive Creep of Geosynthetic Materials Based on Time-Temperature Superposition Using the Stepped Isothermal Method. West Conshohocken: ASTM International.

Barbour, L. S., and Krahn, J. 2004. Numerical Modelling - Prediction or Process? Geotechnical News, pp. 44-52. Retrieved September 10, 2014, from http://www.geo-slope.com/res/numerical%20modelling%20-%20prediction%20or%20process.pdf

Bear J 1972. Dynamics of Fluids in Porous Media, Dover Publications, Inc. New York City

Beaven RP 1994. The technical aspects of controlled waste management: Assessment of the physical and hydraulic properties of tyres for leachate collection and drainage systems in landfills. Wastes Technical Division, Department of the Environment, London, UK.

Beaven RP, Hudson AP, Knox K et al 2013. Clogging of landfill tyre and aggregate drainage layers by methanogenic leachate and implications for practice. Waste Management 33(2): 431-444.

Beaven, R. P., 2000, "The hydrogeological and geotechnical properties of household waste in relation to sustainable landfilling", PhD Dissertation, University of London, London, England, pp. 81-89

Beaven, R. P., Powrie, W., and Zardava, K. 2008. Geotechnical characterization, field measurement, and laboratory testing of Municipal Solid Waste: Hydraulic properties of MSW. Proceedings of the 2008 International Synposium on Waste Mechanics. Geotechnical Special Publication No. 209, pp. 1-15. New Orleans, Louisiana: American Society of Civil Engineers (ASCE).

Beaven, R. P., Powrie, W., Hudson, A. P., and Parkes, D. J. 2006. Compressibility of tyres for use in landfill drainage systems. Proceedings of the Institution of Civil Engineers - Waste and Resource Management, 159(4): 173–180. Available from https://doi.org/10.1680/warm.2006.159.4.173 [last accessed October 14, 2019].

Cooke AJ and Rowe RK, 2008a. 2D modelling of clogging in landfill leachate collection systems. Canadian Geotechnical Journal 45(10): 1393-1409.

Cooke AJ and Rowe RK, 2008b. Modelling landfill leachate-induced clogging of field-scale test cells (mesocosms). Canadian Geotechnical Journal 45(11): 1497-1513.

Cooke AJ, Rowe RK, Rittman BE et al 2001. Biofilm Growth and Mineral Precipitation in Synthetic Leachate Columns. Journal of Geotechnical and Geoenvironmental Engineering 127(10): 849-856.

Cooke AJ, Rowe RK, VanGulck J et al 2005. Application of the BioClog model for landfill leachate clogging of gravel-packed columns. Canadian Geotechnical Journal 42(6): 1600-1614.

Cooke, A. J., Rowe, R. K., Rittmann, B. E., and Fleming, I. R. 1999. Modelling biochemically driven mineral precipitation in anaerobic biofilms. Wat. Sci. Tech., 39(7), 57-64.

Cooke, A. J., Rowe, R. K., VanGulck, J., and Rittman, B. E. 2005. Application of the BioClog model for landfill leachate clogging of gravel-packed columns. Canadian Geotechnical Journal, 42(6), 1600-1614.

Das BM 1983. Advanced Soil Mechanics, Hemisphere Publishing, USA

Dickinson, S. and Brachman, R. W. 2008. Assessment of alternative protection layers for a geomembrane - geosynthetic clay liner (GM-GCL) composite liner. Canadian Geotechnical Journal, 45(11): 1594-1610. Available from https://doi.org/10.1139/T08-081 [last accessed February 5, 2020].

Domenico PA and Schwartz FW 1997. Physical and Chemical Hydrogeology. John Wiley and Sons, New York, USA.

Donovan, R., Dempsey, J., and Owen, S. 1996. Scrap tire utilization in landfill applications. Presented at the 17th Biennial Waste Processing Conference, Atlantic City, NJ, American Society of Civil Engineers, Reston, VA, pp. 353–383.

Duffy, D. P. 1995. Using tire chips as leachate drainage layer. Waste Age, 26(9): 113–122.

Dunicliff, J., 1988. Geotechnical Instrumentation for Monitoring Field Performance, John Wiley and Sons, New York, pp. 165 -177

Evans, P. 1997. Use of tire shred in landfill construction. In Proceedings of the Third Annual Symposium Environmentally Friendly Technologies in Geotechnical Engineering, Edmonton, Canada, Geotechnical Society of Edmonton, Edmonton, Canada, pp. 1–8.

Fleming, I. R., 2011. "Indirect measurements of field scale hydraulic conductivity of waste from two landfill sites, "Waste Management", Vol. 31, pp. 2455-2463.

Fleming, I. R., and Rowe, R. K. 2004. Laboratory studies of clogging of landfill leachate collection and drainage systems. Canadian Geotechnical Journal, 41(1): 134–153. Available from https://doi.org/10.1139/t03-070 [last accessed October 14, 2019].

Fleming, I. R., Rowe, R. K., and Cullimore, D. R. 1999. Field observations of clogging in landfill leachate collection systems. Canadian Geotechnical Journal, 36(4): 685–707. Available from https://doi.org/10.1139/t99-036 [last accessed October 14, 2019].

Fleming, I., and Marshall, P. 2013. Tire-derived aggregate in landfill leachate collection systems. A presentation made at SWANA: Northern Lights Chapter.

Freeze RA and Cherry JA 1979. Groundwater. Prentice-Hall, Englewoods Cliffs, New Jersey, USA.

Geosyntec. 2008. Guidance manual for engineering uses of scrap tires. Prepared for Maryland Department of the Environment, Project No. ME0012-11, Geosyntec Consultants, Columbia, Maryland.

Ghaaowd, I., McCartney, J.S., Thielmann, S., Sanders, M. and Fox, P.J. 2017. Shearing behavior of tire derived aggregate with large particle sizes. I: Internal and concrete

interface direct shear behavior. ASCE Journal of Geotechnical and Geoenvironmental Engineering. 143(10): 1-11. doi: 10.1061/(asce)gt.1943-5606.0001775.

Giroud, J. P., and Houlihan, M. F., 1995 "Design of leachate collection layers, “In proceedings of the 5th International Landfill Symposium, S.Margherita di Pula, Cagliari, Italy, Vol. 2, pp. 613-640.

Hall TJ 1991. Reuse of shredded tire material for leachate collection systems. In Proceedings of the 14th Annual Madison Waste Conference, University of Madison, Wisconsin, pp. 367-376.

Huang M, Rodger H and Barbour L 2015. An evaluation of air permeability measurements to characterize the saturated hydraulic conductivity of soil reclamation covers. Canadian Journal of Soil Science 95(1): 15-26.

Huang M, Zettl JD, Barbour LS et al 2016. Characterizing the spatial variability of the hydraulic conductivity of reclamation soils using air permeability. Geoderma 262: 285-293.

Hudson, A. P., Beaven, R. P., Powrie, W., and Parkes, D. 2007. Hydraulic conductivity of tyres in landfill drainage systems. Proceedings of the Institution of Civil Engineers - Waste and Resource Management, 160(2): pp. 63–70.

Humphrey, D. N, and Sandford, T. C. 1993. Tire chips as lightweight subgrade fill and retaining wall backfill. In Symposium on Recovery and Effective Reuse of Discarded Materials and By-Products for Construction of Highway Facilities Denver, Colorado October 19-22, Vol 5, pp 87-99.

Humphrey, D. N. 1999. Civil engineering application of tire shreds. Presented at: The Tire Industry Conference Hilton Head, South Carolina March 3, 1999

Humphrey, D.N. and Eaton, R.A. 1993. Tire chips as subgrade insulation – field trial. In Proceedings of the Symposium on Recovery and Effective Reuse of Discarded Materials and By-Products for Construction of Highway Facilities, Federal Highway Administration, Denver, Colorado, USA, pp. 5-55 - 5-68.

Humphrey, D.N. and Eaton, R.A. 1994. Performance of tire chips as an insulating layer beneath gravel surface roads. In Proceedings of the Fourth International Symposium on Cold Region Development, Espoo, Finland, pp. 125-126.

Humphrey, D.N. and Eaton, R.A. 1995. Field performance of tire chips as subgrade insulation for rural roads. In Proceedings of the Sixth International Conference on Low-Volume Roads, Transportation Research Board, Washington, D.C., USA, Vol. 2, pp. 77-86.

Humphrey, D.N., Whetten, N., Weaver, J., and Recker, K. 2000. Tire shreds as lightweight fill for construction on weak marine clay. In Proceedings of the International Symposium on Coastal Geotechnical Engineering in Practice, Balkema, Rotterdam, pp. 611-616.

Long RP, Demars KR, Mankbadi RR et al 1988. Final Report: The Relationship between Permeability Coefficients for Soil Obtained Using Liquid and Gas. University of Connecticut, Department of Civil Engineering.

Manion, W. and Humphrey, D. N. 1992. Use of tire chips as lightweight and conventional embankment fill, Phase I – laboratory. Dept. Civil Engineering, Technical Paper 91-1, Technical Services Division, Maine Department of Transportation, Augusta, Maine, USA.

Marcotte, B., and Fleming, I. 2020. Damage to geomembrane liners from tire derived aggregate. Geotextiles and Geomembranes, 48(2): 198-209. Available from https://doi.org/10.1016/j.geotexmem.2019.11.005 [last accessed February 5, 2020].

McIsaac RS, Rowe RK, Fleming IR et al 2000. Leachate collection system design and clog development. In Proceedings of the 6th Environmental Engineering Specialty Conference of the CSCE & 2nd Spring Conference of the Geoenvironmental Division of the Canadian Geotechnical Society, London, Ontario, pp. 66-73.

McIsaac, R. S., Rowe, R. K., Fleming, I. R., and Armstrong, M. D. 2000. Leachate collection system design and clog development. 6th Environmental Engineering Specialty Conference of the CSCE & 2nd Spring Conference of the Geoenvironmental Division of the Canadian Geotechnical Society, (pp. 66-73). London, Ontario. Retrieved December 6, 2013, from http://www.civil.queensu.ca/Research/Environmental/R-Kerry-Rowe/publications/documents/ConfLondon83_90%20Leachate%20Collection.p

McIsaac, R., and Rowe, R. K. 2005. Change in leachate chemistry and porosity as leachate permeates through tire shreds and gravel. Canadian Geotechnical Journal, 42(4): 1173–1188. Available from https://doi.org/10.1139/t05-050 [accessed October 14, 2019].

Meles, D., Bayat, A., and Chan, D. 2014. One-dimensional compression model for tire-derived aggregate using large-scale testing apparatus. International Journal of Geotechnical Engineering, 8(2): 197-204. Available from https://doi.org/10.1179/1939787913Y.0000000019 [last accessed February 5, 2020].

Meles, D., Chan, D., Yi, Y., and Bayat, A. 2016. Finite-Element analysis of highway embankment made from Tire-Derived Aggregate. Journal of Materials in Civil Engineering, 28(2): 1-8. doi: 10.1061/(asce)mt.1943-5533.0001371.

Moo-Young, H., Sellasie, K., Zeroka, D., and Sabnis, G. 2003. Physical and chemical properties of recycled tire shreds for use in construction. Journal of Environmental Engineering, 129(100): 921-929. doi:10.1061/(ASCE)0733-9372(2003)129:10(921).

Mwai, M., Wichuk, K., and McCartney, D. 2010. Implications of using tire-derived aggregate for landfill leachate collection and drainage systems. Presented at the Solid Waste Association of North America, Fifth Canadian Symposium, Banff, Canada.

Mwai M, (2016) Evaluating the performance of tire derived aggregate in the leachate collection systems of Alberta landfills, PhD Thesis, University of Alberta, Edmonton, Alberta.

Narejo, D. B., and Shettima, M. 1995. Use of recycled automobile tires to design landfill components. Geosynthetics International, 2(3): 619-624.

Olson, R. E. 1986. State of the art: consolidation testing. In Consolidation of soils: testing and evaluation, ASTM STP892. Edited by R. N. Yong and F. C. Townsend. ASTM International, West Conshohocken, PA. pp. 7–70.

Qian, X., Koerner, R. M., and Gray, D. H. 2002. Geotechnical Aspects of Landfill Design and Construction, Prentice-Hall Inc., Upper Saddle River, New Jersey, USA. pp. 280-330

Rao, V. G. and Dutta, R. K. 2006. Compressibility and strength behaviour of sand-tyre chip mixtures. Geotechnical and Geological Engineering, 24: 711-724. Available from https://doi.org/10.1007/s10706-004-4006-x [last accessed February 5, 2020].

Reddy KR and Marella A 2001. Properties of different size scrap tire shreds: Implications on using as drainage material in landfill cover systems. In Proceedings of the Seventeenth International Conference on Solid Waste Technology and Management, Philadelphia, PA, USA, 2001, pp. 1-16.

Reddy KR and Saichek RE 1998. Characterization and performance assessment of shredded scrap tires as leachate drainage material in landfills. In Proceedings of the Fourteenth International Conference on Solid Waste Technology and Management, Philadelphia, PA, USA.

Reddy, K. R. and Marella, A. 2001. Properties of different size scrap tire shreds: Implications on using as drainage material in landfill cover systems. In Proceedings of the Seventeenth International Conference on Solid Waste Technology and Management, Philadelphia, PA, USA, pp. 1-16.

Rowe KR and Babcock D 2007. Modelling the clogging of coarse gravel and tire shreds in column tests. Canadian Geotechnical Journal 44(11): 1273-1285.

Rowe KR and McIsaac R 2005. Clogging of tire shreds and gravel permeated with landfill leachate. Journal of Geotechnical and Geoenvironmental Engineering 131(6): 682-693.

Rowe KR and Yu Y 2013. A Practical technique for estimating service life of MSW leachate collection systems. Canadian Geotechnical Journal 50(2): 165-178.

Rowe RK, Armstrong MD and Cullimore DR 2000a. Mass loading and the rate of clogging due to municipal solid waste leachate. Canadian Geotechnical Journal 37(2): 355-370.

Rowe RK, Armstrong MD and Cullimore DR 2000b. Particle size and clogging of granular media permeated with leachate. Journal of Geotechnical and Geoenvironmental Engineering ASCE 126(9): 775-786.

Rowe, K. R., and Yu, Y. 2013. A Practical technique for estimating service life of MSW leachate collection systems. Canadian Geotechnical Journal, 50, 165-178. doi:dx.doi.org/10.1139/cgj-2012-0257

Rowe, R. K. 2005. Long-term performance of contaminant barrier systems. Géotechnique, 55(9): 631–678. Available from https://doi.org/10.1680/geot.2005.55.9.631 [accessed October 14, 2019].

Rowe, R. K. and Babcock, D. 2007. Modelling the clogging of coarse gravel and tire shreds in column tests. Canadian Geotechnical Journal, 44(11):1273–1285. Available from https://doi.org/10.1139/T07-057 [last accessed October 14, 2019].

Rowe, R. K. and Fleming, I. R. 1998. Estimating the time for clogging of leachate collection systems. Presented at the Third International Congress on Environmental Geotechniques, Lisbon, Portugal, A. A. Balkema, Rotterdam, the Netherlands, pp. 23–28.

Rowe, R. K. and McIsaac, R. 2005. Clogging of tire shreds and gravel permeated with landfill leachate. Journal of Geotechnical and Geoenvironmental Engineering, 131(6): 682–693. Available from https://doi.org/10.1061/(ASCE)1090-0241(2005)131:6(682) [last accessed October 14, 2019].

Rowe, R. K., Quigley, R. M., Brachman, R. W., and Booker, J. R., 2004, Barrier Systems for Waste Disposal Facilities, Taylor and Francis Books Ltd (E and FN Spon), London, pp. 587

Sarsby, R. W., and Vickers, B. 1986. "Side Friction in Consolidation Tests on Fibrous Peat," Consolidation of Soils: Testing and Evaluation, ASTM STP 892, R.N. Yong and F.C. Townsend, Eds., American Society for Testing and Materials, Philadelphia, pp.485-489.

Seidelt, S, Mu¨ller-Hagedorn, M., and Bockhorn, H. 2006. Description of tire pyrolysis by thermal degradation behaviour of main components. Journal of Analytical and Applied Pyrolysis, 75(1):11–18. doi:10.1016/j.jaap.2005.03.002.

Strenk, P. M., Wartman, J., Grubb, D. G., Humprey, D. N., and Natale, M. F. 2007. Variability and scale-dependency of tire-derived aggregate. Journal of Materials in Civil Engineering, 19(3): 233–241. Available from https://doi.org/10.1061/(ASCE)0899-1561(2007)19:3(233) [last accessed October 14, 2019].

Tweedie, J. J., Humphrey, D. N., and Sandford, T. C. 1998. Tire shreds as lightweight retaining wall backfill: active conditions. Journal of geotechnical and geoenvironmental engineering, 124(11): 1061-1070. Available from https://ascelibrary.org/doi/10.1061/(ASCE)1090-0241(1998)124:11(1061) [last accessed February 5, 2020].

Warith, M. A., Evgin, E., and Benson, P. A. 2004. Suitability of shredded tires for use in landfill leachate collection systems. Waste Management, 24(10): 967–979. Available from https://doi.org/10.1016/j.wasman.2004.08.004 [last accessed October 14, 2019].

Wartman, J., Natale, M. F., and Strenk, P. M. 2007. Immediate and time dependent compression of tire derived aggregate. Journal of Geotechnical and Geoenvironmental Engineering, 133(3): 245-256.

Wells T, Fityus S and Smith DW 2007. Use of in situ airflow measurements to study permeability in cracked clay soils. Journal of Geotechnical and Geoenvironmental Engineering 133(12): 1577-1586.

Wells T, Fityus S, Smith DW et al 2006. The indirect estimation of saturated hydraulic conductivity of soils, using measurements of gas permeability. Australian Journal of Soil Research 44(7): 719-725.

Williams, P. T., and Besler, S. 1995. Pyrolysis-thermogravimetric analysis of tyres and tyre components. Fuel, 74(9): 1277-1283. doi:0016-2361(95)00083-6.

Yi, Y., Meles, D., Nassiri, S., and Bayat, A. 2014. On the compressibility of tire-derived aggregate: comparison of results from laboratory and field tests. Canadian Geotechnical Journal, 52(4): 442-458. Available from https://doi.org/10.1139/cgj-2014-0110 [last accessed February 5, 2020].

Youwai, S., and Bergado, D. T. 2003. Strength and deformation characteristics of shredded rubber tire sand mixtures. Canadian Geotechnical Journal, 40(2): 254-264. Available from https://doi.org/10.1139/t02-104 [last accessed February 5, 2020].

Yu, Y. and Rowe, K. R. 2012. Modelling leachate-induced clogging of porous media. Canadian Geotechnical Journal, 49(8): 877–890. Available from https://doi.org/10.1139/t2012-052 [last accessed October 14, 2019].

Zekkos, D., Bray, J. D., Kavazanjian, E., Jr., Matasovic, N., Rathje, E. M., Reimer, M. F., and Stokoe, K. H. II. 2006. Unit weight of municipal solid waste. Journal of Geotechnical and Geoenvironmental Engineering, 132(10): 1250–1261. Available from https://doi.org/10.1061/(ASCE)1090-0241(2006)132:10(1250) [last accessed October 14, 2019].

Zeng Z and Grigg R 2006. A Criterion for Non-Darcy Flow in Porous Media. Transport in Porous Media 63(1): 57–69.

Zimmerman PS, 1997. Compressibility, Hydraulic Conductivity and Soil Infiltration of Tire Shreds and Field Testing of a Shredded Tire Horizontal Drain, MS Thesis, Iowa State University, Ames, Iowa.